Enzyme Application for Chemical Transformations:

A Pathway to Green Synthesis

Inaugural dissertation
of the Faculty of Science,
University of Bern

presented by

Lucia Robustini

from Italy

Supervisor of the doctoral thesis :
Prof. Dr. Francesca Paradisi

University of Bern

Accepted by the Faculty of Science.

Bern, **07.05.2024**

The Dean
Prof. Dr. Marco Herwegh

Trust the process

Table of Contents

AADCs Aromatic Amino acid decarboxylases

AI   Auto-induction Media

APIs   Active Pharmaceutical Ingredients

ara   Arabinose

CLEAs   Cross-linked enzyme aggregates

DCM   Dichloromethane

E. coli *Escherichia coli*

EcTnaA Tryptophanase A from *E. coli*

EncMh Encapsulin from *Mycolicibacterium hassiacum*

FITC   Fluorescein isothiocyanate

FMOC   Fluorenylmethyloxycarbonyl

Fwd   Forward

GC   Guanine-Cytosine

HCl   Hydrochloric acid

HeP5CR   Pyrroline-2-carboxylate reductase from *Halomonas elongata*

HeWT ω-Transaminase from *Halomonas elongata*

HPLC   High Performance Liquid Chromatography

IDA   Iminodiacetic acid

IMAC   Immobilized metal affinity chromatography

IPTG   Isopropyl β-D-1-thiogalactopyranoside

KM   Michaelis constant

MsAcT Acyltransferase from *Mycobacterium smegmatis*

NAD   Nicotinamide adenine dinucleotide

PBR   Packed Bed Reactors

PEG   Poly ethylene glycole

PLP   Piridoxyal-5'-phosphate

PMP   Pyridoxamine-5'-phosphate

Rev   Reverse

RgTDC Decarboxylase from *Rumignococcus gnavus*

TA   Aminotransferase/ Transaminase

TB   Terrific Broth

VLP   virus-like proteins

Amino acids

A - Ala Alanine

C - Cys Cysteine

D – Asp   Aspartic acid

E - Glu   Glutamic acid

F - Phe   Phenylalanine

G - Gly   Glycine

H - His   Histidine

I - Ile   Isoleucine

K - Lys   Lysine

L - Leu   Leucine

M - Met   Methionine

N - Asn   Asparagine

P - Pro   Proline

Q - Gln   Glutamine

R - Arg   Arginine

S - Ser   Serine

T - Thr   Threonine

V - Val   Valine

W - Trp   Tryptophan

Y - Ty   Tyrosine

DNA nucleotides

A   Adenine

C   Cytosine

T   Thymine

G   Guanine

Units of measure /symbols

%   Percentage

bp Base pair

°C Celsius

CV Column Volume

Da Dalton

ee enantiomeric excess

Ɛ Extinction coefficient

g Gram

h Hour

L Litre

M Molarity

m meter

min Minute

mol Mole

rpm Rotation per minute

Rt Resident Time

s Second

U Units of activity

V Volume

λ wavelength

In recent decades, the urge to reduce emissions and the environmental impact of industrial processes has driven to the exploration of alternative synthetic methods for industrial and chemical production. Within this context, biocatalysis has gained increasing interest as a complementary tool to classical chemistry. Biocatalysis operates under favourable reaction conditions, maintaining high selectivity. However, the use of enzymes at large production scale is not without limitations. Challenges include catalyst stability, cofactor reusability, and reaction setup (e.g., batch processes), all of which necessitate optimization for cost-effective industrial applications.

Significant efforts focused on implementing enzymatic applications. For instance, the use of immobilized enzymes and the transition to automated flow systems have expanded biocatalysis beyond its initial restricted applications. These advancements enabled gram-scale production of fine chemicals and high degree of enantiospecificity of the final product.

In this work, several critical aspects for efficient biocatalyst utilization are investigated. By screening reaction conditions, the impact of retained enantiopreference in an industrially significant transaminase will be assessed. Factors such as ionic strength, co-solvent, pH, and reaction time are investigated, leading to enhanced or inverted specificity of the final enantiomer. The ultimate goal is to manipulate these factors to optimize enzymatic enantiopreference, thereby enhancing the efficiency and specificity of biocatalytic synthesis.

An important aspect of this research focuses on the downside of the immobilisation approach. While immobilized biocatalysts offer numerous advantages for industrial applications, the structural alterations that occur upon immobilization can be detrimental for the enzyme

activity. To mitigate this effect, a possible solution is proposed which leverage on a proteinaceous cage, a structure identified in bacteria as compartmentalisation strategy, where is serves to preserve the native conformation of the enzyme In this work, we thoroughly investigated the impact of encapsulation on two enzymes, which occurs *in vivo* during enzyme expression. Furthermore, we assessed the potential application of this strategy for immobilization purposes, creating a protective microenvironment that could lead to more efficient industrial processes.

Additionally, we explore the combination of enzymatic and chemical processes highlighting the complementarity of these two synthetical approaches. By combining an enzymatic cascade with the final chemical step, we propose to achieve the production of valuable psychoactive compounds. The sequential use of two enzymes lead to the synthesis of the intermediate which will be converted in the final product, effectively upcycling starting materials and adding value to the overall process.

Through these objectives, we aim to expand the role of biocatalysis, positioning it as a viable and sustainable choice for environmentally friendly industrial applications.

Introduction

1.1 History and State of the Art

Over the past few decades, the necessity for more sustainable industrial practices has become indisputable. Our collective efforts aim to protect the environment and ensure a more promising future for succeeding generations by eliminating processes which are deemed ecologically unfriendly. This commitment was initially formalized in the Rio Declaration of 1992 and has remained a recurring endeavour ever since. Most recently, at COP28 in (Dubai, December 2023), the definition of environmental action was further refined by setting rules for countries to measure, report, and verify their greenhouse gas emissions, as well developing guidelines to enhance their climate action plans.[1,2]

The branch of Green Chemistry, initially introduced by Anastas in 2009, underscores several critical principles of sustainability of chemical reactions and processes. These include the production and efficient use of materials and energy, the advancement of renewable resources, and the deliberate design of processes to minimize hazards. Green Chemistry plays a pivotal role in our ongoing global efforts to address climate change, to foster sustainable solutions, and mitigate emissions, and provides essential guidelines for designing environmentally sustainable chemical processes through 12 principles.[3] These principles place and emphasis on waste reduction, the use of safer chemicals, energy efficiency, and a focus on renewable resources. By adhering to these principles, the goal is to minimize the environmental impact and promote a more sustainable and eco-friendly approach to chemistry.

Figure 1.1. The twelve principles of green chemistry adapted from Anastas *et al.*[3]

In this context, biocatalysis— a series of processes employing natural catalysts, including enzymes or whole cells—plays a significant role in adhering to these principles. Its capacity to perform highly selective and efficient chemical transformations under mild conditions makes it a valuable tool for advancing green and sustainable chemical processes. In contrast to traditional organic synthesis, the use of expensive and often toxic catalysts or reagents is avoided. Furthermore, biocatalysis can be regarded as a complementary tool alongside synthetic chemistry, propelling us toward a green revolution.

1.2 Enzymes in Industrial Applications

The use of enzymes in industrial field faced an exponential growth in the last 50 years .[4,5] Interest in the use of this approach has transitioned from traditional applications, such as those in the bakery and brewery sectors, to cutting-edge practices that revolutionize entire industries while emphasizing sustainability.[6–8] A remarkable milestone in this field was the

synthesis of Islatravir—a nucleoside reverse transcriptase translocation inhibitor (NRTTI) involved in the treatment for HIV infection—achieved exclusively by enzymatic route by Merck in 2019.[9]

Throughout this thesis, we will encounter various industrially-relevant enzymes. The following sections will therefore provide an initial comprehensive overview of enzymes relevant for this research, before discussing techniques for enzyme stabilization and the application of enzymes in continuous flow.

1.2.1 Aminotransferases

Aminotransferases (TAs, EC 2.6.1) play a crucial role in amino acid metabolism within biological systems.[10] These enzymes, which belong to the largest fold type among PLP-dependent enzymes (Type I), facilitate the stereoselective transfer of an amino group from a substrate to a donor (ketone, keto acid, or aldehyde) resulting in the formation of chiral amines or amino acids and a corresponding ketone product (Figure 1.2).
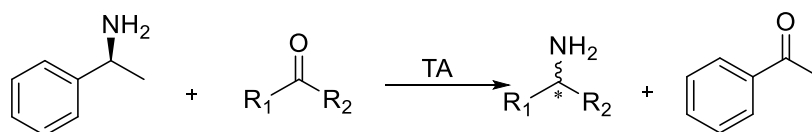
Figure 1.2 Oxidative transamination of pro-chiral substrate from general transaminase (TA). (*S*)-MBA is used here as an example for amino donor.

The catalytic cycle of these enzymes relies on pyridoxal-5'-phosphate (PLP), a derivative of Vitamin B_6. This cycle follows a ping-pong process, which is divided into two half-reactions. Initially, in the PMP half cycle, the amino donor reacts with the internal aldimine (PLP which is bound to a catalytic lysine in the active site through a dehydration reaction) to form the external aldimine (Figure 1.3). The external aldimine is then hydrolysed to form pyridoxamine-5'-phosphate (PMP) and the deaminated amino donor. Subsequently, PMP reacts with the amino acceptor and, in a second dehydration reaction, results in the formation of the final amine product and the regeneration of PLP back in the original internal aldimine state.
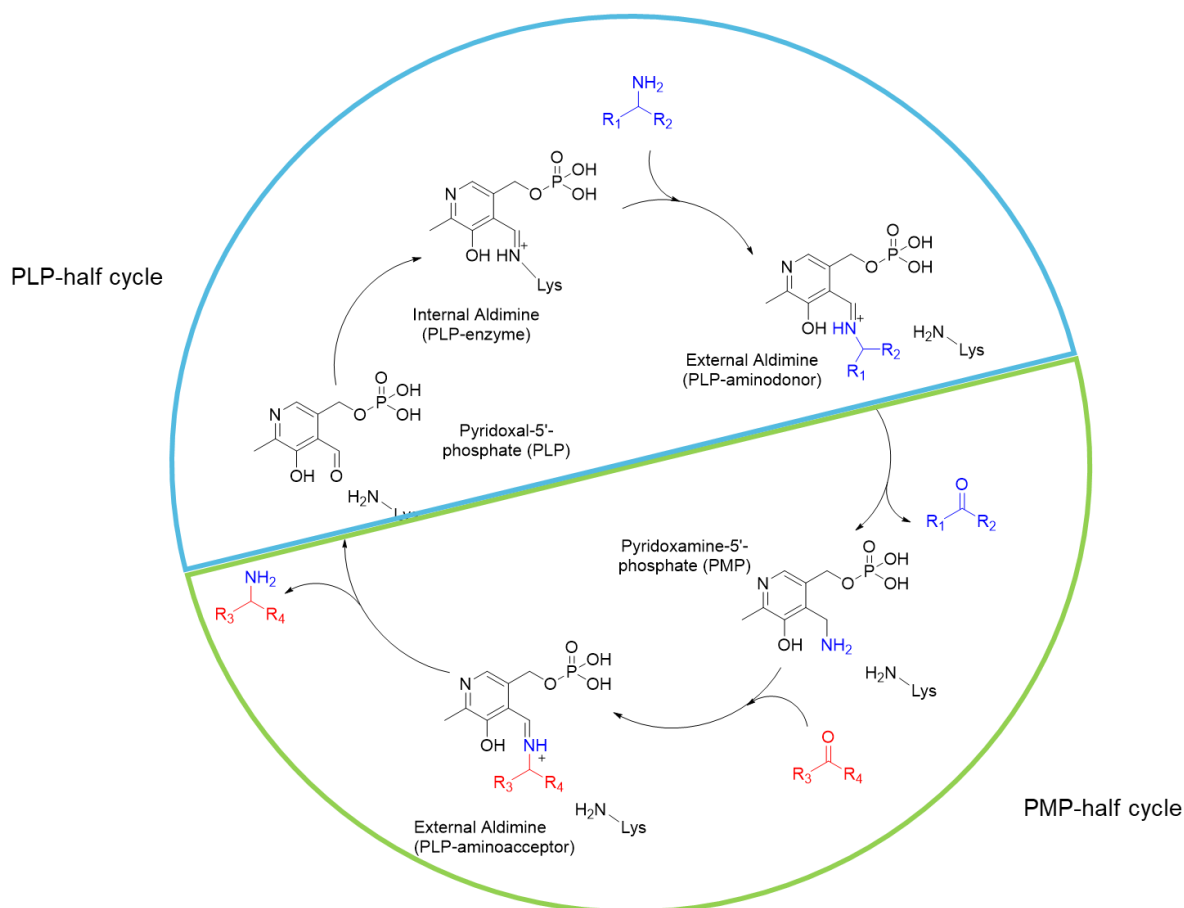
Figure 1.3 Catalytic mechanism of PLP-dependent TAs. The amino donor is highlighted in blue in the PLP-half cycle, while the carbonyl amino acceptor is highlighted in red in the PMP-half cycle. Figure adapted from Roura-Padrosa *et al*.[11]

Numerous studies have investigated the biosynthesis of pharmaceutical drugs and agrochemical compounds, or the intermediates required for their synthesis, mediated by transaminases (TAs). [12–14] . Over the course of time, a number of examples involve the use of TAs derived from *Arthrobacter sp.* (Arth-TAm). Following its discovery in soil, *Arth*-TAm, both in its wild-type form and its genetically modified variants, found application in the field of pharmaceutical manufacturing.[15,16] These enzymes facilitated the asymmetric synthesis of various active APIs, including the production of a dual orexin receptor antagonist (suvorexant),[17] a pro-drug for treating benign prostatic hypertrophy called silodosin, [18] and an anti-arrhythmic medication (mexiletine),[19] among others. In recent years, the application of transaminases has extended to other pharmacologically significant compounds, including carbocyclic nucleosides,[20] steroids derivatives,[21] and for the synthesis of ß- and γ- aromatic amino acids. [22] An important milestone was achieved in 2010 when Savile and collaborators

successfully used the transaminase ATA-117 in a biocatalytic process to replace a rhodium-catalysed asymmetric enamine hydrogenation, enabling efficient, economically viable, and environmentally advantageous processes for pharmaceutical manufacturing.[14] Through enzyme engineering, the research group achieved selective amination of the pro-sitagliptin precursor with high regio- and stereo-selectivity. This strategic modification led to a remarkable 13% improvement in overall yield and an 53% increase in productivity. Moreover, this innovative approach reduced the total waste by 19% when compared to the conventional synthetic method (as illustrated in Figure 1.4)
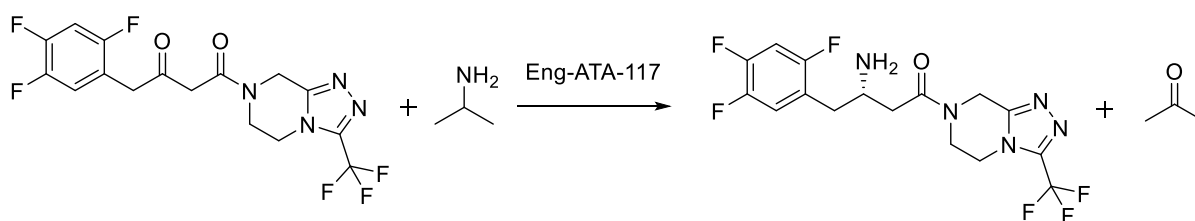
Figure 1.4 Synthesis of sitagliptin using engineered ATA-117 as alternative process developed by Savile *et al.* [14]

Another remarkable example involves the synthesis of (*S*)-Rivastigmine, a potent pharmaceutical employed in the treatment of patients in the early stages of Alzheimer's disease but which exhibited favourable effects also in patients with Parkinson's-related dementia. In 2010, the group of Faber devised a chemo-enzymatic synthetic route for the production of this molecule.[23] This process initiated with the enantioselective reductive amination of *m*-methoxymethyl acetophenone with L-alanine with a ω-transaminase from *Vibrio fluvialis* (*Vf*-ωTA) , achieving an excellent 99% conversion and with a 99% *ee*. This biocatalytic step was coupled with regeneration system (not depicted in the figure), mediated by a glucose dehydrogenase (GDH) and a lactate dehydrogenase (LDH) which allowed to shift the equilibrium of the reaction toward the formation of the aminated product. By starting from the (*S*)-precursor, three synthetic steps were successfully executed, resulting in the production of (*S*)-Rivastigmine in excellent overall yield with a remarkable 99% *ee* (as illustrated in Figure 1.5).
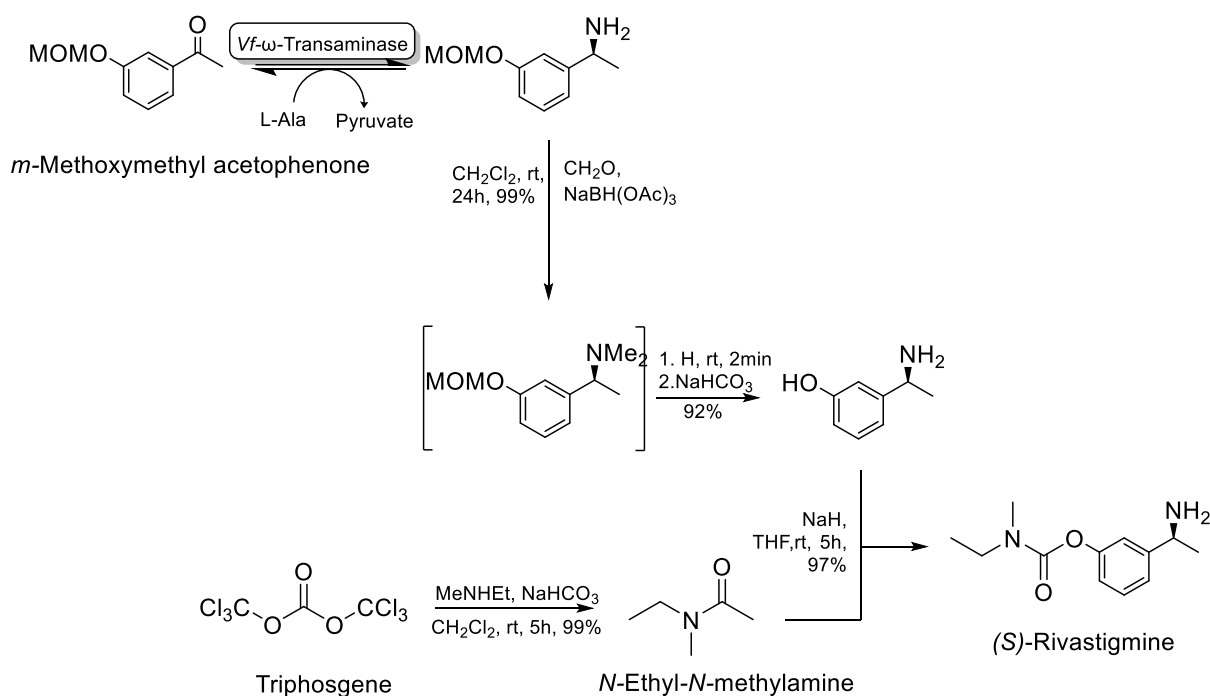
Figure 1.5 The chemoenzymatic synthesis of (*S*)-Rivastigmine developed by Faber *et al.* [23]The first step is enantiospecific resolution of the prochiral precursor, *m*-methoxymethyl acetophenone, catalysed by ω*Vf*TA. An enzymatic transamination (as opposed to a synthetic one) introduces a single stereoisomer into the synthesis, which ensures consistent stereochemistry throughout the synthetic process.

Our group dedicated significant effort to the exploration and engineering of various transaminases, including those sourced from *Chromobacterium violaceum* (*Cv*TA), *Pseudomonas fluorescens* (*Pf*TA), and *Thermomyces stellatus* (*Ts*RTA).[25–28] In 2015 a transaminases from *Halomonas elongata* (*He*WT) was widely characterised and subsequently used for both batch and flow reactions, enabling the catalysis of a series of industrially significant chiral amines.[29–31] The same enzyme was also reported to switch its enantiopreference depending on the reaction condition, topic which will be further studied in Chapter 4.

1.2.2 Oxidoreductases

Oxidoreductases (E.C. 1) are an important class of enzymes with a diverse range of applications in industrial biotechnology. These enzymes play crucial roles in various processes, including lignin degradation, carbohydrate modification, and also find application as cross-linking agents in the food industry to enhance physicochemical properties of the end product

(such as texturization in baking industry or polyphenol removal from juices).[32–35] These proteins catalyse the transfer of electrons from one molecule (the reductant) to another (the oxidant), therefore, in nature, they are essential for a plethora of cellular processes, including energy production, metabolism, and redox homeostasis. [32,36–38] Oxidoreductases are subclassed based on their catalytic properties and coenzyme interactions and can be categorized into four main groups: oxidases, peroxidases, oxygenase/hydroxylases, and dehydrogenases/reductases.[39]

A class redox enzymes identified as imine reductases (IREDs) have emerged as a valuable tool for the asymmetric synthesis of optically active amines. These enzymes facilitate the NAD(P)H-dependent reduction of broad range of imine precursors, including monocyclic, bicyclic, and even large tricyclic imines and iminiums, yielding the corresponding amines with high enantioselectivity. Initially applied in the synthesis of 3,4-dihydroisoquinones and 3,4-dihydro-ß-carbolines, their application has expanded to encompass the one-pot reaction for the production, for instance, of pyrrolidines and piperidines, which serve as scaffolds for alkaloid synthesis.[40,41]

Given the pharmaceutical importance of their products, substantial efforts by both academic and industrial research groups have been directed towards this enzyme class, involving the use of enzyme engineering, aiming to enhance their integration into processes and facilitate the transition from small- (mg) to industrial-scale (tons) production of pharmaceutical relevant molecules.[42,43]

In a more recent advancement within this field, in 2023, the group of Ward identified 29 novel IREDs capable of synthesizing five tetrahydroisoquinolines (THIQs) by asymmetric reduction of the correspondent dihydroisoquinolines (DHIQs). These compounds are known to exhibit therapeutic properties against HIV, tumours, inflammation, as well as possessing bronchodilator and antibiotic activities (Figure 1.6).[44]
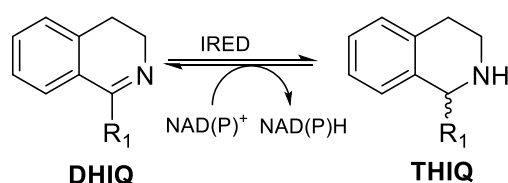
Figure 1.6 Schematic asymmetric reaction of dihydroisoquinolines (DHIQs) into tetrahydroisoquinolines (THIQs) catalysed by IRED.[44]

Despite their relevance, the extensive use of oxidoreductases in industrial processes can face limitations due to their dependence on expensive redox counterparts, which significantly contributes on the overall cost of the process. In addition to whole-cell reactors, which naturally have a regeneration system, various strategies have been devised for cofactor regeneration to achieve a better cost-effectiveness. One common approach involves coupling the initial reduction reaction with a secondary enzymatic cofactor regeneration step, where a sacrificial substrate participates in the reduction of the cofactor. It is therefore important that this sacrificial substrate is affordable and does not interfere with the primary reaction or downstream processes.[45,46] [47]The implementation of such recycling systems enables process intensification at an industrial scale, avoiding the need of continuous feeding of expensive cofactors. This approach has found a significant application in the production of active pharmaceutical ingredients (APIs).[47,48]

1.2.3 Tryptophanase

Tryptophanases, also known as tryptophan indole-lyases (EC 4.1.99.1), are a class of enzymes that play a crucial role in cleaving C-C, C-O, or C-S bonds in their respective substrates in biological systems. Initially identified by Baker and Dawson during their investigation on the tryptophan mechanism in *E. coli*, these enzymes are ubiquitous in plants, fungi, and bacteria.[49] Particularly in the gut, microorganisms which are directly involved in serotonin/melatonin metabolism, use a tryptophanase to produce compounds, such as serotonin (5-hydroxytryptamine), kynurenine (Kyn), and indole derivatives, which are essential for their survival. These molecules also play critical roles in maintaining metabolic and nutritional homeostasis, supporting the immune system, and influencing cerebral activity of the symbiotic organisms.[50–52] Tryptophanases are classified within the fold-type 2 of PLP-dependent enzymes, and operates through the participation of two catalytic amino acids (lysine and aspartate). Its function encompasses either the formation of L-tryptophan *via* the ß-addition of indole to dehydroalanine, or the degradation of L-tryptophan to indole and serine *via* ß-elimination.[53,54] The presence of other residues in the active pocket (Phe, Tyr, His)

are fundamental to stabilise the substrate conformation and facilitate catalysis (Figure 1.8).[55–58]
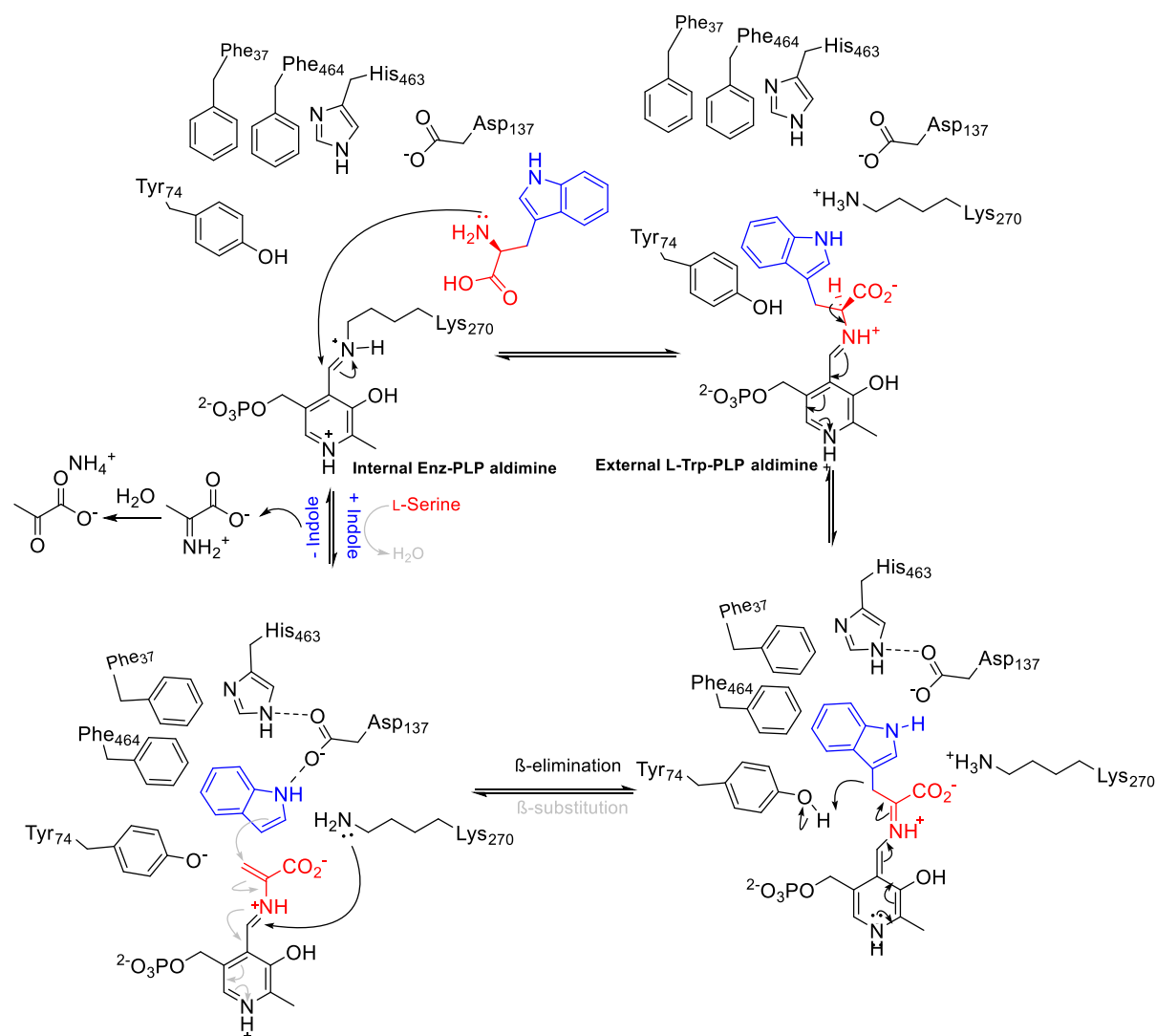
Figure 1.8 The proposed catalytic mechanism of tryptophanase. The biosynthesis of L-tryptophan (black pathway), or its degradation to indole, ammonia, and pyruvate (grey pathway).

L-Tryptophan and its various analogues have recently gained an increased amount of attention. These compounds serve not only as dietary supplements (for example, in melatonin and serotonin), but also find application as pest control agents in agriculture and play a role in textile manufacturing for pigment and dye production (Figure 1.9).[60–63]
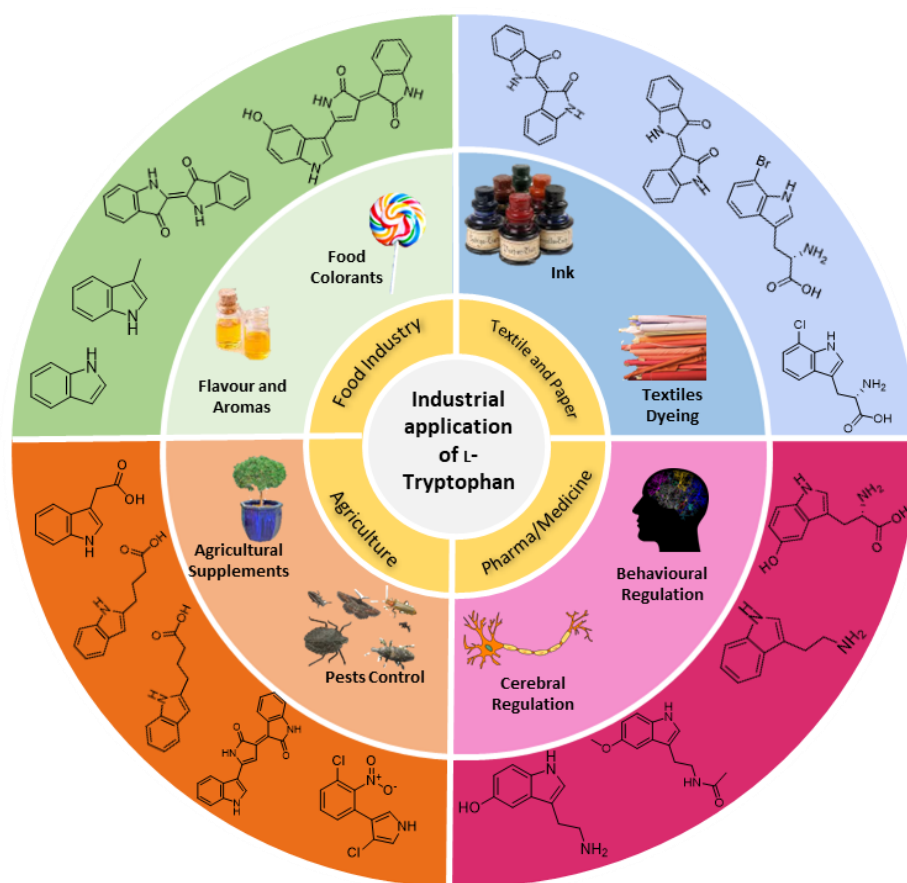
Figure 1.9 Commercially relevant applications of L-tryptophan and its derivatives. Figure adapted from Zhang *et al.*[64]

In Chapter 6, will be investigated the biosynthesis of tryptophan and two 5- substituted analogues, mediated by a tryptophanase from *E. coli*. In a telescopic cascade, this enzyme will be the starting point for a biosynthetic pathway to synthesize precursors for physiologically active molecules, including melatonin, serotonin, and dimethylated tryptamines.

1.2.4 Decarboxylase

Decarboxylases, also referred to as carboxy-lyases (EC number 4.1.1), constitute an enzyme group that plays a pivotal role in many important biochemical processes. Their function involves the removal (or addition) of a carboxyl group from a diverse range of substrates, including amino acids and α- or β-keto acids.[65–67] Due to the importance of their biological role, decarboxylases have been the subject of extensive investigation over the last decade, collecting substantial insights concerning the decarboxylation mechanisms in biological systems. While more than 90 distinct classes of these enzymes have been identified, a

significant differentiation lies in their catalytic mechanisms, which may or may not rely on cofactors (Table 1.1).

Table 1.1 Examples of Decarboxylases classified on the cofactor.

Example	Cofactor	Biological Role	Reference
Orotidine 5'-monophosphate decarboxylase (OMPDC)	none	Involved in uridine monophosphate biosynthesis	Appleby et al. [68]
Methylmalonyl-CoA decarboxylases	Biotin	Decarboxylation of (S)-methylmalonyl-CoA into propionyl-CoA (Succinate pathway)	Beening et al. [69]
Peptidyl-cysteine decarboxylase (EpiD)	Flavin	Formation of reactive (Z)-enethiol from cysteine residue in epidermine biosynthesis	Blaesse et al. [70]
4-Hydroxyphenylacetate decarboxylase (HPAD)	Glycyl radical	Kolbe-type decarboxylation for tyrosine synthesis in Clostridii sp.	Selmer et al. [71]
UDP-glucuronate decarboxylase	NAD^+/$NADP^+$	Conversion of UDP-glucuronate into UDP-xylose in nucleotide sugars metabolism.	Li et al [72]
Aromatic L-amino acid decarboxylases (AADC)	Pyridoxal 5'-phosphate (PLP)	Regulation of L-DOPA, L-Phenylalanine, L-Tyrosine, L-Histidine, L-Tryptophan and Serotonin	Wen et al. [73]
L-Aspartate-alpha-decarboxylase	Pyruvoyl-group	Metabolism of aspartate and microbial beta-alanine	Pei et al. [74]
SEPHCHC-synthase	Thiamine diphosphate (ThDP)	Chorismate and isochorismate pathway in bacteria and plants	Fries et al. [75]
Oxalate decarboxylase	Metal or O_2	Conversion of oxalate to carbon dioxide and formate	Conter et al. [76]

From an industrial perspective, decarboxylases have been used in various applications, from the production of amino acid derivatives to bio-based materials. Noteworthy examples include the synthesis of β-alanine (which has applications in food and feed additives,[77,78] in pharmaceuticals,[79] polymer industry[80], pantothenic acid and carnosine synthesis[81,82]), GABA synthesis (involved in the treatment of stress reduction or as functional foods)[83], Bio-Nylon production (*via* lysine decarboxylase) [84] and CO_2 fixation.[85]

In Chapter 6, a class of pyridoxal 5'-phosphate (PLP)-dependent decarboxylases, specifically active on aromatic amino acids (AADCs), will be used for the decarboxylation of L-tryptophan (Section 6.4). The decarboxylation process relies on the use of PLP as a cofactor, which resides in the active site of the enzyme. The mechanism of action of PLP initiates with the formation of a Schiff's base with a lysine residue to form an aldimine (internal aldimine). Upon substrate binding, the amino group of the substrate undergoes nucleophilic attack at the C4' carbon of the internal aldimine, before a transaldimination reaction leads to the displacement of PLP from the catalytic lysine residue and resulting in the formation of a new Schiff's base (external aldimine). Decarboxylation is then performed, cleaving the C–C bond between the Cα and the carboxylated substrate, accompanied by the release of CO_2. The resulting carbanion is stabilized through resonance by the pyridine ring of PLP, leading to the formation of a quinonoid intermediate. Subsequent protonation of the α-C occurs. Finally, the lysine in the active site reacts with the resultant imine, regenerating the internal aldimine, and effectively restoring the state of the enzyme to the original PLP-enzyme complex, releasing the decarboxylated product (as illustrated in Figure 1.9).[86]
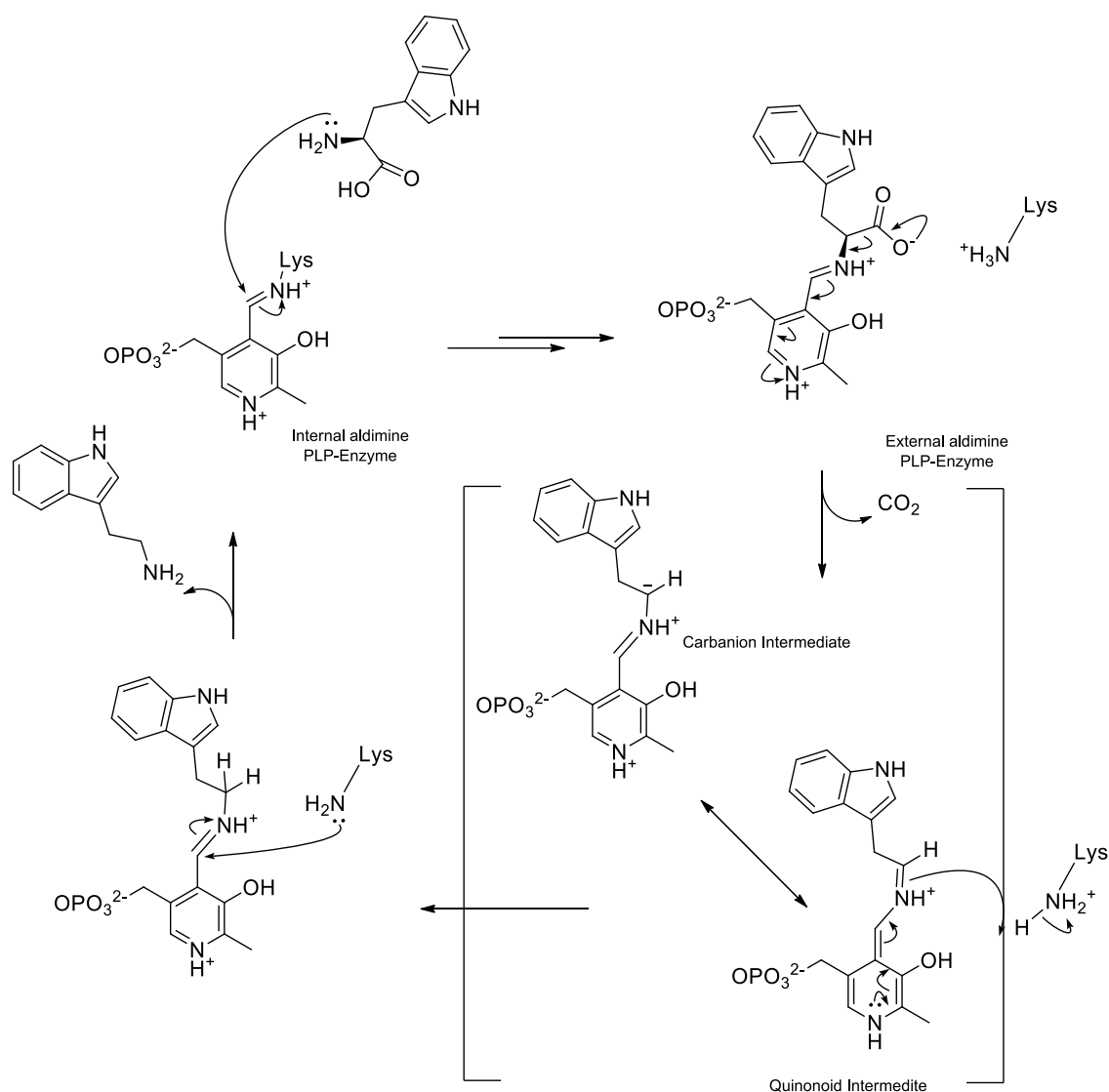
Figure 1.10 Proposed catalytic mechanism of tryptophan decarboxylase.

1.2.5 Acyltransferases

Acyltransferases are a class of enzymes which fall within the broader category of transferases (E.C. 2.3.1). These enzymes catalyse the transfer of acyl groups and alkyl chains from one molecule to another and play crucial roles in lipid metabolism, polyketide biosynthesis. Moreover, they are prevalent in various plant metabolic pathways, especially those associated with secondary metabolism.[87,88] A general scheme of the transacylation reaction is outlined in Figure 1.11.
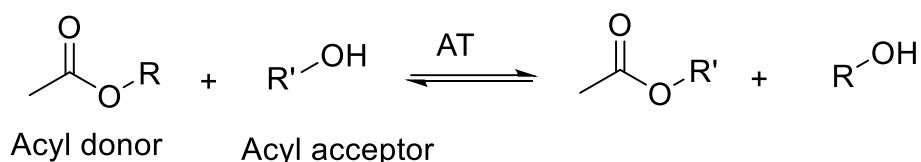
Figure 1.11 Generic scheme of transacylation reaction.

Acyltransferases play a crucial role in various applications, including the synthesis of flavonoids such as Rutin, Naringin, and Isoquercitin, [89,90] as well as terpenes [91] and coumarins. [92] However, their significance extends beyond these compounds to encompass biofuel production and vegetable oil synthesis. Specifically, these enzymes participate in the biosynthesis of triacyl glycerides (TAGs) in both plants and microalgae therefore recent efforts have focused on genetically engineering strains to enhance their TAG content. [93,94] By harnessing natural catalysts, such lipases/acyl transferases, biocatalysis enables the conversion of renewable feedstocks (such as plant biomass or waste materials) into valuable biofuels. These biofuels not only mitigate greenhouse gas emissions but also contribute to the preservation of non-renewable fossil resources. [93]

Enabling acylation reactions in aqueous media represents a significant objective in the field of biocatalysis. Classical chemical acylation of molecules suffers from the need to operate under dry conditions to prevent unwanted hydrolysis. Therefore, biocatalytic acylation has the potential to unlock a wide range of applications at an industrial scale, accessing important molecules while circumventing the need for anhydrous solvents. Lipases, which belong to the α/β hydrolase family, are capable of catalysing transesterification reactions. [95] Recent reports have revealed the transacylation activity of lipases in aqueous environments, expanding their applicability on a larger scale in the synthesis of flavour esters with agro-industrial significance. [96] These molecules are commonly derived from fossil fuels which, as mentioned earlier, pose critical challenges related to energy scarcity and environmental impact. [97] Furthermore, in 2019, Molinari and collaborators successfully synthesized 24 flavour esters using a biphasic system. This achievement involved combining a flow system with an immobilised acetyltransferase from *Mycobacterium smegmatis* and a set of poorly hydrophilic acetyl donors for the synthesis of esters under aqueous conditions, demonstrating the power in the use of enzymes in aroma technology while maintaining the greenness of the

methodology. [98] Related to the scope of this thesis, MsAcT, which catalytic cycle is reported in Figure 1.12, is employed in the final stage of the previously mentioned cascade (Chapter 6). Tryptamine (or its 5-hydroxy/5-methoxy analogues), generated through two consequential enzymatic transformations, serves as the acetyl donor in the ultimate step, enabling the synthesis of melatonin, acetyl-serotonin, or acetyl-tryptamine.
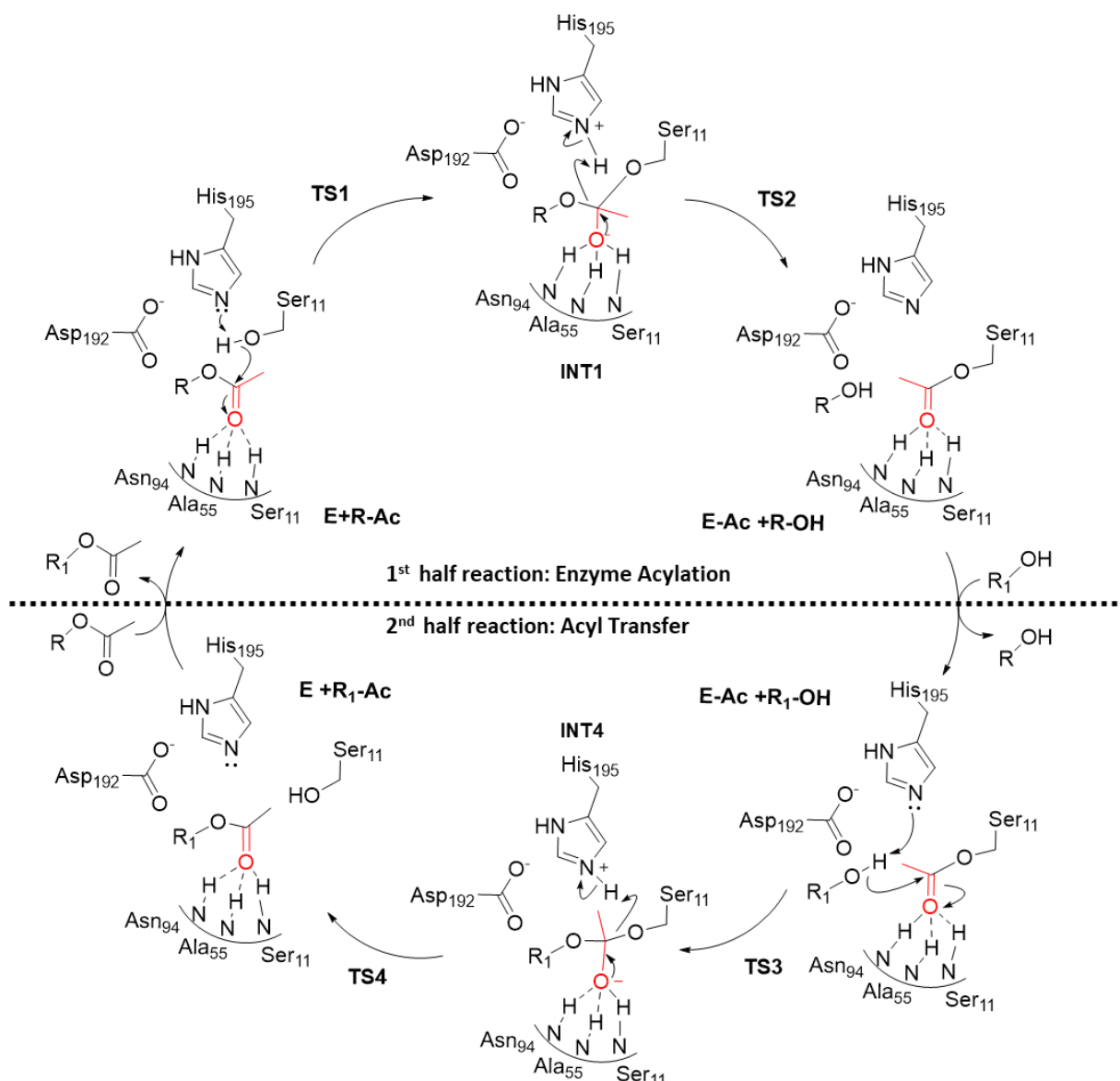
Figure 1.12 Reaction mechanism of MsAcT. Initially, the enzyme (**E**) binds with an acyl donor (**R-Ac**), forming a complex. This complex then proceeds to form an oxyanion tetrahedral intermediate (**INT1**). The alcoholic moiety is then released together with the acylated enzyme (**E-Ac + R-OH**). Following this step, the intermediate **E-Ac** undergoes nucleophilic attack by the incoming acyl acceptor (**R1-OH**) on the carbonyl, forming a secondary tetrahedral intermediate (**INT4**). Finally, the ester is released after transesterification, completing the reaction cycle.

1.3 Immobilised Enzymes and their Application in Biocatalysis

The advent of the use of immobilized biocatalysts has allowed a significant amount of progress in the industrial application of enzymes. This technique involves the anchoring of an enzyme to a solid support, resulting in the formation of an enzyme-support complex that remains immiscible within the reaction mixture, allowing the separation and recycling of the enzyme post-reaction. The earliest reports of enzyme immobilization dates back to late 1916, when Griffin and Nelson successfully adsorbed invertase onto activated charcoal and amorphous aluminium hydroxide observing that the immobilized enzyme retained comparable activity to its free form.[99] Since that point in time, the scientific community has shown keen interest in this technique and, in 1950, a significant milestone was reached when proteins were covalently immobilized onto carriers for the first time, enabling their utilization in continuous processes. [100] This approach has indeed demonstrated significant advantages, particularly in terms of biocatalyst recycling, which effectively reduces production costs by minimizing the requirement for enzyme re-isolation or disposal. During the period of 1960-1980, the use of immobilized enzymes expanded due an increase in the number of immobilisation chemistries. This broader range of approaches facilitated their widespread application across various sectors, including food and pharmaceutical industries.[101–105] A noteworthy example is the pioneering process employed by Bayer in 1972, where immobilized penicillin acylase, obtained from *E. coli*, was used to synthesize (+)-6-aminopenicillanic acid. This compound serves as an intermediate in the production of a semisynthetic penicillin-like antibiotic (Figure 1.13).[106]
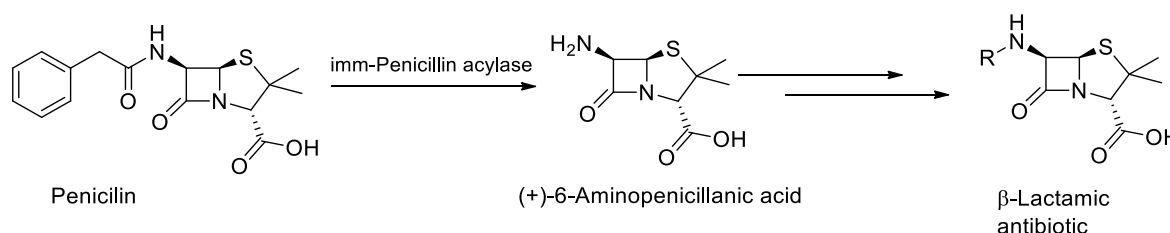
Figure 1.13 Bayer's semi-synthetic process for the synthesis of ß-lactamic antibiotic. The hydrolysis of then phenylacetyl moiety that leads to (+)-6-Aminopenicillanic acid (6-APA) is performed by an immobilised penicillin acylase isolated from *E.coli*. R represents a various side chain found in ß-lactamic antibiotic derivatives.

The use of an immobilised biocatalyst often offers several advantages: [107]

- **Improved Isolation**: By preventing direct mixing of the enzyme with the final product, the necessary work-up steps for purification are significantly minimized;

- **Reusability**: immobilized enzymes can be separated from the solution *via* filtration. Unlike soluble enzymes, which are single-use, immobilized enzymes can be repeatedly recycled;

- **Enhanced Stability**: upon immobilization, enzyme typically show an improvement in stability due to reduced flexibility, resulting in enhanced tolerance to variations in temperature, solvent, and pH;

- **Co-Immobilisation:** it is feasible to immobilize multiple enzymes on the surface of a carrier. This proves advantageous, especially in scenarios where a recycling system is required (as previously discussed). Additionally, it is even possible to immobilize the co-factor itself, either through covalent or non-covalent means.[108,109]

While the enhancements associated with immobilization render it an attractive strategy for industrial applications, it is crucial to acknowledge that the process also entails certain drawbacks that necessitate careful evaluation:

- **Reduced enzyme activity:** Structural distortions arising from multi-point attachments or rigidification can lead to diminished enzyme activity;

- **"Immobilisation" added costs:** The use of carriers and necessary chemicals for enzyme immobilisation introduces additional costs to the overall process;

- **Waste disposal:** While enzymes themselves exhibit high biocompatibility and adherence to sustainable guidelines, the use of carriers which are composed of non-biodegradable polymers necessitates proper disposal procedures;

- **Co-factor supplements:** In contrast to whole-cell bioreactors, the requirement of a continuous supplementation of cofactor must be carefully considered.

Protein immobilization often affects both enzymatic activity and stability and, in specific cases, may also modulate the selectivity of the reaction.[110,111]Therefore, a precise evaluation is essential to optimize process efficiency, taking into account the stability of the protein and the intended final application.[112,113]

The categorization of immobilization techniques depends on the nature of the bond (reversible or irreversible), and the chemical and physical methods employed to integrate the enzyme onto the support matrix. The main classes are represented in Figure 1.14.
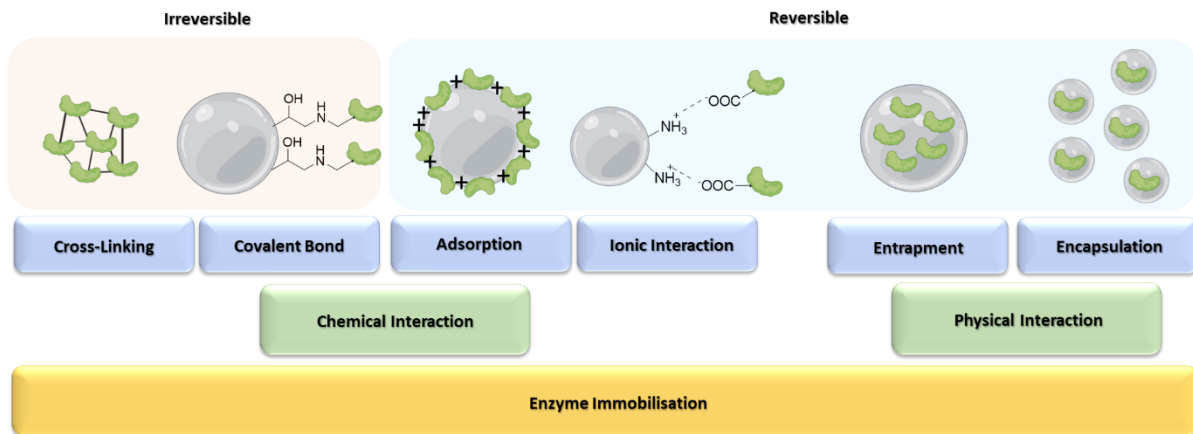
Figure 1.14 Representation of the common immobilisation techniques and their relative properties.

When using chemical methods, enzymes can either be aggregated between different units through the use of a cross-linker (*i.e.* glutaraldehyde), resulting in cross-linked aggregates (known as CLEAs), or the functional groups exposed on the surface of the enzyme can be used to establish an irreversible bond with functional groups of the carrier.[114–116] This approach has gained widespread interest, particularly due to significant advancements in recent years. For example, it is feasible to achieve multi-point covalent immobilization (dependent on derivatization), thereby enhancing the stabilization effect. An interesting strategy involves the use of a divalent metal ion (such as Co^{2+}), which in presence of a His-tagged protein, can facilitate precise positioning of the enzyme on the substrate, leading to enhanced exposure of the active site (Figure 1.15). This strategic arrangement ensures proper orientation of the catalytic side. Through covalent immobilization, the bond formed is robust and stable, resulting in enhanced enzyme resistance to denaturation. [117–119]
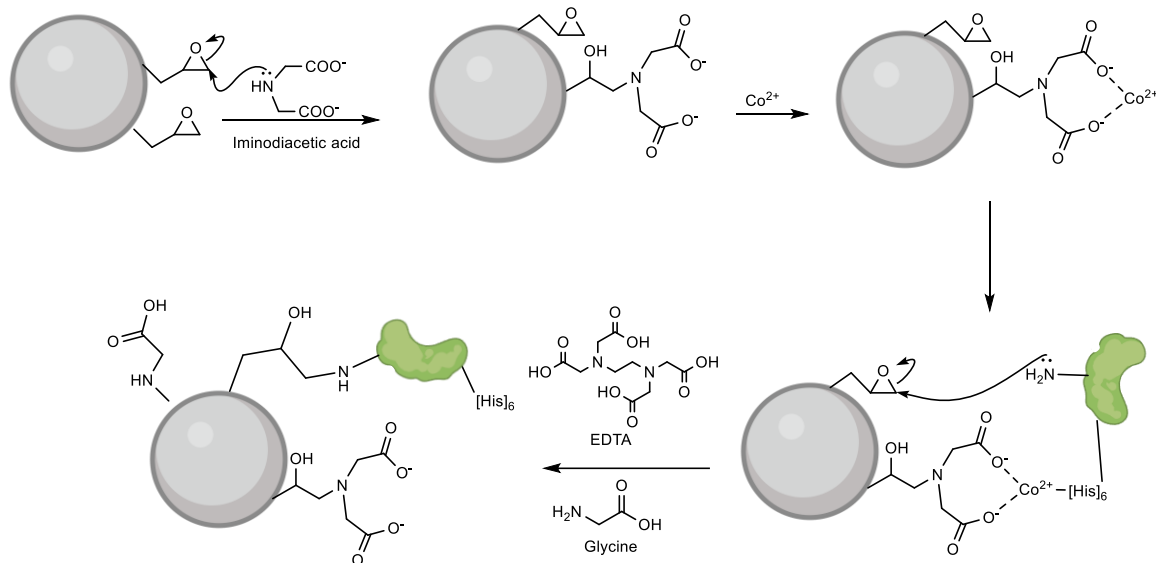
Figure 1.15. Covalent immobilisation of protein on an epoxy-derivatised agarose bead. Some of the epoxy groups are opened by reaction with iminodiacetic acid. This step inserts two carboxylate moieties on the surface of the resin, which can coordinate a Co^{2+} (or a divalent metal) atom needed to interact with the tag of 6 histidine tail present on the enzyme. A last passage of ethylenediaminetetraacetic acid (EDTA) is required to strip the cations present while glycine (or any other primary amine) is used as capping agent to react with any unreacted epoxy-groups on the surface.

Alternatively, reversible chemical immobilization of biocatalysts can occur through direct adsorption onto a carrier, where the enzyme is retained by weak interactions, such as hydrophobic or ionic interactions. Compared to covalent bonds, these interactions cause minimal distortion to the secondary structure of proteins, resulting in higher retained enzymatic activity. However, it is important to acknowledge that the character of these interactions is influenced by environmental factors, including fluctuations in pH or ionic strength. Such variations may render the bonds reversible, consequently contributing to a leaching effect.[120]

Through encapsulation and entrapment techniques, enzymes can be incorporated within a macroscopic matrix, either individually or by compartmentalization of multiple enzymatic units. This approach proves particularly valuable when the enzyme is sensitive to changes in flexibility or binding to a support. Alginate and alginate-based beads exemplify this application. These materials not only provide protection against mechanical stress and protease activity, but also exhibit an excellent degree of compatibility with biological

systems[121] serving as promising materials for clinical applications.[122] Although enzyme-polymer interactions are minimized, a limitation of this retention system is its inability to prevent enzyme leakage. However, alternative encapsulation approaches have emerged in recent years, tailored for specific applications or the production of nanocarriers[123-125]

1.4 A Proteinaceous Shell as New Player in Enzyme Immobilisation

In the realm of enzyme immobilization, both encapsulation and microencapsulation are two well-established techniques. While traditional encapsulation methods have been explored extensively (spray-drying,[126] coacervation,[127] or liposome entrapment[128], polylactic acid (PA)/polyethylene glycol (PEG) coating[129] to mention some), Chapter 5 of our study proposes an alternative strategy. This novel approach leverages on a microbial structure, offering a fresh perspective on enzyme immobilization techniques.

In 1994, Scherer and colleagues discovered proteinaceous structures widely spread in prokaryotes resembling 'shells' or 'cages.' These structures, measuring 24 to 32 nm, consist of 60 to 180 identical subunits with 5 to 9 Å porous between the junctions, capable of self-assembling *in vivo* (Figure 1.16). The studies demonstrated that these type of virus-like proteins (VLPs), named encapsulin, serve as containers, harbouring one or more proteins associated with oxidative stress within their cavities. [130,131]
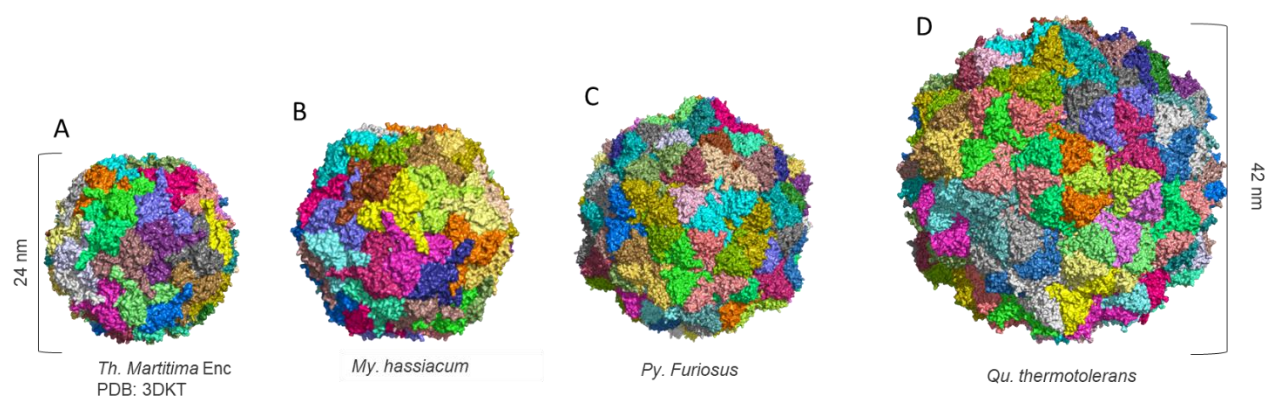
Figure 1.16 Examples of encapsulins found in A) *Thermatoga maritima* (PDB:3DKT); B) *Mycolcibacterium hassiacum* (PDB:6I9G); C) *Pyrococcus furiosus* (PDB: 2E0Z) and; D) *Quasibacillus thermotolerans* (2E0Z). [132–134] Pictures were generated with PyMol 2.4.1.

Numerous attempt have been conducted to engineer encapsulins, rendering them a viable platform for applications in nanotechnology and molecular diagnostics.[135,136] These modifications include the replacement of the cargo-protein (Figure 1.17), modification of the shell surface or its structure (*e.g.* pore size)[137,138] Remarkably, it has been observed that non-native cargo proteins, upon encapsulation, exhibit enhanced resistance to harsh conditions, including heat or pH fluctuations. Additionally, their enzymatic activity can increase, which can possibly be attributed to the increased local substrate concentration (molecular crowding), which favours the catalytic reaction.
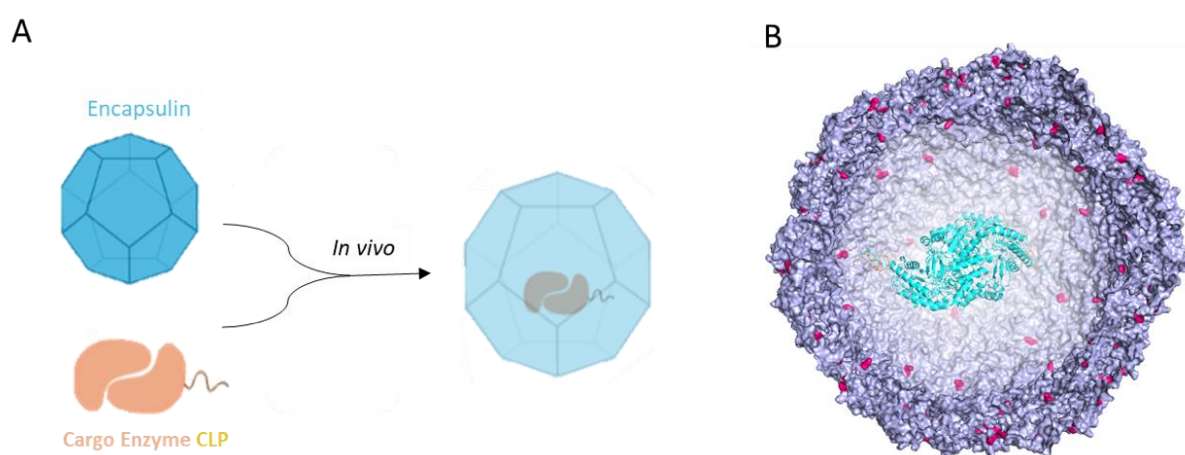
Figure 1.17 A) Schematic representation of the encapsulation of a cargo protein into the encapsulin shell; B) Model of a non-natural cargo protein (HeWT) into encapsulin derived from *M. hassiacum* . Models were generated with PyMol2.4.1.

Encapsulins have been recognised as promising players in the realm of biocatalysis as tools for enzyme immobilization and as nanobiorecators.[139] The possibility to use its proteinaceous surface is seen as intercalator, bridging the enzyme structure and the support matrix, maintaining the original enzymatic activity while leveraging on the benefits of immobilization, including enhanced stability and reusability.

1.5 Flow Biocatalysis

In the context of enzyme-catalysed reactions, the conventional batch approach involving immobilized biocatalysts has made significant progress, leveraging its several advantages with respect to sustainability and efficiency of the reactions. The last century also witnessed an

exponential growth in flow chemistry, technique that decreased the environmental impact of classical synthesis.[140] The principle of flow chemistry refers to chemical reactions occurring within a continuously flowing stream, enabling precise and efficient production of the final compound.[141,142] The advantages of this setup are multiple, including improved mass transfer, higher local substrate concentration, and/or the recycling of expensive metal catalysts.[143] Flow chemistry has gained widespread application on a larger scale, particularly in the production of high-value compounds, such as active pharmaceutical ingredients (APIs).[144] The application of continuous-flow techniques has undergone significant advancements since its initial use in 1932 when Whitmore and Karnatz reported the dehydration of diethylcarbinol into olefins with phosphoric acid using a flow reactor. [145] However, it was not until the early 2000s that this technology gained widespread acceptance due to the groundbreaking work of Ley and colleagues. In that same period, the group of Ley achieved the complete synthesis of (±)-oxomaritidine and grossamide through a fully automated, continuous-flow process.[146,147] Since then, flow chemistry has continued expanding also coupling with other strategies to increase the greenness of chemical process. A remarkable example is the development of solar photochemical reactors, which catalyse photoredox reactions leveraging on UV-vis light.[148] In this context, Nagornîi *et al*. (2024) integrated a continuous flow reactor with UV-A irradiation sources, facilitating the transference of hydrogen atoms generated *via* photocatalysis to a spectrum of alkanes, followed by their subsequent reaction with sulfur dioxide (SO_2) to yield the respective sulfinate derivatives, converting challenging substrates into valuable products.[149] [148]

While flow chemistry is by now a well assessed methodology, flow biocatalysis has only emerged recently. From research conducted on the Scopus database (Figure 1.18), it is clear that, despite the first appearance of flow bioreactor reported in the 80s, the first real practical application of biotransformation in continuous flow took place only in 1990, for the isomerisation of glucose-fructose, and only from 2002 the use of flow biocatalyses started to see a broader application. Examples of that year reported the use of immobilised hydrolytic enzymes for flow applications: CalB for the synthesis of a (*S*)-γ-fluoroleucine ethyl ester in a flow column reactor,[150] a β-glycosyl hydrolase from *Pyrococcus furiosus* for lactose hydrolysis,[151] and a CLEA of L-aminoacylase from the thermophilic organism, *Thermococcus litoralis,* for the enzymatic resolution of a racemic mixture of *N*-acetyl-DL-tryptophan.[152]
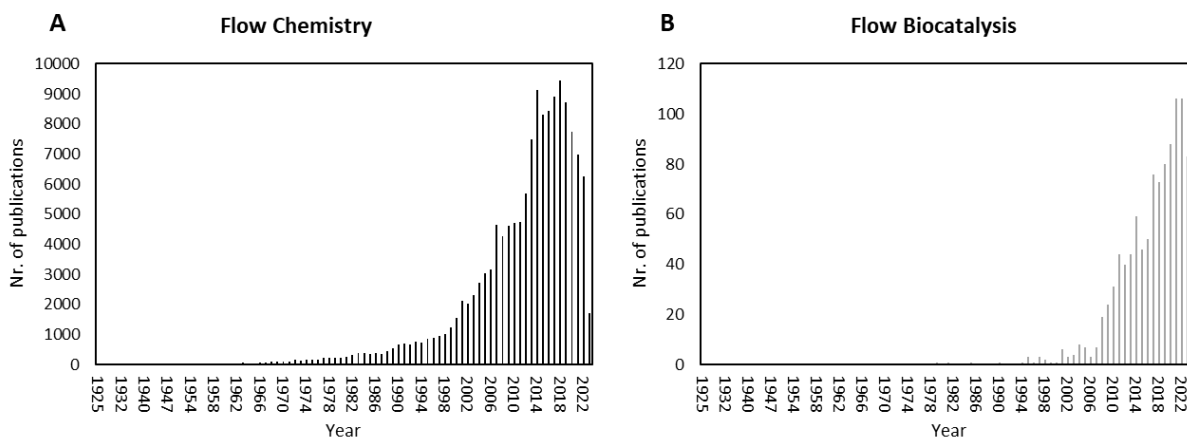
Figure 1.18 Publication trend in scientific articles related to A) Flow chemistry and B) Flow biocatalysis from 1925 to 2023 recorded on the Scopus database.

The benefits gained from this combination stem from the inherent advantages of enzyme utilization while harnessing the enhanced efficiency offered by flow chemistry. Continuous flow processes, unlike batch reactors, excel in both heat and mass transfer. They ensure the efficient mixing and uniform distribution of reactants, resulting in enhanced reaction rates and overall process efficiency. The reaction time is significantly reduced, and challenges, such as product/substrate inhibition, can be circumvented. Furthermore, the scalability of these reactions becomes safer and more straightforward, especially in cases where highly reactive or potentially explosive reagents, such as azide, are used.

A general flow biocatalytic setup is presented in Figure 1.19. Briefly, substrates 1 and 2 are introduced into the bioreactor at a controlled flow rate using two pumps (either peristaltic or high-performance syringe pumps). After passing this solution through the PBD—which can be loaded with various types of resins and enzymes—an inlet for an organic solvent is introduced for the in-line workup of the reaction. Downstream, a back pressure regulator (BPR) is commonly employed to maintain stable pressure levels. Finally, the sample is collected using a fraction collector, which can be thermostatted based on specific requirements.
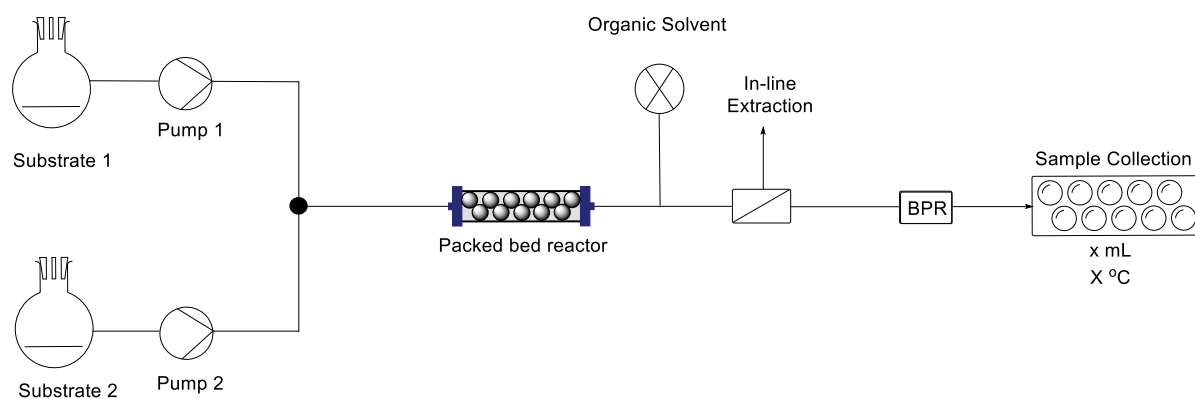
Figure 1.19 General scheme of flow system setup.

The transition from batch biotransformations to an automated flow system also confers a degree of flexibility. In particular, multiple packed bed reactors can be combined in series to better align with process requirements. In many cases, this technology has been applied with successful outcomes. For instance, in 2020, Rinaldi and collaborators developed a system for the in-flow continuous synthesis of nucleoside analogues through two enzymatic routes, reporting conversion yields of between 50 to 88%.[153] In 2022, Mutti and coworkers furthered this work by integrating 3D-printing technology with flow biocatalysis. Within this system, a thermostable amine dehydrogenase and formate dehydrogenase were co-entrapped in an agarose hydrogel and casted in a customised 3D printed mould. The resulting reactor enhanced the stability of the immobilised biocatalysts (over 120 hours) and space-time yield (7.4 g/L/day) in the reductive amination of benzaldehyde, demonstrating the improved efficiency of a tailored bioreactor design.[154] An example from our group reports a work focused on the synthesis of optically pure alcohols catalysed by a multi-step reaction originating from chiral amines.[155] In Figure 1.20, the process setup that was used is depicted: solutions containing the amine substrate, pyruvate, PLP, and NADH were fed into the first bioreactor. In the reactor, a reductive amination, catalysed by an immobilised transaminase (HeWT), yields the corresponding aldehyde (or ketone) and L-alanine. A second sequential enzymatic step, catalysed by a dehydrogenase (HLADH), reduces the prochiral carbonyl group to the corresponding alcohol. Notably, the first and second steps operate under distinct conditions (37 °C and 28 °C), proof of the tunability of the system. The final product, along with any unreacted aldehyde, is isolated from the solution through an initial extraction using

organic solvent (to separate cofactors and by-products), followed by an in-line purification process to selectively retain the unwanted aldehyde on a packed column of benzylamine polymer (QuadraPure™ QP-BZA polymer). Overall, this strategic approach enables the production of the desired alcohol in excellent yield (80% to >90%) and high enantiomeric purity (>99% ee). [155]
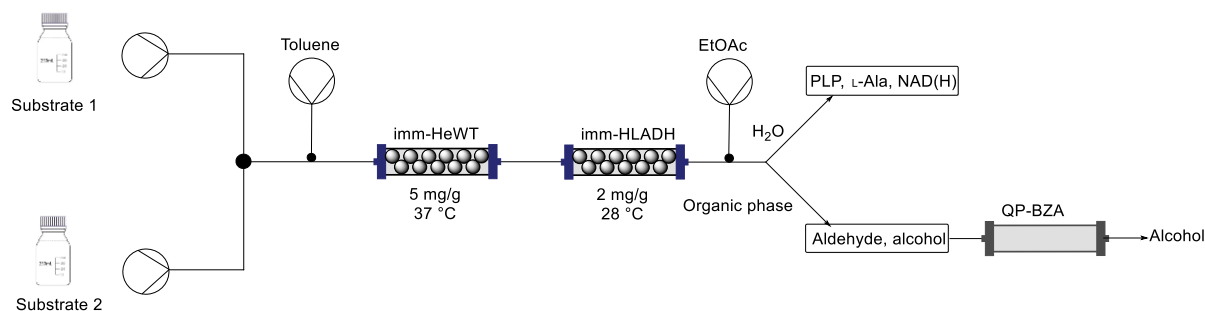
Figure 1.20 Scheme of the multi-step flow strategy for the production of chiral alcohols, incorporating an in-line purification system. Figure adapted from Paradisi *et al.*[155]

This methodology exemplifies how flow biocatalysis can play a pivotal role in transitioning toward greener synthesis of valuable molecules. Nowadays, flow biocatalysis has emerged as a fundamental sustainable approach, overcoming the limitations of classical batch methods. Over the past years, its applications have transitioned from laboratory-scale to industrial implementation and, despite the remaining challenges, its contribution to the green revolution is unequivocal.[156]

References

(1)   Nations, U. A/CONF.151/26/Vol.I: Rio Declaration on Environment and Development. **1992**.

(2)   *COP28   Declaration   On   Climate,   Relief,   Recovery   And   Peace*. https://www.cop28.com/en/cop28-declaration-on-climate-relief-recovery-and-peace (accessed 2024-02-18).

(3)   Anastas, P.; Eghbali, N. Green Chemistry: Principles and Practice. *Chem Soc Rev* **2009**, *39* (1), 301–312. https://doi.org/10.1039/B918763B.

(4)   Singh, R.; Kumar, M.; Mittal, A.; Mehta, P. K. Microbial Enzymes: Industrial Progress in 21st Century. *3 Biotech* **2016**, *6* (2), 1–15. https://doi.org/10.1007/S13205-016-0485-8/FIGURES/2.

(5)   Heckmann, C. M.; Paradisi, F. Looking Back: A Short History of the Discovery of Enzymes and How They Became Powerful Chemical Tools. *ChemCatChem* **2020**, *12* (24), 6082–6102. https://doi.org/10.1002/CCTC.202001107.

(6)   Bajwa, U. Effects of Glyceryl Monostearate and α-Amylase Supplements on Rheological and Breadmaking Properties of Medium Protein Wheat Flour. *J Sci Food Agric* **1990**, *52* (1), 97–105. https://doi.org/10.1002/JSFA.2740520111.

(7)   Uzuner, S. Enzyme Technology in Value Addition of Wine and Beer Processing. *Value-Addition in Beverages through Enzyme Technology* **2023**, 63–76. https://doi.org/10.1016/B978-0-323-85683-6.00003-X.

(8)   Buller, R.; Lutz, S.; Kazlauskas, R. J.; Snajdrova, R.; Moore, J. C.; Bornscheuer, U. T. From Nature to Industry: Harnessing Enzymes for Biocatalysis. *Science* **2023**, *382* (6673). https://doi.org/10.1126/SCIENCE.ADH8615.

(9)   Huffman, M. A.; Fryszkowska, A.; Alvizo, O.; Borra-Garske, M.; Campos, K. R.; Canada, K. A.; Devine, P. N.; Duan, D.; Forstater, J. H.; Grosser, S. T.; Halsey, H. M.; Hughes, G. J.; Jo, J.; Joyce, L. A.; Kolev, J. N.; Liang, J.; Maloney, K. M.; Mann, B. F.; Marshall, N. M.; McLaughlin, M.; Moore, J. C.; Murphy, G. S.; Nawrat, C. C.; Nazor, J.; Novick, S.; Patel, N. R.; Rodriguez-Granillo, A.; Robaire, S. A.; Sherer, E. C.; Truppo, M. D.; Whittaker, A. M.; Verma, D.; Xiao, L.; Xu, Y.; Yang,

H. Design of an in Vitro Biocatalytic Cascade for the Manufacture of Islatravir. *Science (1979)* **2019**, *366* (6470), 1255–1259. https://doi.org/10.1126/SCIENCE.AAY8484/SUPPL_FILE/AAY8484-HUFFMAN-SM.PDF.

(10) Bezsudnova, E. Yu.; Popov, V. O.; Boyko, K. M. Structural Insight into the Substrate Specificity of PLP Fold Type IV Transaminases. *Appl Microbiol Biotechnol* **2020**, *104* (6), 2343–2357. https://doi.org/10.1007/s00253-020-10369-6.

(11) Roura Padrosa, D.; Alaux, R.; Smith, P.; Dreveny, I.; López-Gallego, F.; Paradisi, F. Enhancing PLP-Binding Capacity of Class-III ω-Transaminase by Single Residue Substitution. *Front Bioeng Biotechnol* **2019**, *7*, 484947. https://doi.org/10.3389/FBIOE.2019.00282/BIBTEX.

(12) Ghislieri, D.; Turner, N. J. Biocatalytic Approaches to the Synthesis of Enantiomerically Pure Chiral Amines. *Top Catal* **2014**, *57* (5), 284–300. https://doi.org/10.1007/S11244-013-0184-1/SCHEMES/27.

(13) Process for Producing Optically Active Amino Compounds. WO/1997/015682, April 20, 1998.

(14) Savile, C. K.; Janey, J. M.; Mundorff, E. C.; Moore, J. C.; Tam, S.; Jarvis, W. R.; Colbeck, J. C.; Krebber, A.; Fleitz, F. J.; Brands, J.; Devine, P. N.; Huisman, G. W.; Hughes, G. J. Biocatalytic Asymmetric Synthesis of Chiral Amines from Ketones Applied to Sitagliptin Manufacture. *Science (1979)* **2010**, *329* (5989), 305–309. https://doi.org/10.1126/SCIENCE.1188934/SUPPL_FILE/SAVILE.SOM.PDF.

(15) Wang, C.; Tang, K.; Dai, Y.; Jia, H.; Li, Y.; Gao, Z.; Wu, B. Identification, Characterization, and Site-Specific Mutagenesis of a Thermostable ω-Transaminase from Chloroflexi Bacterium. *ACS Omega* **2021**, *6* (26), 17058–17070. https://doi.org/10.1021/ACSOMEGA.1C02164/ASSET/IMAGES/LARGE/AO1C02164_0010.JPEG.

(16) YAMADA, Y.; IWASAKI, A.; KIZAKI, N.; IKENAKA, Y.; OGURA, M.; HASEGAWA, J. Process for Producing Optically Active Amino Compounds, May 1, 1997.

(17) Mangion, I. K.; Sherry, B. D.; Yin, J.; Fleitz, F. J. Enantioselective Synthesis of a Dual Orexin Receptor Antagonist. *Org Lett* **2012**, *14* (13), 3458–3461. https://doi.org/10.1021/ol3014123.

(18) Simon, R. C.; Sattler, J. H.; Farnberger, J. E.; Fuchs, C. S.; Richter, N.; Zepeck, F.; Kroutil, W. Enzymatic Asymmetric Synthesis of the Silodosin Amine Intermediate. *Tetrahedron Asymmetry* **2014**, *25* (3), 284–288. https://doi.org/10.1016/J.TETASY.2013.12.012.

(19) Koszelewski, D.; Pressnitz, D.; Clay, D.; Kroutil, W. Deracemization of Mexiletine Biocatalyzed by Omega-Transaminases. *Org Lett* **2009**, *11* (21), 4810–4812. https://doi.org/10.1021/OL901834X.

(20) Liang, C.; Duan, X.; Shahab, M.; Zheng, G. Biocatalytic Synthesis of Chiral Five-Membered Carbasugars Intermediates Utilizing CV2025 ω-Transaminase from Chromobacterium Violaceum. *J Biosci Bioeng* **2023**, *135* (5), 369–374. https://doi.org/10.1016/J.JBIOSC.2023.02.009.

(21) Kaličanin, N.; Kovačević, G.; Spasojević, M.; Prodanović, O.; Jovanović-Šanta, S.; Škorić, D.; Opsenica, D.; Prodanović, R. Immobilization of ArRMut11 Omega-Transaminase for Increased Operational Stability and Reusability in the Synthesis of 3α-Amino-5α-Androstan-17β-Ol. *Process Biochemistry* **2022**, *121*, 674–680. https://doi.org/10.1016/J.PROCBIO.2022.08.016.

(22) Mathew, S.; Nadarajan, S. P.; Chung, T.; Park, H. H.; Yun, H. Biochemical Characterization of Thermostable ω-Transaminase from Sphaerobacter Thermophilus and Its Application for Producing Aromatic β- and γ-Amino Acids. *Enzyme Microb Technol* **2016**, *87–88*, 52–60. https://doi.org/10.1016/J.ENZMICTEC.2016.02.013.

(23) Fuchs, M.; Koszelewski, D.; Tauber, K.; Kroutil, W.; Faber, K. Chemoenzymatic Asymmetric Total Synthesis of (S)-Rivastigmine Using ω-Transaminases. *Chemical Communications* **2010**, *46* (30), 5500–5502. https://doi.org/10.1039/C0CC00585A.

(24) Koszelewski, D.; Pressnitz, D.; Clay, D.; Kroutil, W. Deracemization of Mexiletine Biocatalyzed by ω-Transaminases. *Org Lett* **2009**, *11* (21), 4810–4812. https://doi.org/10.1021/ol901834x.

(25) Guidi, B.; Planchestainer, M.; Contente, M. L.; Laurenzi, T.; Eberini, I.; Gourlay, L. J.; Romano, D.; Paradisi, F.; Molinari, F. Strategic Single Point Mutation Yields a Solvent- and Salt-Stable Transaminase from Virgibacillus Sp. in Soluble Form. *Scientific Reports 2018 8:1* **2018**, *8* (1), 1–11. https://doi.org/10.1038/s41598-018-34434-3.

(26) Roura Padrosa, D.; Alaux, R.; Smith, P.; Dreveny, I.; López-Gallego, F.; Paradisi, F. Enhancing PLP-Binding Capacity of Class-III ω-Transaminase by Single Residue Substitution. *Front Bioeng Biotechnol* **2019**, *7*, 484947. https://doi.org/10.3389/FBIOE.2019.00282/BIBTEX.

(27) Heckmann, C. M.; Paradisi, F. GPhos Ligand Enables Production of Chiral N-Arylamines in a Telescoped Transaminase-Buchwald-Hartwig Amination Cascade in the Presence of Excess Amine Donor. *Chemistry – A European Journal* **2021**, *27* (67), 16616–16620. https://doi.org/10.1002/CHEM.202103472.

(28) Benítez-Mateos, A. I.; Contente, M. L.; Velasco-Lozano, S.; Paradisi, F.; López-Gallego, F. Self-Sufficient Flow-Biocatalysis by Coimmobilization of Pyridoxal 5'-Phosphate and ω-Transaminases onto Porous Carriers. *ACS Sustain Chem Eng* **2018**, *6* (10), 13151–13159. https://doi.org/10.1021/acssuschemeng.8b02672.

(29) Hegarty, E.; Paradisi, F. Implementation of Biocatalysis in Continuous Flow for the Synthesis of Small Cyclic Amines. *Chimia (Aarau)* **2020**, *74* (11), 890. https://doi.org/10.2533/chimia.2020.890.

(30) Heckmann, C. M.; Dominguez, B.; Paradisi, F. Enantio-Complementary Continuous-Flow Synthesis of 2-Aminobutane Using Covalently Immobilized Transaminases. **2021**. https://doi.org/10.1021/acssuschemeng.0c09075.

(31) Cerioli, L.; Planchestainer, M.; Cassidy, J.; Tessaro, D.; Paradisi, F. Characterization of a Novel Amine Transaminase from Halomonas Elongata. *J Mol Catal B Enzym* **2015**, *120*, 141–150. https://doi.org/10.1016/j.molcatb.2015.07.009.

(32) Little, A. S.; Younker, I. T.; Schechter, M. S.; Bernardino, P. N.; Méheust, R.; Stemczynski, J.; Scorza, K.; Mullowney, M. W.; Sharan, D.; Waligurski, E.; Smith, R.; Ramanswamy, R.; Leiter, W.; Moran, D.; McMillin, M.; Odenwald, M. A.; Iavarone, A. T.; Sidebottom, A. M.; Sundararajan, A.; Pamer, E. G.; Eren, A. M.; Light, S. H. Dietary- and Host-Derived Metabolites Are Used by Diverse Gut Bacteria for Anaerobic Respiration. *Nature Microbiology 2024 9:1* **2024**, *9* (1), 55–69. https://doi.org/10.1038/s41564-023-01560-2.

(33) Younus, H. Oxidoreductases: Overview and Practical Applications. *Biocatalysis: Enzymatic Basics and Applications* **2019**, 39–55. https://doi.org/10.1007/978-3-030-25023-2_3/TABLES/1.

(34)   Labat, E.; Morel, M. H.; Rouau, X. Effects of Laccase and Ferulic Acid on Wheat Flour Doughs. *Cereal Chem* **2000**, *77* (6), 823–828. https://doi.org/10.1094/CCHEM.2000.77.6.823.

(35)   Tanriöven, D.; Ekşi, A. Phenolic Compounds in Pear Juice from Different Cultivars. *Food Chem* **2005**, *93* (1), 89–93. https://doi.org/10.1016/J.FOODCHEM.2004.09.009.

(36)   Daußmann, T.; Hennemann, H. -G.; Rosen, T. C.; Dünkelmann, P. Enzymatische Technologien Zur Synthese Chiraler Alkohol-Derivate. *Chemie Ingenieur Technik* **2006**, *78* (3), 249–255. https://doi.org/10.1002/cite.200600004.

(37)   Patrick, G. L. Miscellaneous Targets. *Antimalarial Agents: Design and Mechanism of Action* **2020**, 547–594. https://doi.org/10.1016/B978-0-08-101210-9.00016-0.

(38)   Munro, A. W.; Taylor, P.; Walkinshaw, M. D. Structures of Redox Enzymes. *Curr Opin Biotechnol* **2000**, *11* (4), 369–376. https://doi.org/10.1016/S0958-1669(00)00112-9.

(39)   May, S. W.; Padgette, S. R. Oxidoreductase Enzymes in Biotechnology: Current Status and Future Potential. *Nat Biotechnol* **1983**, *1* (8), 677–686. https://doi.org/10.1038/nbt1083-677.

(40)   Huber, T.; Schneider, L.; Präg, A.; Gerhardt, S.; Einsle, O.; Müller, M. Direct Reductive Amination of Ketones: Structure and Activity of S-Selective Imine Reductases from Streptomyces. *ChemCatChem* **2014**, *6* (8), 2248–2252. https://doi.org/10.1002/CCTC.201402218.

(41)   France, S. P.; Hussain, S.; Hill, A. M.; Hepworth, L. J.; Howard, R. M.; Mulholland, K. R.; Flitsch, S. L.; Turner, N. J. One Pot Cascade Synthesis of Mono- and Di-Substituted Piperidines and Pyrrolidines Using Carboxylic Acid Reductase (CAR), ω-Transaminase (ω-TA) and Imine Reductase (IRED) Biocatalysts. *ACS Catal* **2016**, *6* (6), 3753–3759. https://doi.org/10.1021/ACSCATAL.6B00855.

(42)   Gilio, A. K.; Thorpe, T. W.; Turner, N.; Grogan, G. Reductive Aminations by Imine Reductases: From Milligrams to Tons. *Chem Sci* **2022**, *13* (17), 4697. https://doi.org/10.1039/D2SC00124A.

(43)   Cigan, E.; Eggbauer, B.; Schrittwieser, J. H.; Kroutil, W. The Role of Biocatalysis in the Asymmetric Synthesis of Alkaloids – an Update. *RSC Adv* **2021**, *11* (45), 28223. https://doi.org/10.1039/D1RA04181A.

(44) Cárdenas-Fernández, M.; Roddan, R.; Carter, E. M.; Hailes, H. C.; Ward, J. M. The Discovery of Imine Reductases and Their Utilisation for the Synthesis of Tetrahydroisoquinolines. *ChemCatChem* **2023**, *15* (3). https://doi.org/10.1002/CCTC.202201126.

(45) Mordhorst, S.; Andexer, J. N. Round, Round We Go – Strategies for Enzymatic Cofactor Regeneration. *Nat Prod Rep* **2020**, *37* (10), 1316–1333. https://doi.org/10.1039/D0NP00004C.

(46) García-Junceda, E.; Lavandera, I.; Rother, D.; Schrittwieser, J. H. (Chemo)Enzymatic Cascades-Nature's Synthetic Strategy Transferred to the Laboratory. *J Mol Catal B Enzym* **2015**, *114*, 1–6. https://doi.org/10.1016/j.molcatb.2014.12.007.

(47) Liao, L.; Zhang, Y.; Wang, Y.; Fu, Y.; Zhang, A.; Qiu, R.; Yang, S.; Fang, B. Construction and Characterization of a Novel Glucose Dehydrogenase-Leucine Dehydrogenase Fusion Enzyme for the Biosynthesis of l-Tert-Leucine. *Microb Cell Fact* **2021**, *20* (1), 1–12. https://doi.org/10.1186/S12934-020-01501-2/FIGURES/7.

(48) Rocha, R. A.; North, A. J.; Speight, R. E.; Williams, C. C.; Scott, C. Cofactor and Process Engineering for Nicotinamide Recycling and Retention in Intensified Biocatalysis. *Catalysts 2022, Vol. 12, Page 1454* **2022**, *12* (11), 1454. https://doi.org/10.3390/CATAL12111454.

(49) Baker, J. W.; Happold, F. C.; Walker, N. The Tryptophanase-Tryptophan Reaction. *Biochemical Journal* **1946**, *40* (3), 420–426. https://doi.org/10.1042/bj0400420.

(50) Barik, S. The Uniqueness of Tryptophan in Biology: Properties, Metabolism, Interactions and Localization in Proteins. *International Journal of Molecular Sciences 2020, Vol. 21, Page 8776* **2020**, *21* (22), 8776. https://doi.org/10.3390/IJMS21228776.

(51) Agus, A.; Planchais, J.; Sokol, H. Gut Microbiota Regulation of Tryptophan Metabolism in Health and Disease. *Cell Host Microbe* **2018**, *23* (6), 716–724. https://doi.org/10.1016/j.chom.2018.05.003.

(52) Roager, H. M.; Licht, T. R. Microbial Tryptophan Catabolites in Health and Disease. *Nature Communications 2018 9:1* **2018**, *9* (1), 1–10. https://doi.org/10.1038/s41467-018-05470-4.

(53) Phillips, R. S.; Demidkina, T. V.; Faleev, N. G. Structure and Mechanism of Tryptophan Indole-Lyase and Tyrosine Phenol-Lyase. *Biochim Biophys Acta Proteins Proteom* **2003**, *1647* (1–2), 167–172. https://doi.org/10.1016/S1570-9639(03)00089-X.

(54) Phillips, R. S.; Buisman, A. A.; Choi, S.; Hussaini, A.; Wood, Z. A. The Crystal Structure of *Proteus Vulgaris* Tryptophan Indole-Lyase Complexed with Oxindolyl- <scp>L</Scp> -Alanine: Implications for the Reaction Mechanism. *Acta Crystallogr D Struct Biol* **2018**, *74* (8), 748–759. https://doi.org/10.1107/S2059798318003352.

(55) Snell, E. E. Tryptophanase: Structure, Catalytic Activities, and Mechanism of Action; 1975; pp 287–333. https://doi.org/10.1002/9780470122877.ch6.

(56) Phillips, R. S.; Buisman, A. A.; Choi, S.; Hussaini, A.; Wood, Z. A. The Crystal Structure of *Proteus Vulgaris* Tryptophan Indole-Lyase Complexed with Oxindolyl- <scp>L</Scp> -Alanine: Implications for the Reaction Mechanism. *Acta Crystallogr D Struct Biol* **2018**, *74* (8), 748–759. https://doi.org/10.1107/S2059798318003352.

(57) Watanabe, T.; Snell, E. E. Reversibility of the Tryptophanase Reaction: Synthesis of Tryptophan from Indole, Pyruvate, and Ammonia. *Proceedings of the National Academy of Sciences* **1972**, *69* (5), 1086–1090. https://doi.org/10.1073/pnas.69.5.1086.

(58) Li, G.; Young, K. D. Indole Production by the Tryptophanase TnaA in Escherichia Coli Is Determined by the Amount of Exogenous Tryptophan. *Microbiology (Reading)* **2013**, *159* (Pt 2), 402–410. https://doi.org/10.1099/MIC.0.064139-0.

(59) Watkins-Dulaney, E.; Straathof, S.; Arnold, F. Tryptophan Synthase: Biocatalyst Extraordinaire. *Chembiochem* **2021**, *22* (1), 5–16. https://doi.org/10.1002/CBIC.202000379.

(60) Veldmann, K. H.; Dachwitz, S.; Risse, J. M.; Lee, J.-H.; Sewald, N.; Wendisch, V. F. Bromination of L-Tryptophan in a Fermentative Process With Corynebacterium Glutamicum. *Front Bioeng Biotechnol* **2019**, *7*. https://doi.org/10.3389/fbioe.2019.00219.

(61) Raveendran, S.; Parameswaran, B.; Ummalyma, S. B.; Abraham, A.; Mathew, A. K.; Madhavan, A.; Rebello, S.; Pandey, A. Applications of Microbial Enzymes in Food Industry. *Food Technol Biotechnol* **2018**, *56* (1). https://doi.org/10.17113/ftb.56.01.18.5491.

(62) Lee, J.; Kim, J.; Song, J. E.; Song, W.-S.; Kim, E.-J.; Kim, Y.-G.; Jeong, H.-J.; Kim, H. R.; Choi, K.-Y.; Kim, B.-G. Production of Tyrian Purple Indigoid Dye from Tryptophan in Escherichia Coli. *Nat Chem Biol* **2021**, *17* (1), 104–112. https://doi.org/10.1038/s41589-020-00684-4.

(63) Xiao, S.; Wang, Z.; Wang, B.; Hou, B.; Cheng, J.; Bai, T.; Zhang, Y.; Wang, W.; Yan, L.; Zhang, J. Expanding the Application of Tryptophan: Industrial Biomanufacturing of Tryptophan Derivatives. *Front Microbiol* **2023**, *14*, 1099098. https://doi.org/10.3389/FMICB.2023.1099098/BIBTEX.

(64) Xiao, S.; Wang, Z.; Wang, B.; Hou, B.; Cheng, J.; Bai, T.; Zhang, Y.; Wang, W.; Yan, L.; Zhang, J. Expanding the Application of Tryptophan: Industrial Biomanufacturing of Tryptophan Derivatives. *Front Microbiol* **2023**, *14*. https://doi.org/10.3389/fmicb.2023.1099098.

(65) Ferris, J. P.; Miller, N. C. The Decarboxylation of β-Keto Acids. II. An Investigation of the Bredt Rule in Bicyclo[3.2.1]Octane Systems [1,2]. *J Am Chem Soc* **1966**, *88* (15), 3522–3527. https://doi.org/10.1021/ja00967a011.

(66) Sutiono, S.; Carsten, J.; Sieber, V. Structure-Guided Engineering of A-Keto Acid Decarboxylase for the Production of Higher Alcohols at Elevated Temperature. *ChemSusChem* **2018**, *11* (18), 3335–3344. https://doi.org/10.1002/cssc.201800944.

(67) Burkhard, P.; Dominici, P.; Borri-Voltattorni, C.; Jansonius, J. N.; Malashkevich, V. N. Structural Insight into Parkinson's Disease Treatment from Drug-Inhibited DOPA Decarboxylase. *Nat Struct Biol* **2001**, *8* (11), 963–967. https://doi.org/10.1038/nsb1101-963.

(68) Appleby, T. C.; Kinsland, C.; Begley, T. P.; Ealick, S. E. The Crystal Structure and Mechanism of Orotidine 5'-Monophosphate Decarboxylase. *Proceedings of the National Academy of Sciences* **2000**, *97* (5), 2005–2010. https://doi.org/10.1073/pnas.259441296.

(69) Benning, M. M.; Haller, T.; Gerlt, J. A.; Holden, H. M. New Reactions in the Crotonase Superfamily: Structure of Methylmalonyl CoA Decarboxylase from *Escherichia Coli* ⸳. *Biochemistry* **2000**, *39* (16), 4630–4639. https://doi.org/10.1021/bi9928896.

(70) Blaesse, M. Crystal Structure of the Peptidyl-Cysteine Decarboxylase EpiD Complexed with a Pentapeptide Substrate. *EMBO J* **2000**, *19* (23), 6299–6310. https://doi.org/10.1093/emboj/19.23.6299.

(71) Selmer, T.; Andrei, P. I. P -*Hydroxyphenylacetate Decarboxylase from* Clostridium Difficile. *Eur J Biochem* **2001**, *268* (5), 1363–1372. https://doi.org/10.1046/j.1432-1327.2001.02001.x.

(72) Li, Z.; Chen, R.; Wen, Y.; Liu, H.; Chen, Y.; Wu, X.; Yang, Y.; Wu, X.; Zhou, Y.; Liu, J. Comprehensive Analysis of the UDP-Glucuronate Decarboxylase (UXS) Gene Family in Tobacco and Functional Characterization of NtUXS16 in Golgi Apparatus in Arabidopsis. *BMC Plant Biol* **2023**, *23* (1), 551. https://doi.org/10.1186/s12870-023-04575-3.

(73) Wen, Y.; Wang, J.; Zhang, Q.; Chen, Y.; Bao, X. The Genetic and Clinical Characteristics of Aromatic L-Amino Acid Decarboxylase Deficiency in Mainland China. *J Hum Genet* **2020**, *65* (9), 759–769. https://doi.org/10.1038/s10038-020-0770-6.

(74) Pei, W.; Zhang, J.; Deng, S.; Tigu, F.; Li, Y.; Li, Q.; Cai, Z.; Li, Y. Molecular Engineering of L-Aspartate-α-Decarboxylase for Improved Activity and Catalytic Stability. *Appl Microbiol Biotechnol* **2017**, *101* (15), 6015–6021. https://doi.org/10.1007/s00253-017-8337-y.

(75) Fries, A.; Mazzaferro, L. S.; Grüning, B.; Bisel, P.; Stibal, K.; Buchholz, P. C. F.; Pleiss, J.; Sprenger, G. A.; Müller, M. Alteration of the Route to Menaquinone towards Isochorismate-Derived Metabolites. *ChemBioChem* **2019**, *20* (13), 1672–1677. https://doi.org/10.1002/cbic.201900050.

(76) Conter, C.; Oppici, E.; Dindo, M.; Rossi, L.; Magnani, M.; Cellini, B. Biochemical Properties and Oxalate-degrading Activity of Oxalate Decarboxylase from Bacillus Subtilis at Neutral PH. *IUBMB Life* **2019**, *71* (7), 917–927. https://doi.org/10.1002/iub.2027.

(77) Tomonaga, S.; Matsumoto, M.; Furuse, M. β-Alanine Enhances Brain and Muscle Carnosine Levels in Broiler Chicks. *Journal of Poultry Science* **2012**, *49* (4), 308–312. https://doi.org/10.2141/JPSA.0110165.

(78) Wang, L.; Mao, Y.; Wang, Z.; Ma, H.; Chen, T. Advances in Biotechnological Production of β-Alanine. *World J Microbiol Biotechnol* **2021**, *37* (5), 1–11. https://doi.org/10.1007/S11274-021-03042-1/TABLES/1.

(79) Hoffman, J. R.; Stout, J. R.; Harris, R. C.; Moran, D. S. β-Alanine Supplementation and Military Performance. *Amino Acids* **2015**, *47* (12), 2463–2474. https://doi.org/10.1007/S00726-015-2051-9/TABLES/1.

(80) Song, C. W.; Lee, J.; Ko, Y. S.; Lee, S. Y. Metabolic Engineering of Escherichia Coli for the Production of 3-Aminopropionic Acid. *Metab Eng* **2015**, *30*, 121–129. https://doi.org/10.1016/J.YMBEN.2015.05.005.

(81)   Bellinger, P. M. β-Alanine Supplementation for Athletic Performance: An Update. *J Strength Cond Res* **2014**, *28* (6), 1751–1770. https://doi.org/10.1519/JSC.0000000000000327.

(82)   Artioli, G. G.; Franchini, E.; Iglesias, R. T.; Gualano, B.; Kashiwagura, D. B.; Fuchs, M.; Solis, M. Y.; Takesian, M.; Lancha, A. H. Role of B-Alanine Supplementation on Muscle Carnosine and Exercise Performance. *Med Sci Sports Exerc* **2010**, *42* (5), 1162–1173. https://doi.org/10.1249/01.mss.0000384497.49519.49.

(83)   Hyun, T. K.; Eom, S. H.; Jeun, Y. C.; Han, S. H.; Kim, J.-S. Identification of Glutamate Decarboxylases as a γ-Aminobutyric Acid (GABA) Biosynthetic Enzyme in Soybean. *Ind Crops Prod* **2013**, *49*, 864–870. https://doi.org/10.1016/j.indcrop.2013.06.046.

(84)   Xi, Y.; Ye, L.; Yu, H. Enhanced Thermal and Alkaline Stability of L-Lysine Decarboxylase CadA by Combining Directed Evolution and Computation-Guided Virtual Screening. *Bioresour Bioprocess* **2022**, *9* (1), 24. https://doi.org/10.1186/s40643-022-00510-w.

(85)   Ohde, D.; Thomas, B.; Bubenheim, P.; Liese, A. Enhanced CO2 Fixation in the Biocatalytic Carboxylation of Resorcinol: Utilization of Amines for Amine Scrubbing and in Situ Product Precipitation. *Biochem Eng J* **2021**, *166*, 107825. https://doi.org/10.1016/J.BEJ.2020.107825.

(86)   Han, S. W.; Shin, J. S. Aromatic L-Amino Acid Decarboxylases: Mechanistic Features and Microbial Applications. *Applied Microbiology and Biotechnology 2022 106:12* **2022**, *106* (12), 4445–4458. https://doi.org/10.1007/S00253-022-12028-4.

(87)   Yu, X. H.; Gou, J. Y.; Liu, C. J. BAHD Superfamily of Acyl-CoA Dependent Acyltransferases in Populus and Arabidopsis: Bioinformatics and Gene Expression. *Plant Mol Biol* **2009**, *70* (4), 421–442. https://doi.org/10.1007/S11103-009-9482-1.

(88)   Mugford, S. T.; Milkowski, C. Serine Carboxypeptidase-like Acyltransferases from Plants. *Methods Enzymol* **2012**, *516*, 279–297. https://doi.org/10.1016/B978-0-12-394291-3.00006-X.

(89)   Ziaullah; Bhullar, K. S.; Warnakulasuriya, S. N.; Rupasinghe, H. P. V. Biocatalytic Synthesis, Structural Elucidation, Antioxidant Capacity and Tyrosinase Inhibition Activity of Long Chain Fatty Acid Acylated Derivatives of Phloridzin and Isoquercitrin. *Bioorg Med Chem* **2013**, *21* (3), 684–692. https://doi.org/10.1016/J.BMC.2012.11.034.

(90) Céliz, G.; Martearena, M. R.; Scaroni, E.; Daz, M. Kinetic Study of the Alkyl Flavonoid Ester Prunin 6"-O-Laurate Synthesis in Acetone Catalysed by Immobilised Candida Antarctica Lipase B. *Biochem Eng J* **2012**, *69*, 69–74. https://doi.org/10.1016/J.BEJ.2012.08.008.

(91) Staudt, A.; Brack, Y.; Jr, I. I.; Leal, I. C. R. Biocatalytic Synthesis of Monoterpene Esters − A Review Study on the Phylogenetic Evolution of Biocatalysts. *Molecular Catalysis* **2022**, *528*, 112464. https://doi.org/10.1016/J.MCAT.2022.112464.

(92) Vanholme, R.; Sundin, L.; Seetso, K. C.; Kim, H.; Liu, X.; Li, J.; De Meester, B.; Hoengenaert, L.; Goeminne, G.; Morreel, K.; Haustraete, J.; Tsai, H. H.; Schmidt, W.; Vanholme, B.; Ralph, J.; Boerjan, W. COSY Catalyses Trans–Cis Isomerization and Lactonization in the Biosynthesis of Coumarins. *Nature Plants 2019 5:10* **2019**, *5* (10), 1066–1075. https://doi.org/10.1038/s41477-019-0510-0.

(93) Yang, M.; Fan, Y.; Wu, P. C.; Chu, Y. D.; Shen, P. L.; Xue, S.; Chi, Z. Y. An Extended Approach to Quantify Triacylglycerol in Microalgae by Characteristic Fatty Acids. *Front Plant Sci* **2017**, *8*, 312102. https://doi.org/10.3389/FPLS.2017.01949/BIBTEX.

(94) Yu, R.; Chang, L.; Cao, J.; Yang, B.; Chen, H.; Chen, W. Applications of Diacylglycerol Acyltransferase for Triacylglycerol Production in Mortierella Alpina. *Journal of Fungi* **2023**, *9* (2). https://doi.org/10.3390/JOF9020219/S1.

(95) Garlapati, V. K.; Kant, R.; Kumari, A.; Mahapatra, P.; Das, P.; Banerjee, R. Lipase Mediated Transesterification of Simarouba Glauca Oil: A New Feedstock for Biodiesel Production. *Sustainable Chemical Processes 2013 1:1* **2013**, *1* (1), 1–6. https://doi.org/10.1186/2043-7129-1-11.

(96) Subileau, M.; Jan, A. H.; Dubreucq, E. Lipases/Acyltransferases for Lipid Modification in Aqueous Media. *Lipid Modification by Enzymes and Engineered Microbes* **2018**, 45–68. https://doi.org/10.1016/B978-0-12-813167-1.00003-7.

(97) Bayout, I.; Bouzemi, N.; Guo, N.; Mao, X.; Serra, S.; Riva, S.; Secundo, F. Natural Flavor Ester Synthesis Catalyzed by Lipases. *Flavour Fragr J* **2020**, *35* (2), 209–218. https://doi.org/10.1002/FFJ.3554.

(98) Perdomo, I. C.; Gianolio, S.; Pinto, A.; Romano, D.; Contente, M. L.; Paradisi, F.; Molinari, F. Efficient Enzymatic Preparation of Flavor Esters in Water. **2019**. https://doi.org/10.1021/acs.jafc.9b01790.

(99) Nelson, J. M.; Griffin, E. G. Adsorption of Invertase. *J Am Chem Soc* **1916**, *38* (5), 1109–1115. https://doi.org/10.1021/ja02262a018.

(100) Grubhofer, N.; Schleit, L. Protein Coupling with Diazotized Polyaminostyrene. *Hoppe Seylers Z Physiol Chem* **1954**, *297* (2), 108–112.

(101) Quiocho, F. A.; Richards, F. M. The Enzymic Behavior of Carboxypeptidase-A in the Solid State *. *Biochemistry* **1966**, *5* (12), 4062–4076. https://doi.org/10.1021/bi00876a041.

(102) Pennington, S. N.; Brown, H. D.; Patel, A. B.; Chattopadhyay, S. K. Silastic Entrapment of Glucose Oxidase–Peroxidase and Acetylcholine Esterase. *J Biomed Mater Res* **1968**, *2* (4), 443–446. https://doi.org/10.1002/jbm.820020404.

(103) Mosbach, K.; Mosbach, R.; Wentrup, C.; Møller, J.; Sjöberg, B.; Bunnenberg, E.; Djerassi, C.; Records, R. Entrapment of Enzymes and Microorganisms in Synthetic Cross-Linked Polymers and Their Application in Column Techniques. *Acta Chem Scand* **1966**, *20*, 2807–2810. https://doi.org/10.3891/acta.chem.scand.20-2807.

(104) Hicks, G. P.; Updike, S. J. The Preparation and Characterization of Lyophilized Polyacrylamide Enzyme Gels for Chemical Analysis. *Anal Chem* **1966**, *38* (6), 726–730. https://doi.org/10.1021/ac60238a014.

(105) Tosa, T.; Mori, T.; Fuse, N.; Chibata, I. Studies on Continuous Enzyme Reactions. IV. Preparation of a DEAE-sephadex–Aminoacylase Column and Continuous Optical Resolution of Acyl-<scp>DL</Scp> -amino Acids. *Biotechnol Bioeng* **1967**, *9* (4), 603–615. https://doi.org/10.1002/bit.260090413.

(106) Fritz Dr Hueper. Wasserloesliche, Kovalent an Polymere Traeger Gebundene Penicillinacylase, Verfahren Zu Ihrer Herstellung, Sowie Ihre Verwendung Zur Herstellung von 6-Aminopenicillansaeure. **1973**.

(107) Attique, S. A.; Qurat ul ain; Hussain, N.; Bilal, M.; Iqbal, H. M. N. Enzyme Immobilization Approaches. *Biocatalyst Immobilization* **2023**, 37–54. https://doi.org/10.1016/B978-0-323-91317-1.00007-4.

(108) Velasco-Lozano, S.; Benítez-Mateos, A. I.; López-Gallego, F. Co-immobilized Phosphorylated Cofactors and Enzymes as Self-Sufficient Heterogeneous Biocatalysts for Chemical Processes. *Angew Chem Int Ed Engl* **2017**, *56* (3), 771. https://doi.org/10.1002/ANIE.201609758.

(109) Benítez-Mateos, A. I.; Paradisi, F. Advanced Enzyme Immobilization Technologies: An Eco-Friendly Support, a Polymer-Stabilizing Immobilization Strategy, and an Improved Cofactor Co-Immobilization Technique. *Methods in Molecular Biology* **2022**, *2397*, 263–276. https://doi.org/10.1007/978-1-0716-1826-4_14/TABLES/1.

(110) Aleku, G. A.; Man, H.; France, S. P.; Leipold, F.; Hussain, S.; Toca-Gonzalez, L.; Marchington, R.; Hart, S.; Turkenburg, J. P.; Grogan, G.; Turner, N. J. Stereoselectivity and Structural Characterization of an Imine Reductase (IRED) from Amycolatopsis Orientalis. *ACS Catal* **2016**, *6* (6), 3880–3889. https://doi.org/10.1021/ACSCATAL.6B00782/SUPPL_FILE/CS6B00782_SI_001.PDF.

(111) Rodrigues, R. C.; Ortiz, C.; Berenguer-Murcia, Á.; Torres, R.; Fernández-Lafuente, R. Modifying Enzyme Activity and Selectivity by Immobilization. *Chem. Soc. Rev.* **2013**, *42* (15), 6290–6307. https://doi.org/10.1039/C2CS35231A.

(112) Rodrigues, R. C.; Ortiz, C.; Berenguer-Murcia, Á.; Torres, R.; Fernández-Lafuente, R. Modifying Enzyme Activity and Selectivity by Immobilization. *Chem. Soc. Rev.* **2013**, *42* (15), 6290–6307. https://doi.org/10.1039/C2CS35231A.

(113) Illanes, A.; Wilson, L. Parameters for the Evaluation of Immobilized Enzymes Under Process Conditions; 2020; pp 65–81. https://doi.org/10.1007/978-1-0716-0215-7_3.

(114) Sheldon, R. A.; van Pelt, S. Enzyme Immobilisation in Biocatalysis: Why, What and How. *Chem. Soc. Rev.* **2013**, *42* (15), 6223–6235. https://doi.org/10.1039/C3CS60075K.

(115) Sampaio, C. S.; Angelotti, J. A. F.; Fernandez-Lafuente, R.; Hirata, D. B. Lipase Immobilization via Cross-Linked Enzyme Aggregates: Problems and Prospects – A Review. *Int J Biol Macromol* **2022**, *215*, 434–449. https://doi.org/10.1016/J.IJBIOMAC.2022.06.139.

(116) Chibata, I.; Tosa, T.; Sato, T. Biocatalysis: Immobilized Cells and Enzymes. *Journal of Molecular Catalysis* **1986**, *37* (1), 1–24. https://doi.org/10.1016/0304-5102(86)85134-3.

(117) López-Gallego, F.; Fernandez-Lorente, G.; Rocha-Martin, J.; Bolivar, J. M.; Mateo, C.; Guisan, J. M. Stabilization of Enzymes by Multipoint Covalent Immobilization on Supports Activated with Glyoxyl Groups. *Methods in Molecular Biology 1051*. https://doi.org/10.1007/978-1-62703-550-7_5.

(118) Fernández-Lafuente, R.; Rodríguez, V.; Mateo, C.; Penzol, G.; Hernández-Justiz, O.; Irazoqui, G.; Villarino, A.; Ovsejevi, K.; Batista, F.; Guisán, J. M. Stabilization of Multimeric Enzymes via Immobilization and Post-Immobilization Techniques. *J Mol Catal B Enzym* **1999**, *7* (1–4), 181–189. https://doi.org/10.1016/S1381-1177(99)00028-4.

(119) Zucca, P.; Fernandez-Lafuente, R.; Sanjust, E. Agarose and Its Derivatives as Supports for Enzyme Immobilization. **2016**. https://doi.org/10.3390/molecules21111577.

(120) Mohamad, N. R.; Marzuki, N. H. C.; Buang, N. A.; Huyop, F.; Wahab, R. A. An Overview of Technologies for Immobilization of Enzymes and Surface Analysis Techniques for Immobilized Enzymes. *Biotechnol Biotechnol Equip* **2015**, *29* (2), 205. https://doi.org/10.1080/13102818.2015.1008192.

(121) Lee, K. Y.; Mooney, D. J. Alginate: Properties and Biomedical Applications. *Prog Polym Sci* **2012**, *37* (1), 106. https://doi.org/10.1016/J.PROGPOLYMSCI.2011.06.003.

(122) Weng, Y.; Yang, G.; Li, Y.; Xu, L.; Chen, X.; Song, H.; Zhao, C.-X. Alginate-Based Materials for Enzyme Encapsulation. *Adv Colloid Interface Sci* **2023**, *318*, 102957. https://doi.org/10.1016/j.cis.2023.102957.

(123) Bobone, S.; Miele, E.; Cerroni, B.; Roversi, D.; Bocedi, A.; Nicolai, E.; Di Venere, A.; Placidi, E.; Ricci, G.; Rosato, N.; Stella, L. Liposome-Templated Hydrogel Nanoparticles as Vehicles for Enzyme-Based Therapies. *Langmuir* **2015**, *31* (27), 7572–7580. https://doi.org/10.1021/acs.langmuir.5b01442.

(124) Lindhoud, S.; de Vries, R.; Norde, W.; Stuart, M. A. C. Structure and Stability of Complex Coacervate Core Micelles with Lysozyme. *Biomacromolecules* **2007**, *8* (7), 2219–2227. https://doi.org/10.1021/bm0700688.

(125) Markwalter, C. E.; Pagels, R. F.; Hejazi, A. N.; Gordon, A. G. R.; Thompson, A. L.; Prud'homme, R. K. Polymeric Nanocarrier Formulations of Biologics Using Inverse Flash NanoPrecipitation. *AAPS J* **2020**, *22* (2), 18. https://doi.org/10.1208/s12248-019-0405-z.

(126) Jafari, S.; Jafari, S. M.; Ebrahimi, M.; Kijpatanasilp, I.; Assatarakul, K. A Decade Overview and Prospect of Spray Drying Encapsulation of Bioactives from Fruit Products: Characterization, Food Application and in Vitro Gastrointestinal Digestion. *Food Hydrocoll* **2023**, *134*, 108068. https://doi.org/10.1016/J.FOODHYD.2022.108068.

(127) Wang, B.; Akanbi, T. O.; Agyei, D.; Holland, B. J.; Barrow, C. J. Coacervation Technique as an Encapsulation and Delivery Tool for Hydrophobic Biofunctional Compounds. *Role of Materials Science in Food Bioengineering* **2018**, 235–261. https://doi.org/10.1016/B978-0-12-811448-3.00007-3.

(128) Cruz, M. E. M.; Corvo, M. L.; Martins, M. B.; Simões, S.; Gaspar, M. M. Liposomes as Tools to Improve Therapeutic Enzyme Performance. *Pharmaceutics* **2022**, *14* (3). https://doi.org/10.3390/PHARMACEUTICS14030531.

(129) Kelly, J. M.; Gross, A. L.; Martin, D. R.; Byrne, M. E. Polyethylene Glycol-b-Poly(Lactic Acid) Polymersomes as Vehicles for Enzyme Replacement Therapy. *Nanomedicine* **2017**, *12* (23), 2591–2606. https://doi.org/10.2217/NNM-2017-0221.

(130) McHugh, C. A.; Fontana, J.; Nemecek, D.; Cheng, N.; Aksyuk, A. A.; Heymann, J. B.; Winkler, D. C.; Lam, A. S.; Wall, J. S.; Steven, A. C.; Hoiczyk, E. A Virus Capsid-like Nanocompartment That Stores Iron and Protects Bacteria from Oxidative Stress. *EMBO J* **2014**, *33* (17), 1896–1911. https://doi.org/10.15252/embj.201488566.

(131) Giessen, T. W.; Orlando, B. J.; Verdegaal, A. A.; Chambers, M. G.; Gardener, J.; Bell, D. C.; Birrane, G.; Liao, M.; Silver, P. A. Large Protein Organelles Form a New Iron Sequestration System with High Storage Capacity. *Elife* **2019**, *8*. https://doi.org/10.7554/ELIFE.46070.

(132) Lončar, N.; Rozeboom, H. J.; Franken, L. E.; Stuart, M. C. A.; Fraaije, M. W. Structure of a Robust Bacterial Protein Cage and Its Application as a Versatile Biocatalytic Platform through Enzyme Encapsulation. *Biochem Biophys Res Commun* **2020**, *529* (3), 548–553. https://doi.org/10.1016/J.BBRC.2020.06.059.

(133) Cassidy-Amstutz, C.; Oltrogge, L.; Going, C. C.; Lee, A.; Teng, P.; Quintanilla, D.; East-Seletsky, A.; Williams, E. R.; Savage, D. F. Identification of a Minimal Peptide Tag for *in Vivo* and *in Vitro* Loading of Encapsulin. *Biochemistry* **2016**, *55* (24), 3461–3468. https://doi.org/10.1021/acs.biochem.6b00294.

(134) Andreas, M. P.; Giessen, T. W. Large-Scale Computational Discovery and Analysis of Virus-Derived Microbial Nanocompartments. *Nat Commun* **2021**, *12* (1). https://doi.org/10.1038/S41467-021-25071-Y.

(135) MaHam, A.; Tang, Z.; Wu, H.; Wang, J.; Lin, Y. Protein-Based Nanomedicine Platforms for Drug Delivery. *Small* **2009**, *5* (15), 1706–1721. https://doi.org/10.1002/SMLL.200801602.

(136) Ma, Y.; Nolte, R. J. M.; Cornelissen, J. J. L. M. Virus-Based Nanocarriers for Drug Delivery ☆. **2012**. https://doi.org/10.1016/j.addr.2012.01.005.

(137) Putri, R. M.; Allende-Ballestero, C.; Luque, D.; Klem, R.; Rousou, K. A.; Liu, A.; Traulsen, C. H. H.; Rurup, W. F.; Koay, M. S. T.; Castón, J. R.; Cornelissen, J. J. L. M. Structural Characterization of Native and Modified Encapsulins as Nanoplatforms for in Vitro Catalysis and Cellular Uptake. *ACS Nano* **2017**, *11* (12), 12796–12804. https://doi.org/10.1021/ACSNANO.7B07669/SUPPL_FILE/NN7B07669_SI_001.PDF.

(138) Tamura, A.; Fukutani, Y.; Takami, T.; Fujii, M.; Nakaguchi, Y.; Murakami, Y.; Noguchi, K.; Yohda, M.; Odaka, M. Packaging Guest Proteins into the Encapsulin Nanocompartment from Rhodococcus Erythropolis N771. *Biotechnol. Bioeng* **2015**, *112*, 13–20. https://doi.org/10.1002/bit.25322/abstract.

(139) Jones, J. A.; Benisch, R.; Giessen, T. W. Encapsulin Cargo Loading: Progress and Potential. *J. Mater. Chem. B* **2023**, *11*, 4377. https://doi.org/10.1039/d3tb00288h.

(140) Volk, A. A.; Campbell, Z. S.; Ibrahim, M. Y. S.; Bennett, J. A.; Abolhasani, M. Flow Chemistry: A Sustainable Voyage Through the Chemical Universe En Route to Smart Manufacturing. *https://doi.org/10.1146/annurev-chembioeng-092120-024449* **2022**, *13*, 45–72. https://doi.org/10.1146/ANNUREV-CHEMBIOENG-092120-024449.

(141) Hartman, R. L. Flow Chemistry Remains an Opportunity for Chemists and Chemical Engineers. *Curr Opin Chem Eng* **2020**, *29*, 42–50. https://doi.org/10.1016/J.COCHE.2020.05.002.

(142) Gutmann, B.; Kappe, C. O. Forbidden Chemistries — Paths to a Sustainable Future Engaging Continuous Processing. *J Flow Chem* **2017**, *7* (3–4), 65–71. https://doi.org/10.1556/1846.2017.00009.

(143) Wegner, J.; Ceylan, S.; Kirschning, A. Ten Key Issues in Modern Flow Chemistry. *Chemical Communications* **2011**, *47* (16), 4583–4592. https://doi.org/10.1039/C0CC05060A.

(144) Díaz-Kruik, P.; Paradisi, F. Rapid Production of the Anaesthetic Mepivacaine through Continuous, Portable Technology. *Green Chem* **2024**, *26* (4). https://doi.org/10.1039/D3GC04375D.

(145) Karnatz, F. A.; Whitmore, F. C. Dehydration of Diethylcarbinol. *J Am Chem Soc* **1932**, *54* (8), 3461–3461. https://doi.org/10.1021/ja01347a509.

(146) Baxendale, I. R.; Griffiths-Jones, C. M.; Ley, S. V.; Tranmer, G. K. Preparation of the Neolignan Natural Product Grossamide by a Continuous-Flow Process. *Synlett* **2006**, *2006* (3), 427–430. https://doi.org/10.1055/S-2006-926244/ID/3/BIB.

(147) Baxendale, I. R.; Deeley, J.; Griffiths-Jones, C. M.; Ley, S. V.; Saaby, S.; Tranmer, G. K. A Flow Process for the Multi-Step Synthesis of the Alkaloid Natural Product Oxomaritidine: A New Paradigm for Molecular Assembly. *Chemical Communications* **2006**, No. 24, 2566–2568. https://doi.org/10.1039/B600382F.

(148) Rossi, S.; Puglisi, A. Stereoselective Photocatalytic Transformations in Continuous Flow. *Reference Module in Chemistry, Molecular Sciences and Chemical Engineering* **2024**. https://doi.org/10.1016/B978-0-32-390644-9.00150-5.

(149) Nagornîi, D.; Raymenants, F.; Kaplaneris, N.; Noel, T. C(Sp3)–H Sulfinylation of Light Hydrocarbons with Sulfur Dioxide via Hydrogen Atom Transfer Photocatalysis in Flow. **2024**. https://doi.org/10.26434/CHEMRXIV-2024-DJX7B.

(150) Truppo, M. D.; Pollard, D. J.; Moore, J. C.; Devine, P. N. Production of (S)-γ-Fluoroleucine Ethyl Ester by Enzyme Mediated Dynamic Kinetic Resolution: Comparison of Batch and Fed Batch Stirred Tank Processes to a Packed Bed Column Reactor. *Chem Eng Sci* **2008**, *63* (1), 122–130. https://doi.org/10.1016/J.CES.2007.09.022.

(151) Microfluidic Reactor for Continuous Flow Biotransformations with Immobilized Enzymes: The Example of Lactose Hydrolysis by a Hyperthermophilic b-Glycoside Hydrolase. **2008**. https://doi.org/10.1002/elsc.200720223.

(152) Toogood, H. S.; Taylor, I. N.; Brown, R. C.; Taylor, S. J. C.; McCague, R.; Littlechild, J. A. Immobilisation of the Thermostable L-Aminoacylase from Thermococcus Litoralis to Generate a Reusable Industrial Biocatalyst. *Biocatal Biotransformation* **2002**, *20* (4), 241–249. https://doi.org/10.1080/10242420290029472.

(153) Rinaldi, F.; Fernández-Lucas, J.; de la Fuente, D.; Zheng, C.; Bavaro, T.; Peters, B.; Massolini, G.; Annunziata, F.; Conti, P.; de la Mata, I.; Terreni, M.; Calleri, E. Immobilized Enzyme Reactors Based on Nucleoside Phosphorylases and 2'-Deoxyribosyltransferase for the in-Flow Synthesis of Pharmaceutically Relevant Nucleoside Analogues. *Bioresour Technol* **2020**, *307*, 123258. https://doi.org/10.1016/J.BIORTECH.2020.123258.

(154) Croci, F.; Vilím, J.; Adamopoulou, T.; Tseliou, V.; Schoenmakers, P. J.; Knaus, T.; Mutti, F. G. Continuous Flow Biocatalytic Reductive Amination by Co-Entrapping Dehydrogenases with Agarose Gel in a 3D-Printed Mould Reactor. *ChemBioChem* **2022**, *23* (22). https://doi.org/10.1002/CBIC.202200549.

(155) Contente, M. L.; Paradisi, F. Self-Sustaining Closed-Loop Multienzyme-Mediated Conversion of Amines into Alcohols in Continuous Reactions. *Nat Catal* **2018**, *1* (6), 452–459. https://doi.org/10.1038/s41929-018-0082-9.

(156) Santi, M.; Sancineto, L.; Nascimento, V.; Azeredo, J. B.; Orozco, E. V. M.; Andrade, L. H.; Gröger, H.; Santi, C. Molecular Sciences Flow Biocatalysis: A Challenging Alternative for the Synthesis of APIs and Natural Compounds. **2021**. https://doi.org/10.3390/ijms22030990.

Chapter 2

Aims and Objectives

Biocatalysis has emerged as a sustainable and environmentally friendly strategy for use in the industrial synthesis of molecules. The approach is particularly relevant in the production of active pharmaceutical ingredients (APIs) as it offers high enantiopreference. However, challenges arise during the implementation and scale-up of reactions due to enzymatic stability issues. To address this, enzyme immobilization techniques have been shown to enhance catalyst stability and resistance, enabling a broader application of this process at larger scales. Despite these advantages, drawbacks, such as reduced biocatalyst flexibility and activity, hinder a complete industrial revolution in favour of biocatalysis. In this PhD work, we will delve into the diverse aspect of biocatalysis with the following aims:

1. Propose a Novel Approach to Biocatalysis and Immobilization:

Investigate the utilization of protein nanocompartments (encapsulins) as a novel method for biocatalysis and enzyme immobilization. We will explore how encapsulins can enhance enzyme stability and activity by providing a protective microenvironment. The use of encapsulins could lead to more efficient industrial processes, both enhancing the catalytic activity and resistance of the enzyme, providing a system which prevents the distortion of the enzyme upon immobilisation.

2. Understand factors and conditions which influence the variation of enantiopreference of a ω-Transaminase from *Halomonas elongata* (HeWT):

Enzymes often exhibit different affinities for enantiomeric substrates. In Chapter 5, the enantiopreference of HeWT, and how it changes in response to varying reaction conditions, is investigated. Understanding the factors (such as temperature, pH, and substrate concentration) that influence the selectivity of the enzyme can guide the design of tailored enzymatic reactions.

3. Chemoenzymatic Cascade Synthesis in Continuous Flow Systems:

We will develop and optimize a sequential reaction cascade that integrates chemical and enzymatic steps to synthesize pharmacologically active compounds. Our specific focus will be on the production of diverse alkylated tryptamines through a three-step reaction, both in batch processes and continuous flow systems.

By achieving these objectives, our work aims to significantly contribute to the advancement of biocatalysis, positioning it as a viable choice for sustainable and environmentally friendly industrial applications.

Materials and Methods

3.1 Reagents

Q5 High-fidelity DNA polymerase, 5x Q5 reaction buffer, and dNTPs were obtained from New England Biolabs (NEB). New England Biolabs (NEB) also provided the restriction enzymes (BamHI, HindIII), CutSmart buffer, 6x gel loading dye, and unstained protein standard (broad range 10-200 kDa). Primers were ordered and synthesised by Microsynth. Plasmids pBAD-EncMh, pENC-VsHb and pENC-HeWT were kindly donated by Dr. Nicola Loncar GECCO Biotech B.V.(Groningen, ND). Molecular biology kit such as GeneJET Plasmid Miniprep kit and GeneJET Gel Extraction kit were purchased by GeneAid. *E. coli* strain tn5:tna- was kindly provided by Dr. Robert S. Phillips from the Department of Chemistry at the University of Georgia, USA.

The following compounds were purchased from Merck: LB broth, LB broth with Agar, imidazole, ampicillin sodium salt, kanamycin sulfate, sodium chloride (NaCl), sodium hydroxide, tris base, HEPES buffer, sodium borohydride ($NaBH_4$), sodium cyanoborohydride ($NaCNBH_3$), picoline borane (pib-BH_3),formaldehyde, SYBR Safe DNA gel stain, agarose, Pyridoxal 5'-phosphate monohydrate (PLP), N,N,N',N' tetramethylethylenediamine (TEMED), magnesium sulfate ($MgSO_4$), potassium iodide (KI), trifluoracetic acid (TFA), dimethyl sulfoxide (DMSO) chloroform, deuterated water, methanol and deuterated methanol. Toluene, acetonitrile (MeCN) HPLC grade, ethyl acetate (EtOAc) glacial acetic acid and isopropanol were purchased from the same supplier.

The following substances were procured from Sigma Aldrich: yeast extract, N-Z-amine, glycerol, potassium phosphate dibasic and monobasic, ammonium sulfate, α-lactose monohydrate, isopropyl β-D-thiogalactoside (IPTG), L-glycine, D-glucose, ethylenediaminetetraacetic acid (EDTA), calcium chloride ($CaCl_2$), magnesium chloride hexahydrate ($MgCl_2x6H_2O$) , nickel (II) chloride hexahydrate ($NiCl_2·2H_2O$), cobalt (II) chloride ($CoCl_2$), copper (II) chloride dihydrate ($CuCl_2·2H2O$), iron (III) chloride hexahydrate($FeCl_3x 6H_2O$), manganese (II) chloride tetrahydrate ($MnCl_2· 4H_2O$), sodium pyruvate, sodium dodecyl sulphate (SDS), 2-mercaptoethanol (ß-ME), acrylamide/bis-acrylamide 30% solution, ammonium persulfate (APS), Instant blue, Bradford reagent, bovine serum albumin solution (BSA), sodium periodate ($NaIO_4$), boric acid, sodium tetraborate decahydrate, sodium bicarbonate ($NaCO_3$), iminodiacetic acid (IDA), Fmoc-HCl, Fluoresceine isothiocyanate (FITC). L-Alanine, (*S*)-methyl benzylamine (*S*-MBA), thiazolidine-4-carboxylic acid (T4C), cadaverine, indole, L-serine, 5-hydroxy indole, 5-methoxy indole, L-tryptophan 5-hydroxy-L-tryptophan, 5-

mehtoxy-L-tryptophan, tryptamine, 5-hydroxytryptamine (serotonin), 5-methoxytryptamine, *N,N*-acetyl-tryptamine, *N,N*-acetyl 5-hydroxytryptamine, *N,N*-acetyl 5-methoxytryptamine (melatonin), ascorbic acid, sodium borohydride (NaBH$_4$), picoline borane (pic-BH$_4$), sodium cyano borohydride (NaCNBH$_3$), formic acid were ordered from Merck. NAD$^+$, tetrahydro furan ketone (THF-O) purchased from Apollo Scientific. Benzothiophene, benzofuran and ethanolamine were kindly donated by Prof.Dr. Martin Albrecht and Prof. Dr. Eva Hevia.

Metacrylic resins ReliSorb EP400/SS, EP403/S and HFA403/S were kindly donated by Resindion S.R.L.. 4% BCL Agarose Bead Standard (50-150μm) were obtained from Agarose eBeads Technologies. Amberlite HPR4811, Amberlite MB-3 and Amberlite XAD-4 were acquired from DuPont.

3.2 Bacterial strains

Plasmids pET28-b were cloned into *E. coli* DH5(α) or XL10-gold strains for plasmid propagation and sequencing. *E. coli* BL 21AI-one Shot, BL 21(DE3), BL21(DE3)-star BL21(DE3) *tn5:tna*$^-$ were used for protein expression accordingly with the requirements of the experiments.

3.3 Plasmid

Plasmids used for cloning and transformation are reported in the Table 3.1.

Table 3.1 Genes used in this work with specific vectors, promotor, source, and resistance.

Plasmid	Backbone	Induction	Organism	Resistance
pBAD-EncMh	pBAD	Arabinose	*Mycolicibacterium hassiacum*	Amp
pENC-VsHb	pEN-C	IPTG	*Vitreoscilla stercoraria*	Kan
pENC-HeWT	pEN-C	IPTG	*Halomonas elongata*	Kan
pENC-HeP5C	pEN-C	IPTG	*Halomonas elongata*	Kan
HeWT	pET28-b	IPTG	*Halomonas elongata*	Kan
EcTnaA-WT or EcTnaA-L51A-V394A	pET28-b	IPTG	*Escherichia coli*	Amp
RgTDC-WT or RgTDC-W349F	pET28-b	IPTG	*Rumignococcus gnavus*	Kan
MsAcT	pET26-a(+)	IPTG	*Mycolicibacterium hassiacum*	Kan

3.5 General Procedures

3.5.1 Preparation of chemically competent cells

From a glycerol stock of the appropriate *E. coli* strain, a Petri dish (antibiotic-free) was made by spreading the cells with a sterile spreader and grown at 37 °C. Ater 16 hours, one colony was picked and used to inoculate 50 mL LB medium and grown at 37°C, 150 rpm until on OD_{600} of 0.35-0.4 was reached. The culture was then placed on ice for 30 minutes and harvested by centrifugation at 3000 g for 15 minutes at 4 °C (centrifuge NU-C200R, rotor NU-RX625). The cells were resuspended in 50 mL of an ice-cold 100 mM $MgCl_2$ and centrifuged again as before. The pellet was resuspended in 25 mL of an ice-cold solution of 100 mM $CaCl_2$ and incubated for 30 minutes in ice. After the last step (2000 g, 15 minutes, 4 °C), the pellet was resuspended in 1 mL of ice cold 85 mM $CaCl_2$ (15% *v/v* glycerol) and aliquoted in 40 µL in 1.5 mL sterile microcentrifuge tubes and stored at -80 °C until needed.

3.5.2 Transformation of competent *E. coli* cells

The appropriate strain of *E.coli* cells was transformed by adding 1 µL (80-100 ng) of the plasmid to a 40 µL competent cells directly in the microcentrifuge tube. The sample was left

on ice for 30 minutes before heat-shock at 42 °C for 60 seconds and immediately cooled on ice for 5 minutes. 300 µL of LB media pre heated at 37 °C was added to the tube and incubated for 45min at 37 °C and 180 rpm. After this time, 50 to 100 µL of the solution were spread onto two LB-agar plates containing the appropriate antibiotic and incubated overnight at 37 ℃.

3.5.3 Gene cloning

The construction of pENC-HeP5C was done starting from pENC-HeWT *via* Gibson Assembly technology. After amplification of the insert and the vector, the products were analysed on agarose gel under UV (λ=345 nm), excised and purified *via* purification kit (Thermo Fisher or GeneAid). Either HeP5C gene and pENC vector were digested with DpnI before ligation, which was performed overnight at 16 °C using T4-DNA ligase from New England Biolabs (1 µL/25 µL PCR reaction). After this step, *E. coli* DH5α or XL10-Gold were transformed with the entire construct (pENC-HeWT-C-ter, pENC-HeP5C-C-ter), purified with GeneJET PCR Purification Kit (Thermo Fischer) and sent for sequencing.

Table3.2 Primers sequences for gene and vector amplification

Primer	Primers Sequence	Amplicon
FW-pENC	5'-GTC GAA TCA CCG CCG CCG CTG CCG GAT T-3'	pENC vector
Rev-pENC	5'-ATG GCT GCC GCG CGG CAC CAG-3'	pENC vector
FW-HeP5C	5'-CGC GCG GCA GCC ATA TGG CAA GCC AAG TCA CC-3'	HeP5C
Rev-HeP5C	5'-CGGCGGTGATTCGACGCGCTTGCCGAGTTCGTC-3'	HeP5C

The composition of the reaction mix and the PCR condition to amplify pENC vector are reported in Tables 3.3 and 3.4.

Table 1.3- Q5 High Fidelity PCR Setup for pENC amplification. Total volume: 25 µL

Description	Volume (µL)	Final Concentration
5X Q5 Reaction Buffer	5	1x
Q5® High-Fidelity DNA Pol	0.25	0.02 U/µl
dNTPs	0.5	97 ng/ µL
10 µM Primer Forward	1.25	0.5 µM
10 µM Primer Reverse	1.25	0.5 µM
10 mM dsDNA template	2.5	200 µM
Nuclease free dH$_2$O	14.5	-

C

Table3. 4-Touch-Down PCR Condition for pENC amplification

PCR Cycle Step	Temperature (°C)	Time	Ramp (°C/min)
Q5® High-Fidelity DNA Pol Activation	98	30 sec	
Denaturation	98	10 sec	
Annealing	69 to 59	3.30 min	0.5°C/min
Elongation	72	2	
Number of cycles		10	
Enzyme Deactivation	80	4 min	-

The composition of the reaction mix and the PCR condition to amplify HeP5C insert are reported in Tables 3.5 and 3.6.

Table3.5 Q5 High Fidelity PCR Reaction Setup for HeP5C amplification. Total volume is 25 μL

Description	Volume (μL)	Final Concentration
5X Q5 Reaction Buffer	5	1x
Q5® High-Fidelity DNA Pol	0.25	0.02 U/μl
dNTPs	0.5	97 ng/ μL
10 μM Primer Forward	1.25	0.5 μM
10 μM Primer Reverse	1.25	0.5 μM
10 mM dsDNA template	5	200 μM
Nuclease free dH$_2$O	11.75	-

Table3. 6-Touch-Up PCR Condition for HeP5C amplification

PCR Cycle Step	Temperature (°C)	Time	Ramp (°C/min)
Q5® High-Fidelity DNA Pol Activation	98	30 sec	
Denaturation	98	10 sec	
Annealing	67 to 72	3.30 min	0.5°C/min
Elongation	72	2	
Number of cycles		20	
Enzyme Deactivation	80	4 min	-
Final Storage	4	∞	-

3.5.4 Agarose Gel Electrophoresis

Upon amplification of the desired fragment by PCR, the DNA samples were run on an agarose gel at 0.8% (*w/v*) (Figure 3.1). The gel was prepared as follows: 0.32 g of agarose powder were mixed with 40 mL TAE buffer 1% (243 g Tris base, 57 mL glacial acetic acid, 0.5 M EDTA in 100 mL) in a conical flask were heated for approx. 3 min until completely dissolved. Once the solution cooled down sufficiently, 4 μL of SYBR safe DNA staining were added and subsequently poured in the pre-assembled mould (Biorad). PCR samples were prepared by 2μL of Gel Loading Dye Purple (6x) to 12 μL. 10 μL of each sample were loaded into the

respective well and the gel was run at 75V and 150 mA for approx. 45 minutes. To visualise the results, a UV lamp was used (λ = 260 nm).

3.5.5 Culture media

The bacterial cultures used to produce all the proteins were expressed in LB, ZYM-50 ZYP-5052 Auto-Induction or TB medium. Media and plates were prepared as follows:

- <u>LB-Medium</u>: Premixed lyophilised broth 25 g/L. Final concentration: Tryptone (10 g), yeast extract (5g), NaCl (10g) and distilled H_2O (1 L).
- <u>LB-Agar Plates</u>: Premixed lyophilised broth 40 g/L. Final concentration: Tryptone (10 g), yeast extract (5 g), NaCl (10 g), agar (15 g) and distilled H_2O (1 L).
- <u>ZYP-5052 Auto-Induction media</u>: N-Z-Amine (3 g), yeast extract (1.5 g), 1M K_2HPO_4 (15 mL), 1M H_2PO_4 (15 mL), 1M $(NH_4)_2SO_4$, (7.5 mL) 1000x trace element solution (0.6 mL) consists of: $FeCl_2$ (50 mM), $CaCl_2$ (20 mM), $MnCl_2$ (10 mM), $ZnSO_4$ (10 mM), $CoCl_2$ (2 mM), $CuCl_2$ (2 mM), $NiCl_2$ (2mM), HCl (60 mM), Na_2MoO_4 (2mM), Na_2SeO_4 (2 mM) and H_3BO_3 (2 mM) (sterilized by filtration); 50x 5052 solution (6 mL) consists of: glycerol (25 g), glucose (2.5 g), α-lactose monohydrate (10 g) and dH_2O (to 100 mL) in dH_2O (to 300 mL);[1]
- <u>TB medium</u>: N-Z amine (12g), yeast extract (24g), glycerol (5g), K_2HPO_4 (2.2 g) and KH_2PO_4 (9.4 g) and distilled H_2O (1 L).

Each culture (liquid or solid) was supplemented with the appropriate antibiotic in a final concentration of 50 (Amp) or 100 (Kan) µg/mL

3.5.6 Protein expression, purification and quantification

Production and purification of the desired protein was performed after transformation of the appropriate BL21(DE3) strain (in case of encapsulated protein, the strain was co-transformed with 1 µL of pBAD-MbEnc and 1 µL of pENC-HeWT or pENC-HeP5C, accordingly to the experiment. See section 4.4) and grew on a Petri dish supplied with the appropriate antibiotic. The expression was initiate by adding 1 colony from the plate to 5 mL LB medium with the appropriate antibiotic for the pre-inoculum and incubated at 37 °C overnight at 180 rpm. After due time, an adequate volume of pre-inoculum (3-4 mL) was added to 300mL of ZYP-5052 Auto-Induction or TB medium (initial OD_{600}= 0.1), supplemented with the right antibiotic. The

expression of proteins under *lac* operon was induced, in case of TB broth, with 0.1mM IPTG once the OD_{600} reached 0.6. In case of encapsulin expression, the induction was done by subsequent addition of arabinose(1% *w/v*) at OD_{600} of 1.[2] The cultures were generally grown overnight at 37 °C in all cases, except for MsAcT which required an expression temperature of 25 °C. Successively, the cells were harvested at 2500 rpm for 20 minutes at 4 °C; the supernatant was discarded, and the cells were washed with 50mM KP_i buffer pH 7.8 before a second centrifugation step under the same conditions. Once again, the supernatant was discarded to quantify the biomass yield before proceeding with the purification.

To recover the protein of interest, the culture was mixed with the appropriate loading buffer (Table 3.7) (approx. 3mL buffer per g of pellet were added) for protein purification. The suspension was sonicated for 8 or 10 min in an ice bath, activating the pulse for 5-seconds with 10-second pause in between at 40% amplitude. A sample of the lysate (100 µL) was withdrawn for SDS-PAGE electrophoresis, the rest was centrifuged for 45 minutes at 4 °C at 12500 g at 4 °C (centrifuge NU-C200R, rotor NU-RA8-50). A sample (100 µL) of the supernatant was taken for SDS-PAGE analyses and the remainder was filtered through a 0.45 µm Millex PVDF before loading on to NiNTA 5mL columns for affinity purification with an AKTA Start system. Similarly, approx. 50 mg of the pellet was resuspended in dH_2O and saved for SDS-PAGE analyses. Before any purification, the column (1 or 5 mL) was pre-loaded with 4 column volume of 0.1 M $NiSO_4$, washed with 4 column volumes of dH_2O, and equilibrated with 5 column volumes of loading buffer A, all at 1 mL/min flow rate.

With the exception of encapsulated proteins, upon application of the sample on the column the flow through was discarded, followed by a washing step (5 CV) with loading buffer and a second step (5 CV) with 10 % elution buffer (Table 3.7), to remove unspecific proteins that eventually bound to the column. The retained protein was then eluted with 100 % elution buffer, collecting the appropriate tube by monitoring the variation in absorption at 280 nm. The fractions were pooled together in a dialyses membrane (cellulose membrane, 14 kDa MWCO (Sigma Aldrich) and dialysed twice against 50 - 100 mM KP_i buffer pH 7.8 at 4 °C, supplemented with 10 mM PLP when needed. The dialysis solution was replaced after 1 hour, followed by a second dialysis step in 500 mL buffer at 4 °C overnight. The specific buffer for each protein is summarised in Table 3.7.

The encapsulated biocatalysts (HeWT or HeP5C) and the hollow structure were purified by PEG-precipitation. The flowthrough was collected in a falcon tube, dialyzed against 50 mM KPi buffer pH 8 to remove the indole, and further purified *via* PEG8000. The purification was done by mixing the sample with a 10 % PEG 8000 solution (dropwise) in a ratio 1:1. The tube was left on an orbital shaking tray for 1 h at 4 °C and centrifuged for 20 min at 5000 rpm. The precipitate was resuspended in 50 mM KPi buffer pH 8, 150 mM NaCl 5 % glycerol and left under agitation at 4 °C for 20 hours.

Table 3.7 Specific conditions for protein purification by Ni-NTA.

Enzyme	Loading Buffer	Elution Buffer	Dialyses/ Storage Buffer
HeWT (Cargo Protein)	50 mM KPi Buffer pH 8, 100 mM NaCl 30 mM Imidazole, 0.1 mM PLP	50 mM KPi Buffer pH 8, 100 mM NaCl , 300 mM Imidazole, 0.1 mM PLP	50 mM KPi Buffer pH 8, 0.1 mM PLP
HeP5C (Cargo Protein)	50 mM KPi Buffer pH 8, 100 mM NaCl 30 mM Imidazole	50 mM KPi Buffer pH 8, 100 mM NaCl , 300 mM Imidazole	50 mM KPi Buffer pH 8,
HeWT	50 mM KPi Buffer pH 8, 100 mM NaCl 30 mM Imidazole, 0.1 mM PLP	50 mM KPi Buffer pH 8, 100 mM NaCl , 300 mM Imidazole, 0.1 mM PLP	50 mM KPi Buffer pH 8, 0.1 mM PLP
EcTnaA-WT or EcTnaA-L51A-V394A	100 m KPi Buffer pH 7, 100 mM KCl, 0.1 mM PLP, 10 mM 2-mercaptoethanol	100 m KPi Buffer pH 7, 100 mM KCl, 0.1 mM PLP, 300 mM Imidazole 10 mM 2-mercaptoethanol	100 m KPi Buffer pH 7, 0.1 mM PLP
RgTDC-WT or RgTDC-W349F	50 mM KPi Buffer pH 8.0 100 mM NaCl, 0.1 mM PLP 10 mM Imidazole	50 mM KPi Buffer pH 8.0 100 mM NaCl, 0.1 mM PLP 300 mM Imidazole	100 m KPi Buffer pH 7, 0.1 mM PLP
MsAcT	100 mM KPi Buffer pH 8, 100 mM NaCl, 6 mM Imidazole	100 mM KPi Buffer pH 8, 100 mM NaCl, 250 mM Imidazole	100 mM KPi Buffer pH 8

At the end of the dialyses, the purified proteins were quantified by absorbance at 280 nm with a BioTek Tek3 plate reader. The extinction coefficients of each protein were determined *via* ProtParam (Table 3.8). This parameter was needed for the estimation of the concentration, which follows the Lambert-Beer law (Figure 3.1), [3]

$$A = \varepsilon b C$$

Figure 3.1 Lambert-Beer equation. With *A* = absorbance, ε = extinction coefficient ($M^{-1}cm^{-1}$), *b* = length of light path (cm), C = analyte concentration (M).

Table 3.8 Extinction coefficients and molecular weight of the enzymes involved in this work obtained *via* ProtParam.

Enzyme	Extinction coefficient ($M^{-1}cm^{-1}$)	Molecular Mass (kDa)
EncMh	28545	28.9
HeWT-Ctag (Cargo Protein)	62840	57.5
HeP5C-Ctag (Cargo Protein)	17085	34.1
HeWT	62800	54.0
HeP5C	18450	32.4
EcTnaA-WT	51230	57.1
EcTnaA-L51A-V394A	50115	53.4
RgTDC-WT	70360	58.5
RgTDC-W349F	65110	54.9
MsAcT	28100	25.6
VsHb	11460	21.1

Due to the complexity of the encapsulin-cargo protein system, protein quantification could not be performed as for the other proteins. Therefore, to estimate the amount of included biocatalyst we coupled two quantification methods. Initially, the use of a Bradford assay permits the estimation of the total protein, calculated by extrapolation from a standard curve of BSA (1.4 mg/mL, 1 mg/mL, 0.5 mg/mL, 0.25 mg/mL, 0.125 mg/mL).The samples were prepared by adding 250µL of Bradford reagent to each well of a 96 micro-well plate, together with 5µL of the BSA standard solutions or sample. The plate was incubated for 5 min at 25 °C before reading the absorbance at 595 nm. At the same time, a sample of the same protein solution was treated and analysed by SDS-PAGE electrophoresis, prepared as it will be described in the next section. As reference, a known amount of non-encapsulated biocatalyst

(either HeWT- Ctag or HeP5C-Ctag) was used to create a 6-points calibration curve, 2 wells were dedicated to the Encapsulin-Cargo protein sample and one for the protein ladder. The results were analysed with Image-J software, which based on the calibration curve can lead us to estimate the concentration of the cargo protein comprised, hence understand the ratio between the shell and the catalyst. [4,5] An example of SDS-PAGE used for this approach is shown in Figure 3.2. Lanes 5 to 10 were dedicated to the HeWT C-tag calibration curve, where the protein is visible at 56 kDa. In Lane 3 and 4 a sample of EncHeWT was loaded, the two bands are for the cargo (56 kDa) and the Encapsulin (29 kDa). Lane 2 was a sample of HeWT C-tag at 2.5 mg/mL.
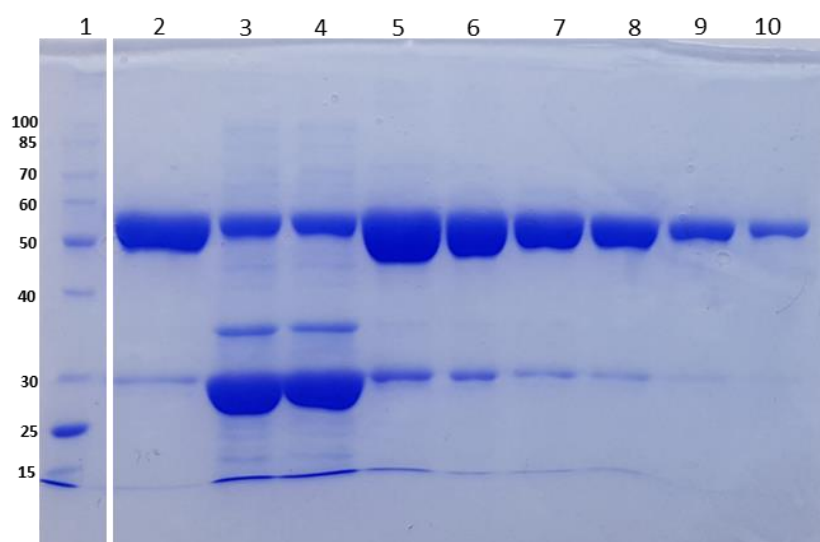

Figure 3.2 Quantification *via* SDS-PAGE of Enc-HeWT. Lanes: 1- Protein Ladder, 2- HeWT C-tag, 3-EncHeWT, 4-EncHeWT, 5- HeWT C-tag 2.5 mg/mL, 6- HeWT C-tag 2 mg/mL, 7- HeWT C-tag 1.5 mg/mL, 8- HeWT C-tag 1 mg/mL, 9- HeWT C-tag 0.5 mg/mL, 10- HeWT C-tag 0.25 mg/mL

3.5.7 SDS-PAGE electrophoresis

To make 12 % SDS running gel for SDS-PAGE, the following components were mixed: 1.9mL deionized H_2O, 2.45 mL 1 M Tris-HCl buffer pH 8.8, 1.5 mL acrylamide 40%, 70 µL SDS 10%, 70 µL of a 10% solution, 7 µL tetramethylethylenediamine (TEMED). Once the mixture was ready, it was loaded to the casted support, as specified from the supplier (BioRad), and polymerized with a layer of 2-propanol to ensure an even edge. During the polymerisation time, 6 % stacking gel was prepared as follows: 1.2 mL deionized H_2O, 0.5mL of 0.5 M Tris-HCl buffer pH 6.8, 0.25 mL acrylamide 40 %, 20 µL SDS 10%, 20 µL ammonium persulfate 10%, 3 µL TEMED.

The 2-propanol was discarded, the stacking gel was added on top, and a 10-wells comb was inserted. During the last polymerisation step the samples were prepared by adding to 30 μL pre-boiled diluted protein sample, either 10 μL of 4x loading Buffer (for 40 mL stock solution: 2.5mL dH₂O, bromophenol Blu 100mg, 1 M Tris pH 6.8 10 mL, SDS 4g, glycerol 20 mL, EDTA 1.5 g, ß-mercaptoethanol 5 mL) or 10 μL of Protein Loading Dye (GeneAId) supplemented with ß-mercaptoethanol.

Once the cast was assembled and the samples were loaded into the wells, the separation was performed by running the gel at 33 mA, 120 V for about an hour in glycine buffer (3.1 g Tris Base, 14 g glycine, 10 mL SDS 10% for 100 mL solution) pH 8.3. After this time, or once the front reached nearly the bottom edge of the glass, the gel was removed, briefly rinsed in dH₂O, and stained for an hour in Staining solution (InstantBlue® Coomassie Protein Stain, BioHelix).

3.6 Activity assay

Assess the activity of each enzyme before setting up any experiment was a mandatory to set the specific activity of the initial biocatalyst. Each enzyme involved in this study has its specific substrates, therefore a tailored setup for each biocatalyst was necessary. [6]

- **HeWT Specific Assay:**
  2.5 mM S-MBA; 2.5 mM pyruvate; 0.1 mM PLP, KPi buffer 50 mM pH 8 were added to a 1 mL cuvette. The product formation (acetophenone) was monitored at 245 nm at 37 °C over 2 minutes with an Agilent Cary 60 Scan UV–Visible spectrophotometer equipped with a Cary single cell Peltier temperature controller.[7]

- **HeP5C Specific Assay:**
  10mM Thiazolidine-4-carboxylic acid, 1 mM NAD⁺, KPi Buffer 50 mM pH 8 in 1mL volume at 25 °C. The activity of the enzyme was monitored indirectly *via* cofactor consumption at 345 nm. To follow the signal, the same Cary 60 as mentioned before was used.[8]

- **EcTnaA Specific Assay:**
  10 mM of Indole, 125 mM ʟ-serine, 0.1 mM PLP, KPi Buffer 50mM pH 8 in 1 mL volume at 37 °C. Before starting the assay, the enzyme was activated by incubation at 37 °C for minimum 2 hours. The tryptophan generated was monitored by RP-HPLC (Thermo Fischer Ultimate 3000 UHPLC supplied with Waters XBridge BEH C18 Column, 130 Å,

3.5 μm, 2.1 mm X 150 mm) withdrawing 50 μL from the reaction at 0, 2,5,7,10, and 15 minutes. The samples were mixed with MeCN and dH$_2$O+ 0.2% HCl and filtering on an PTFE filter with a 0.45 μm cut-off limit. The mobile phase used was MeCN (HPLC grade) 0.1% TFA (A) and dH$_2$O 0.1% (B): 0-1 min 95% A: 5% B; 1-5 min 5% A:95% B; 5.1-6.6 min 100% B; 6.6-7 min 95% A:5%B; 7-10 min 95% A:5%B.

- **RgTDC Specific Assay:**
  10 mM L-tryptophan, 0.1 mM PLP, KPi Buffer 50 mM pH 8 in 1 mL volume at 37 °C. The reaction was monitored for 1 hour and 50 μL of sample was withdrawn at 0, 10. 30 and 60 minutes and analysed by RP-HPLC as mentioned before. The final concentration of the biocatalyst in reaction tube was kept at 1mg/mL.

- **MsAcT Specific Assay:**
  Activity of MsAcT was monitored spectrophotometrically with an Agilent BioTek3 Epoch on a 96-well plate. The assay set up was prepared by mixing 0.1 mM *p*-nitrophenyl acetate, 1 μg/mL MsAcT, in KPi 100 mM pH 8. Under this condition, the hydrolytic activity of the enzyme cleaves the substrate into *p*-nitrophenol, and its production is monitored at 400 nm for 2 min at 25 °C. [9]

For all the activity assays, a blank reaction was done in parallel, where the enzyme was replaced by an equivalent volume of 50 mM KPi buffer pH 8.

In general, the specific activity of an enzyme, number of units per milligram of protein, is calculated by the following equation (Figure 3.3) and expresses the efficiency of an enzyme in catalysing a specific reaction. 1 unit (U) is defined as the amount of enzyme required to catalyse the reaction of 1 nmol of substrate per minute under standard conditions specified from the assay. The slope is given by the variation of absorbance at certain wavelength over a specific period.

$$Specific\ Activity\left(U/mg\right) = \frac{slope(mAu/min) \times reaction\ volume\ (mL)}{\varepsilon(M^{-1} \times cm^{-1}) \times enzyme\ concentration\ (mg/mL)\ \times volume\ of\ enzyme\ (mL)}$$
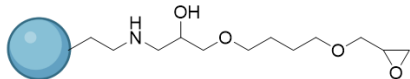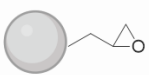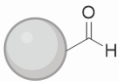
Figure 3.3 General formula for specific activity.

3.7 Enzyme Immobilisation

Enzyme immobilisation was done on different type of carriers and strategies. As showed in Section 1.3, depending on the operational conditions the choice of the nature of the resin and

the chemistry of the immobilisation may vary . Table 4 shows the resin used in this work (metal coordination not shown).[10–12]

Table 3.4 Support and immobilisation strategies.

Carrier	Identifier	Features	Functionalisation
	EP400/S	Methacrylate Particle size: 100-300 μm Pores diameter: 40-60 nm	Epoxy
	HFA403/S	Methacrylate Particle size: 100-300 μm Pores diameter: 40-60 nm	Amino Epoxy
	Sephabeads 6CL	Agarose Particle size: 50-150 μm Pores diameter: 200 nm	Epoxy Glyoxyl
	EziG Opal	Glass Particle size: 120-200 μm Pores diameter: 500 nm	Ionic interaction
	EziG Coral	Polymer coated Glass Particle size: 2-50 μm Pores diameter: 250-350 nm	Ionic interaction
	EziG Amber	Polymer coated Glass Particle size: 50-150 μm Pores diameter: 250-350 nm	Ionic interaction

3.7.1 Enzyme Immobilisation on Epoxy Supports via Co^{2+} coordination.

Immobilisation of biocatalysts on an epoxy support were done either on agarose or methacrylic support accordingly to the application. For agarose immobilisation, the carrier was firstly functionalised with epoxy groups: 10 g di Agarose (Sephabeads 6CL) were mixed with 44 mL of H_2O and 16 mL of acetone, 3.38 g of NaOH, 0.4 g of $NaBH_4$. and 11 mL of epichlorohydrin dropwise. All the steps were performed on ice. The tube was incubated at room temperature overnight (or at least 16 hours) and the day after thoroughly washed and filtered until further use. A syringe with 1 g of epoxy or amino epoxy functionalised carrier was mixed with 2 mL modification buffer (0.1 M sodium borate, 2 M iminodiacetic acid, pH 8.0) for 2 hours. The resin was filtered, washed with H_2O, mixed with 5 mL metal solution (30 mg/mL of $CoCl_2$ in H_2O) and mixed at room temperature. After 1 hour, the carrier was washed again with an excess of dH_2O and the enzyme solution was added to the syringe. Incubation time and temperature were adjusted depending on the requirements of the enzyme. When

no more protein was detectable on the supernatant (checked at 280 nm, SDS-PAGE and/or activity assay), the resin was filtered and mixed with 3 mL of desorption buffer (50 mM EDTA, 0.5 M NaCl in 50 mM KPi buffer, pH 7.2) to remove any excess cobalt, washed again with water and incubated with 4 mL 3 M glycine buffer (pH 8.5) to block the aldehyde group that may cross-react. The last blocking step was done at room temperature (or at 4° C in case of RgTDC) temperature overnight under agitation.

3.7.2 Quantification of the Epoxy-Groups

The quantification of the epoxy groups available for immobilisation was done by mixing 50 mg of resin with 0.5 mL of 0.5 M H_2SO_4 and incubated for 1 hour to open all the epoxy groups. The resin was washed thoroughly with water and mixed for 1 hour with 0.5 mL of 10 mM $NaIO_4$ to oxidise the obtained diols to the corresponding aldehydes. The suspension was centrifuged, and 100 µL of the supernatant was added to a solution of saturated $NaCO_3$:KI 10% 1:1. and analysed in triplicate on a 96-well plate. A blank and a control were also included, using H_2O 100 µL of 10 mM $NaIO_4$ respectively. The unreacted $NaIO_4$ in contact with KI releases I^-, which peak of absorbance is at 405 nm The difference in the absorbance between the control with $NaIO_4$ and the samples indicates the µmol of $NaIO_4$ that did not react and therefore indirectly the amount of epoxy groups that are available per gram of agarose bead. 1 g of agarose 6BCL is stated to harbour 70-75 µmol of diols available.[12]

3.7.3 Immobilisation on Glyoxyl Group

1 g of epoxy support was mixed with 10 mL of 100 mM H_2SO_4 and incubated overnight. After washing with deionized water, the resin was treated with 10 mL of 30 mM $NaIO_4$ for 2 hours, followed by washing with water. The aldehyde groups were quantified at 405 nm using the aforementioned procedure for the quantification of epoxy groups. Upon derivatisation with aldehyde solution containing the enzyme was prepared in a 100 mM $NaHCO_3$ buffer, pH 10. After washing the resin with the same buffer, the protein solution was added and incubated for at least 4 hours. The Schiff bases, formed upon the reaction of the ε-amino groups of lysine residues and the aldehydes, were reduced by adding 10 mg of $NaBH_4$ to the suspension, then left under gentle shaking for 30 minutes at 4 °C.[12]

3.7.4 Ionic Immobilisation on Glass Bead

Immobilization on glass beads was done by adding the protein solution to the support. The EziG beads were thoroughly washed with dH$_2$O and mixed with the enzyme at RT under gentle shaking until no protein was detected in the supernatant. After the due time, the support was washed with dH$_2$O and the immobilised enzyme was stored at 4 °C until needed.[13]

3.7.5 Spatial Analyses Distribution by Laser Scanning Confocal Microscopy (LSCM)

The spatial analyses distribution of MhEnc covalently bound on agarose beads was performed with a Confocal microscopy Nikon Ti2 Eclipse with a X-light V2 spinning disk equipped with 20x, 60x and 100x objectives. Fluorescein isothiocyanate (FITC) was incubated in a molar ratio 1:20 with the protein solution (prepared in Tris-HCl buffer pH 7) and left under gentile shaking at RT for 1 hour. The excess of labelling agent was removed by filtration using an Amicron membrane (10 kDa), centrifuging the sample at 11000 g for 10 minutes at 4 °C. The step was repeated 3 times and the retained protein was resuspended in 100 mM NaHCO$_3$ buffer, pH 10 for the immobilisation on glyoxyl-agarose (Section 3.7.3). To measure the fluorescence, the sample was diluted 50-fold in dH$_2$O and analysed with an excitation wavelength of 510 nm and emission wavelength of 470 nm. The analysis included a negative control with a non-labelled MhEnc immobilized.

3.9 Analytical Methods

3.9.1 RP-HPLC Analyses

For enzymatic assays and biotransformation, the production of the final compound was analysed via HPLC. The instrument, a Dionex UltiMate 3000, Waters is equipped with Waters XBridge BEH C18 Column (130 Å, 3.5 μm, 2.1 mm X 150 mm). MeCN (Eluent A) and milliQ H$_2$O 0.1% TFA (Eluent B) were used as mobile phase and the elution program was as follows: injection volume 2 μL. Flow rate 0.8 mL/min, elution at 45 °C . Elution method (A: 0.1% TFA in water, B: 0.1% TFA in acetonitrile): 0-5 min (50% to 100% A); 5-6.6 min (100% A); 6.6-10 min (95% A).

To detect chiral molecules, the HPLC system was equipped with Phenomenex Lux Cellulose-2 chiral column (5 μm, 44.6 x 250 mm). The injection volume was 20 μL, at 30 °C with a flow rate of 1 mL/min. The analyses were done with an isocratic method 40% A - 60% B.

For both methods, the samples were prepared mixing 50 μL of reaction with 225 μL MeCN and 225 μL dH$_2$O containing 0.2% HCl.

3.9.2. Fmoc derivatization

Compounds which were not UV-active was derivatised with Fmoc-Cl. Borate buffer (100 mM, pH 9; 200 μL), the sample to be analysed (diluted to a total amine concentration not exceeding 25 mM; 100 μL), and Fmoc–Cl (15 mM in MeCN; 400 μL) were combined and thoroughly mixed for 30 seconds. 200 μL of that mixture were added to 800 μL of HCl (0.2%) and MeCN (1:1 *v/v*) and analysed by RP-HPLC.

3.9.3. Thin Layer Chromatography

TLC plates used in work were ALUGRAM Xtra SIL G UV254, 40x60 mm (Machery-Nagel). Depending on the final application the mobile phase was composed by *n*-butanol:acetic acid:dH$_2$O in a proportion of 7:2:1 for the visualisation of the production of tryptamines analogue from the corresponding tryptophan (Section 5.6). The mobile phase for the resolution of dimethylated tryptamines was done either using methanol or a mixture of dichloromethane and triethylamine in proportion 5:1. To stain the compound, the plate was visualised at 260 nm or stained with a solution of ninhydrin (1.5% *w/v* ninhydrin, 3% *v/v* acetic acid in absolute ethanol).

3.10 Continuous Flow Biotransformations

The flow system used in this work was a Vapourtec® R2S supplied with pumping module and R-4 reactor heater. The packed bed reactors (PBR) used was a Omnifit glass columns (6.6 mm bore x 150 mm length), incorporating glass heat exchangers in the setup. When needed, a T-tube connection was used to a connect the system to an organic phase supply. The flow rates

were set up considering the desired residence times and the volume of the PBR, according to the following formula depicted in Figure 3.3.

$$Total\ volume\ (mL) = Column\ length\ (cm)/0.3421$$

Figure 3.3 Formula for the calculation of the volume of a bioreactor.

3.11 Chemical dimethylation of Tryptamine Analogues

In Chapter 7, a chemical synthesis was used to synthetise the dimethylated tryptamine or the 5-substituted analogues (5-hydroxy, 5-methoxy). The reaction was conducted using various reducing agents: NaCNBH3, NaBH4, or picoline borane, with formaldehyde serving as the alkyl donor. The reaction mixture (5 mL) was placed in glass vials, stirred continuously, and maintained at a controlled temperature of 25°C. For analysis, 100 μL of the reaction mixture was mixed with 600 μL D2O and subjected to ^{1}H-NMR, RP-HPLC or HRMS. When formic acid was used as the reducing agent, the reaction was heated to 150°C in an oil bath and the samples were prepared similarly to the previous method.

After completion of the reaction, the mixture was applied to a TLC (Alugram Xtra SIL G/UV) using MeOH:EtOAc 5:1 as running phase and the plates were visualized at 260 nm. To extract the dimethylated compound, the silica from the TLC plate was removed and flushed with CD3OD. Finally, the sample was collected and analysed using 1H-NMR. ^{1}H-NMR.

References

(1)   Studier, F. W. Protein Production by Auto-Induction in High Density Shaking Cultures. *Protein Expr Purif* **2005**, *41* (1), 207–234. https://doi.org/10.1016/J.PEP.2005.01.016.

(2)   Studier, F. W. T7 Expression Systems for Inducible Production of Proteins from Cloned Genes in E. Coli. *Curr Protoc Mol Biol* **2018**, *124* (1). https://doi.org/10.1002/cpmb.63.

(3)   Beer. Bestimmung Der Absorption Des Rothen Lichts in Farbigen Flüssigkeiten. *Ann Phys* **1852**, *162* (5), 78–88. https://doi.org/10.1002/andp.18521620505.

(4)   Schneider, C. A.; Rasband, W. S.; Eliceiri, K. W. NIH Image to ImageJ: 25 Years of Image Analysis. *Nat Methods* **2012**, *9* (7), 671–675. https://doi.org/10.1038/NMETH.2089.

(5)   Schindelin, J.; Arganda-Carreras, I.; Frise, E.; Kaynig, V.; Longair, M.; Pietzsch, T.; Preibisch, S.; Rueden, C.; Saalfeld, S.; Schmid, B.; Tinevez, J. Y.; White, D. J.; Hartenstein, V.; Eliceiri, K.; Tomancak, P.; Cardona, A. Fiji: An Open-Source Platform for Biological-Image Analysis. *Nat Methods* **2012**, *9* (7), 676–682. https://doi.org/10.1038/NMETH.2019.

(6)   Bisswanger, H. Enzyme Assays. *Perspect Sci (Neth)* **2014**, *1* (1–6), 41–55. https://doi.org/10.1016/J.PISC.2014.02.005.

(7)   Cerioli, L.; Planchestainer, M.; Cassidy, J.; Tessaro, D.; Paradisi, F. Characterization of a Novel Amine Transaminase from Halomonas Elongata. *J Mol Catal B Enzym* **2015**, *120*, 141–150. https://doi.org/10.1016/j.molcatb.2015.07.009.

(8)   Roura Padrosa, D.; Benítez-Mateos, A. I.; Calvey, L.; Paradisi, F. Cell-Free Biocatalytic Syntheses of l -Pipecolic Acid: A Dual Strategy Approach and Process Intensification in Flow. *Green Chemistry* **2020**, *22* (16), 5310–5316. https://doi.org/10.1039/D0GC01817A.

(9)   Contente, M. L.; Pinto, A.; Molinari, F.; Paradisi, F. Biocatalytic *N* -Acylation of Amines in Water Using an Acyltransferase from *Mycobacterium Smegmatis*. *Adv Synth Catal* **2018**, *360* (24), 4814–4819. https://doi.org/10.1002/adsc.201801061.

(10)   Maghraby, Y. R.; El-Shabasy, R. M.; Ibrahim, A. H.; Azzazy, H. M. E. S. Enzyme Immobilization Technologies and Industrial Applications. *ACS Omega* **2023**, *8* (6), 5184–5196. https://doi.org/10.1021/ACSOMEGA.2C07560/ASSET/IMAGES/LARGE/AO2C07560_0003.JPEG.

(11)   Mateo, C.; Abian, O.; Fernández-Lorente, G.; Pedroche, J.; Fernández-Lafuente, R.; Guisan, J. M.; Tam, A.; Daminati, M. Epoxy Sepabeads: A Novel Epoxy Support for Stabilization of Industrial Enzymes via Very Intense Multipoint Covalent Attachment. *Biotechnol. Progr.* **2002**, *18* (3), 629–634. https://doi.org/10.1021/bp010171n.

(12)   Mateo, C.; Grazu, V.; Palomo, J. M.; Lopez-Gallego, F.; Fernandez-Lafuente, R.; Guisan, J. M. Immobilization of Enzymes on Heterofunctional Epoxy Supports. *Nature Protocols 2007 2:5* **2007**, *2* (5), 1022–1033. https://doi.org/10.1038/nprot.2007.133.

(13)   Cassimjee, K. E.; Federsel, H. J. EziG: A Universal Platform for Enzyme Immobilisation. *RSC Catalysis Series* **2018**, *2018-January* (29), 345–362. https://doi.org/10.1039/9781782629993-00345.

Influence of reaction conditions on enzymatic

enantiopreference: the curious case of HewT in the

synthesis of THF-amine

4.1 Aim of the Project

In biocatalysis, enzymatic enantiopreference stands out as a crucial feature. This project focuses on a deep exploration of this phenomenon, with a specific emphasis on the synthesis of small cyclic compounds as 3-aminotetrahydrofuran (THF-amine).[1] The primary enzyme of interest is the (*S*)-selective transaminase from *Halomonas elongata (*HeWT) which displayed a dynamic of enantiopreference in dependence of the reaction conditions during the synthesis of 3-aminotetrahydrofuran (THF-amine).[2] Furthermore, we explored the impact of varying additives, *e.g.* ionic strength and co-solvent content in the reaction mixture. Our goal is to discern how these factors can be manipulated to optimize enzymatic enantiopreference, thereby enhancing the efficiency and specificity of biocatalytic synthesis.

The work presented in this chapter has been published in: "Heckmann CM, Robustini L, Paradisi F. Influence of Reaction Conditions on Enzymatic Enantiopreference: the Curious Case of HEwT in the Synthesis of THF-Amine. Chembiochem. 2022 Aug 3;23(15):e202200335. doi: 10.1002/cbic.202200335. Epub 2022 Jul 1"

4.2 Introduction

Enantioselectivity stands as a main advantage within the field of biocatalysis, often addressed as a point of contrast when compared to canonical synthetic synthesis.[3] This inherent characteristic, spread among the majority of biological catalysts, serves as a powerful tool in overcoming laborious separations and facilitates straightforward reaction workup under mild conditions.[4] Of major importance is the downstream purification process, where the extraction of the desired product from contaminants, including heavy metals, side-products, solvents, and undesired stereoisomers, significantly influences the overall cost of a chemical process [5] This becomes particularly critical in the production of Active Pharmaceutical Ingredients (APIs)[6–8] and in industries such as fragrances, where variations in enantiomers impart distinct active and olfactive properties, influencing characteristics such as biological response or intensity (Figure 4.1). [9,10]
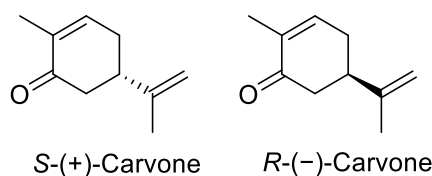
S-(+)-Carvone   R-(−)-Carvone

Figure 4.1 Example of enantiomers with distinct characteristics. To the left, *S*-(+)-carvone exudes a mentholated, spicy aroma complemented by bready notes of moderate intensity. On the right, *R*-(-)-carvone presents a medium-strength fragrance characterized by herbal, minty, and sweetish undertones.[11]

In the production of chiral amines, crucial components in many active pharmaceutical ingredients, conventional chemical catalysts often struggle to achieve significant enantiomeric excess (*ee*), especially when dealing with aliphatic amines. In contrast, a broad group of enzymes exhibits remarkable ability in synthesizing chiral amines with exceptional enantioselectivity. [12–14]

Among these enzymes, ω-transaminases (TAs) represent a prominent class, facilitating the formal reductive amination of pro-chiral ketones by utilizing a sacrificial amine donor that undergoes oxidation to the carbonyl state.[15]

4.2.1 *Halomonas elongata* transaminase (HeWT)

ω-Transaminases (ω-TAs) are pyridoxal-5'-phosphate (PLP)-dependent enzymes known for their key role in catalysing the formal reductive amination of prochiral substrates. This process involves the conversion of ketones into their corresponding chiral amines, with a well-established mechanism.[16–18] TAs typically demonstrate high enantioselectivity, often yielding only one detectable enantiomer, attributed to steric discrimination facilitated by a small and a large binding pocket. [19] In 2015 our group focused on the characterisation of a transaminase from *Halomonas elongata* (HeWT) which established the stereospecificity of this enzyme toward the synthesis of *S*-amines from pro-chiral ketones. [20] In a second study though, during the synthesis of four aliphatic cyclic amines, our group reported some discrepancies (Figure 4.2). In fact, when challenged with the steric discrimination on either face of the pro-chiral cyclic ketone, only moderate enantiomeric excess was achieved. [21]
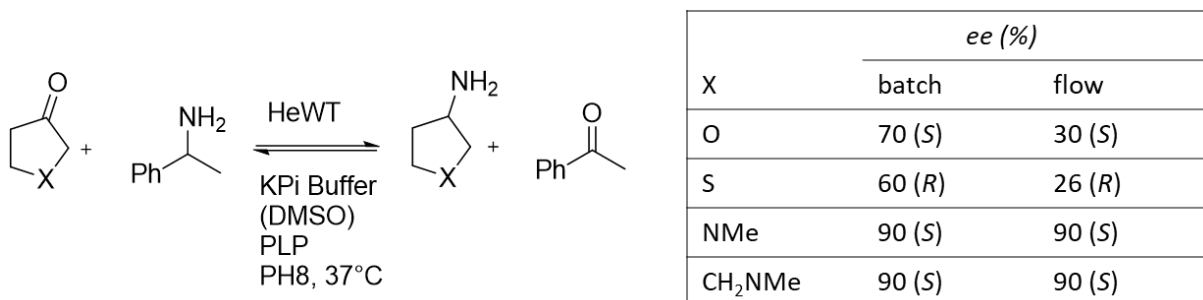
	ee (%)	
X	batch	flow
O	70 (*S*)	30 (*S*)
S	60 (*R*)	26 (*R*)
NMe	90 (*S*)	90 (*S*)
CH$_2$NMe	90 (*S*)	90 (*S*)

Figure 4.2 Previous work involved the synthesis of THF-amine, along with 3-aminotetrahydrothiophene, N-methyl-3-aminopyrrolidine, and N-methyl-3-aminopiperidine, showcasing varying enantiomeric excess (*ees*) in batch versus flow conditions.[21]

In this chapter, the focus is on the synthesis of THF-amine from THF-ketone, utilizing the (*S*)-selective transaminase HeWT, investigating *ees* in batch reactions and their dependence on the specific reaction conditions.

To gain a deeper understanding of this phenomenon, we systematically examined various parameters known to influence the stereoselectivity of a biocatalyst.[22,23] These parameters, such as catalyst loading, reaction temperature and duration, enzyme immobilisation, and substrate loading, would favour the outcome of a thermodynamic rather than a kinetic equilibrium. Similar behaviour has been documented in the past with chiral organo catalysts.[24]
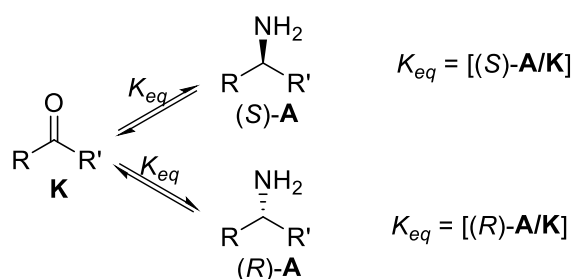

Figure 4.3 Schematic equilibrium for a generic reductive amination: given that both enantiomers share identical thermodynamic properties (standard Gibbs free energy), the equilibrium constants between the prochiral ketone (K) and each enantiomer of the amine (A) are also identical. As both equations possess the same concentration of ketone in the denominator, it requires that the concentration of each enantiomer must be identical for both equilibria to be fulfilled.

72

The formation of the thermodynamic product was monitored over time, as, by definition, it represents the most stable compound, whereas the kinetic product is the one that forms more rapidly.

4.3 Results

4.3.1 Expression and purification of HeWT

The expression of HeWT was performed as reported in Chapter 3.5. The biomass yield was consistent around 15g of cell pellet per litre of culture while the volumetric yield was between 50 and 90 mg of protein per litre of culture. Those results were consistent with previous reports. [25] The purification steps were monitored also *via* 12% SDS PAGE (Figure 4.4).
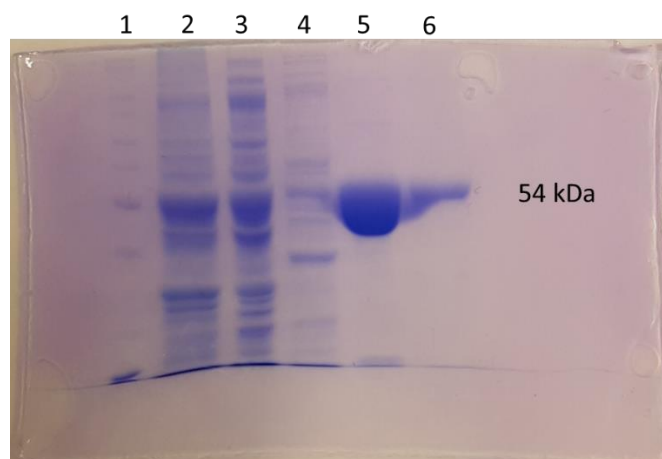

Figure 4.4 12% SDS page of HeWT purification. Lane 1: Ladder; Lane 2: pellet; Lane 3: Crude Extract; Lane 4: Flow Through; Lane 5: Purified HeWT, Lane 6: Flanking Fraction at lower concentration.

Before each experiment, the specific activity was assessed following standard protocols (see Chapter 3.6) [19] and it ranged between 1.7 to 4.4 U/mg depending on the batch.

4.3.2 Role of amino acceptor in the enantiopreference inversion: kinetic vs. thermodynamic product

The first scenario of the enantiopreference switch was observed at different THF-ketone concentrations: the conversion into (*S*)-THF-amine showed a slight decrease with the

progressive increase of the co-substrate (Table 4.1). Particularly significant is the shift in the enzymatic enantiopreference from (*S*) to (*R*) at the highest substrate concentration when lyophilised cell extract was used. In fact, before each purification step, a specific assay was performed on a sample of the crude extract to have first esteem of its activity. Upon observing the presence of an active biocatalyst in the results, preliminary experiments were conducted using samples of a similar nature.

Scale (mM)	%Conversion[a]	*ee*[b] (%)
10	82±3	11 (*S*)
100	76±1	4 (*R*)
300	54±2	17 (*R*)

[a] Conversion determined by RP-HPLC, following the production of THF-amine (after FMOC derivatization), using a calibration curve ± 1 standard deviation (n=2).
[b] *ee* determined by chiral GC-FID following acetylation.

Table 4.1 Biotransformations employing HeWT for the production of THF-amine. Reactions were conducted on a scale of 10, 100, or 300 mM, comprising HeWT (lyophilized cell-free extract, 50 mg/mL), Isopropyl amine (IPA) (5 eq.), PLP (1 mM), KPi-buffer (50 mM), and DMSO (10%); pH 8. The reactions were allowed to incubate at 30 °C for 48 hours.

To exclude the influence of other enzymes in the crude mixture, biotransformations were set up with a sample of HeWT purified as mentioned above with a good degree of purity (Figure 4.5). It was expected that optimal *ees* would be achieved with shorter reaction times and lower enzyme concentrations, while *ees* were expected to diminish with prolonged reaction times or higher enzyme concentrations. In Figure 4.5 the conversion (on the primary axes) and the *ee* (on the secondary axes) are reported over time and at different enzyme concentrations (Figure 4.5 B-C).
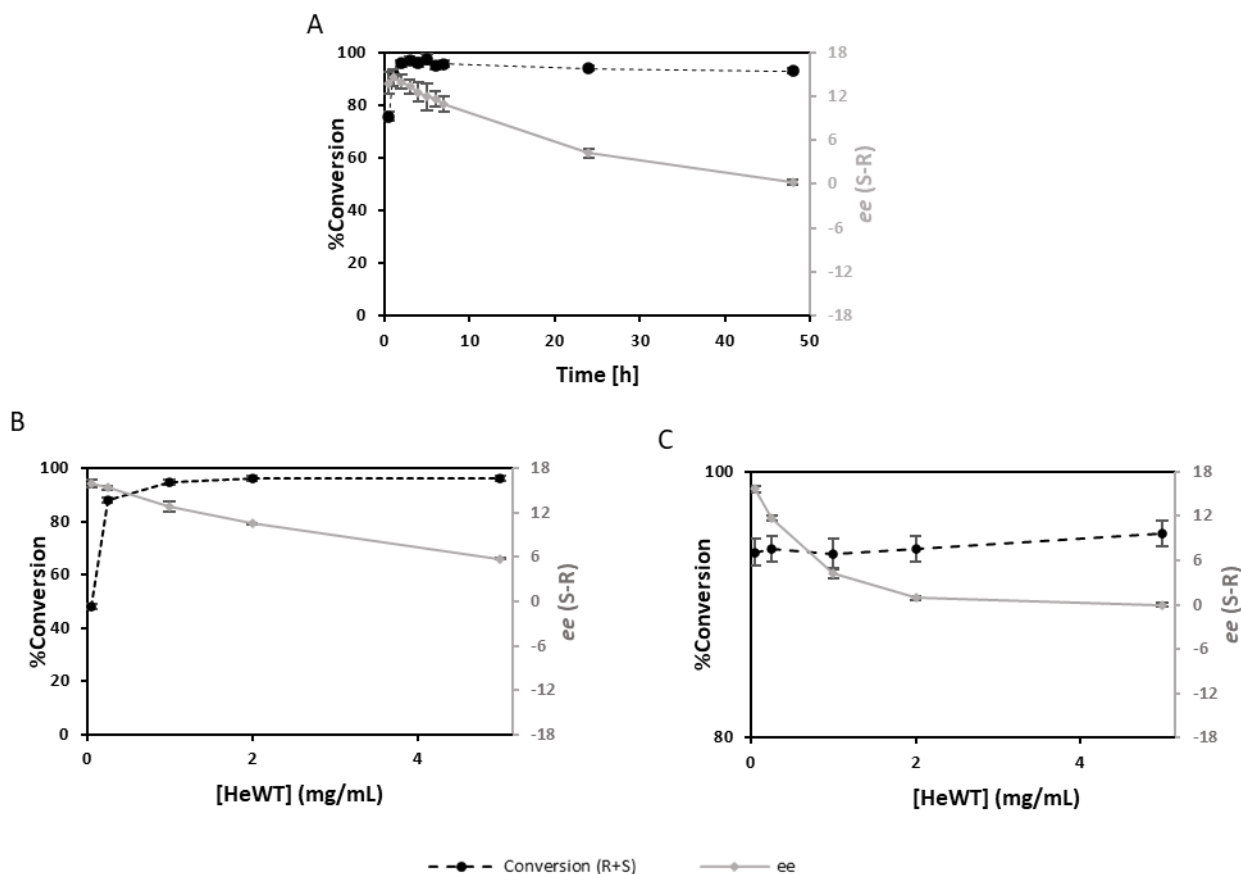
Figure 4.5 Production of THF-amine from THF-ketone over time (A) and in dependence of biocatalysts concentration after 3 hours(B) and 24 hours (C). Biotransformation setup includes THF-ketone (10 mM), (S)-α-methyl benzylamine (SMBA) (1 eq.), pyridoxal-5-phosphate (PLP) (0.01 eq.) in KPi-buffer (100 mM); pH 8, 30 °C. In (A), the concentration of HeWT is maintained at 1 mg/mL. Conversions determined by chiral RP-HPLC, after FMOC-derivatization.

Even if the switch in enantiopreference was indeed reported at higher reaction times and concentration, the maximum *ee*s obtained under those conditions were approximately 56% (*S*). Hence, it seemed improbable that these effects alone are sufficient to justify the observed spectrum of *ee*s seen previously. The use of a purified enzyme at increasing substrate concentrations was supposed to promote the formation of the kinetic product with high *ee* for the (*S*)-enantiomer. However, our observations contradict this hypothesis (Figure 4.6).
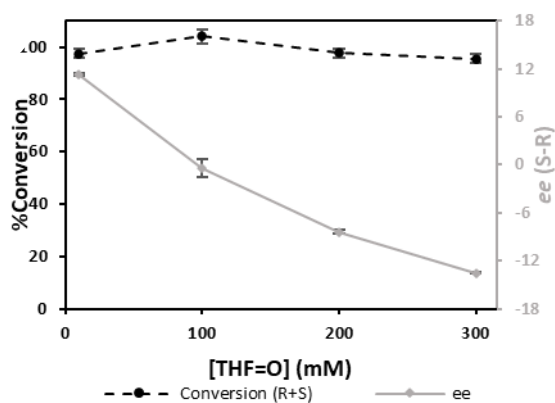
Figure 4.6 The production of THF-amine from THF-ketone (THF=O) at increasing substrate concentrations, in biotransformations containing IPA (5 eq.), and purified HeWT (0.72 mg/mL). Samples taken after 3 h.

4.3.3 Impact of co-substrates

Having excluded thermodynamic effects and the synergic action of other enzymes in the crude as potential sources for this phenomenon, our attention was redirected to how the reaction environment influences the enantiopreference of the enzyme. Previous studies have indicated that the enantioselectivity of lipases and proteases can be influenced by the polarity of the organic solvent and its water content when these enzymes are employed in organic media, resulting in an inversion in enantioselectivity.[25–27] To establish whether the observed behaviour in HeWT is the result of the increased concentration of one of the substrates, we ran two sets of reactions, maintaining constant concentrations of the respective co-substrate. Figure 4.7 shows how raising the THF-ketone concentration from 10 to 300 mM (with fixed IPA at 50 mM) maintains the enantiopreference for the (*S*)-enantiomer with minor fluctuations. On the other side, varying IPA from 50 to 1500 mM (with THF-ketone fixed at 100 mM) results in the same switching behaviour observed when both substrates were changed proportionally.
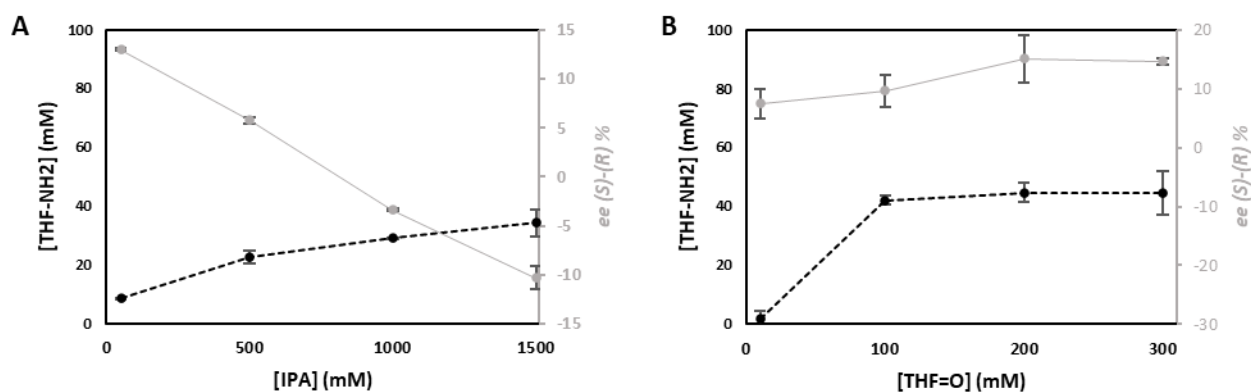
Figure 4.7 A: The synthesis of THF-amine from increasing concentrations of IPA in biotransformations containing a fixed concentration of THF-ketone (100 mM) B: Synthesis of THF-amine from increasing concentrations of THF-ketone (THF=O) was investigated (fix concentrations IPA at 50mM). The reaction set up contained purified HeWT (1 mg/mL), 0.1 mM PLP in KPi buffer 100 mM pH 8. Samples were collected after 3 hours.

4.3.4 Effect of pH

As described in other studies, the optimal pH for HeWT is between 8 and 9. [20] In fact, as shown in Figure 4.8, full conversion is reached indeed at these values, and it decreases progressively at pH 11 with a conversion dropping to 48%. Notably, the enantiopreference is enhanced at higher pH values (Figure 4.8). The protonation/deprotonation status of the residues within the active site directly influences the affinity for the substrate, and under these conditions, the (*S*)-enantiomer is the preferred configuration.
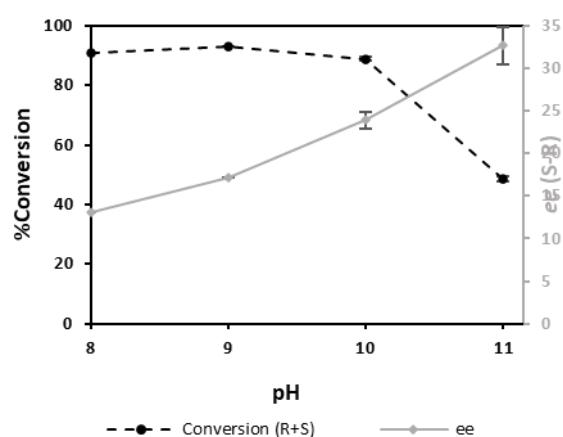

Figure 4.8 The production of THF-amine from THF-ketone (THF=O) in biotransformations containing THF-ketone (10 mM), SMBA (1 eq.), purified HeWT (1mg/mL), PLP (1 mM), and KPi-buffer (100 mM. pH 8-11. Samples taken after 3 h. All reactions were carried out at 30 °C.

In previous *in silico* investigations, it was proposed that the enantioselectivity of HeWT in relation to this substrate could be explained by the hydrogen bonding between the oxygen of the ring and tryptophan 56, as the substrate gets in the active site (Figure 4.9).[21] The docking analysis revealed that the neighbouring C (yellow) faces the active site entrance and may potentially interact with the solvent. A competition for hydrogen bonding between THF-ketone and the co-substrate (*i.e.,* with IPA, which is protonated at pH 8 with a pK_a of 10.63)[28] could promote the entry of the substrate into the active site in a "C5-first" fashion rather than "oxygen-first," hence promoting the production of (*R*)-THF-amine. However, other aspects should be considered: alterations in the enzyme structure due to increased organic solvent content or elevated ionic strength might preferentially lead to the production of the (*R*)-enantiomer.
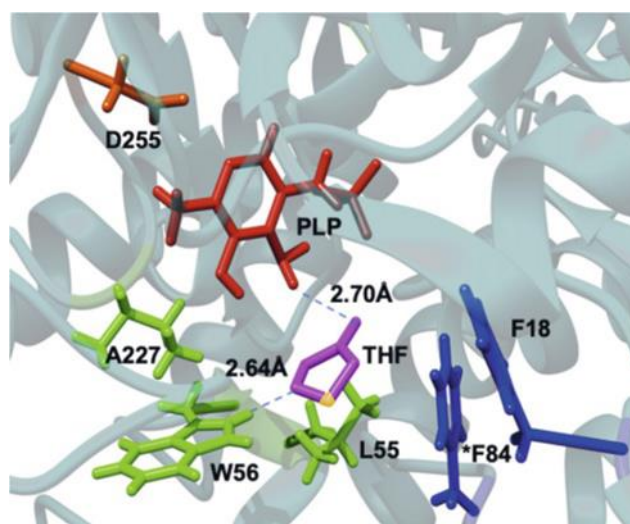

Figure 4.9: Docking of THF-ketone into the entrance of the active site of wild-type HeWT, showing the hydrogen bond to W56. Figure reproduced from ref.[21] (CC BY 4.0 license).

4.3.5 Effect of Additives

To differentiate between the impact of hydrogen bonding, organic solvent content, and ionic strength and the effect they might have on HeWT enantiopreference, experiments were set up using (*S*)-methylbenzylamine (SMBA) as the amino donor. Varying concentrations of different additives such as isopropyl alcohol (^{i}PrOH), NaCl, and NH$_4$Cl were screened to understand each condition separately.

i. Addition of Isopropyl alcohol

The addition of [i]PrOH was used to confirm or exclude the possibility that the switch is induced by the conformational characteristics of the co-substrate. In fact, [i]PrOH is a weaker hydrogen bond donor than protonated IPA, with a comparable size and structure. In Figure 4.10, it can be noted that the enantiopreference of HeWT is enhanced at higher concentrations of co-solvent, and at 5M the *ee* of the resulting amine goes from 62 (50 mM [i]PrOH) to 79% (*S*).
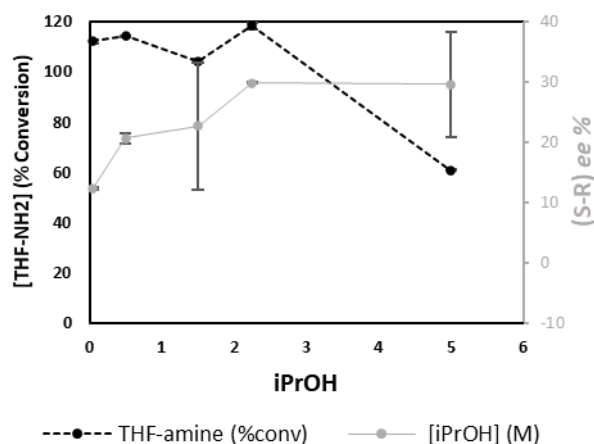

Figure 4.10 Production of THF-amine from THF-ketone (THF=O) at different concentrations of [i]PrOH: 0.05-5M. Biotransformations containing THF-ketone (10 mM), SMBA (1 eq.), purified HeWT (0.25 mg/mL), PLP (0.1 mM), and KPi-buffer (50 mM); pH8. Samples taken after 3 hours. n=2

These results indicate that the [i]PrOH is not inducing any inversion of enantiopreference, therefore the structural conformation of the biocatalyst does not appear to be the reason that triggers such behaviour.

ii. Addition of NaCl

The choice of NaCl as an additive is primarily driven by the need to increase ionic strength without altering the concentration of hydrogen bond donors or organic solvent content. The ratio of the two enantiomers was observed with respect to the rising concentration of NaCl, ranging from 10 mM to 3 M. In this test, the *ee* of the (*S*)-enantiomer was 13% at a low salt concentration, shifting in favour of the (*R*)-enantiomer, reaching a maximum *ee* of 76% at 3 M (Figure 4.11)
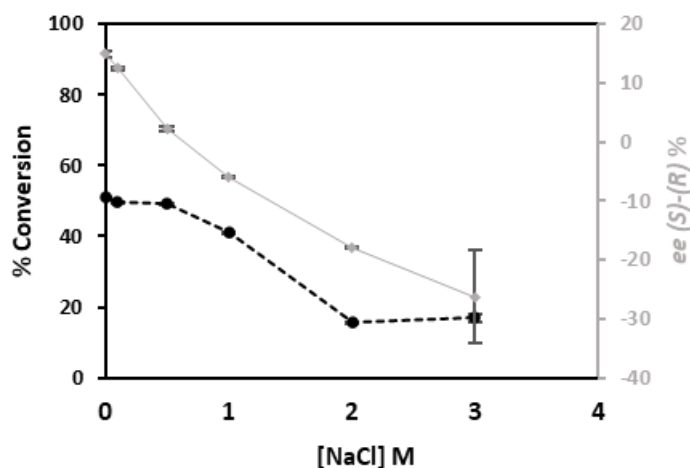
Figure 4.11 Production of THF-amine from THF-ketone (THF=O) at different concentrations of NaCl (0.01 to 3 M). Biotransformations containing THF-ketone (10 mM), SMBA (1 eq.), purified HeWT (0.25 mg/mL), PLP (0.1 mM), and KPi-buffer (50 mM); pH8. Samples taken after 3 hours. n=2

iii. Addition of NH₄Cl

Ammonium chloride (NH₄Cl), despite having a lower pK_a than IPA (9.21 instead of 10.63), is still protonated at pH 8 and is expected to provide a comparable hydrogen bond donor capacity to IPA, while avoiding an increase in organic solvent content. Therefore, similarly to what was done in the previous experiment, we monitored the *ee* at concentrations of NH₄Cl between 50mM and 1.5M. Results are depicted in Figure 4.12.
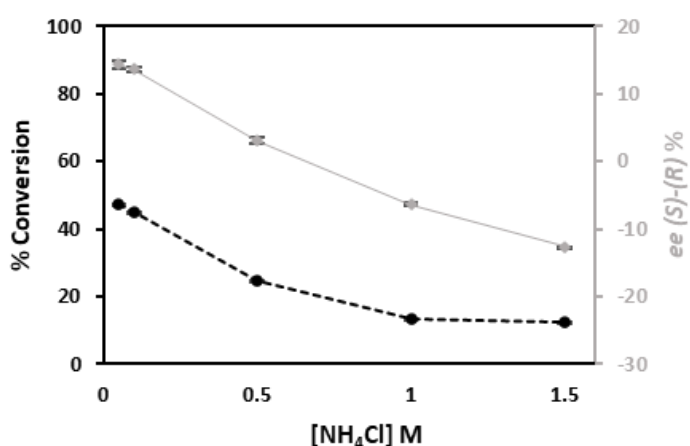

Figure 4.12 Production of THF-amine from THF-ketone (THF=O) at different concentrations of NH₄Cl (50 mM to 1.5M). Biotransformations containing THF-ketone (10 mM), SMBA (1 eq.), purified HeWT (0.25 mg/mL), PLP (0.1 mM), and KPi-buffer (50 mM); pH8. Samples taken after 3 hours. n=2

As observed before, the enantiopreference shifts from (*S*) to (*R*) progressively at increasing concentrations of NH$_4$Cl: from 54 % (*S*) at 50 mM to 64% (*R*) at 1.5 M. This result shows that the ability of the environment to induce hydrogen bond, is a key factor for the prevalence of one enantiomer over the other.

4.3.6 Screening Different Co-substrate

Another aspect to investigate was whether employing other co-substrates would trigger a similar behaviour. The inversion in enantiopreference is already seen when either IPA or SMBA is used as the amino donor. However, due to the substrate inhibition by the latter, [20] it was not possible to increase its concentration while keeping THF-ketone constant, as it was done with IPA. Therefore cadaverine was also tested. Cadaverine is a small diamine categorized as a "smart amino-donor" due to its ability to cyclise and therefore to significantly shift the reaction equilibrium. In 2016, such small molecules were effectively utilized in challenging transamination reactions, resulting in high conversion rates and no by-products.[29] The screening was done at 3 different concentrations: 50, 100, and 250 mM, while the amino acceptor (THF-ketone) was kept constant at 100 mM. The results showed the same trend: the product, initially with a dominance of the (*S*)-enantiomer at 50 mM, progressively shifted to a racemic mixture at higher concentrations (250 mM) (Figure 4.13-A). In analogy to this experiment, the effect of an alternative amino acceptor was also investigated. The setup of the reaction consisted of increasing concentrations of 2-butanone (and 5 equimolar of isopropyl amine), which was reported to reduce the enantioselectivity of the enzyme at high substrate concentrations (Figure 4.13-B).[30] In contrast to what was obtained with THF-ketone (Figure 4.6), no major shift towards the (*R*)-enantiomer is noted at high substrate concentration, suggesting that the enantioselectivity for butanone, unlike that for THF-ketone, is predominantly influenced by steric factors.
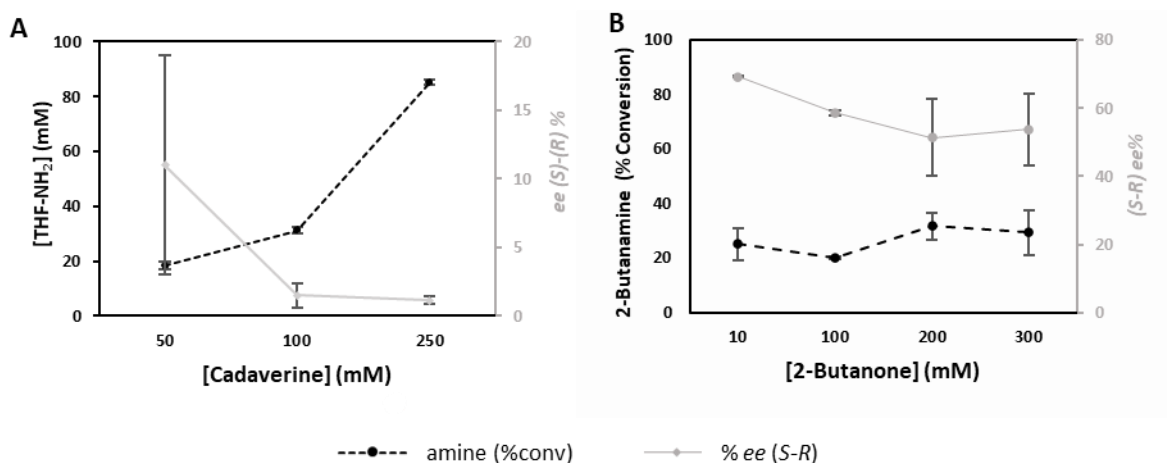
Figure 4.13 A Production of THF-amine from THF-ketone (THF=O) at increasing concentrations of cadaverine (50-250 mM) and fixed concentration of THF-ketone (100 mM). **B**: The production of 2-butanamine from 2-butanone at increasing concentration (2-butanone: 10, 100, 200, 300) and IPA 5eq.. Each biotransformation contains purified HeWT (1 mg/mL), PLP (0.1 mM), KP_i-buffer (50 mM); pH 8, 30 °C Samples taken after 3 h.

4.3.7 Screening Different Co-Solvents

The impact of co-solvent in the reaction, proportionally reducing the water content, was assessed. Having already screened ^{i}PrOH in a previous experiment, we included here dimethyl sulfoxide (DMSO), methanol (MeOH), and acetonitrile (ACN) based on their partition coefficient (*log*P). The biotransformations were performed in standard conditions (THF-ketone 10 mM, SMBA 1 eq., 0.1 mM PLP, in KP_i-buffer (100 mM); pH 8, 30 °C), with the addition of 1.5 M of organic solvent. Figure 4.14 shows that an increase in *log*P aligns with enhanced (*S*)-selectivity, as seen before, however, neither the solvent excluded volume, nor the protic/aprotic nature of the solvent displayed a linear trend. In related research, it was reported that carboligations catalysed by thiamine diphosphate-dependent (TPP) enzymes shows a direct correlation between the spatial hindrance of a solvent and a reduction in (*S*)-enantiopreference, leading to an inversion to (*R*)-selectivity.[31]

This was interpreted as evidence that smaller solvent molecules could obstruct the binding pocket for these enzymes, favouring the binding of the substrate in a flipped orientation. The absence of such size dependency in the present case appears to eliminate the possibility of a direct binding to the active site.
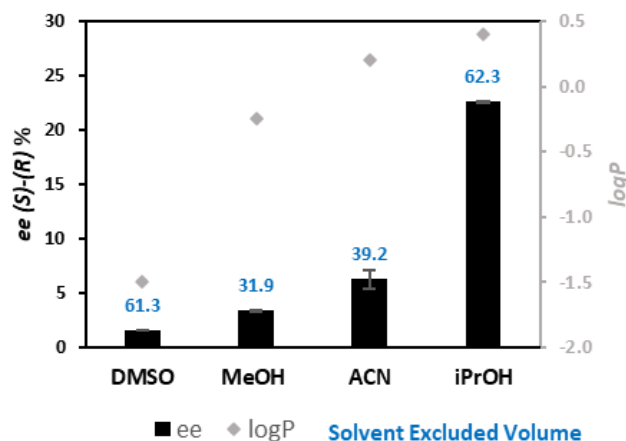
Figure 4.14 Influence of diverse co-solvents on the enantioselectivity of HeWT in the synthesis of THF amine from THF-ketone. Biotransformations setup: THF-ketone (10 mM), SMBA (1 eq.), purified HeWT (0.25 mg/mL), PLP (0.1 mM) in KPi-buffer (50 mM); pH 8, 30 °C, co-solvents 1.5 M. Samples were collected after 3 hours. In blue, Conolly solvent excluded volume of each solvent (ChemDraw v. 20.0).

4.4 Conclusions

While attempting to enhance the previously reported synthesis of THF-amine using HeWT, an unexpected shift in enantiopreference was observed. While this was initially noted with increasing substrate concentrations, it was then determined to be induced also at higher ionic strength of the reaction mixture. Further experiments revealed that an increase in the polarity of the co-solvent corresponds to an increase of the (*S*)-selectivity of the enzyme, whereas increasing the ionic strength induces the (*R*)-enantiopreference. This effect does not seem to relate to the size of the co-solvent molecule, making a direct binding to the active site an improbable explanation for this switch. The effect is likely attributed to structural changes in the enzyme under varying conditions specifically, an increase in the ionic strength of the medium is expected to bolster hydrophobic interactions within the protein structure, while increasing the organic content of the medium would diminish these interactions, hence influencing the overall structure. Notably, a similar effect could not be observed with butanone as amino acceptor, suggesting that the enantiopreference is dominated by steric discrimination within the binding pocket. However, if the enantioselectivity of HeWT is indeed determined by the orientation in which the substrate enters the active site, a direct impact of the reaction medium on that orientation due to solvation effects on the substrate is also possible. Additional research, which includes screening analogous conditions on similar

substrates or those with increased steric hindrance, with a more comprehensive emphasis on enantiopreference, would lead to a deeper understanding of the relationship between the reaction environment and enantiopreference. Moreover, the structure characterisation of the enzyme under varying ionic strengths/organic solvent content, circular dichroism spectroscopy, and point mutations, with a special focus on W56, will help to get a better insight into the conformation under different conditions. Additionally, molecular dynamic simulations can provide further insights into the trajectory and interactions with solvent/residues of THF-ketone as it enters the active site. Possible applications include the identification of key factors influencing enzymatic enantiopreference, the establishment of protocols for controlled inversion or alteration of enantiopreference, and the development of optimized conditions for the biocatalytic synthesis of pharmaceutically relevant chiral amines using (*S*)-selective ω-transaminases. Beyond these practical advancements, the project holds significance in contributing to the broader knowledge of enzymatic processes, thereby opening the way for innovations in biocatalysis and green chemistry.

References

(1) Heckmann, C. M.; Robustini, L.; Paradisi, F. Influence of Reaction Conditions on Enzymatic Enantiopreference: The Curious Case of HEwT in the Synthesis of THF-Amine. *ChemBioChem* **2022**, *23* (15). https://doi.org/10.1002/cbic.202200335.

(2) Hegarty, E.; Paradisi, F. Implementation of Biocatalysis in Continuous Flow for the Synthesis of Small Cyclic Amines. *Chimia (Aarau)* **2020**, *74* (11), 890. https://doi.org/10.2533/chimia.2020.890.

(3) Enders, D.; Jaeger, K. E. Asymmetric Synthesis with Chemical and Biological Methods. *Asymmetric Synthesis with Chemical and Biological Methods* **2007**, 1–441. https://doi.org/10.1002/9783527610648.

(4) Winkler, C. K.; Schrittwieser, J. H.; Kroutil, W. Power of Biocatalysis for Organic Synthesis. *ACS Cent Sci* **2021**, *7* (1), 55–71. https://doi.org/10.1021/ACSCENTSCI.0C01496.

(5) van Schie, M. M. C. H.; Spöring, J. D.; Bocola, M.; Domínguez de María, P.; Rother, D. Applied Biocatalysis beyond Just Buffers – from Aqueous to Unconventional Media. Options and Guidelines. *Green Chemistry* **2021**, *23* (9), 3191–3206. https://doi.org/10.1039/D1GC00561H.

(6) McConathy, J.; Owens, M. J. Stereochemistry in Drug Action. *Prim Care Companion CNS Disord* **2003**, *5* (2). https://doi.org/10.4088/PCC.v05n0202.

(7) Yan, J.; Xiang, B.; Wang, D.; Tang, S.; Teng, M.; Yan, S.; Zhou, Z.; Zhu, W. Different Toxic Effects of Racemate, Enantiomers, and Metabolite of Malathion on HepG2 Cells Using High-Performance Liquid Chromatography–Quadrupole–Time-of-Flight-Based Metabolomics. *J Agric Food Chem* **2019**, *67* (7), 1784–1794. https://doi.org/10.1021/acs.jafc.8b04536.

(8) Kumar, V.; Bansal, V.; Madhavan, A.; Kumar, M.; Sindhu, R.; Awasthi, K.; Binod, P.; Saran, S. Active Pharmaceutical Ingredient (API) Chemicals: A Critical Review of Current Biotechnological Approaches. **2022**. https://doi.org/10.1080/21655979.2022.2031412.

(9)   Caillet, C.; Chauvelot-Moachon, L.; Montastruc, J.-L.; Bagheri, H. Safety Profile of Enantiomers *vs* . Racemic Mixtures: It's the Same? *Br J Clin Pharmacol* **2012**, *74* (5), 886–889. https://doi.org/10.1111/j.1365-2125.2012.04262.x.

(10)   Bentley, R. The Nose as a Stereochemist. Enantiomers and Odor. *Chem Rev* **2006**, *106* (9), 4099–4112. https://doi.org/10.1021/cr050049t.

(11)   Turin, L. *The Secret of Scent: Adventures in Perfume and the Science of Smell*; Ecco; Reprint edition (October 23, 2007), 2006.

(12)   Patil, M. D.; Grogan, G.; Bommarius, A.; Yun, H. Oxidoreductase-Catalyzed Synthesis of Chiral Amines. *ACS Catal* **2018**, *8* (12), 10985–11015. https://doi.org/10.1021/ACSCATAL.8B02924.

(13)   Breuer, M.; Ditrich, K.; Habicher, T.; Hauer, B.; Keßeler, M.; Stürmer, R.; Zelinski, T. Industrial Methods for the Production of Optically Active Intermediates. *Angewandte Chemie - International Edition* **2004**, *43* (7), 788–824. https://doi.org/10.1002/ANIE.200300599.

(14)   Ghislieri, D.; Turner, N. J. Biocatalytic Approaches to the Synthesis of Enantiomerically Pure Chiral Amines. https://doi.org/10.1007/s11244-013-0184-1.

(15)   Slabu, I.; Galman, J. L.; Lloyd, R. C.; Turner, N. J. Discovery, Engineering, and Synthetic Application of Transaminase Biocatalysts. *ACS Catal* **2017**, *7* (12), 8263–8284. https://doi.org/10.1021/ACSCATAL.7B02686.

(16)   Van Oosterwijk, N.; Willies, S.; Hekelaar, J.; Terwisscha Van Scheltinga, A. C.; Turner, N. J.; Dijkstra, B. W. Structural Basis of the Substrate Range and Enantioselectivity of Two (S)-Selective ω-Transaminases. **2016**. https://doi.org/10.1021/acs.biochem.6b00370.

(17)   Schiroli, D.; Peracchi, A. A Subfamily of PLP-Dependent Enzymes Specialized in Handling Terminal Amines. *Biochimica et Biophysica Acta (BBA) - Proteins and Proteomics* **2015**, *1854* (9), 1200–1211. https://doi.org/10.1016/j.bbapap.2015.02.023.

(18)   Kwon, S.; Ho Park, H. Structural Consideration of the Working Mechanism of Fold Type I Transaminases From Eubacteria: Overt and Covert Movement. **2019**. https://doi.org/10.1016/j.csbj.2019.07.007.

(19)   Mutti, F. G.; Fuchs, C. S.; Pressnitz, D.; Sattler, J. H.; Kroutil, W. Stereoselectivity of Four (R)-Selective Transaminases for the Asymmetric Amination of Ketones. *Adv Synth Catal* **2011**, *353* (17), 3227–3233. https://doi.org/10.1002/ADSC.201100558.

(20)   Cerioli, L.; Planchestainer, M.; Cassidy, J.; Tessaro, D.; Paradisi, F. Characterization of a Novel Amine Transaminase from Halomonas Elongata. *J Mol Catal B Enzym* **2015**, *120*, 141–150. https://doi.org/10.1016/j.molcatb.2015.07.009.

(21)   Hegarty, E.; Paradisi, F. Implementation of Biocatalysis in Continuous Flow for the Synthesis of Small Cyclic Amines. *Chimia (Aarau)* **2020**, *74* (11), 890. https://doi.org/10.2533/chimia.2020.890.

(22)   Causevic, A.; Gladkauskas, E.; Olofsson, K.; Adlercreutz, P.; Grey, C. Impact of Critical Parameters Influencing Enzymatic Production of Structured Lipids Using Response Surface Methodology with Water Activity Control. *Biochem Eng J* **2022**, *187*, 108610. https://doi.org/10.1016/j.bej.2022.108610.

(23)   Raczyńska, A.; Jadczyk, J.; Brzezińska-Rodak, M. Altering the Stereoselectivity of Whole-Cell Biotransformations via the Physicochemical Parameters Impacting the Processes. *Catalysts* **2021**, *11* (7), 781. https://doi.org/10.3390/catal11070781.

(24)   Rulli, G.; Duangdee, N.; Baer, K.; Hummel, W.; Berkessel, A.; Gröger, H. Direction of Kinetically versus Thermodynamically Controlled Organocatalysis and Its Application in Chemoenzymatic Synthesis. *Angewandte Chemie International Edition* **2011**, *50* (34), 7944–7947. https://doi.org/10.1002/anie.201008042.

(25)   Kawashiro, K.; Sugahara, H.; Sugiyama, S.; Hayashi, H. Effects of Water Content on the Enantioselectivity of α-Chymotrypsin Catalysis in Organic Media. *Biotechnol Lett* **1995**, *17* (11), 1161–1166. https://doi.org/10.1007/BF00128378.

(26)   Kawashiro, K.; Sugahara, H.; Tsukioka, T.; Sugiyama, S.; Hayashi, H. Effect of Ester Moiety of Substrates on Enantioselectivity of Protease Catalysis in Organic Media. *Biotechnol Lett* **1996**, *18* (12), 1381–1386. https://doi.org/10.1007/BF00129339.

(27)   Riva, S. Laccases: Blue Enzymes for Green Chemistry. *Trends Biotechnol* **2006**, *24* (5), 219–226. https://doi.org/10.1016/j.tibtech.2006.03.006.

(28) Hall, Jr. , H. K. Additions and Corrections - Correlation of the Base Strength of Amines. *J Am Chem Soc* **1964**, *86* (24), 5709–5709. https://doi.org/10.1021/ja01078a602.

(29) Gomm, A.; Lewis, W.; Green, A. P.; O'Reilly, E. A New Generation of Smart Amine Donors for Transaminase-Mediated Biotransformations. *Chemistry - A European Journal* **2016**, *22* (36), 12692–12695. https://doi.org/10.1002/chem.201603188.

(30) Heckmann, C. M.; Dominguez, B.; Paradisi, F. Enantio-Complementary Continuous-Flow Synthesis of 2-Aminobutane Using Covalently Immobilized Transaminases. **2021**. https://doi.org/10.1021/acssuschemeng.0c09075.

(31) Gerhards, T.; MacKfeld, U.; Bocola, M.; Lieres, E. Von; Wiechert, W.; Pohl, M.; Rother, D. Influence of Organic Solvents on Enzymatic Asymmetric Carboligations. *Adv Synth Catal* **2012**, *354* (14–15), 2805–2820. https://doi.org/10.1002/ADSC.201200284.

A Cage Protein for Encapsulated Biocatalysts –

Tackling the downside of the Immobilisation

5.1 Aim of the Project

Our primary objective revolved around the design and optimisation of a methodology that would combine the advantages associated with an immobilized biocatalyst, such as enhanced stability and reduced product inhibition, with a higher catalytic activity typical of free enzymes. As introduced in Chapter 1.1, one of the major drawbacks of the immobilisation is the loss of activity resulting from the distortion to the quaternary structure and rigidification of the enzyme. In this work we investigated the potential application of encapsulin from *Mycolicybacterium hassiacum* (MhEnc) as a protective shell for a transaminase (HeWT) and a pyrroline-2-carboxylate reductase (HeP5CR) from *Halomonas elongata* to act as an intercalator between the enzyme structure and the support. We aimed in this way to retain the original activity of the free enzyme, while benefiting from the advantages of an immobilized biocatalyst, such as extended stability and reusability (Figure 5.1).

Furthermore, we assessed the ability of the encapsulin structure to confer structural protection of the encapsulated proteins from additives, such as organic solvents, surfactants, and salts.
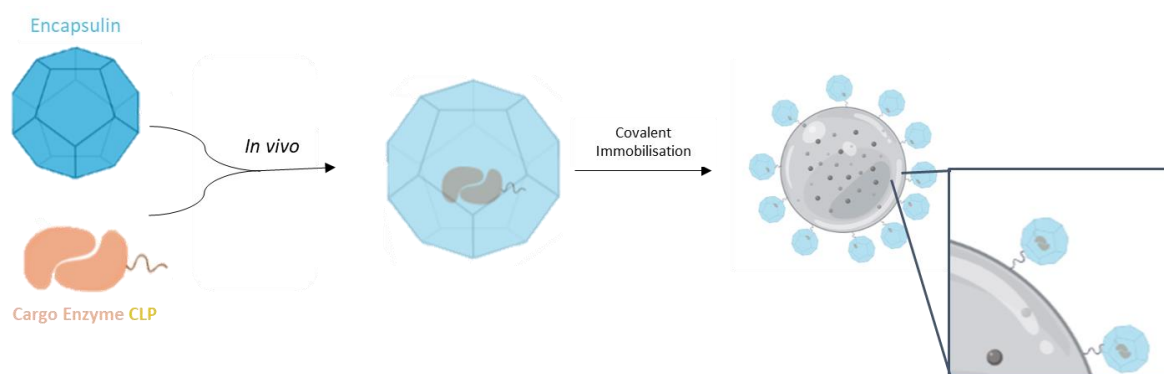

Figure 5.1 Expression, encapsulation and immobilisation of a Cargo Enzyme inside MhEnc. By providing a proteinaceous shell to the biocatalyst, our objective is to mitigate the structural distortions that typically arise when enzymes are directly covalently immobilized onto solid supports.

5.2 Introduction

The use of covalently immobilized biocatalysts for biocatalytic transformations offers distinct advantages, particularly in the context of industrial scale-up. Despite significant progress in the development of this technique, certain limitations persist.

Covalent immobilization induces structural constraints on enzymes, leading to reduced flexibility and, consequently, diminished specific activity compared to native enzymes. [1–3] Various strategies, including the formation of aggregates (CLEAs), affinity immobilization, adsorption (potentially coated with polymers), and entrapment, have been explored to address these challenges.

While some of these approaches demonstrate improved retained activity, issues such as leaching during longer reaction time or reuse of the immobilised catalyst often arise. [4,5] As mentioned in Chapter 1, an elegant solution to this problem involves the encapsulation of proteins within a vesicle-like structure. One prominent example of this is the use of the bacterial proteins – encapsulins – as nanocompartments for the storage of molecules.

In 1994, Valdés-Stauber et *al.* identified proteinaceous aggregates with a high molecular weight in *Brevidobacterium linens* M18, revealing repetitive subunits of 20 to 30 nm diameters.[6] The compartmentalizing role of this structure became apparent over the next decade, leading to the discovery of multiple encapsulin families with similar features and functions: icosahedral compartments with diameters of approximately 24 to 42 nm with pores of 5–10 Å at the junctures, able to isolate their contents from the cell lumen in simple organisms, such as prokaryotes, which lack a complex compartmentalization system.[6]

This case is an example of how Nature uses proteinaceous structures, named Virus-Like Particles (VLPs) as compartmentalisation strategies. In general, VLPs are structures that mimic the outer shell of viruses in shape and size but lack in pathogenicity as they contain no viral genetic material. Formerly known as linocin-like proteins, encapsulins are a subclass of VLP and have been identified in association with proteins related to oxidative stress, such as ferritin. This interaction results in the oxidation of Fe(II) ions, leading to the storage of insoluble ferrihydrite in nanocompartments, effectively mitigating cytotoxicity. Another example is their association with a dye-decolorizing peroxidase (DyP) derived from *Rhodococcus jostii.*, which catalyse lignin degradation and the resulting toxic products are safely encapsulated preventing harm to the host. [6]

Despite these discoveries, the potential applications of nanocompartments still remained relatively underexplored for an additional decade.[7-8]

5.2.1 Architectural structures

Since their first isolation, more than 6,000 encapsulin-like systems have been identified and classified into different families.[9,10] The most widespread family was identified for the first time in the supernatant of *B. linens* M18. It was described as a homomultimeric bacteriocin with no activity.[6] The general operon structure consists of the gene for the single shell protomer and the cargo protein generally encoded upstream (Figure 5.2). The recruitment of the cargo protein relies on a target peptide (Figure 5.2. red), and such mechanism will be explained in detail the next paragraph. Encapsulins from *Mycobacterium tuberculosis,*[11] *Thermatoga maritima,*[12] and *Mycolicibacterium hassiacum*[13] belong to this family.

Figure 5.2. Schematic representation of an encapsulin operon.

More recently, Fraajie and co-workers identified an operon in *M. hassiacum*, which was found to be dedicated to an encapsulin-cargo system. The gene cluster was found to contain two genes encoding for a putative encapsulin (EncMh, WP_005630281.1) [13] and a putative DyP-type peroxidase (EKF22245.1). The predicted mass of the encapsulin is 29 kDa, and at the *C*-terminal of the DyP there is a 30aa cargo loading peptide (-CLP) **(PPPLPDSEPDREIPADDGSLGIGSLKGTRS)**. The encapsulin structure has been elucidated by X-ray crystallography (PDB: 6I9G) and by cryo-electron microscopy showing the formation of large spherical structures with a 22 nm diameter and 12 pentamers, each made of 5 protein chains (Figure 5.3).
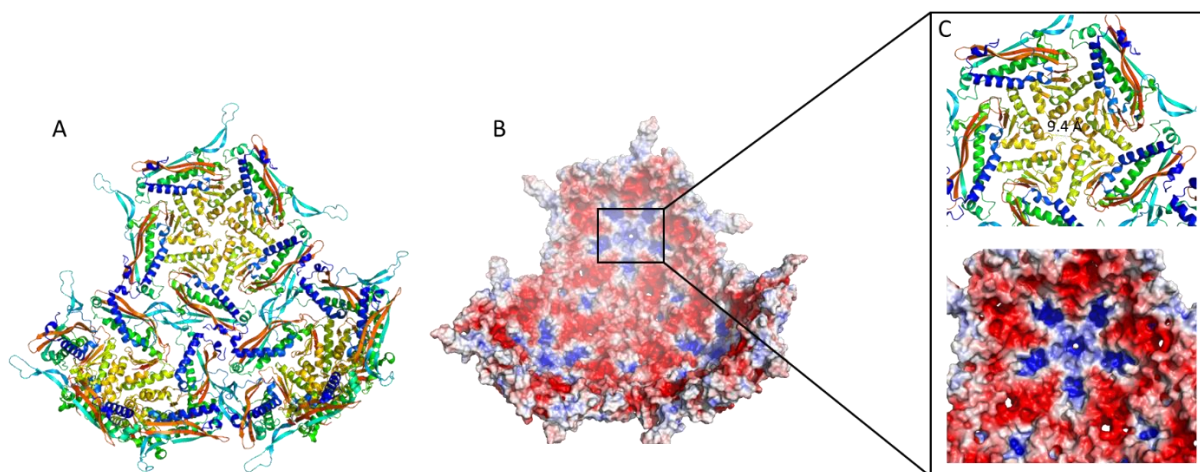
Figure 5.3. Crystal structure (A) and charge display (B) of the encapsuline from *M. hassiacum* (PDB: 6I9G) and a detailed view of the pores (C) at the inner side of the shell. The diameter of the opening is 9.4 Å, similar to that observed in the encapsuline from *T. maritima*. Pictures generated using PyMol software ver. 2.4.1.

A practical example of this application was reported in 2014 by Moon *et al.* [14] The study showcased the practical application of encapsulin as a versatile nanoplatform with the ability to transport therapeutic agents or probes. For instance, it was employed to deliver a cell-specific targeting peptide designed to selectively bind to cell lines associated with Squamous Cell Carcinoma. This finding underscores the adaptability and potential of encapsulin as a promising tool in the targeted delivery of therapeutic payloads or diagnostic probes.[15]

In 2012, Tiago *et al*. sequenced the genome of *M. hassiacum*, highlighting its suitability as a source of heat-stable proteins, given its tolerance to temperatures up to 65 °C.[14] Based on these findings, the group of Fraajie managed to replace the cargo protein associated to the encapsulin from this organism (a DyP gene), with alternative biocatalysts, leveraging the use of the encapsulin shell, thereby enhancing their resistance to degradation to proteinases and to elevated temperatures. The experiment was done on 5 different proteins: a Cu^{2+}- containing laccase and a peroxidase and from *S. viridis* (SviDyP)*;* a catalase from *T. fusca* (TfuCat)*;* a Bayer-Villiger monooxygenase (CHMO); and a small heme-containing protein hemoglobin from *V. stercoraria* (VsHb). After proving the successful encapsulation using SDS-PAGE, they demonstrated resistance of the internalised proteins to proteolysis (the protein was stable up to 25 hours while the unencapsulated SviDyP lost its activity within 30 minutes), increased

activity (due to a molecular crowding effect) and in some of the cases also to higher temperatures.[13,16]

Considering these advantages, we explored the possibility of encapsulating a biocatalyst in the proteinaceous shell to mitigate the effect of structure rigidification upon immobilisation, increase tolerance to co-solvent or harsher operational conditions. At the same time, this strategy aimed to enhance biocatalytic activity by leveraging localized higher substrate concentration.

5.2.2 Cage Self-assemble and Cargo-Protein Recruitment.

As discussed above, the primary function of encapsulin as a nanocompartment is to prevent a particularly toxic compound from inducing damage to the rest of the cell. The inclusion of the cargo protein inside the encapsulin can be achieved through various reported methods, however in most cases, it is accomplished by the encoding of a small tag, which can be either a small peptide(~10 aa) fused to the *C-* or *N-* terminus of the cargo protein or a longer cargo loading peptide (-CLP) of 5 to 30 amino acids in length at the *N-* or *C-* terminus of the cargo protein.[17,18] This peptide is responsible for the electrostatic interactions of the protein with the inner face of the protomers while the shell is self-assembling.

Initially, our investigation into this system involves the use of an enzyme extensively characterized within our research group. Chapter 4 focused on the investigation of the (*S*)-selectivity of ω-transaminase from *Halomonas elongata* (HeWT, DSM 2581), aiming to elucidate the reason for enantiopreference inversion in the amination of small pro-chiral cyclic ketones under varied reaction conditions (presence of co-solvent, alterations in ionic strength, varying substrate concentrations, *etc*). Moreover, we observed that while the highest specific activity for HeWT is measured at 50 °C,[19] the stability of the enzyme diminishes to 90% within 5 minutes of incubation, with the retained activity reaching a maximum of 40%.[20]

In this context, the inactivation of the transaminase could potentially be mitigated through encapsulation as reported by others.[13]

5.3 Results

5.3.1 *H. elongata* as a Cargo Protein

We got the pENC plasmid harbouring the gene for a haemoglobin from *Vitreoscella stercoraria* and the CLP from the group of Fraajie (University of Groeningen). For our interest we required the substitution of the Haemoglobin gene with our transaminase. However, despite several attempts to achieve this, using traditional protocols such as subcloning *hewT* gene into pENC-VsHb, none of them were not successful in our hands.

Figure 5.4 illustrates the map of the pENC-vector, where the -CLP is annotated in pink. In collaboration with Lončar at the University of Groeningen, this was eventually achieved through Golden Gate technology, a technique that by utilizing a series of Type IIS restriction enzymes and DNA ligases allows for the assembly of multiple DNA fragments into a plasmid vector with high efficiency.[21]
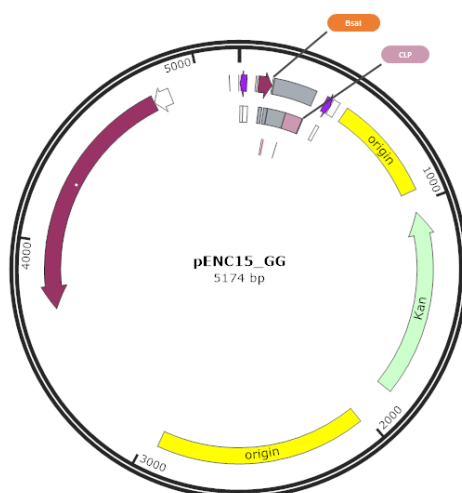

Figure 5.4 The pENC vector map, originating from pET, featuring kanamycin resistance (Kan). The schematic representation highlights the presence of the -CLP in pink, positioned at the C-terminus of a generic gene, with the BsaI restriction site marked in orange. Pictures generated using SnapGene software version 7.0.2.

This construct produced a HeWT variant with the -CLP situated at the *C*-terminus (Figure 5.5a).

To assess the efficacy of the system, the pENC-HeWT-CLP vector was co-transformed with pBAD-Enc (Figure 5.5b) into *E. coli* (BL21-AI One Shot), following a previously described protocol (Chapter 3).
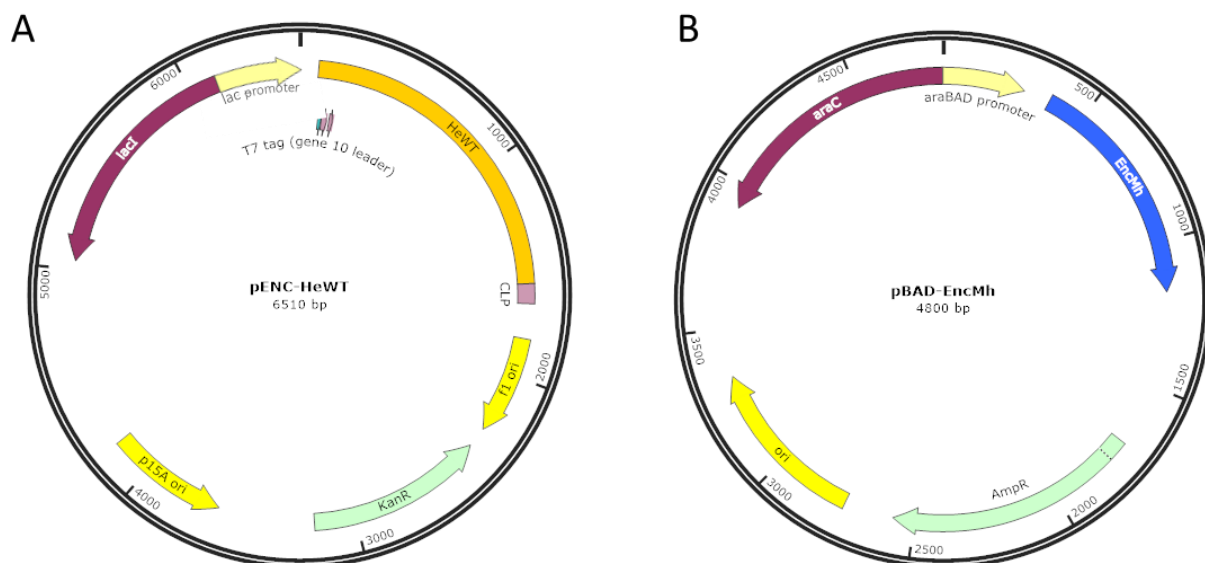
Figure 5.5. (A) Map of the hewT gene, flanked by a 6 x His-Tag at the *N*-terminal (blue) and the -CLP at the *C*-terminal (pink) (HeWT -CLP); (B) Map of MhEnc with *ara* promoter on the left.

Preliminary co-expressions of MhEnc-HeWT screened various growth conditions (see Materials and Methods for details), including culture media (LB, TB, and Auto-Induction) and inducers concentration (arabinose and IPTG). The optimal expression conditions were determined to be in TB medium, inducing encapsulin expression with 1% arabinose, while HeWT-CLP expression was induced with 0.1 mM IPTG. Cultures were incubated at 30 °C for 20 to 24 hours, yielding a biomass yield of 8 g/L of culture (3 g/L for auto-induction).[14] Following sonication, the cell extract is passed through Ni-NTA. In fact, an advantageous feature of the HeWT construct is the presence of both the -CLP and the 6xHis tag, facilitating Ni-NTA purification of the non-encapsulated excess. The overexpression of MhEnc and HeWT was assessed on SDS-PAGE (Figure 5.6) and the non-encapsulated His-tagged HeWT, which was retained in the column, was used as a control in subsequent assays. To purify Enc-HeWT, it

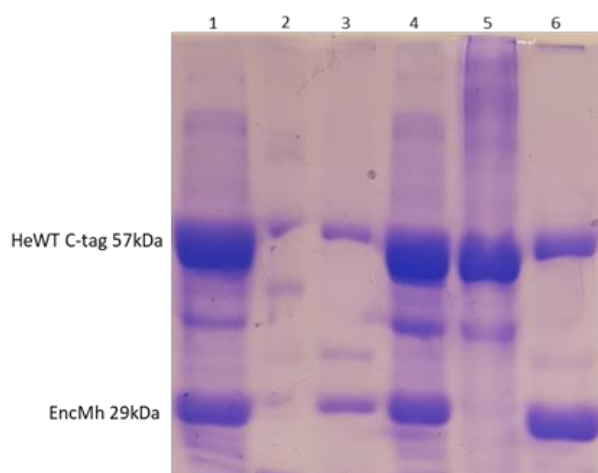was necessary to collect the unbound flow-through, as the encapsulin shell hinders the interaction of the His-tag with Ni^{2+}.

Figure 5.6. SDS-PAGE analysis of distinct purification stages of MhEnc-HeWT. Lane 1: Clarified cell extract; Lane 2: Protein Ladder; Lane 3: Bacterial pellet; Lane 4: Flow-through from the Äkta system revealing bands corresponding to HeWT (50 kDa) and MhEnc (29 kDa) within the protein pool; Lane 5: Non-encapsulated excess HeWT-CLP purified through Ni-NTA; Lane 6: Enc-HeWT after 5% *w/v* PEG precipitation and subsequent resuspension in 5% *w/v* glycerol.

The quantification of MhEnc-HeWT protein was performed using the Bradford assay, which was considered more reliable than measuring absorbance at 280 nm due to the complexity of the encapsulin-biocatalyst system. The resulting protein concentration was 1.9 mg/mL. However, for an accurate assessment of the activity of the catalyst, it was necessary to evaluate the ratio of encapsulin to HeWT -CLP. This was accomplished by means of the Fiji software, allowing the estimation of band intensity on the SDS-PAGE (Figure 5.7).
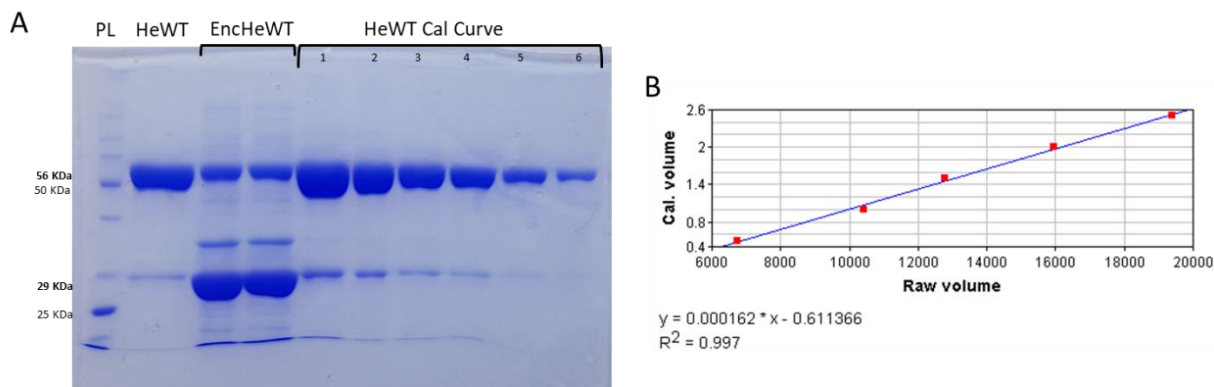
Figure 5.7. (a) the SDS-PAGE was used to assess the ratio of MhEnc:HeWT. 1 = 2.5 mg/mL; 2 = 2 mg/mL, 3 = 1.5 mg/mL; 4 =1 mg/mL; 5 = 0.5 mg/mL; 6 = 0.25 mg/mL. (b) A calibration curve was made using the excess of HeWT -CLP as standard.

The protein ratio between encapsulin and HeWT -CLP was determined to be 1:3 (Table 5.1).

Table 5.1. Concentration of HeWT in Enc-HeWT calculated by Fiji software.

	He**WT** (mg/mL)	**MhEnc (mg/mL)**	**% HeWT**
HeWT	1.7	-	-
Enc-HeWT	0.65	1.3	32.7

With the MhEnc:HeWT ratio in hand, we moved to assess its specific activity through a standard activity test for the reductive amination of (*S*)-methyl benzylamine (S-MBA) into acetophenone, using pyruvate as the co-substrate, which is subsequently converted into alanine (Figure 5.8). The formation of acetophenone is monitored by UV at 245 nm. A non-encapsulated HeWT-CLP, obtained through the same purification process (excess purified by Ni^{2+} affinity), was used as a reference control. The results, at a comparable concentration of active biocatalyst (0.1 mg/mL), revealed a 1.5-fold reduction in activity of HeWT upon encapsulation, 0.8 U/mg for MhEnc-HeWT, while HeWT-CLP exhibited 1.2 U/mg of protein.
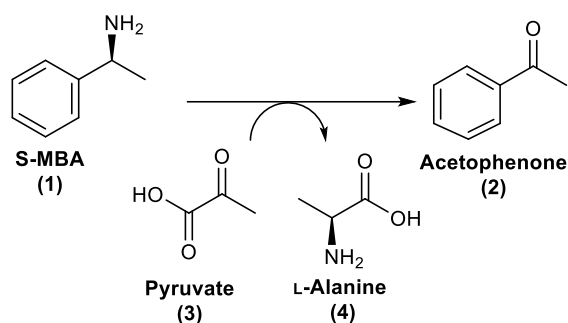
Figure 5.8. Standard activity assay for HeWT.

Since initial results suggested that the encapsulation of HeWT did not enhance the catalysis, we examined the effect of the encapsulated construct under various reaction conditions.

5.3.2 Effect of Additives

Previous studies reported encapsulation as an effective strategy against degradative agents including proteases, high temperatures, and denaturants.[22–24] We included further parameters in our screening that could potentially affect the activity of the enzyme, such as higher ionic strengths and co-solvent.

i. Investigation of Polyethylene glycol (PEG) and Glycerol and their effect on the catalysis

Initially, we checked whether additives present in the protein purification protocol impacted the activity of HeWT. Polyethylene glycol ((PEG) 8000) at a concentration of 5% *w/v* was employed to precipitate the encapsulated biocatalyst from the rest of the host proteins in the early stages of purification. The resulting pellet was subsequently resuspended in Tris-HCl buffer with 5% glycerol.

The catalytic activity in the presence of these two chemicals was evaluated with HeWT (Figure 5.9) at two different concentrations. An assay conducted without PEG at 0.4 mg/mL, corresponding to 1.6 U/mg, was used to determine the baseline level of activity of HeWT. The presence of PEG (Figure 5.9-A) demonstrated a positive impact on the activity at 0.4 mg/mL of enzyme, a 44 % increase in activity was observed, while at 0.2 mg/mL, it was only 10%. However the maximum activity measured is 2.4 U/mg in both cases. This value falls within the

expected activity range for HeWT under standard conditions, leading us to conclude that at that specific concentration, PEG 8000 did not significantly affect the activity of the enzyme.

We then moved on to evaluate the activity of HeWT in the presence of an increasing concentration of glycerol, another additive required during the purification of the enzyme. Compared to the control (2.2 U/mg), no significant differences were observed. The concentrations of glycerol screened ranged between 5% and 20%, and the activity remained consistent at 2.6-2.7 U/mg in all cases.
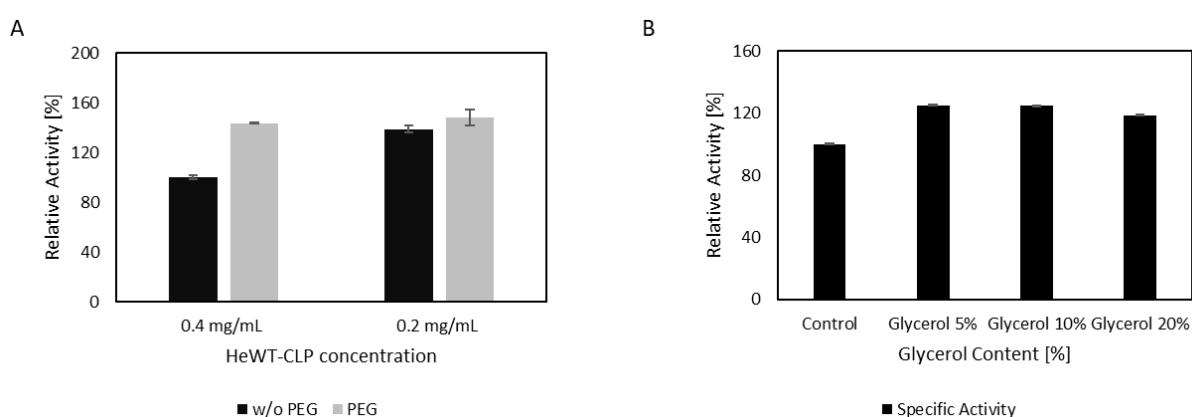

Figure 5.9. Comparative assessment of the relative activity of HeWT -CLP in(A) the presence or absence of 5% PEG 8000. The standard assay for activity contained 2.5 mM *S*-MBA, 2.5 mM pyruvate, and 0.1 mM PLP in 50 mM KPi pH 8 at 30 °C for 2 minutes, with the addition of the specified additive. The enzyme concentrations screened were 0.2 and 0.4 mg/mL. In B, the assessment of varying concentrations of glycerol. The specific activity of the control without addition of glycerol at 0.4 mg/mL is assigned at 100%. The standard assay for activity contained 2.5 mM *S*-MBA, 2.5 mM pyruvate, and 0.1 mM PLP in 50 mM KPi pH 8 at 30 °C with 1 mg/mL of enzyme for 2 minutes, with the addition of the specified additive (n=2).

ii.   Investigation into the effect of the use of dimethyl sulfoxide (DMSO) a co-solvent and cetyltrimethylammonium bromide (CTAB) as a surfactant.

Our investigation continued with an evaluation on the impact of encapsulation on resistance to co-solvents and additives, particularly to surfactants. Our focus was on dimethyl sulfoxide (DMSO), a co-solvent commonly used for solubilizing non-polar substrates under aqueous conditions, and cetyltrimethylammonium bromide (CTAB) (Figure 5.10) as a cationic surfactant.
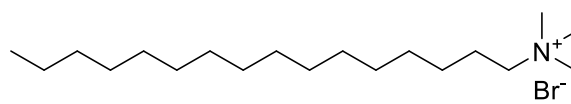
Cetyltrimethylammonium bromide (CTAB)

Figure 5.10. Structure of cetyltrimethylammonium bromide (CTAB) used as surfactant.

Initial investigations involved the addition of the co-solvent at various concentrations with HeWT-CLP and MhEncHeWT. We observed, in both scenarios, that the activity of HeWT was negatively impacted by the presence of dimethyl sulfoxide (DMSO), demonstrating that the encapsulation of HeWT does not confer any benefits to the enzyme. Furthermore, we observed that the inhibitory effect becomes more intense at increasing concentrations of DMSO. For example, at 10% DMSO, the activity of MhEncHeWT and HeWT decreased by 27% and 39%, respectively. At a concentration of 20% DMSO, the loss in activity increased to 60% and 52% for the encapsulated and non-encapsulated biocatalysts, respectively (Figure 5.11A). The reduced activity at increased DMSO concentration is likely due to a loss of the secondary structure of the enzyme under these conditions.

We then investigated the effect of a surfactant on catalysis, screening four concentrations of CTAB (1, 10, 20, and 50 mM). Compared to the control, a significant loss in enzyme activity was already observed at the lowest concentration (24-27% of residual activity). In this case, and similarly to the previous scenario of co-solvent addition, both encapsulated and non-encapsulated HeWT showed equivalent susceptibility towards surfactant addition (Figure 5.11 B).
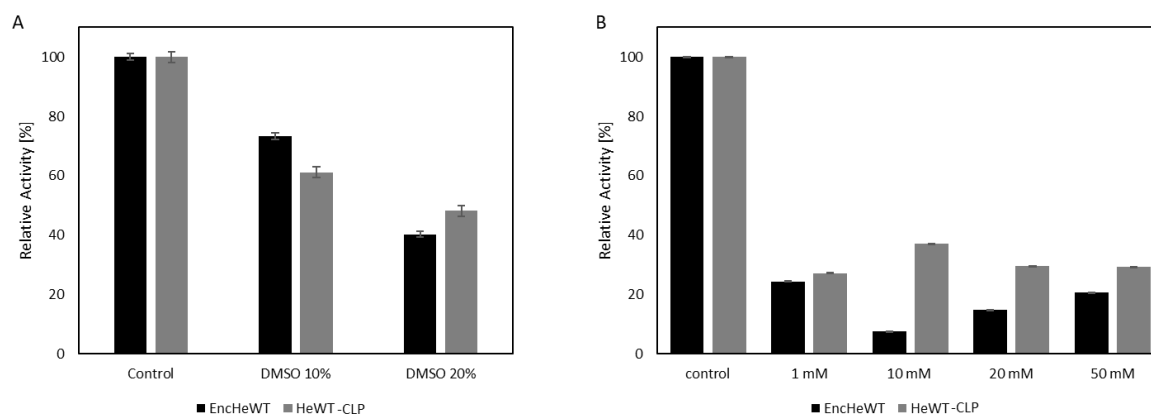

Figure 5.11. Activity of EncHeWT and HeWT in the presence of DMSO (A) and CTAB (B) at varying concentrations. In the first case, the activity decreased by approximately 2-fold when HeWT was not encapsulated and by approximately 2.5-fold when encapsulated in the

encapsulin, at 10 and 20% DMSO, respectively. Similarly, the addition of CTAB reduced the activity of both HeWT and EncHeWT by 3-fold at a concentration of 1 mM. Overall, the activity of the free enzyme was slightly less affected than the encapsulated one. The activity test was conducted as previously described: 2.5 mM *S*-MBA, 2.5 mM pyruvate, 0.1 mM PLP, 1 mg/mL HeWT in 50 mM KPi pH 8 at 30 °C for 2 min, with the addition of the additive at specified concentrations. (n=2) Add the SA at 100% for the two controls.

5.3.3 Investigation of the encapsulated biocatalyst at different ionic strength

In our previous work, we observed that the enzyme activity was negatively affected at increasing salt concentrations.[19] Therefore, we explored whether the encapsulation of HeWT-CLP could potentially mitigate the effect of salts on the protein in the media. The experiments were conducted preparing the protein solution of MhEncHeWT with buffers at two different concentrations of KCl and NaCl (1 and 2 M) and incubating for one hour at 37 °C. A comparisons in activity were made with a control reaction (*i.e.* without the addition of salts). The results are presented in Figure 5.12.
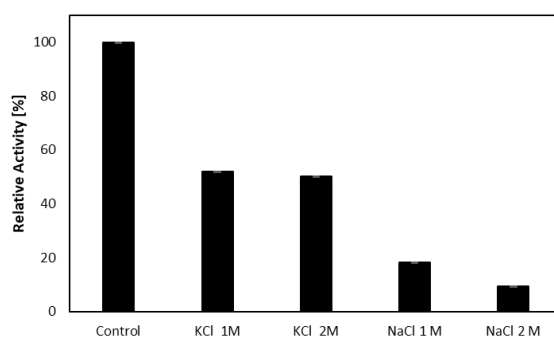

Figure 5.12. Relative activity of MhEncHeWT in the presence of KCl and NaCl at 1 and 2 M following 1h incubation at 37°C. Each experiment was performed with 2.5 mM *S*-MBA, 2.5 mM pyruvate, 0.1 mM PLP, 1 mg/mL MhEncHeWT in 50 mM KPi pH 8 (control), or KCl 1M, KCl 2M, NaCl 1M or 2M accordingly with the condition screened. n=2

We observed a consistent reduction in activity in all cases: in the presence of KCl, the retained activity remained at 50%, irrespective of the salt concentration. However, with NaCl, the reduction in the specific activity of MhEncHeWT was more considerable, with the biocatalyst retaining only 18% and 9% of the activity at 1 M and 2 M concentrations, respectively. These results are in line with the findings previously obtained for HeWT.[19] In that case, the presence of NaCl had a lower impact (retained activity was 21% at 1 M and 27% at 2 M). These results

indicate that the encapsulation of HeWT-CLP was not effective in preventing the destabilization of the biocatalyst in the presence of high salt concentrations.

5.3.4. Extended operational stability at 50°C.

We were then interested in testing the impact of encapsulation on temperature stability. As mentioned, HeWT has an optimal activity temperature at 50 °C but low stability at the same temperature.

To assess the activity of the enzyme at higher temperatures, we compared the reaction rates of the biotransformation of S-MBA to acetophenone at 30 °C and 50 °C, respectively, for 10 minutes (Figure 5.13). At 50°C, the activity of the biocatalyst increased, as expected, but the encapsulated enzyme exhibited lower activity at both temperatures.
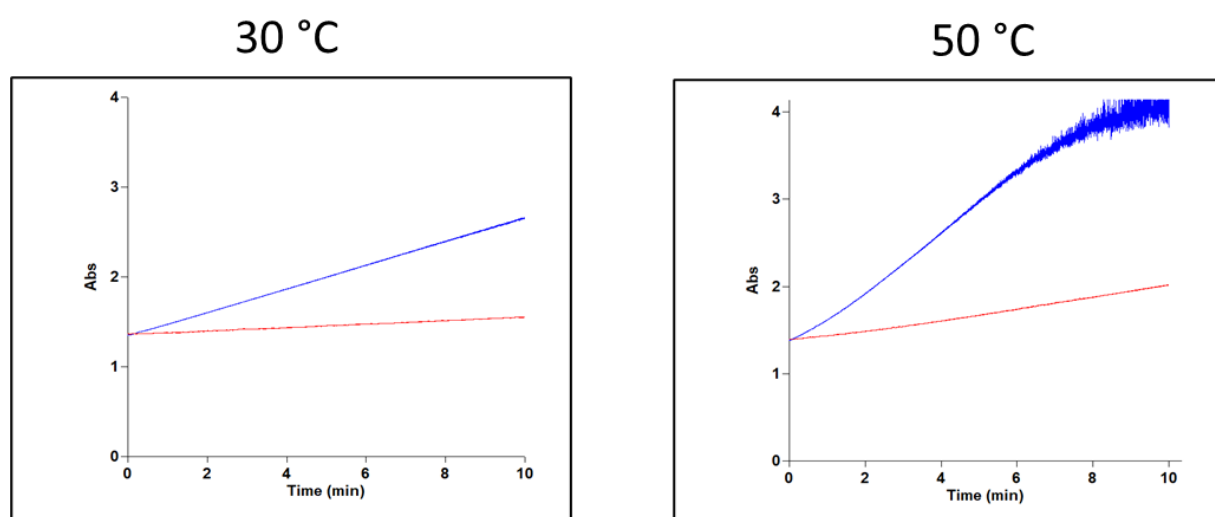

Figure 5.13. Activity rates at 30 °C and 50 °C for HeWT-CLP (blue) and EncHeWT (red). Right: At 50°C, the enzyme had higher activity than at 30 °C (left), irrespective of encapsulation. The assay was performed by the incubating the enzyme with 2.5 mM *S*-methyl benzylamine (*S*-MBA), 2.5 mM pyruvate, and 0.1 mM PLP, in 50 mM KPi buffer pH 8. 0.15 mg/mL HeWT for 10 mins.

In both experiments, HeWT was equally influenced by the temperature. The observed increase was 3 times for the non-encapsulated (from 0.7 to 1.7 U/mg) and 2.5 times for the encapsulated biocatalyst (from 0.4 to 1.2 U/mg).

The stability of HeWT to higher temperatures was assessed by storing the biocatalyst at 50 °C and checking the retained activity over time. In this vein, MhEncHeWT was incubated in KPi at 50 °C for 0.5, 1, 2, 3, 15 and 24 hours (Figure 5.14). Free HeWT-CLP was incubated under the same conditions as a control.
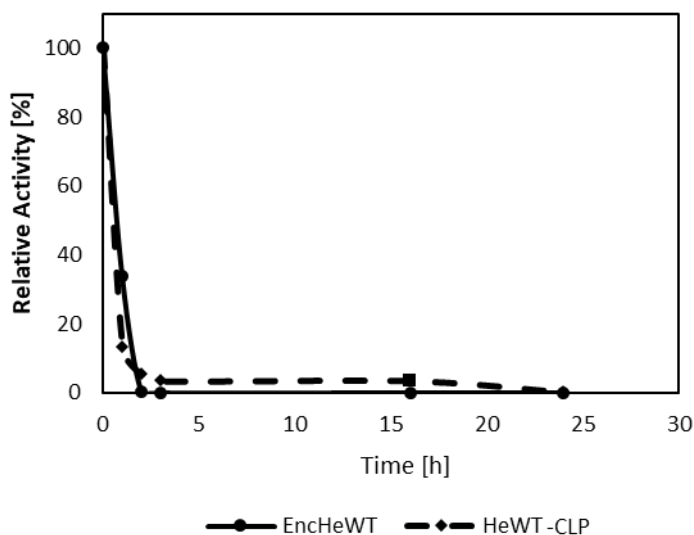

Figure 5.14. Stability of MhEncHeWT at 50 °C over 24 hours. HeWT was also incubated under the same conditions as a control. The specific activity assay was then carried out as previously described: 2.5 mM *S*-MBA, 2.5 mM pyruvate, 0.1 mM PLP, 1 mg/mL HeWT in 50 mM KPi pH 8 at 30 °C for 2 min.

As can be seen in Figure 5.14, again the encapsulation of HeWT does not benefit the biocatalyst stability, as both EncHeWT and the control lost all activity after just 30 minutes of incubation.

5.3.5 Benefits of encapsulation over immobilisation: can the proteinaceous shell prevent the rigidification of the structure?

We previously highlighted one of the drawbacks of enzyme covalent immobilization: the secondary structure of the protein undergoes rigidification upon immobilization, resulting in a decrease in retained activity, but this is generally compensated by an increased stability over time. We reasoned that HeWT would retain freedom of movement within encapsulin but that the complex still allowed for immobilisation through the outer shell.

We therefore aimed to exploit the outer surface of encapsulin for immobilisation, serving as a "protective layer" between the resin and the catalyst. This approach also aimed to maintain the native quaternary structure of HeWT, preserving 100% of the specific activity while not compromising the stability of the protein over time.

A preliminary investigation was conducted using MhEnc to determine the overall feasibility of immobilization using the exposed lysins. *In silico* analysis done with CapiPy[25] showed that the surface of MhEnc has 8.15% exposed lysins (Figure 5.15 A) and a predominancy of negative charges exposed on the surface (Figure 5.15 B).[26]
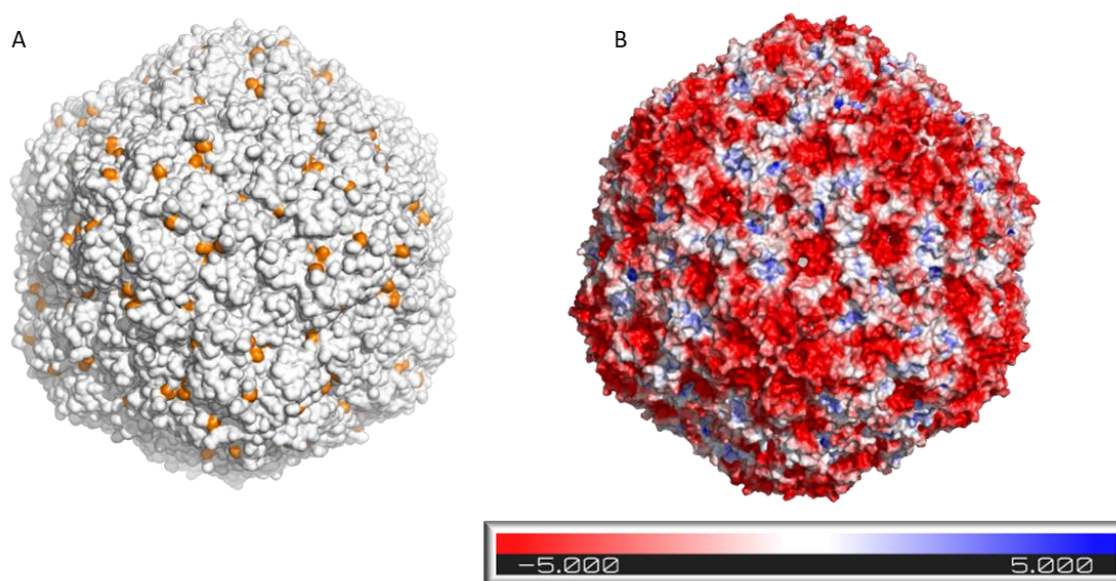

Figure 5.15. Surface of MhEnc. (A) the exposed lysines (21 per chain) available for immobilization are highlighted in orange; (B) the charge distribution on the protein's surface, from negative (in red) to positive (in blue). The model shows clearly that the surface is predominantly negatively charged and the positive regions are mostly concentrated at the porous level. (PDB: 6I9G)

5.3.6 Spatial distribution analyses using Laser Scanning Confocal Microscopy (LSCM)

Before screening various types of carriers for the immobilization of MhEncHeWT, we conducted a preliminary test using agarose beads. The choice of this resin was based on its translucent feature, making it suitable for visualization with LSCM. Initially, we tested the hollow encapsulin labelled with fluorescein isothiocyanate (FITC) immobilized on glyoxyl-agarose. This chemistry offers a robust covalent bond between the protein and the resin, resulting in a high immobilization yield (Figure 5.16)
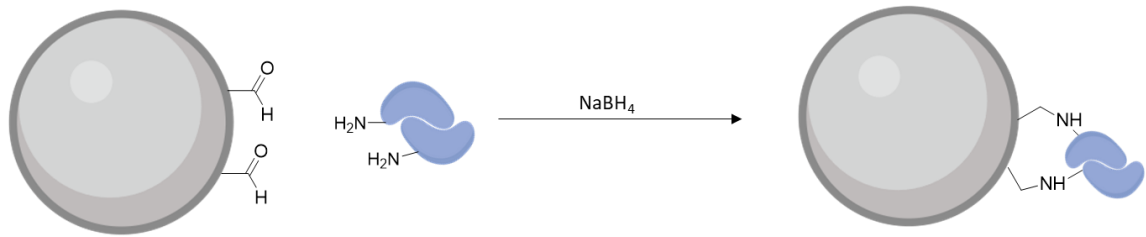
Figure 5.16. Immobilisation scheme on agarose beads (in grey) *via* aldehydes and amine groups from exposed lysins of the protein (purple).

The labelling procedure requires a molar ratio of FTIC to MhEnc at 1:20. The glyoxyl-support was prepared as described by Guìsan *et al*. and Mateo *et al*.[27,28] In this protocol, the epoxy groups are hydrolysed with aq. H_2SO_4 (100 mM) and the subsequent diols, oxidised with 30 mM $NaIO_4$ to yield the final aldehyde. Protein immobilization was performed at pH 10, where half of the lysins are deprotonated. Under these conditions, the amines form an unstable Schiff's base with the reactive aldehydes on the resin, and the covalent linkage between protein and resin is made by the addition of $NaBH_4$ as a reducing agent

The results reported in Figure 5.17 A-C show beads evenly fluorescent, indicating the presence of protein on the surface. The bottom row shows the control, to confirm the absence of any unwanted background fluorescence(Figure 5.17 D-F).
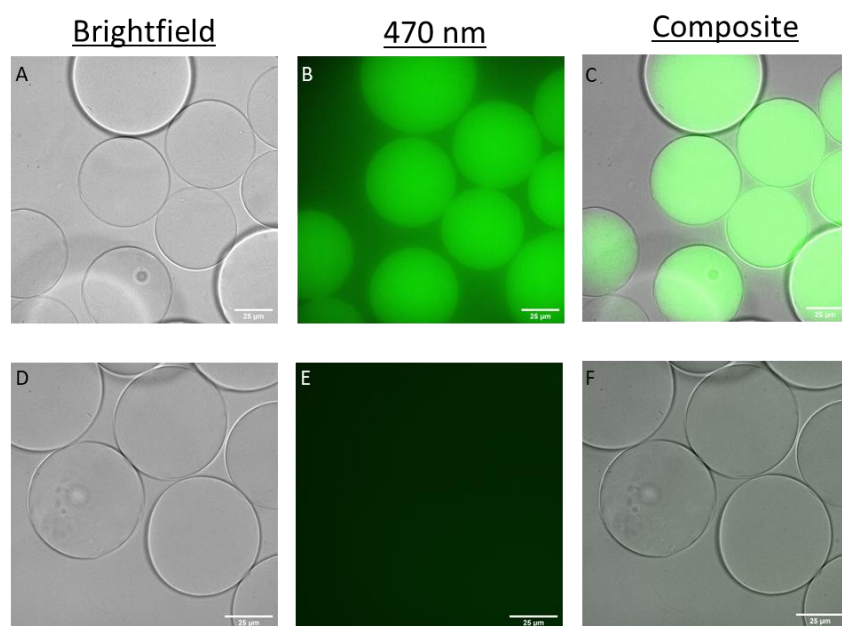
Figure 5.17. Laser Scanning Confocal Microscopy (LSCM) of MhEnc immobilized on glyoxyl-agarose. Upper row: 60x magnification of the immobilized MhEnc sample, observed in brightfield (A), at 510 nm emission (B), and the composite figure combining both (C). Bottom row: a sample of non-labelled MhEnc was analysed after immobilization on the same support. Images in brightfield (D), upon excitation (E), and their overlaid representation (F) are also presented here. A 2 second exposure time was used to obtain these images.

Although the immobilization method has yielded positive results, its applicability is limited due to the underlying chemical requirements. Specifically, the chemistry necessitates the reduction of the Schiff's base formed between the aldehyde group of the resin and the exposed amino group of the encapsulin. This same Schiff's base is also crucial in the catalytic site, where it forms an internal aldimine with the cofactor. Any reduction of this Schiff's base adversely affects the regeneration of pyridoxal phosphate (PLP). [29]

5.3.7 Immobilisation on Methacrylic Carriers and Effects on the Catalytical Activity

Once the immobilisation of the hollow structure was confirmed by LCMS, we explored the immobilization of encapsulin containing HeWT at different protein loadings and evaluated its activity in comparison with immobilised HeWT -CLP as control. Given the limitations identified by using glyoxyl agarose as an immobilization strategy, we redirected our focus toward alternative resins and chemistries: ReliZyme EP403/S, EP400/S, and HFA403/SS from Resindion, along with ECR8204F from Purolite were the resins of choice. Each of these resins features a methacrylic core functionalized with either epoxy or amino epoxy spacers (Figure 5.19 A-B).
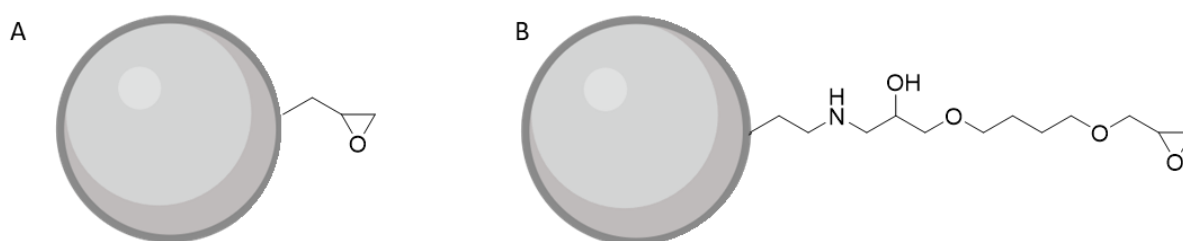

Figure 5.19. Scheme of epoxy and amino epoxy resin. The carrier represented by the grey beads is made from methacrylic resin while the functionalisation contains an epoxy (A) or epoxy amino group (B) which can interact with the exposed residues of the enzyme.

EP400/SS and ECR8204F share a similar composition, with the beads functionalized with epoxy groups and spacers of different lengths. HFA403/S, illustrated in Figure 5.19, features a

long spacer containing an amino group, enhancing ionic interactions with the enzyme surface. The immobilization procedure was consistent across all cases, maintaining a 4:1 ratio of protein solution to resin, and monitoring the supernatant concentration for 20 hours. The retained activity was then evaluated (2.5 mM S-MBA, 2.5 mM pyruvate, and 0.1 mM PLP, in 50 mM KPi pH 8 with 10 mg of resin at 30 °C for 20 minutes) with samples withdrawn every 2 minutes for acetophenone quantification at 245 nm. The summarized results are presented in Table 5.1.

Table 5.1. Immobilisation of MhEncHeWT on diverse methacrylic resins at 5 mg/g$_{resin}$ as protein loadings

Resin	Supplier	Protein Loading (mg/g $_{resin}$)	Immobilisation Yield (%)	Retained Activity (%)	Residual Activity U/mg$_{enzyme}$
ECR8204F	Purolite		>99	2	0.03
EP400/SS	Resindion	5	>99	22	0.28
EP403/SS	Resindion		>99	13	0.10
HFA403/SS	Resindion		>99	35	0.44

Our investigations demonstrated that immobilization on epoxy resin led to a diminished residual activity (-30%) compared to the reported literature value for HeWT. The use of aminoepoxy resin yielded the most favourable outcome, with a 35% residual activity. Although this value remains lower than the literature-reported residual activity (42%) for the free enzyme, we selected this resin to carry on further experiments.[30]

Then, we investigated three protein loadings of MhEncHeWT (1, 5, and 10 mg/g resin) on HFA403/SS, which was demonstrated to be the best candidate. The immobilization process involved adding the appropriate volume of the protein solution to Tris-HCl buffer (50 mM, pH 8) to achieve the desired final concentration. The ratio of protein solution to resin was maintained at 4:1 in all cases. Samples of the supernatant were collected to monitor the immobilization progress until the detected protein in reached a constant or zero.

Within 4 hours, immobilization was almost complete in all cases, resulting in an immobilization yield ranging from 71% to 81% (results not shown). Thus, we left the mixture incubating overnight until the immobilization was complete.

The confirmation of the covalent nature of the bond between the protein and the resin was assessed by boiling a small sample of the resin (approximately 10 mg), resuspension in dH_2O (200 µL), centrifuged, and resolving 10 µL of the supernatant on a 12% SDS-PAGE gel. The absence of specific bands at 55 and 29 kDa confirmed that the proteins were not attached by ionic interaction. The retained activity was measured with the aforementioned method.

Table 5.2 summarises the observations of the assay, indicating that the best compromise is achieved at 5 mg/mL of protein loading and recovered activity.

Table 5.2. Immobilisation of MhEncHeWT on HFA 403/SS at different protein loadings. Overall, the best results are achieved at 5 mg/ g_{resin}. The immobilisation yield is comparable with 1 mg/g and the recovered activity is higher than 10 mg/g, leading to a higher catalytic unit.

Protein Loading	Immobilisation Yield (%)	Recovered Activity (%)	Residual Activity U/mg_{enzyme}
1	>99	33	0.4
5	>99	34	0.4
10	71	12	0.01

Based on the experimental results, we conclude that not only does the proteinaceous shell fail to prevent immobilization distortion, but it also adversely impacts enzyme activity. A plausible explanation for this behaviour stems from the cumulative effects of both mass-transfer limitations and alterations in the secondary structure of the enzyme, which persist despite the encapsulation process.

5.3.8 Stability Study of MhEncHeWT and imm-MhEncHeWT

Given that encapsulin inherently possesses resistance to various degradative factors, we investigated the different stability observed over a 1-month storage period at 4 °C. The retained activity after 1 week was found to be 7-fold higher for MhEncHeWT than for HeWT -

CLP. However, after 1 month, both biocatalysts experienced a substantial loss of activity resulting in a comparable negligible remaining activity (Figure 5.20).
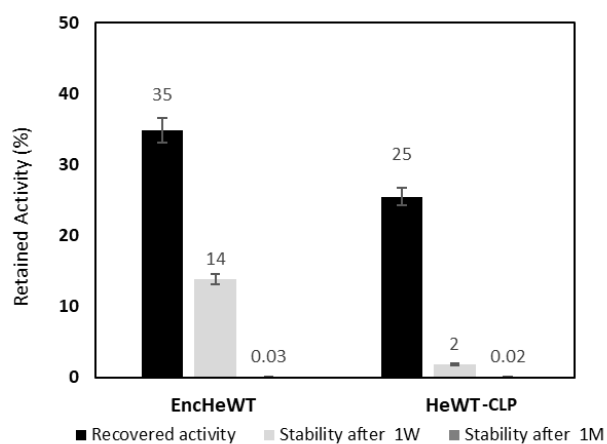

Figure 5.20. Stability study on MhEncHeWT and HeWT over 1 month. The sample was stored at 4 °C.

We noted a similar trend for imm-MhEncHeWT (on HFA 403/SS) at diverse protein loadings, reducing the investigation time to 3 weeks. Under these conditions, the variation in retained activity fluctuated between 12% and 26% across the different loadings with respect to the encapsulated MhEncHeWT, showing stability over the entire 3-week period in all cases (Figure 5.21).
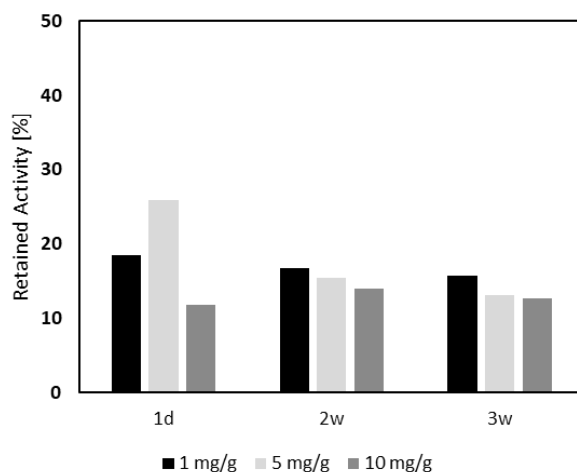

Figure 5.21. Stability study on imm-MhEncHeWT over 3 weeks at different protein loadings.

5.3.9 *H. elongata* pyrroline-2-carboxylate reductase (HeP5CR) as a Cargo Protein

Having determined that encapsulation did not provide tangible benefits in terms of catalytic activity or immobilization for HeWT-CLP, our attention shifted to the redox enzyme, pyrroline-

2-carboxylate reductase from *H. elongata* (HeP5CR). HeP5CR is known for its good activity when used in soluble form, however the enzyme faces limitations when ionically immobilised and used in a flow system due to rapid leaching. The goal was to leverage the high immobilisation yield obtained with the encapsulin shell to effectively retain the enzyme. We cloned the HeP5CR gene into the original vector pENC-VsHb using Gibson Assembly (Figure 5.22).[31]
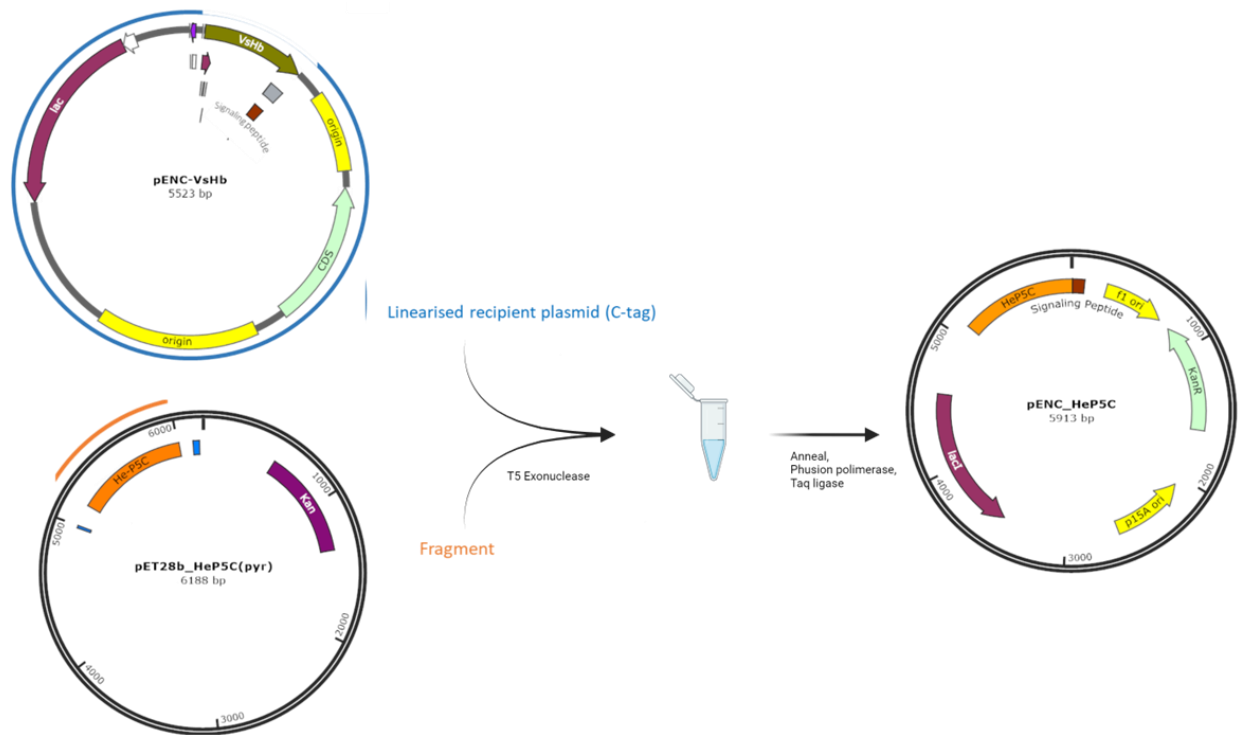

Figure 5.22. A simplified scheme of Gibson Assembly for the construct HeP5CR -CLP

In a similar fashion to the HeWT procedure, the co-transformed strain was expressed in 300 mL TB media supplemented with kanamycin and ampicillin at the appropriate concentrations and the two proteins were induced with 1% arabinose and 0.1% IPTG when the optical density at 600 nm was between 0.6 and 1.

After 16 hours, the culture was harvested and purified using the same purification protocol as before. The purification of non-encapsulated excess HeP5CR-CLP was done as previously described for HeWT-CLP and was used as the control. The quantification of the biocatalyst enclosed in the shell was determined using SDS-PAGE, utilizing Fiji for quantification of the encapsulated HeP5CR and the purified excess as a standard for the calibration curve (Figure 5.23).
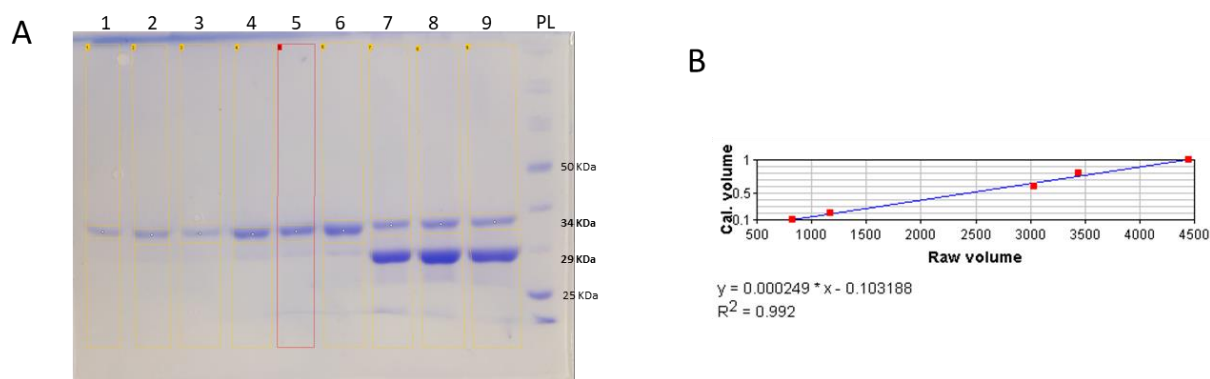
Figure 5.23. 12% SDS-PAGE for quantification of various HeP5CRs. (a) Lanes 1-6: HeP5CR STD 0, 0.2, 0.4, 0.6, 0.8, and 1 mg/mL of protein; Lanes 7-9: triplicate of 1 mg/mL EncHeP5CR; (b) Calibration curve generated with Fiji based on HeP5CR std. The molecular weight of HeP5CR was determined to be 34 kDa (ProtParam).

The estimated amount of HeP5CR-CLP from the gel was approximately 25%, and this value was taken into consideration for all following calculations. The determination of specific activity involved the reduction of 10 mM L-thiazolidine carboxylate (T4C) to (R)-4,5-dihydrothiazole-4-carboxylic acid, utilizing 0.1 equivalents of NAD+ as a co-factor (Figure 5.24). The reaction mixture was prepared in 50 mm KPi buffer at pH 8, and the reaction slope was determined by monitoring the production of NADH at 340 nm at 30 °C.
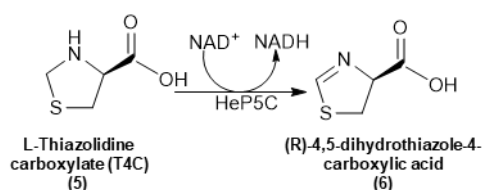

Figure 5.24. Reaction catalysed by HeP5CR to assess the specific activity.

The specific activity of MhEncHeP5CR was found to be 3.5 U/mg, which is nearly half of the non-encapsulated enzyme (6.2 U/mg). These results are consistent with those observed previously, where the activity of MhEncHeWT ranged between 0.3 to 0.8 U/mg, and HeWT -CLP exhibited activity in the range of 1.2-2.2 U/mg. The stability of HeP5CR-CLP and its encapsulated variant was further assessed at different temperatures.

To gain a comprehensive understanding of the impact of the -CLP, we included a sample of HeP5CR lacking the -CLP, expressed as described by Roura Padrosa *et al.*, with a specific activity of 8.4 U/mg. The three samples were incubated at 30, 37, and 45 °C for 135 hours,

with specific assays conducted under standard conditions. The results, presented in Figure 5.25, illustrate that both the presence of the -CLP and encapsulin, irrespective of temperature, negatively influenced the stability of HeP5CR, maintaining a consistent trend across all conditions. Interestingly, native HeP5CR exhibited robust stability throughout the entire incubation period at all tested temperatures.
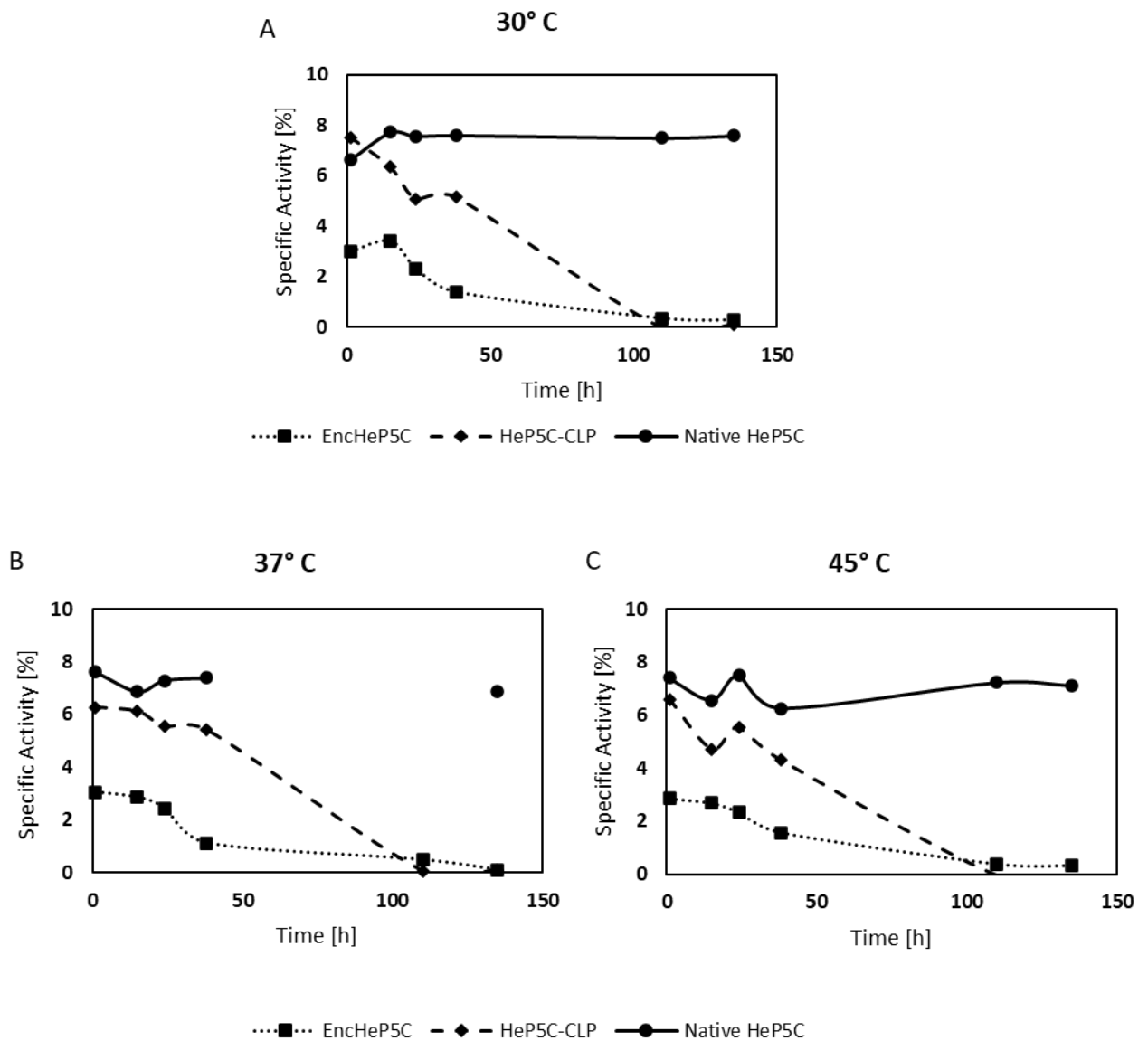

Figure 5.25. Stability of MhEnc HeP5CR, HeP5CR-CLP, and native HeP5CR upon incubation at 30, 37 and 45 °C up to 135 hours. Aliquots were taken at 1, 15, 24, 38, 110 and 135 hours and subjected to an activity test. The activity test was performed under standard conditions: 10 mM T4C and 1 mM NAD$^+$ in 50 mm KPi 50 mM at pH 8 at 30°C.

We then moved to assay the retained activity of MhEnc HeP5CR upon immobilisation. On this occasion, 5 mg/g$_{resin}$ on HFA403/SS was directly used to have a reliable comparison of activity with the immobilised MhEncHeP5CR.

The final protein immobilisation yielded 80 and 76% for HeP5CR (with and without -CLP, respectively Table 5.2) and 68% for MhEncHeP5CR. A confirmation of the covalent nature of the bond formed between the enzyme and the resin was given by a boiled sample (10 mg of resin in dH$_2$O) of the immobilised carrier.

The recovered activity was then determined, whereby 50 mg of resin was resuspended in 10 mL of reaction mixture containing 10 mM T4C and 1 mM NAD$^+$ in 50 mM KPi at pH 8 and the reaction was monitored for 20 minutes, withdrawing aliquots every 2 minutes. The retained activity (Figure 5.26) was found to be very low in comparison with the respective free catalyst in all the conditions screened, never exceeding 4% (HeP5CR -CLP).

Interestingly, we noted that the native HeP5CR exhibited the least recovered activity (1.8%) compared to the other screened variants. However, additional investigations are required to explore the impact of CLP on the specific activity, considering that the reported values may fall within the of error.
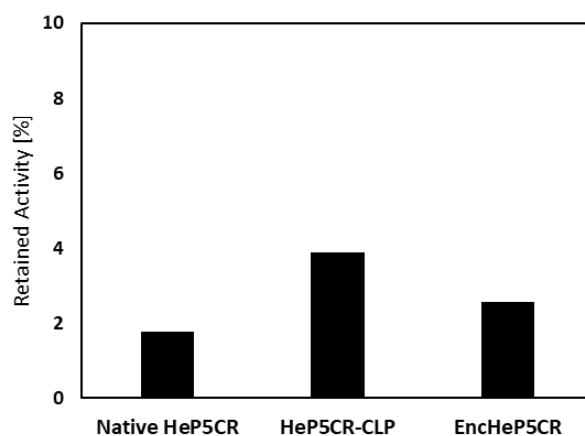

Figure 5.26. Retained activity of HeP5CR, EncHeP5CR, and native HeP5CR on HFA 403/SS. The reactions, containing 10 mM T4C and 1 mM NAD$^+$ in 50 mM KPi, pH 8, were performed at 30 °C for 20 minutes. A sample was aliquoted every two minutes, and the absorbance of the mixture was analysed at 340 nm.

5.4 Conclusions

In this chapter, investigations into the molecular nanocompartment, encapsulin *from M. hassiacum*, was carried out to address key issues associated with the immobilization of biocatalysts, and to potentially enhance local substrate concentration, thereby influencing activity. Genetic modifications allowed the cloning of the loading peptide at the C-terminal and subsequent *in vivo* encapsulation of both HeWT and HeP5CR.

Quantification of the encapsulated biocatalysts, HeWT and HeP5CR, revealed content levels of 33% and 25%, respectively, determined by 12% SDS-PAGE analysis with imaging software (Fiji). These values were employed to calculate the specific activity of the encapsulated enzymes, named EncHeWT and EncHeP5CR, which were found to be 2-fold lower than the control. It appears that molecular crowding effects may not induce benefits for HeWT and HeP5CR. Moreover, it is possible that substrates and cofactors might encounter limitations in their passage through the encapsulin structure. The permeability and the pore size of the encapsulin may act as molecular sieves, thereby hindering the transfer rate of specific molecules to the active site, seemingly diminishing the activity of the biocatalyst. Additionally, the polarity of the molecules of interest and the charge distribution on the shell surface should also be considered.

EncHeWT and EncHeP5CR exhibited a similar trend upon immobilization. Following an initial screening on various carriers, such as agarose and different types of methacrylic resins, it was concluded that the retained activity of the encapsulated enzyme consistently decreased compared to the control. This reduction, estimated to be over 75%, poses a challenge for the broader application of EncHeWT and EncHeP5CR, as the quantity of enzyme required to achieve a significant catalytic unit would be notably high. One possible explanation for this unexpected behaviour may lie within the cage. The -CLP cloned at the C-terminus of the genes, anchors the subunits to the inner surface of the shell, potentially inducing structural rigidification and limiting the space available for the enzyme to adopt an active conformation.

Possible future outlooks to implement encapsulin in biocatalysis will involve screening smaller enzymes that do not suffer from space constraints, such as monomeric enzymes, nor require migration of cofactors through the pores. Alternatively, exploring larger encapsulins, for example from *Qu. thermotolerance*, which offer a greater inner volume, could be a promising

direction. Furthermore, the assembly-disassembly ability of encapsulin under diverse conditions, along with its potential application in biocatalysis to replace immobilized enzymes at the end of their life cycle, is an aspect that worth further investigation.

References

(1)   Basso, A.; Serban, S. Industrial Applications of Immobilized Enzymes—A Review. *Molecular Catalysis* **2019**, *479*, 110607. https://doi.org/10.1016/j.mcat.2019.110607.

(2)   Homaei, A. A.; Sariri, R.; Vianello, F.; Stevanato, R. Enzyme Immobilization: An Update. *J Chem Biol* **2013**, *6* (4), 185. https://doi.org/10.1007/S12154-013-0102-9.

(3)   Kress, J.; Zanaletti, R.; Amour, A.; Ladlow, M.; Frey, J. G.; Bradley, M. Enzyme Accessibility and Solid Supports: Which Molecular Weight Enzymes Can Be Used on Solid Supports? An Investigation Using Confocal Raman Microscopy. *Chemistry - A European Journal* **2002**, *8* (16), 3769. https://doi.org/10.1002/1521-3765(20020816)8:16<3769::AID-CHEM3769>3.0.CO;2-V.

(4)   Romero-Fernández, M.; Paradisi, F. General Overview on Immobilization Techniques of Enzymes for Biocatalysis. *Catalyst Immobilization: Methods and Applications* **2019**, 409–435. https://doi.org/10.1002/9783527817290.CH12.

(5)   Mohamad, N. R.; Marzuki, N. H. C.; Buang, N. A.; Huyop, F.; Wahab, R. A. An Overview of Technologies for Immobilization of Enzymes and Surface Analysis Techniques for Immobilized Enzymes. *Biotechnol Biotechnol Equip* **2015**, *29* (2), 205. https://doi.org/10.1080/13102818.2015.1008192.

(6)   Valdés-Stauber, N.; Scherer, S. Isolation and Characterization of Linocin M18, a Bacteriocin Produced by Brevibacterium Linens. *Appl Environ Microbiol* **1994**, *60* (10), 3809–3814. https://doi.org/10.1128/aem.60.10.3809-3814.1994.

(7)   Smith, J. L. The Physiological Role of Ferritin-Like Compounds in Bacteria. *Crit Rev Microbiol* **2004**, *30* (3), 173–185. https://doi.org/10.1080/10408410490435151.

(8)   McHugh, C. A.; Fontana, J.; Nemecek, D.; Cheng, N.; Aksyuk, A. A.; Heymann, J. B.; Winkler, D. C.; Lam, A. S.; Wall, J. S.; Steven, A. C.; Hoiczyk, E. A Virus Capsid-like Nanocompartment That Stores Iron and Protects Bacteria from Oxidative Stress. *EMBO J* **2014**, *33* (17), 1896–1911. https://doi.org/10.15252/embj.201488566.

(9)   Giessen, T. W. Encapsulins. *Annu Rev Biochem* **2022**, *91* (1), 353–380. https://doi.org/10.1146/annurev-biochem-040320-102858.

(10)   Andreas, M. P.; Giessen, T. W. Large-Scale Computational Discovery and Analysis of Virus-Derived Microbial Nanocompartments. *Nat Commun* **2021**, *12* (1). https://doi.org/10.1038/S41467-021-25071-Y.

(11)   Rosenkrands, I.; Rasmussen, P. B.; Carnio, M.; Jacobsen, S.; Theisen, M.; Andersen, P. Identification and Characterization of a 29-Kilodalton Protein from *Mycobacterium Tuberculosis* Culture Filtrate Recognized by Mouse Memory Effector Cells. *Infect Immun* **1998**, *66* (6), 2728–2735. https://doi.org/10.1128/IAI.66.6.2728-2735.1998.

(12)   Hicks, P. M.; Chang, L. S.; Kelly, R. M. Homomultimeric Protease and Putative Bacteriocin Homolog from Thermotoga Maritima. *Methods Enzymol* **2001**, *330*, 455–460. https://doi.org/10.1016/S0076-6879(01)30397-X.

(13)   Lončar, N.; Rozeboom, H. J.; Franken, L. E.; Stuart, M. C. A.; Fraaije, M. W. Structure of a Robust Bacterial Protein Cage and Its Application as a Versatile Biocatalytic Platform through Enzyme Encapsulation. *Biochem Biophys Res Commun* **2020**, *529* (3), 548–553. https://doi.org/10.1016/J.BBRC.2020.06.059.

(14)   Tiago, I.; Maranha, A.; Mendes, V.; Alarico, S.; Moynihan, P. J.; Clarke, A. J.; Macedo-Ribeiro, S.; Pereira, P. J. B.; Empadinhas, N. Genome Sequence of Mycobacterium Hassiacum DSM 44199, a Rare Source of Heat-Stable Mycobacterial Proteins. *J Bacteriol* **2012**, *194* (24), 7010–7011. https://doi.org/10.1128/JB.01880-12.

(15)   Moon, H.; Lee, J.; Min, J.; Kang, S. Developing Genetically Engineered Encapsulin Protein Cage Nanoparticles as a Targeted Delivery Nanoplatform. *Biomacromolecules* **2014**, *15* (10), 3794–3801. https://doi.org/10.1021/bm501066m.

(16)   Lončar, N.; Rozeboom, H. J.; Franken, L. E.; Stuart, M. C. A.; Fraaije, M. Molecular Packaging of Biocatalysts Using a Robust Protein Cage. **2020**. https://doi.org/10.26434/CHEMRXIV.12063243.V1.

(17)   Cassidy-Amstutz, C.; Oltrogge, L.; Going, C. C.; Lee, A.; Teng, P.; Quintanilla, D.; East-Seletsky, A.; Williams, E. R.; Savage, D. F. Identification of a Minimal Peptide Tag for *in Vivo* and *in Vitro*

Loading of Encapsulin. *Biochemistry* **2016**, *55* (24), 3461–3468. https://doi.org/10.1021/acs.biochem.6b00294.

(18)   Altenburg, W. J.; Rollins, N.; Silver, P. A.; Giessen, T. W. Exploring Targeting Peptide-Shell Interactions in Encapsulin Nanocompartments. *Sci Rep* **2021**, *11* (1), 4951. https://doi.org/10.1038/s41598-021-84329-z.

(19)   Cerioli, L.; Planchestainer, M.; Cassidy, J.; Tessaro, D.; Paradisi, F. Characterization of a Novel Amine Transaminase from Halomonas Elongata. *J Mol Catal B Enzym* **2015**, *120*, 141–150. https://doi.org/10.1016/j.molcatb.2015.07.009.

(20)   Planchestainer, M.; Contente, M. L.; Cassidy, J.; Molinari, F.; Tamborini, L.; Paradisi, F. Continuous Flow Biocatalysis: Production and in-Line Purification of Amines by Immobilised Transaminase from Halomonas Elongata. **2017**, *19*, 372. https://doi.org/10.1039/c6gc01780k.

(21)   Engler, C.; Kandzia, R.; Marillonnet, S. A One Pot, One Step, Precision Cloning Method with High Throughput Capability. *PLoS One* **2008**, *3* (11), 3647. https://doi.org/10.1371/journal.pone.0003647.

(22)   Sutter, M.; Boehringer, D.; Gutmann, S.; Günther, S.; Prangishvili, D.; Loessner, M. J.; Stetter, K. O.; Weber-Ban, E.; Ban, N. Structural Basis of Enzyme Encapsulation into a Bacterial Nanocompartment. *Nature Structural & Molecular Biology 2008 15:9* **2008**, *15* (9), 939–947. https://doi.org/10.1038/nsmb.1473.

(23)   Putri, R. M.; Allende-Ballestero, C.; Luque, D.; Klem, R.; Rousou, K. A.; Liu, A.; Traulsen, C. H. H.; Rurup, W. F.; Koay, M. S. T.; Castón, J. R.; Cornelissen, J. J. L. M. Structural Characterization of Native and Modified Encapsulins as Nanoplatforms for in Vitro Catalysis and Cellular Uptake. *ACS Nano* **2017**, *11* (12), 12796–12804. https://doi.org/10.1021/ACSNANO.7B07669/SUPPL_FILE/NN7B07669_SI_001.PDF.

(24)   Tamura, A.; Fukutani, Y.; Takami, T.; Fujii, M.; Nakaguchi, Y.; Murakami, Y.; Noguchi, K.; Yohda, M.; Odaka, M. Packaging Guest Proteins into the Encapsulin Nanocompartment from Rhodococcus Erythropolis N771. *Biotechnol. Bioeng* **2015**, *112*, 13–20. https://doi.org/10.1002/bit.25322/abstract.

(25)   Roura Padrosa, D.; Marchini, V.; Paradisi, F. CapiPy: Python-Based GUI-Application to Assist in Protein Immobilization. *Bioinformatics* **2021**, *37* (17), 2761–2762. https://doi.org/10.1093/bioinformatics/btab030.

(26)   Roura Padrosa, D.; Marchini, V.; Paradisi, F. CapiPy: Python-Based GUI-Application to Assist in Protein Immobilization. https://doi.org/10.1093/bioinformatics/btab030.

(27)   *Immobilization of Enzymes and Cells*; Guisan, J. M., Ed.; Methods in Molecular Biology; Humana Press: Totowa, NJ, 2013; Vol. 1051. https://doi.org/10.1007/978-1-62703-550-7.

(28)   Mateo, C.; Abian, O.; Bernedo, M.; Cuenca, E.; Fuentes, M.; Fernandez-Lorente, G.; Palomo, J. M.; Grazu, V.; Pessela, C. C.; Giacomini, C.; Irazoqui, G.; Villarino, A.; Ovsejevi, K.; Batista-Viera, F.; Fernandez-Lafuente, R.; Guisán, J. M. Some Special Features of Glyoxyl Supports to Immobilize Proteins. *Enzyme Microb Technol* **2005**, *37*, 456–462. https://doi.org/10.1016/j.enzmictec.2005.03.020.

(29)   Roura Padrosa, D.; Alaux, R.; Smith, P.; Dreveny, I.; López-Gallego, F.; Paradisi, F. Enhancing PLP-Binding Capacity of Class-III ω-Transaminase by Single Residue Substitution. *Front Bioeng Biotechnol* **2019**, *7*, 484947. https://doi.org/10.3389/FBIOE.2019.00282/BIBTEX.

(30)   Planchestainer, M.; Contente, M. L.; Cassidy, J.; Molinari, F.; Tamborini, L.; Paradisi, F. Continuous Flow Biocatalysis: Production and in-Line Purification of Amines by Immobilised Transaminase from Halomonas Elongata. *Green Chemistry* **2017**, *19*, 372. https://doi.org/10.1039/c6gc01780k.

(31)   Gibson, D. G.; Young, L.; Chuang, R. Y.; Venter, J. C.; Hutchison, C. A.; Smith, H. O. Enzymatic Assembly of DNA Molecules up to Several Hundred Kilobases. *Nature Methods 2009 6:5* **2009**, *6* (5), 343–345. https://doi.org/10.1038/nmeth.1318.

A Three-Step Enzymatic Cascade for Production of

Tryptamine Analogues

6.1 Aim of the Project

This chapter explores the enzymatic synthesis of tryptamine analogues as an alternative method for producing valuable compounds, such as melatonin and serotonin. An L-tryptophanase from *Escherichia coli* (EcTnaA), a decarboxylase from *Rumignococcus gnavus* (RgtDC), and an acyltransferase from *Mycobacterium smegmatis* (MsAcT) are used in a sequential manner to convert serine and indole, or its derivatives (5-hydroxy- and 5-methoxy-indole), into the respective acylated tryptamine (Figure 6.1). The primary objective was to promote the continuous production of the final compounds in flow, maximize the catalytic efficiency of the biocatalyst, and recover the unreacted substrate, thereby increasing the sustainability of the system.
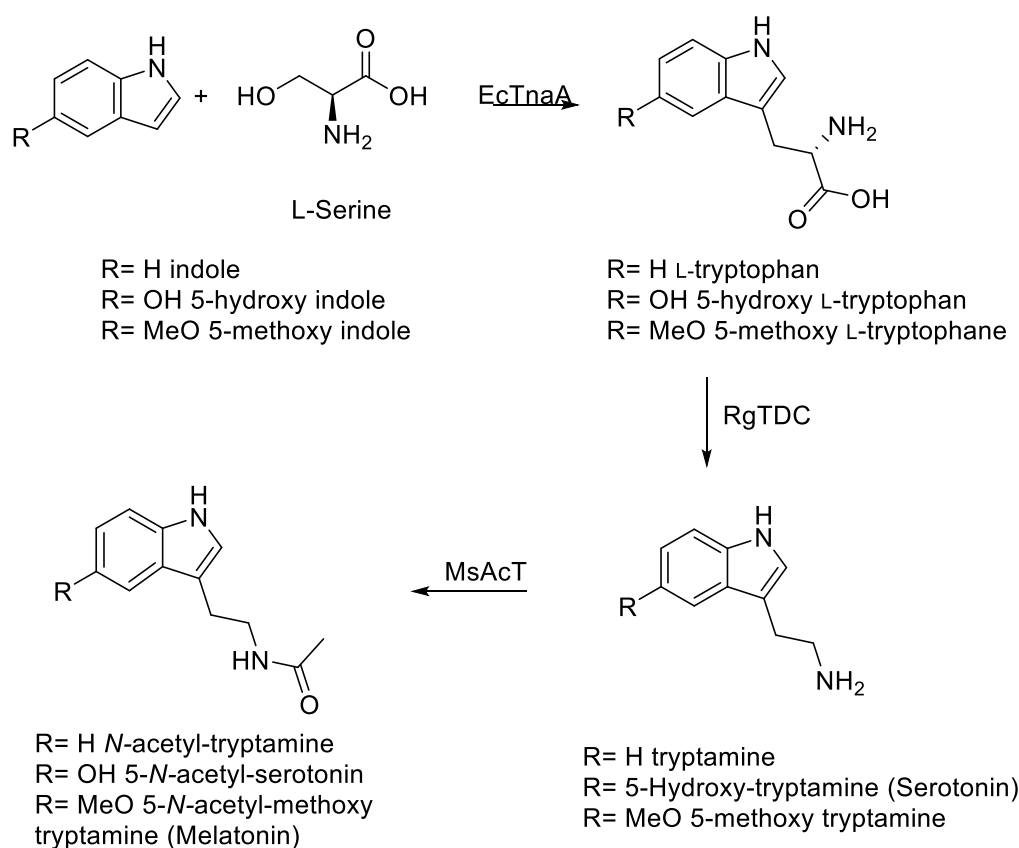

Figure 6.1. Schematic representation of the proposed three-step enzyme cascade for the synthesis of tryptamine analogues. The first enzyme, EcTnaA, catalyses the conversion of L-serine and indole (or analogues) into the corresponding L-tryptophan scaffold. Subsequently, RgTDC, promotes the transformation of L-tryptophan (or analogue) into the respective tryptamine (or analogue). The latter molecule generated serves as the substrate for the final enzyme, MsAcT which catalyses the acylation step, leading to the formation of the final product, such as melatonin.

6.2 Introduction

The cyclic pattern of alternating sleep and wake in response to environmental light fluctuations is known as the circadian cycle. This rhythmic phenomenon repeats approximately every 24 hours and is predominantly regulated by the suprachiasmatic nucleus (SCN) located in the hypothalamus. Stimulation of the SCN initiates a sophisticated metabolic cascade, engaging additional structures, such as the pineal gland.[1–3] In this small organelle, the biosynthesis of melatonin (*N*-acetyl-5-methoxytryptamine) and serotonin (5-hydroxytryptamine, 5-HT) occurs. The habits developed in contemporary society, such as excessive screen usage, shift work, or exposure to jet lag, have led to a disruption in the circadian rhythm governing the sleep-wake cycle.

In response to this dysfunction, melatonin is now commercially available in many countries as an over-the-counter dietary supplement. The trade of melatonin in the United States witnessed an increment from 0.4% to 2.1% between 1999 and 2018, reflecting an increased demand for its production.[4] Currently, melatonin is industrially manufactured through a complex chemical synthesis that involves the utilization of cyanide, lithium aluminium hydride, and multiple iterations of heating and cooling.[5] Nowadays, this traditional method for the production of melatonin faces challenges in alignment with prevailing political and environmental directives, requiring a more sustainable and eco-friendly synthetic approach.

To attain this objective, the research in this chapter will explore an alternative biosynthetic method involving three enzymes, and introducing steps which aim to reduce the environmental impact of the original process. The forthcoming section will provide a detailed description of the biocatalysts, initiating from common precursor molecules like serine and indole (or its analogues), progressing through the condensation, decarboxylation, and acetylation step. This last step of the cascade is a well assessed system developed in 2019 in our research group for an enzymatic synthesis of melatonin in a flow system by means of an acetyl transferase from *Mycobacterium smegmatis*.[6–8] This innovative approach afforded a fully automated alternative process, enabling the conversion of 5-methoxy tryptamine and other biogenic amines into their corresponding acylated products. Under these conditions, an excellent yield was achieved within short reaction times of just 5 minutes.[9] Starting from this initial stage, we explored the possibility of broadening the cascade by employing a more economical substrate and recycling the unreacted starting materials, therefore improving the

overall sustainability of the process. The ultimate outcome is the generation of high-value products, such as serotonin and melatonin by employing sustainable practices from affordable sources while minimising waste.

Preliminary Work and Background on EcTnaA.

The first enzyme of the cascade, EcTnaA (EC 4.1.99.1), naturally catalyses the degradation of L-tryptophan to indole, pyruvate, and ammonia *via* an α,β-elimination in a pyridoxal-5'-phosphate (PLP)-dependant reaction. Previous reports demonstrate that this enzyme shows substrate promiscuity as was highlighted for 12 differently substituted L-tryptophan analogues by Snell *et al.*.[9] Ku and collaborators reported the crystallographic structure of EcTnaA, which was identified as a homotetramer (subunits of 53 KDa).[9] [10] This structure exhibit cold sensitivity and below 25 °C dissociates into dimers, transitioning into its inactive apo-form. Therefore, to facilitate the correct quaternary structure folding, a two-hour incubation at 37 °C is essential prior to any biotransformation. In its natural environment, EcTnaA produces pyruvate, ammonia, and indole (**7**). Notably, **7** acts as a signalling molecule inside microbial cells, responding to environmental stress and triggering functions such as biofilm formation[11], quorum sensing[12] or plasmid stability.[13]

Other investigations have indicated that in the presence of elevated substrate concentrations, EcTnaA can also function in the synthetic direction – that is, it facilitates the production of L-tryptophan (**9**), utilizing indole, pyruvate, and ammonia as starting materials.[14] Interestingly, the synthesis of **9,** from **7** and L-serine (**8**) as substrates, is also possible when **8** in large excess (Figure 6.2).[15]
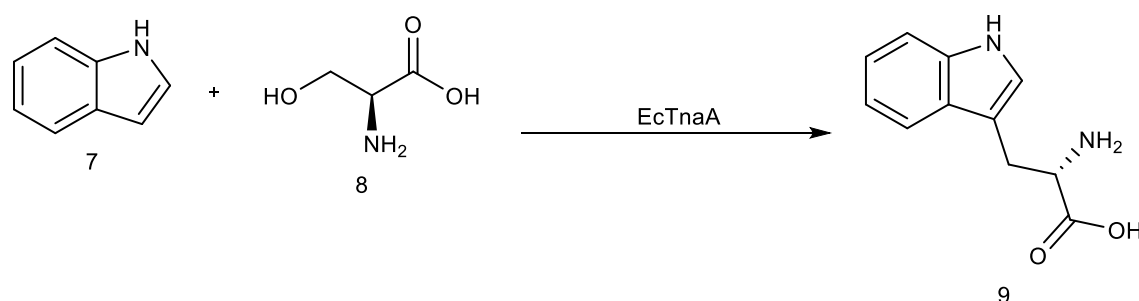

Figure 6.2. Biosynthesis of L-tryptophan **9** from indole **7** and L-serine **8** by EcTnaA.

The objective of this work is to produce a range of tryptamine analogues from 5-X-indole derivatives such as 5-hydroxyindole (**10**) and 5-methoxyindole (**11**). However, to achieve this, the active site of EcTnaA required engineering to accommodate the more voluminous substrates and ensure the successful binding and turnover of these molecules (Figure 6.3).
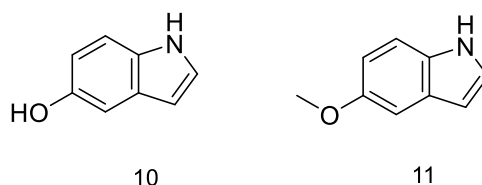

Figure 6.3 Indole analogues as substrates for the biosynthesis of tryptamines analogues. 5-hydroxyindole (**10**) and 5-methoxyindole (**11**) both contain substitutions in position 5 of the indole ring, exhibit larger molecular dimensions compared to the natural substrate **7**, consequently, their accommodation within the active site may pose challenges due to their increased bulkiness

To enhance the available space within the active site, was necessary to introduce specific mutations at positions 51 (replacing alanine with leucine, L51A) and 394 (substituting alanine with valine, V394A) (as depicted in Figure 6.4).
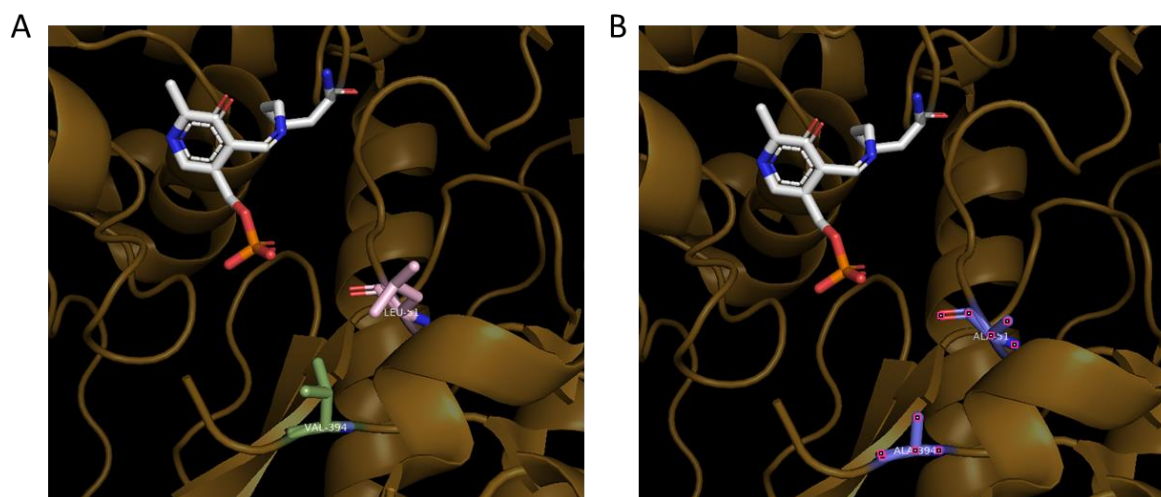

Figure 6.4 EcTnaA wt (A) and the double mutated variant where valine 364 is depicted in green and leucine 51 is depicted in pink. On the right (B) the respective mutation (in purple) where both amino acids are mutated for two alanine.

The substituted amino acids highlighted in purple in Figure 6.4, were rationally *in silico* designed by our research group.[16] Following the successful mutation of the gene, the plasmid was introduced into the *E. coli* strain tn5:tna-, which had been modified to lack the L-

tryptophanase gene. This modified strain was kindly provided by Dr. Robert S. Phillips from the Department of Chemistry at the University of Georgia, USA.[17]

6.3 Results

6.3.1 Enzyme 1: L-Tryptophan indole-lyase from *Escherichia coli* (EcTnaA)

In this work we replicated the expression achieving a good biomass (10 g/L) and protein yield (80 and 150 mg/L for EcTnaA-wt and L51A-V394A, respectively) comparable with what previously done. Upon purification, we established a series of biotransformations involving various (substituted) indole substrates. In all cases, the protein was pre-incubated at 37 °C for 2 hours. The specific activity was measured over 10 minutes and analysed by HPLC at 260 nm. The results are summarised in Table 6.1.

Table 6.1. Specific activity of EcTnaA-wt and EcTnaA-L51A-V394A. n.d. not detected.

Variant	Substrate	Specific Activity (U/mg)
EcTnaA-WT	Indole	5.5 ± 1.2
	5-Methoxyindole	n.d.
	5-Hydroxyindole	4.5 ± 1.8
EcTnaA-L51A-V394A	Indole	0.3 ± 0.2
	5-Methoxyindole	0.7 ± 0.2
	5-Hydroxyindole	n.d

At a concentration of 10 mM of the respective substrate, the wild-type enzyme demonstrated remarkable efficacy: up to 90 % of 5-hydroxyindole was converted to the corresponding 5-hydroxy-L-tryptophan within 1 hour of incubation at 37 °C, using 12.5 equivalents of serine

(Figure 6.5). As expected, the conversion of indole as natural substrate, was 100% in the same time frame.
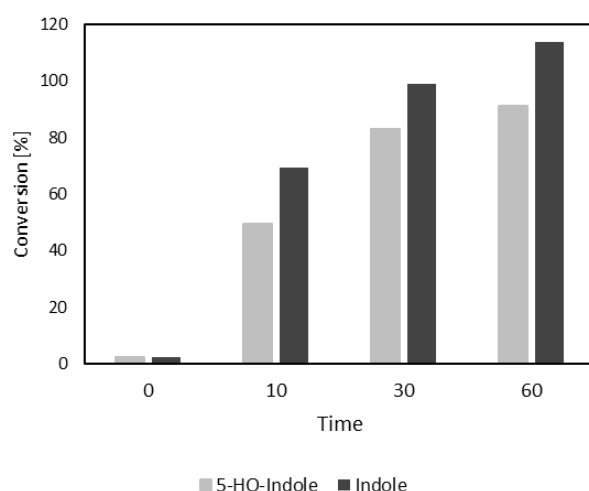

Figure 6.5 Conversion of indole (black) and 5-hydroxyindole (grey) in L-tryptophan and 5-hydroxy-L-tryptophan, respectively, catalysed by EcTnaA-WT. The experimental setup included indole or 5-hydroxyindole at concentrations of 10 mM along with 125 mM serine and 0.1 mM PLP in a KPi buffer (50 mM, pH 8), all reactions were conducted at 37 °C.

Similarly, the variant EcTnaA-L51A-V394A, converted 97 % of 5-methoxyindole (10 mM) to 5-methoxy-L-tryptophan within 1 hour, using the same equivalents of serine (12.5) (as depicted in Figure 6.6A). The rate of conversion decreased progressively as the concentration of 5-methoxyindole was increased, while a fixed concentration of L-serine (125 mM) was maintained (Figure 6.6B).
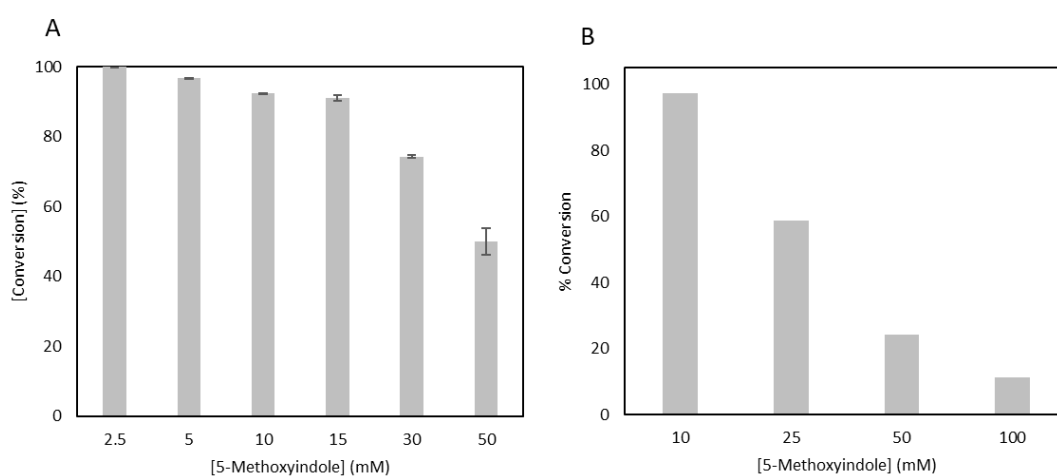

Figure 6.6 (A) Process scale-up for the synthesis of 5-methoxy-L-tryptophan at 1 hour and; (B) 4 hours. The reaction mixture comprised 5-methoxyindole (10-100 mM), serine (125 mM),

127

PLP (0.1 mM), and EcTnaA-L51A V394A (1 mg/mL) in a KPi buffer (50 mM, pH 8). The reaction mixture was maintained at 37 °C. Samples were collected at regular intervals: 2, 5, 7, 10, 30, 60, and 90 minutes and submitted for HPLC analysis.

We investigated the minimum amount of L-serine required for complete conversion of 5-methoxyindole to product. The number of equivalents of L-serine was varied while a fixed concentration of 5-methoxyindole (50 mM) was maintained. The highest conversion was achieved when using 0.625 M of serine (12.5 equivalents, Figure 6.7).
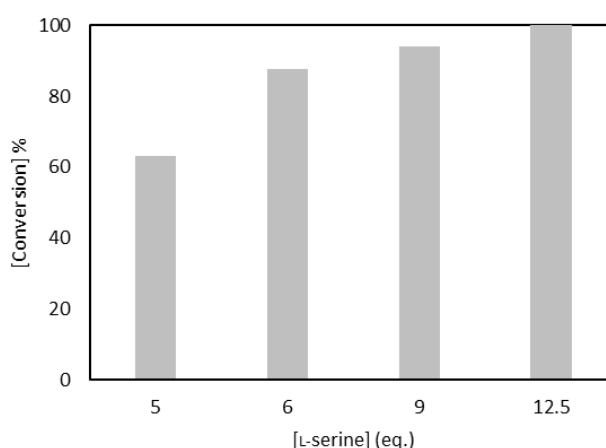

Figure 6.7 Screening of L-serine equivalents for the synthesis of 5-methoxy-L-tryptophan after 90 minutes. The highest conversion rate was achieved when using 12.5 equivalents of serine. The reaction mixture comprised of 5-methoxyindole (50 mM), L-serine (5-12.5 eq.), PLP (0.1 mM), and EcTnaA-L51A-V394A (1 mg/mL) in KPi buffer (50 mM, pH 8). The reaction mixture was maintained at 37 °C. Samples were analysed by HPLC.

With the optimal indole-derivative: serine ratio established, we found the optimal conditions for the production of 5-methoxy-L-tryptophan. Our next step was to investigate how this reaction could be implemented in a flow system. To do that, the biocatalyst must be immobilised on a suitable resin and identify the best operational conditions. Therefore, in the next section will be presented the study that has been carried out in order to identify these parameters.

6.3.2 Immobilization of EcTnaA and Application to Flow

The transition toward an automated system required the identification of the optimal support on which to immobilize the biocatalyst. Our screening process started with two distinct carriers: agarose and a methacrylic resin (EP400/SS), both of which are functionalized with epoxy groups. A protein loading of 5 mg/g was tested. Following a 2-hour pre-incubation of

the free enzymes at 37 °C (WT and mutant), we added the support and an immobilization yield of >99% was estimated for EP400/S after 4 hours. However, with agarose, we observed the formation of a precipitate in the solution (Figure 6.8) and this support was not considered further.
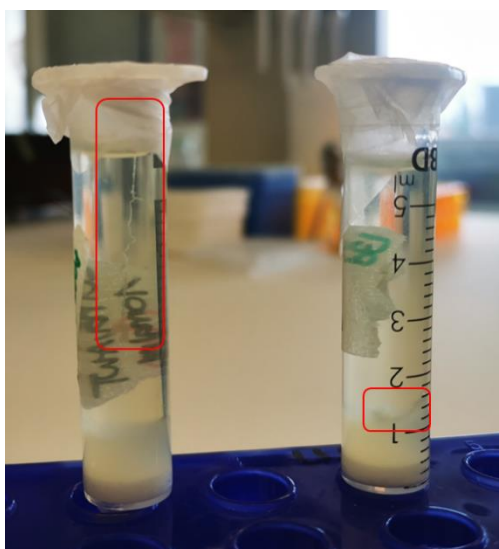

Figure 6.8 Attempted immobilization of EcTnaA-WT (left) and EcTnaA-L51A-V394A (right) on agarose as the support material. The protein loading was 5 mg/g, and the protein solution was diluted to the appropriate amount in KPi buffer (50 mM, pH 8). After 4 hours, the formation of a precipitate in solution was observed (highlighted in the red square).

We then tested a higher protein loading (10 mg/g) with EP400/S to maximize the activity of the resin. While the immobilisation yield was the same, the recovered activity was significantly impacted by the immobilisation process, retaining 4 to 8% at both 5 and 10 mg/g, respectively (Figure 6.9). Hence, we proceed with the highest protein loading for subsequent flow experiments.
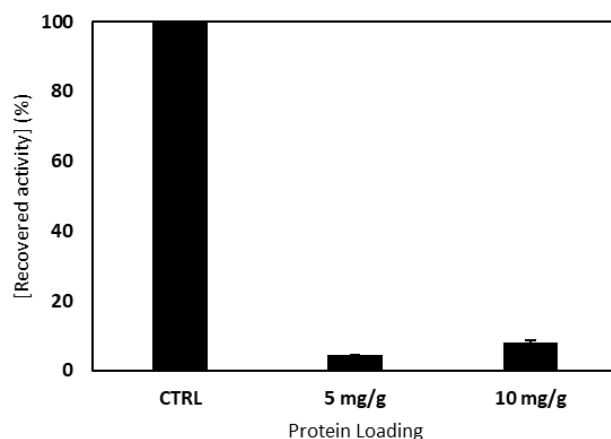
Figure 6.9 Recovered activity of EcTnaA-WT at 5 and 10 mg/g upon immobilisation on EP400/SS. The activities are reported in comparison with the control (soluble enzyme). The immobilised biocatalyst retained 4 and 8% of its initial activity at 5 and 10 mg/g, respectively.

The flow setup included a packed-bed reactor with 2.7 g and 3 g of immobilized EcTnaA-L51A-V394A respectively, both at 10 mg/g and the flow rate was adjusted to achieve a residence time (the duration a chemical species remains within the reactor) of 20 minutes.

We collected several fractions, each corresponding to 1 column volume (3.42 or 3.9 mL) and the amount of 5-hydroxy-/5-methoxy-L-tryptophan in each was quantified by HPLC. The results, depicted in Figure 6.10 A-B, indicate that the concentration of the product in both the experiments never exceeded 0.5 mM (2.25%) in any of the collected fractions, therefore.
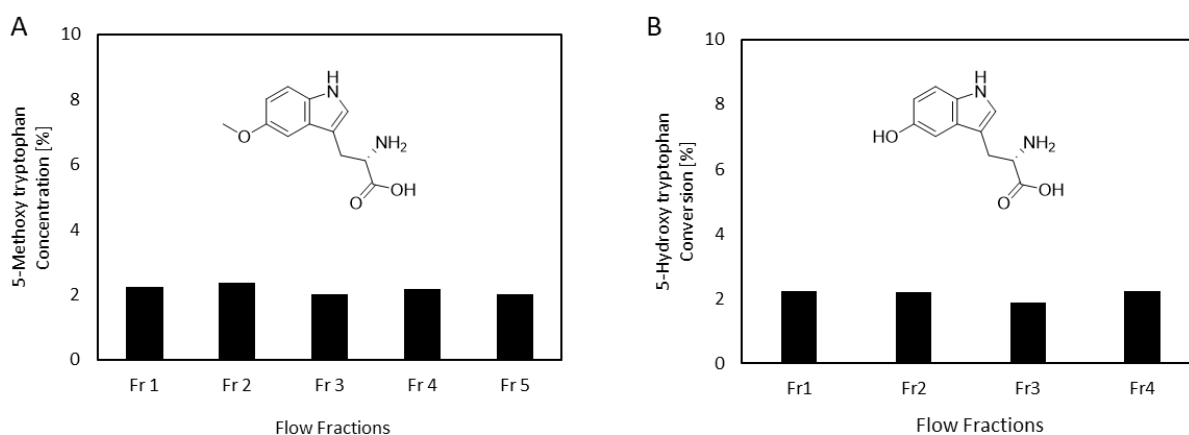

Figure 6.10 (A) Amount of 5-methoxy-L-tryptophan quantified in each flow fraction. (B) Amount 5-Hydroxy-L-tryptophan produced in each flow fraction Each fraction is equivalent to 1 column volume (1 CV). Each fraction was analysed by HPLC, quantifying both the final

products by HPLC. The reaction mixture was prepared with 20 mM of the respective indole-precursor, 250mM-1.25M L-serine, 0.1 mM PLP, and 10% DMSO in 50 mM KPi buffer at pH 8.

After the first fraction, we observed a colour change of the resin, shifting from white to pink (Figure 6.11), likely coming from the degradation of the starting material (5-hydroxyindole).

Figure 6.11 Flow column packed with immobilised EcTnaA before (left) and after (right) the experiment.

This binding effect likely arises from the inherent ability of the substrate to interact and adsorb onto the resin surface. Therefore the indole becomes less available for enzymatic turnover.

To try to optimise the production of 5-methoxy-L-tryptophan in our continuous flow system, the residence time was extended from 20 to 100 minutes. This extension was achieved by combining five individual fractions (19.6 mL) and recirculating the collected volume. We introduced 10% toluene in a segmented flow into the system to extract 5-methoxyindole from the resin. This process was repeated for three cycles, with quantification of the concentration of 5-methoxy-L-tryptophan after each cycle. Despite our efforts, no improvement was noted (Figure 6.12).
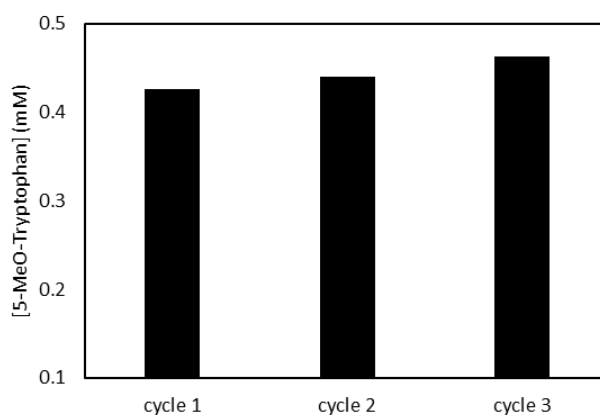
Figure 6.12 Concentration of 5-methoxy-L-tryptophan after 3 cycles. Each cycle is the collection of 5 fractions of 3.9 mL each collected and recirculated for a total residence time of 100 min.

Due to the significant loss of retained activity of immobilised EcTnaA and the inherent limitations of immobilization, we opted for an alternative strategy. In the next section, we employ a membrane to selectively isolate the first enzyme within the reaction mixture. This strategic separation allowed us to substitute the first biocatalyst with the second enzyme in a telescopic reaction once the initial substrates had undergone conversion.

6.3.3 Strategies to avoid product degradation.

During our attempt to scale up the reaction to 50 mM, biotransformation setups with indole, 5-methoxy, and 5-hydroxy indole in 50 mL were established. Noteworthy, with extended reaction times (beyond 4 hours), we observed a gradual change in the colour of the reaction medium. Initially pale yellow, the mixture deepened to a darker yellow and eventually transformed into a dark brownish solution (Figure 6.14A). Remarkably, this colour change correlated with a conversion rate of less than 3% for the indole-like substrate. A colour change in the reaction mixture coupled with a low conversion suggests that the product underwent oxidation, which is influenced by factors such as light exposure, reactive oxygen species (ROS), metal interactions, and thermal effects.[18]

To address this setback, various approaches were employed, including the introduction of an antioxidant, mitigation of light exposure, and conducting the biotransformation under nitrogen gas. To evaluate the impact of the antioxidant, ascorbic acid was chosen for

examination. A standard reaction mixture containing 10 mM indole, 125 mM serine, 0.1 mM PLP, and 0.1 mg/mL of EcTnaA-WT in 50 mM KPi buffer at pH 8, was set up and served as the control.[19] In parallel, a second identical reaction supplemented with 10 mM ascorbic acid was prepared.

Figure 6.13 shows that the presence of the additive significantly diminished L-tryptophan synthesis, resulting in a nearly 50% reduction in conversion after 60 minutes.
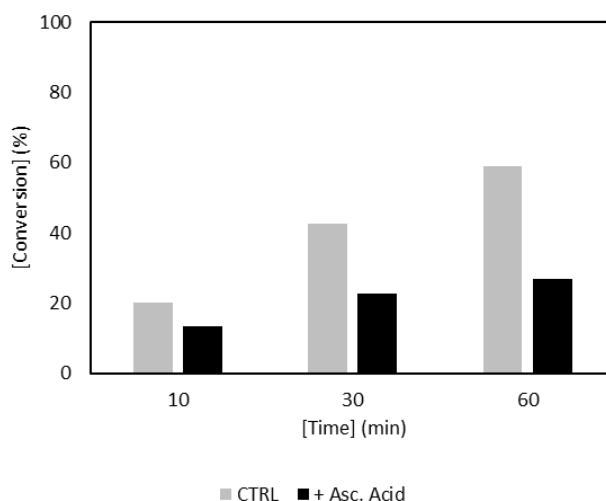

Figure 6.13 Influence of ascorbic acid on L-tryptophan biosynthesis by EcTnaA-wt. The black bars represent the conversion of 10 mM indole and 125 mM serine in the presence of 10 mM ascorbic acid in the reaction mixture. In contrast, the grey bars represent the biotransformation carried out under standard conditions without the addition of antioxidant. The reactions were allowed to proceed for 1 hour at 37 °C, with samples aliquoted for HPLC analysis at 10, 30, and 60 minutes.

The second approach to prevent the degradation of L-tryptophan involved protecting the reaction from exposure to light and oxygen. A vessel containing 50 mL of reaction mixture (50 mM 5-hydroxy- or 5-methoxyindole) was shielded with aluminium foil, and nitrogen gas was purged into the solution prior to the enzyme addition. The reactions were kept under an inert atmosphere throughout the 16-hour process, and samples were extracted using a syringe through a septum. Figure 6.14 illustrates an example of the experimental setup for the reaction involving 5-hydroxyindole.
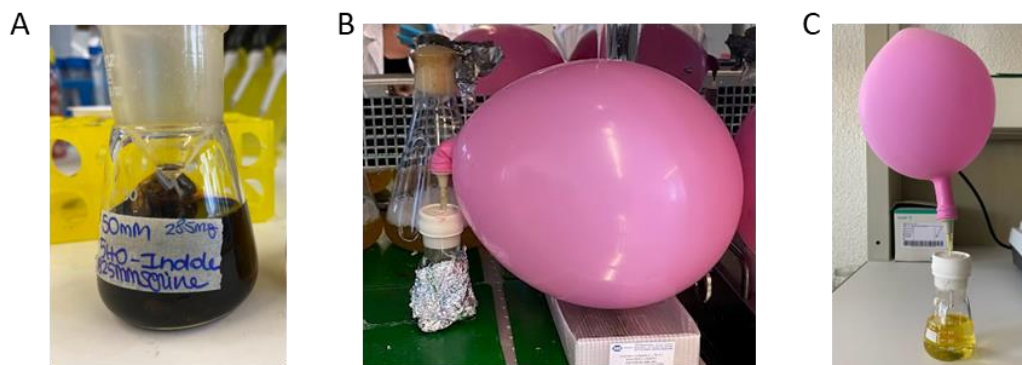
Figure 6.14 5-Hydroxy-L-tryptophan production under different conditions. (A) Production of 5-hydroxy-L-tryptophan without light and air protection; (B) a reaction set-up where the mixture is shielded from light and O_2 and; (C) the resulting solution after 16 hours at 37 °C. The reaction mixture contained 50 mM 5-hydroxyindole, 125 mM serine, 0.1 mM PLP, and 1 mg/mL EcTnaA-WT in 50 mM KPi buffer at pH 8. The balloon is filled with N_2 to maintain an inert atmosphere.

With this method, after 16 hours of reaction time, no colour change was observed. Notably, the conversion to 5-hydroxy-L-tryptophan reached 97% with EcTnaA-WT, while 5-methoxy-L-tryptophan was fully converted only with EcTnaA-L51A-V349A. These results suggest that the oxidation process of either the substrate or the product, is the main major contributor to the low conversions.

6.3.4 Screening of Alternative Substrates

To investigate the substrate promiscuity of EcTnaA, alternative indole analogues were also screened. We first focused on benzothiophene (**12**) and benzofuran (**13**). These compounds are isostructural with indole (**7**), with the nitrogen atom in the ring replaced by sulphur and oxygen, respectively, with 3-benzothienyl-L-alanine (**14**) and D-3-(3-benzofuranyl)-alanine (**15**) as potential products (Figure 6.15). Non-natural amino acids are known to inhibit mitochondrial translation and indoleamine-pyrrole 2,3-dioxygenase (IDO), an enzyme associated with L-tryptophan metabolism in humans. [20,21]
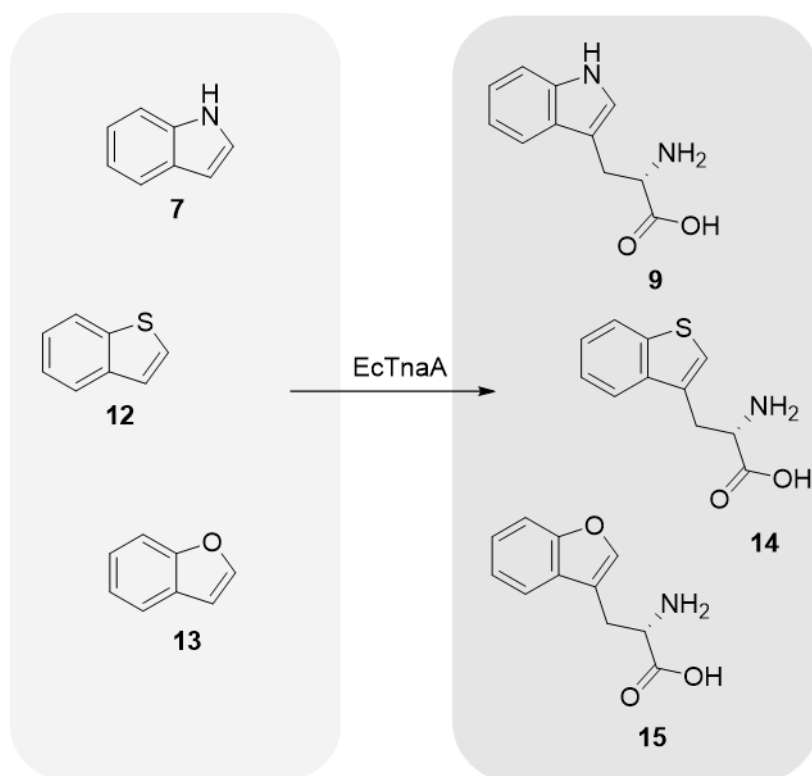
Figure 6.15 Indole-analogues for substrate scope and the corresponding reactions catalysed by EcTnaA (B,C).

Reactions containing 10 mM benzothiophene or benzofuran, 125 mM serine, 0.1 mg/mL PLP, and 1 mg/mL EcTnaA (either wild-type or L51A-V394A) in 50 mM KPi buffer at pH 8 were prepared. The indole analogues exhibited solubility issues under aqueous conditions, so DMSO was added as a co-solvent (5% to 15%). Each reaction was carried out at 37 °C, and samples were aliquoted for HPLC analysis at 10, 30, and 60 minutes.

Unfortunately, the chromatographic profiles of the reaction mixtures did not reveal any product formation, regardless of whether the wild-type or mutant variant of the enzyme was employed.

As part of the screening process, an examination of a serine analogue was conducted. In this instance, ethanolamine (**16**) was evaluated, considering that the reaction would directly yield the formation of tryptamine, thereby by-passing the necessity to decarboxylate tryptophan (Figure 6.16).
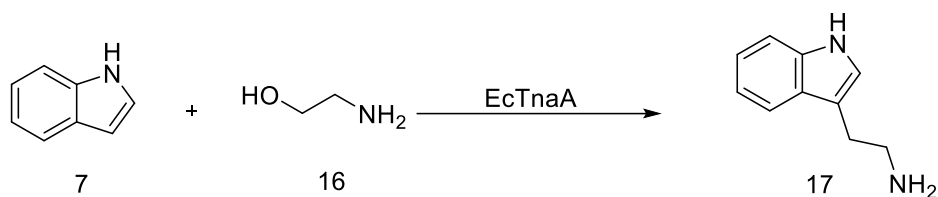
Figure 6.16 Proposed synthesis of tryptamine (**17**) from indole (**7**) and ethanolamine (**16**) catalysed by EcTnaA.

We tested various concentrations of **16** (125, 250, and 500 mM) while the concentration of the other reagents remained constant (5-hydroxy/5-methoxy indole at 10 mM, PLP at 0.1 mM, and EcTnaA (either wild-type or L51A-V394A) at 1 mg/mL). These reactions were conducted in 50 mM KPi buffer at pH 8. Product formation was monitored over 1 hour at 37 °C, with samples collected at intervals of 10, 30, 60 minutes, and 7 hours.

None of the tested conditions however yielded the corresponding amine product, highlighting the critical role of the carboxylic moiety in the condensation step during L-tryptophan synthesis.

6.3.5 Enzyme 2: L-Tryptophan Decarboxylase from *Rumignococcus gnavus* (RgTDC)

The second phase of the cascade relies on a decarboxylase obtained from *Rumignococcus gnavus*, specifically identified as RUMGNA_01526 or RgTDC (EC 4.1.1.105). Fischbach *et al*. isolated this enzyme in 2014 while investigating the influence of gut microbiota and their potential effects on the human brain.[22]

Similar to EcTnaA, RgTDC is a pyridoxal-5'-phosphate (PLP)-dependent enzyme which catalyses the conversion of L-tryptophan to tryptamine (Figure 6.17). [23]

R= H, L-Tryptophan
R=HO, 5-Hydroxy-L-tryptophan
R=MeO, 5-Methoxy-L-tryptophan

R= H, Tryptamin
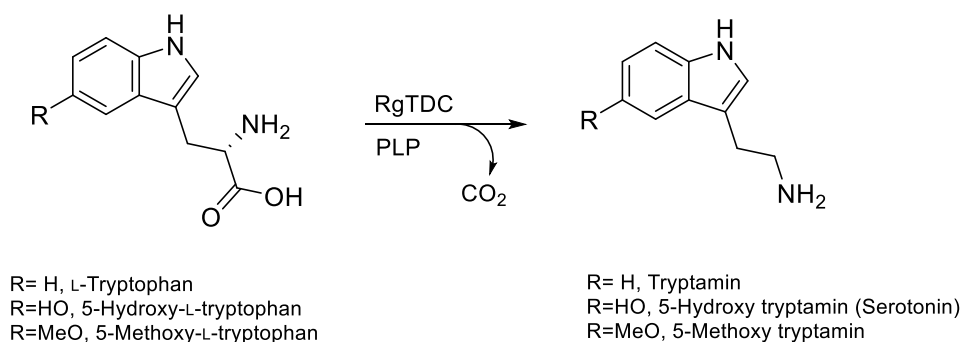R=HO, 5-Hydroxy tryptamin (Serotonin)
R=MeO, 5-Methoxy tryptamin

Figure 6.17 In this step, RgTDC catalyses the decarboxylation of L-tryptophan, resulting in the formation of the corresponding tryptamine by a PLP-mediated reaction.

The crystallographic structure of RgTDC (PDB: 4OBV) reveals a homodimeric enzyme composed of two subunits, each weighing 54.7 kDa, with the active sites situated at the interface of the subunits (Figure 6.18).
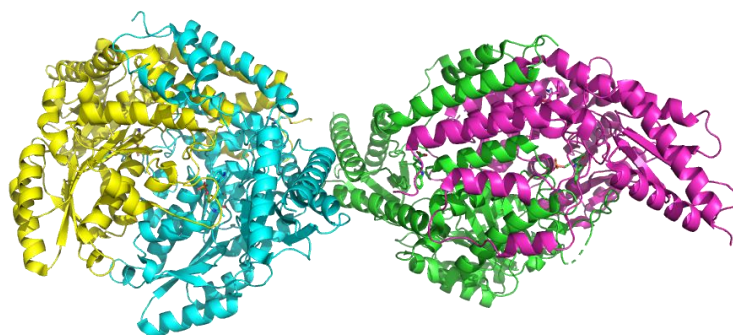

Figure 6.18 Crystal structure of RgTDC crystalised with α-fluoromethyl-D-tryptophan as inhibitor (4OBV). Picture obtained with PyMol ver. 2.4.1.

Given its ability to transform L-tryptophan into tryptamine, our objective was to convert the product generated in the initial enzymatic step into the substrates for the subsequent step. Prior to this work, through *in silico* analysis, two mutants were created to expand the space inside the catalytic pocket and favour the binding of 5-substitutet L-tryptophan analogues.[16]

Figure 6.19A illustrates the design of the mutations: the catalytic pocket of the wild type enzyme features a leucine and a tryptophan at positions 336 and 349, respectively. For one mutant, the leucine residue was replaced with a less bulky alanine (RgTDC-L336A, Fig 6.19B). For a second mutant, the tryptophan residue was substituted with a phenylalanine (RgTDC-W349F, Fig 6.19C), thereby augmenting the space available for the substrate while preserving the aromaticity of the residue in the chain.
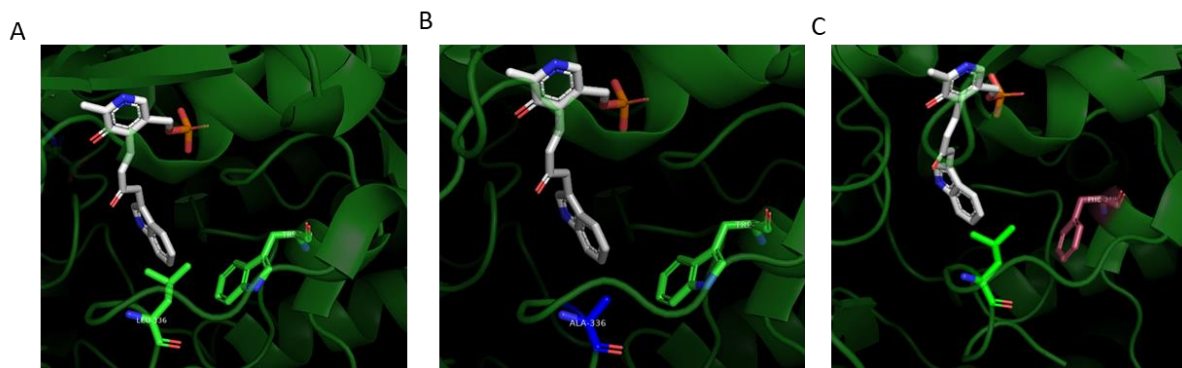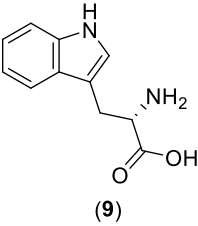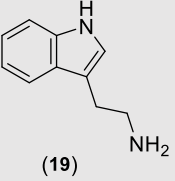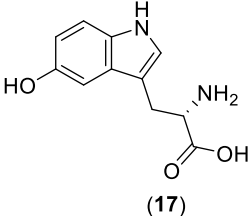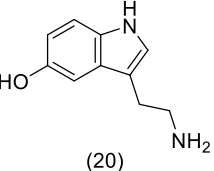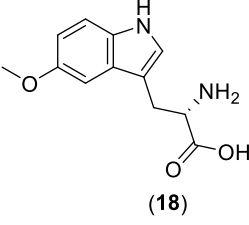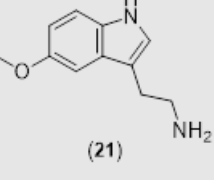
Figure 6.19 Representation of the RgTDC active site model and corresponding mutation, docked with the inhibitor, α-fluoromethyl-D-tryptophan. From left to right, the active site of the wild type enzyme (A) features a leucine and a tryptophan, highlighted in green. To accommodate our larger substrates, the leucine was replaced by an alanine (B, shown in blue), and tryptophan was substituted with a phenylalanine (C, shown in pink). Models were generated using PyMol version 2.4.1.

The wild type and both mutants were soluble expressed in *E. coli* and subsequently evaluated for their activity using the natural substrate.

6.3.6 Activity Assay

With the enzymes in hand, we observed that RgTDC retained the original activity observed in the wild type. The assay was set up as described in Materials and Methods, and with that we tracked the conversion to tryptamine overtime (Figure 6.20). A similar screening was performed using the commercially-available substrates, 5-methoxy-L-tryptophan (**17**) and 5-hydroxy-L-tryptophan (**18**), at a 10 mM scale while keeping the same concentrations of each RgTDC mutant. However, no peak indicative of product formation was observed by HPLC analysis when 5-hydroxy-L-tryptophan (**18**) was used as the substrate. In fact, the peak of the substrate and the product were co-eluted with our elution method, therefore the progression of this reaction was monitored using thin-layer chromatography (TLC). The specific activities obtained from the HPLC assay are presented below in Table 6.2

Table 6.2 Analysis of the specific activity of RgTDC (wt and its variants) with various substrates by HPLC. The specific activity is expressed in U/mg $_{enzyme}$. The reaction was monitored *via* HPLC at specific time intervals: 0, 2, 5, 7, 10, 15, and 30 minutes.

Substrate	Product	RgTDC Variant	Specific Activity (U/mg)
(9)	(19)	Wild type	13±3
		W349F	8±2
		L336A	n.d
(17)	(20)	Wild type	n.d
		W349F	n.d
		L336A	n.d.
(18)	(21)	Wild type	0.4 ±0.1
		W349F	0.7 ±0.3
		L336A	n.d

RgTDC-W349F demonstrated an enhanced conversion of the 5-methoxy-L-tryptophan (**18**) into 5-methoxytryptamine (**21**) compared to the wild type (Figure 6.20). RgTDC-WT achieved a maximum conversion of 11% while RgTDC-W349F yielded 66% conversion after 20 hours which was not improved at longer reaction times.

It is important to highlight that the conclusion of the reaction after 20 hours might be linked to protein degradation, given the continuous incubation of the reaction at 37 °C throughout the entire duration. In further support of our hypothesis, as detailed in the subsequent section, the protein is completely inactivated already after 16 hours at room temperature (as discussed in Session 6.4.2) . The conversion of 5-hydroxy-L-tryptophan (**17**) to serotonin (**20**)

was monitored by TLC since the peaks of **17** and **20** co-eluted in HPLC analysis, and after staining with ninhydrin, we observed full conversion within 2 hours.
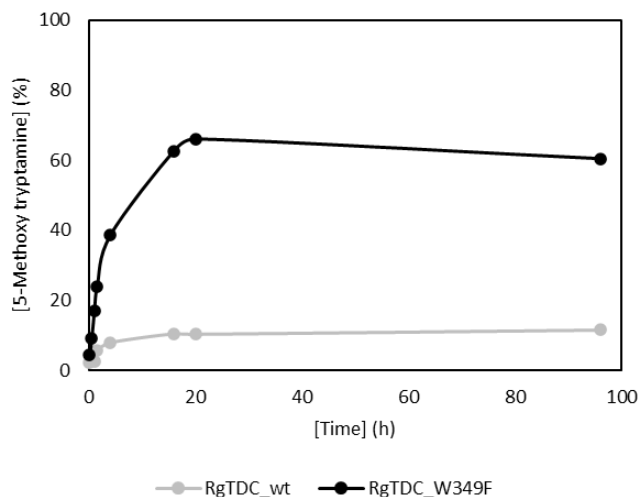
Figure 6.20 Production of 5-methoxytryptamine using RgTDC-WT (in grey) and W349F (in black) over 96 hours. Each biotransformation (2 mL) contained 1 mg/mL of the respective enzyme, 10 mM 5-methoxy L-tryptophan, 0.1 mM PLP in KPi 50 mM pH8, and was incubated at 37°C. Samples were taken at 10, 30, 60, 90 minutes, and 4, 16, 20, and 96 hours and analysed by HPLC at 260 nm.

RgTDC-W349F was therefore chosen as the optimal partner in tandem reactions with EcTnaA, irrespective of the initial substrate (indole, 5-hydroxy, or 5-methoxy-indole).

6.3.7 Immobilisation of RgTDC-W349F on Diverse Supports.

Immobilization of RgTDC-W349F was tested with various conditions and support materials as described for EcTnaA above. A protein loading of 5 mg/g on methacrylic resin EP400/SS carried out at room temperature for 5 hours yielded only negligible activity.

The immobilisation was then repeated, adjusting the incubation temperature and extending the contact time between the resin and the protein. Firstly, the enzyme-resin mixture was incubated under gentle shaking at both room temperature and at 4 °C for 16 hours. The progress of immobilization in the supernatant was monitored at two different time points.

After 4 hours, the sample at 4 °C exhibited a lower immobilization yield (63%) compared to the one at RT (83%) but both reached > 98% in 16 hours (Figure 6.21).
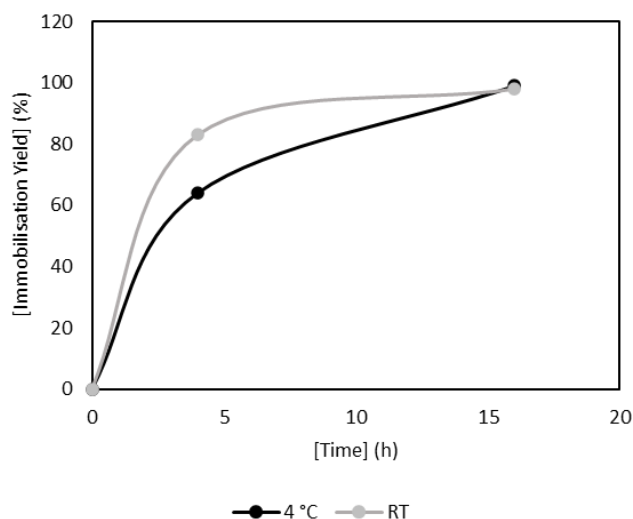
Figure 6.21 Progression of the immobilisation of RgTDC-W349F on EP400/SS at 4 °C (black) and RT (grey). The protein concentration in the supernatant was checked at 3 and at 16 hours at 280 nm.

Under these conditions, the immobilised biocatalyst retained 28% of its initial activity, while the free enzyme used under control remains fully active.

EP400/SS, also considering our similar findings with EcTnaA, was not investigated further. It was also noted that even L-tryptophan is adsorbed on the support by approximately 30% and a less hydrophobic resin was considered to be more suitable. To identify the best candidate, we tested other types of resins available in our lab. Silica beads with varying degrees of surface hydrophobicity (EziG Opal, Coral, and Amber), and agarose were considered. The protein loading was increased to 10 mg/g $_{resin}$ and the appropriate volume of protein solution was added to 100 mg of resin. The mixture was then incubated under gentle shaking at 4 °C. After 3 hours, we achieved >99% immobilization of the protein in all cases.

In terms of retained activity, the best result was obtained with EziG Opal (42% compared to the free biocatalyst). The other two resins showed 28% retained activity for EziG Coral and 12% for EziG Amber (Table 6.3).

Table 6.3 Retained activity of RgTDC-W349F (protein loading of 10 mg/g) on EziG resins.

Resin	Surface	Pore Diameter	Immobilisation Yield	Retained Activity
EziG Opal	Hydrophilic (glass)	500 ± 50 Å	>99%	42
EziG Coral	Hydrophobic (polymer)	30 ± 50 Å	>99%	12
EziG Amber	Semi-hydrophilic (polymer)	300 ± 50 Å	>99%	28

Although EziG Opal showed a good amount of retained activity, enzyme leakage into the solution over time was noted.

Agarose was trialled next. In this case, the resin was derivatized with epoxy groups for covalent immobilization. We tested different protein loadings ranging from 1 to 20 mg/g of resin, achieving full immobilization yield only at the lowest protein loading, but with negligible recovered activity (Table 6.4). As we increased the protein loading, the immobilization yield progressively decreased. At the highest protein loading (20 mg/g), the immobilization yield dropped to 33% and the retained activity never exceeded 37%.

As the immobilisation of nor the first neither the second enzyme was not satisfying, we considered an alternative approach for the cascade setup. We proposed to perform the full process using the enzymes in free form, which can be isolated from the rest of the reaction using a membrane.

Table 6.4 Retained activity of RgTDC-W349F at different protein loadings, upon immobilisation on epoxy-agarose beads.

Protein offered (mg/g $_{resin}$)	Immobilisation yield (%)	Retained activity (%)
1	97	n.d
5	45	32
10	46	37
20	33	17

6.3.8 Co-expression in EcTnaA-WT and RgTDC-W349F in *E.coli*

While screening the different alternative to a cascade setup, we also considered a co-expression of enzymes in a single host. Is reported in several examples that this approach offers different benefits, for instance the possibility to perform the reaction without any further purification, higher local substrate concentration or higher efficiency in substrate channelling. [24–26] [27]In this context, we decided to also investigate the behaviour of EcTnaA and RgTDC within such a co-expression system. To achieve this, we co-transformed *E. coli* BL21 with two plasmids carrying the respective genes and two different antibiotic resistance. The presence of colonies on the plate was confirmation that the host was successfully co-transformed. Unfortunately, the quantification of the protein, which could be done *via* FIJI Software, was not feasible due to the high similarity of the molecular weight of the two proteins, hence, was not possible to properly separate the two bands. (Figure6.22).
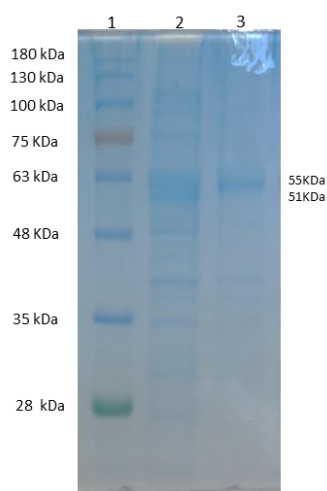
Figure 6.22 SDS-PAGE 12% of co-expressed proteins: lane **1:** crude extract; lane **2:** pellet

The production of tryptamine was then assessed using both the cell extract (100 µL) and whole cells (100 µL), in a reaction mix containing 10 mM indole, 125 mM L-serine, 0.1 mM PLP in KPi buffer 50 mM pH 8. Interestingly, under these conditions only a small fraction of indole was consumed in the both set ups (between 14% and 20%, Figure 6.23A) and the conversion of indole to L-tryptophan did not surpass 5% (Figure 6.23B). The detection of the final product of this two-enzyme cascade (tryptamine) was only noticeable after 30 minutes, but even after 80 minutes, the conversion remained below 4% (Figure 6.23C). Initially, we attributed this discrepancy in the mass balance from indole to tryptophan may be attributed to the presence

of multiple metabolic pathways within whole cells, however, as will be seen in the next section, indole exhibits an inhibitory effect on RgTDC.

A comparative analysis between the two systems (whole cells and crude extract) reveals notable distinctions, particularly in the final stage of product formation. Whole cells catalysed the formation of tryptamine with 50% less efficiency compared to the crude sample. This observation is likely due to mass transfer issues in the transport of the substrates through the outer membrane and the peptidoglycan wall of *E-coli* cells, impeding access of the substrates to the enzyme.

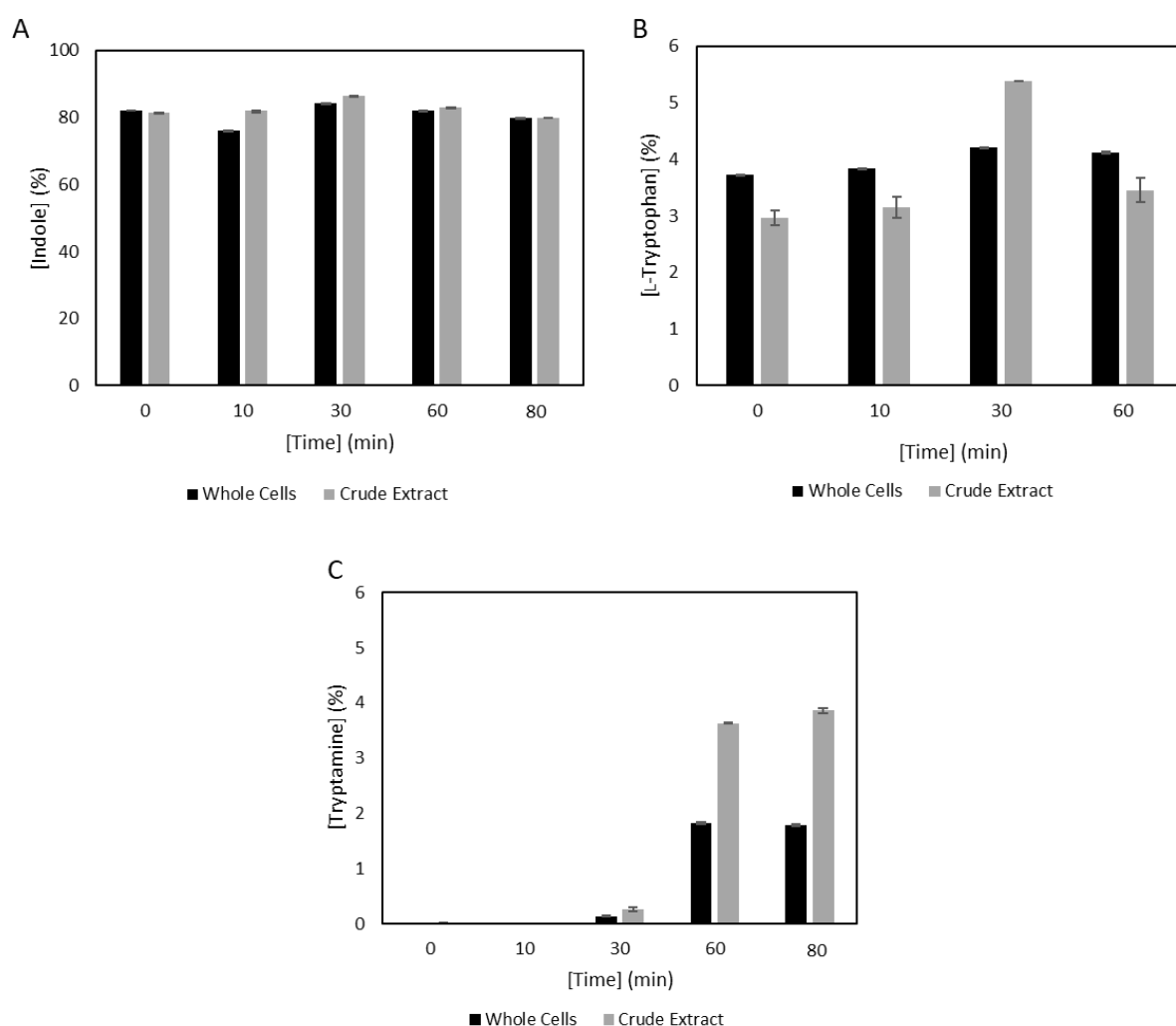**Figure 6.23** Quantification of indole (A), L-tryptophan (B), and tryptamine (C) in the reaction mixture catalysed by *E.coli*-EcTnaA-wt-RgTDC-W349F, employing both whole cells (black) or its crude extract (grey). The reaction mixture contained 10 mM indole, 125 mM serine, and 0.1 mM PLP in 50 mM KPi buffer at pH 8. The reaction was incubated at 37 °C for 80 minutes before an aliquot was taken and analysed by HPLC.

In summary, employing the co-expression of the two enzymes cannot be considered a viable strategy in this case as the initial substrate is not efficiently directed towards the production of tryptamine or its analogues.

6.3.9 Effect of Starting Material on RgTDC-W349F

During the implementation of the cascade, we closely examined the behaviour of RgTDC-W349F when coupled with EcTnaA. While RgTDC-W349F demonstrated the ability to catalyse the conversion of L-tryptophan (and analogues) to the respective amines in an isolated step within a one-pot system alongside the first enzyme, the production of final tryptamine from indole was notably impacted. We postulated that the starting material in solution could influence the second step of the cascade, therefore we conducted a preliminary test by using 3 equivalents (30 mM) of indole in the reaction, which also contained 10 mM L-tryptophan, 0.1 mM PLP, and 0.1 mg/mL RgTDC-W349F in 50 mM KPi buffer at 37 °C. The specific activity dropped by 70% upon the addition of excess indole to the reaction (Figure 6.24).
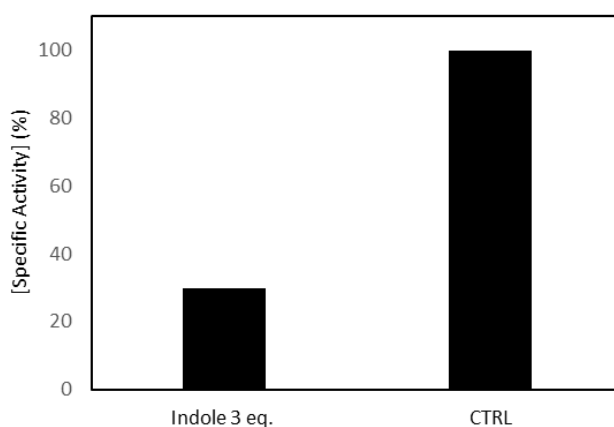
Figure 6.24 Specific activity of RgTDC-W349F in the presence of 3 equivalents of indole (left). The reaction mixture contained 10 mM L-tryptophan, 30 mM indole, 0.1 mM PLP, and 0.1 mg/mL enzyme in 50 mM KPi buffer at pH 8. The reaction mixture was incubated at 37 °C. In this reaction, the specific activity was 70% less than the control (right).

Additional investigations were conducted to determine the minimum indole concentration that RgTDC could tolerate before an inhibitory effect was observed. As illustrated in Figure 6.25 we assessed the conversion of 10 mM L-tryptophan into tryptamine with RgTDC after 1 hour, with varying indole concentrations in the reaction mixture. Notably, the biosynthesis of the product was already impacted in the presence of 0.1 mM of indole. The conversion steadily dropped to 55% at 1 mM.
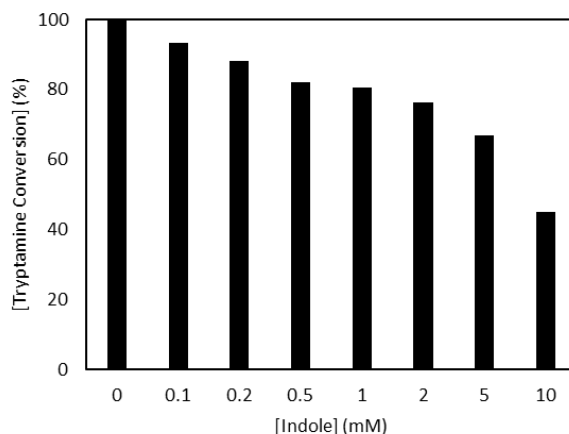
Figure 6.25 Conversion of ʟ-tryptophan into tryptamine catalysed by RgTDC-W349F in the presence of different indole concentrations. The reaction mixture contained 10 mM ʟ-tryptophan, 0.1-10 mM indole, 0.1 mM PLP, and 0.1 mg/mL enzyme in 50 mM KPi buffer at pH 8. The reaction mixture was maintained at 37 °C and the formation of tryptamine was estimated after 1 hour by HPLC. Remarkably, as the indole concentration increases, the conversion progressively decreases from 93% at 0.1 mM to 43% at 10 mM.

To further investigate whether the inhibitory effect was solely attributed to the presence of indole or whether the excess of serine also influenced the reaction, we designed a parallel experiment. 25 mM ʟ-serine was added to a reaction mixture containing 10 mM ʟ-tryptophan, 0.1 mM PLP, and 0.1mg/mL of RgTDC-W349F, and the reaction was monitored over a period of 45 minutes. The trend was found to be comparable to the control, thus ruling out an inhibitory effect from ʟ-serine (Figure 6.26).)

Figure 6.26 Effect of 125 mM ʟ-serine on the production of tryptamine by RgTDC-W349F. The reaction mixture of the control (grey) contained 10 mM ʟ-tryptophan, 0.1 mM PLP, and 0.1 mg/mL enzyme in 50 mM KPi buffer at pH 8. The reaction mixture was maintained at 37 °C. In

our experiment (black), the same reaction was supplemented with 125 mM L-serine. The conversion of tryptamine was quantified using HPLC.

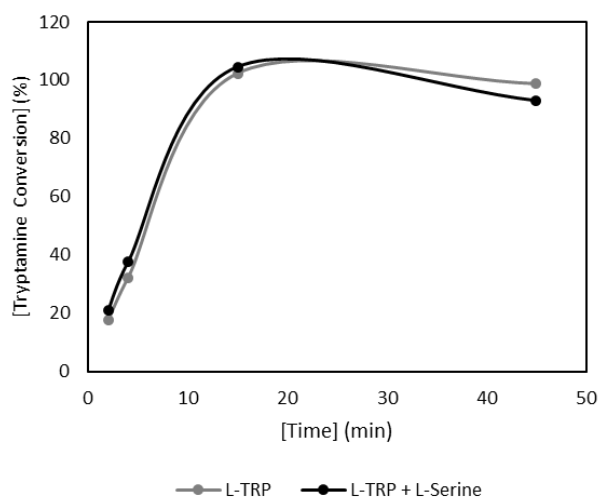It became clear that the two steps must be performed in a sequential manner. While achieving a one-pot-like setup may have been desirable, it is not feasible in this context as introducing RgTDC-W349F to the reaction mixture while indole is still present in the solution will impede the formation of the final amine.

6.3.10 Cascade optimisation: toward a telescopic reaction

In light of the previous results, a cascade with three indole-like substrates and L-serine was established. Each reaction was conducted with the indole analogue (50 mM), PLP (0.1 mM) in 50 mM KPi buffer at pH 8. The reaction mixture was maintained at 37 °C. Depending on the indole analogue used, 1 mg/mL of the corresponding variant of EcTnaA housed in a dialysis bag was introduced into the reaction vessel. Prior to incubation at 37 °C, the mixture was purged with N_2, sealed, and covered with aluminium foil to prevent degradation. When indole (or its analogues) could no longer be detected by TLC in the reaction mixture (approximately 16 hours), the dialysis bag was removed.

In a similar manner, RgTDC-W349F, housed in a dialysis bag, was then added for the second step of the cascade. The conversion of the intermediate into tryptamine (or analogue) was tracked by HPLC (in the case of L-tryptophan, 5-methoxytryptophan) or TLC (in the case of 5-hydroxy-L-tryptophan). The final concentration of decarboxylase in the reaction mixture (50 mL) was 3 mg/mL (two sequential additions of 1.5 mg/mL) and, with this quantity, a good conversion was achieved after 16 hours (Tabe 6.5).
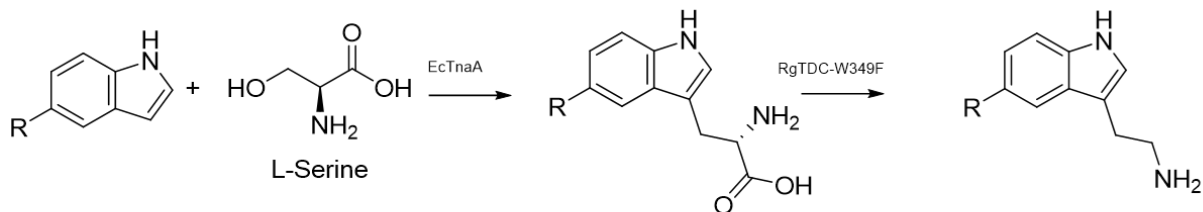
	Substrate	Step 1 EcTnaA	Conversion (%)	Step 2 RgTDC-W349F	Conversion (%)
R= H	Indole (7)	Tryptophan (9)	97	Tryptamine (19)	99
R=OH	5-Hydroxy-Indole (10)	5-Hydroxy-Tryptophan (17)	99	Serotonin (20)	TLC
R=MeO	5-Methoxy-Indole (11)	5-Methoxy-Tryptophan (18)	99	5-Methoxy-Tryptamine (21)	80
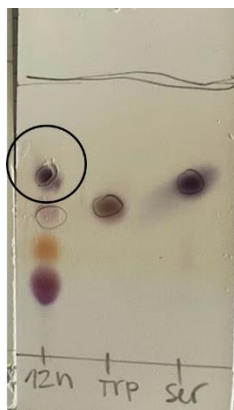
Figure 6.27 Reaction scheme and corresponding conversion of the first 2 cascade steps quantified by HPLC (top) or TLC (bottom). The conversion from indole (and analogues) to the corresponding L-tryptophan (and analogues) was >97% in all the substrates used. After 16 hours, the decarboxylation of tryptophan (and analogues) showed full consumption of L-tryptophan (**9**) and 80% conversion for 5-methoxy-L-tryptophan (**18**) to the corresponding amine. The progress of 5-hydroxy-L-tryptophan (**17**) to serotonin (**20**, highlighted in the black circle) was instead monitored using TLC due to analytical limitations.

Amines **19-21** will then serve as the substrate for the final step of the cascade - the acetylation of the free amino group. This reaction will be catalysed by an acyltransferase from *Mycobacterium smegmatis*, leading to the formation of the final products: melatonin, *N*-acetyl-tryptamine, and *N*-acetyl-serotonin.

6.3.11 Enzyme 3: Acetyl transferase from *Mycobacterium smegmatis* (MsAcT)

The final catalyst of this cascade is an acyltransferase from *Mycobacterium smegmatis* (MsAcT, E.C. 3.1.1.2), belonging to the SGNH hydrolase superfamily and characterized by a distinctive hydrogen bond network that stabilizes their catalytic centres. In the case of MsAcT, the catalytic triad consists of Ser11, Asp192, and His195.[6–8]

The crystal structure of this enzyme, elucidated by Mathews and collaborators, reveals an octameric protein featuring a hydrophobic tunnel and one active site per subunit (PDB 2Q0S, Figure 6.28).[28] The tunnel, located at the junction with three subunits, was initially identified of 26.4 Å lately enlarged of 29.6 Å and leads from the surface of the protein to the buried active site (Figure 6.28-D).[28–30]
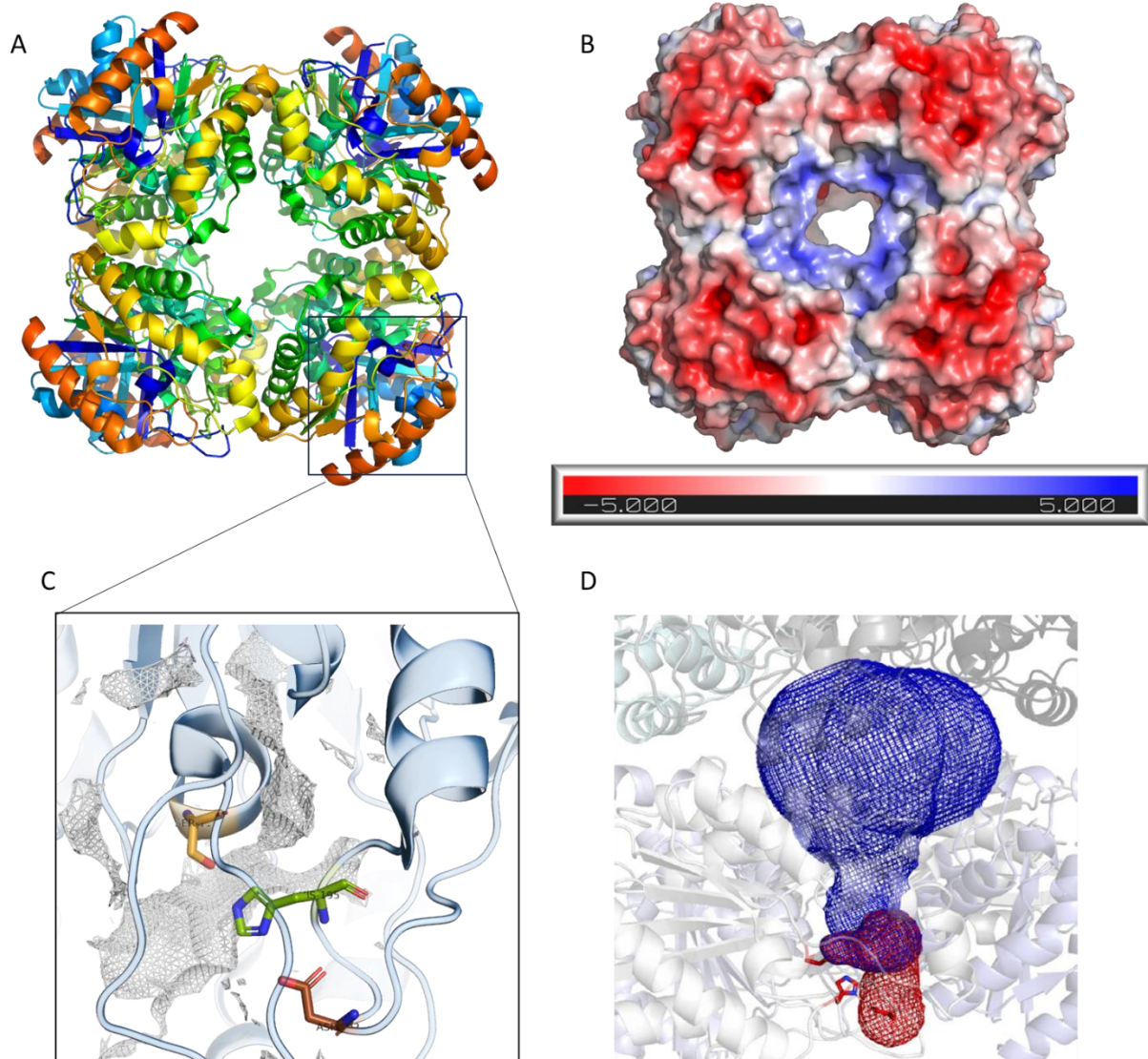
Figure 6.28 Crystal structure of MsAcT showing: (A) a five-stranded parallel β-sheet structure between α-helices and (B) electrostatic charge display, highlighting the hydrophobic tunnel at the protein centre. (C) Shows the active site with the catalytic triad highlighted in yellow (Ser11), green (His191) and pink (Asp194). These figures were generated using PyMol ver. 2.4.1 (D) Hydrophobic tunnel identified by Mathews *et al.* (in red) and the extension identified by Roura Padrosa *et al.* (in blue). Picture from Paradisi *et al.*[29]

The use of ethyl acetate can be seen as attractive way to increase process efficiency by incorporating a cosolvent which is also the acyl donor, as previously reported in 2018 in our group. Therefore, we proposed the use of immobilized MsAcT to catalyse the acetylation of the tryptamines produced in the cascade with the hope that the resulting product could be directly extracted in the co-solvent, while the unreacted amine could be easily recycled.

MsAcT was obtained by a standard expression protocol.[31]The protein was then purified gravimetrically using a Ni-NTA affinity column, yielding a substantial protein yield of 83 mg/L with a specific activity of 98 U/mg, which is in line with what was previously reported in literature (110 U/mg).[32] The immobilization (1 mg/g resin on glyoxyl-agarose) afforded a yield >99% with 60% of retained activity, also in line with previous studies.[33]

The immobilized biocatalyst was then used to replicate the acetylation reaction on a commercial substrate. We began with the amines at a 50 mM scale, resuspended in 100 mM KPi buffer at pH 8, with1 M ethyl acetate as acetyl donor. The reactions were executed at 30 °C, with 10 mg immobilized MsAcT per mL of reaction volume (refer to Figure 6.29 for further details)

Substrate	Acetyl Donor	Product
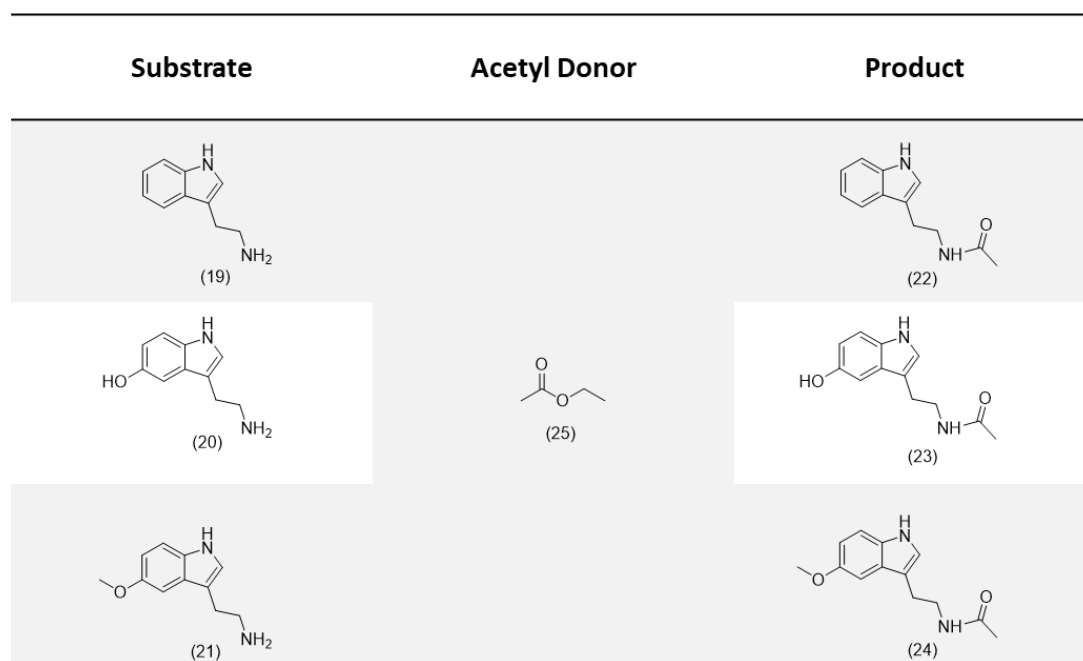
Figure 6.29 Tryptamine (**19**) and analogues (**20** and **21**) and the target *N*-acetylated products (**22**-**24**) formed by MsAcT using ethyl acetate (**25**) as acetyl donor.
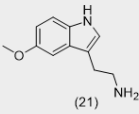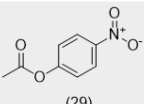
The formation of the corresponding acylated product was evaluated at 5, 20 minutes, 2 hours, and 24 hours. Despite our expectations, HPLC analyses of these reaction mixtures after the indicated time points did not show any sign of product formation. Possible explanation for this behaviour may lie in the substrate concentrations and acyl donors employed in our reaction. The literature reports favourable conversions at a scale 10 times larger than that utilized in our study, thereby in our case the rate of the reaction is significantly reduced.[34]

6.3.12 Screening of Alternative Acetyl Donor

Using 5-methoxytryptamine (**21**) as the substrate, we aimed to identify an effective acyl donor using the following series of esters (listed in order of increasing reactivity): isopropyl acetate (**25**), ethyl acetate (**26**), isopropenyl acetate (**27**), vinyl acetate (**28**), and 4-nitrophenyl acetate (**29**), all at a concentration of 1 M. The free biocatalyst was employed in solution (*i.e.* non-immobilised) with a final concentration of 1 mg/mL. Our results, outlined in Table 6.5, revealed that among the investigated substrates, only vinyl acetate (**28**) exhibited minimal conversion of **21** to **24** (>4%). However, as comparable results were observed in the control, the acetylation of **21** with vinyl acetate in the presence of MsAcT likely occurred through a

non-enzymatic pathway. This spontaneous reaction in fact take place in acidic environment, which is likely induced from the acetic acid that generated from the hydrolysis of **28.** We were expected the same behaviour from **27.** In this context the methyl group that is bonded to the alkyl chain stabilised the charge on the carbonyl, leading to a deceleration in the hydrolysis process.

Table 6.5 Screening of a range of acetyl donors for the synthesis of melatonin (**24**) in batch.

ACYL DONOR (20eq.)	REACTIVITY	SUBSTRATE (50 mM)	Enzyme	Conversion after 2 hours MsAcT	Conversion after 2 hours CTRL
(25)	−			n.d	n.d
(26)			MsAcT 1 mg/mL	n.d	n.d
(27)		(21)		n.d	n.d
(28)				<4%	<4%
(29)	+			n.d	n.d

100 mM KPi buffer pH 8.0, 25 °C

Each reaction was conducted at 30 °C in 100 mM KPi buffer at pH 8. The formation of the final product (melatonin, **24**) was monitored for up to 2 hours. Additionally, a control reaction was included, where all the compounds were added except for MsAcT.

Furthermore, we explored the interaction of vinyl acetate (**28**) with other tryptamine-like substrates (**19** and **20**). We observed conversion to *N*-acetyl-tryptamine (**22**) in both the reaction containing MsAcT and the control. Notably, the conversions were again comparable in both cases, with 4% conversion observed in the enzymatic reaction and 7% in the control. In an aqueous environment, vinyl acetate is susceptible to spontaneous hydrolysis, leading to the release of acetic acid and consequent pH reduction, which is unfavourable for the activity of MsAcT and induces spontaneous acylation of the starting material.[35,36]

6.4 Conclusion

Our attempts to establish a complete cascade to produce melatonin and acetylated melatonin, as an alternative route to the standard synthesis, encountered several challenges. Despite the inability to construct the full cascade, our efforts yielded significant findings, which are essential for a comprehensive understanding and potential future development of similar systems. Initially, in the first step of the cascade, we employed a tryptophanase from *E. coli* (either EcTnaA-WT or L51A-V394A) to combine indole-like molecules with serine to generate the corresponding tryptophan analogues. Subsequent optimization of the reaction conditions highlighted other requirements for EcTnaA-WT and EcTnaA-L51A-V394A, with the latter demanding significantly higher co-substrate equivalents (serine 12.5 eq. instead of 2.5) for full conversion. Our investigations into the second step of the cascade, catalysed by a tryptophan decarboxylase from *Ruminococcus gnavus* (RgTDC), began with a screening of two variants (L225A and W349F) alongside the wild type. Evidence identified RgTDC-W349F as the most promising candidate due to its favourable activity towards all the substrate screened (tryptophan, 5-hydroxytryptophan and 5-methoxytryptophan). However, challenges in the immobilisation of this enzyme and substrate inhibition highlighted additional complexities in cascade design and implementation. The final step of the cascade involved the attempted enzymatic acetylation of the tryptamines, employing an acetyl transferase derived from *Mycobacterium smegmatis* (MsAcT). Regardless of our success in immobilizing MsAcT on glyoxyl agarose, subsequent screening of various acetyl donors with MsAcT, and 5-methoxytryptamine as the substrate, were unsuccessful. In conclusion, we redirect our focus towards other pharmaceutically relevant molecules with emerging medical applications, acknowledging the challenges encountered in realizing the cascade for melatonin synthesis.

References

(1)   Sollars, P. J.; Pickard, G. E. The Neurobiology of Circadian Rhythms. *Psychiatric Clinics of North America* **2015**, *38* (4), 645–665. https://doi.org/10.1016/J.PSC.2015.07.003.

(2)   Leung, J. M.; Martinez, M. E. Circadian Rhythms in Environmental Health Sciences. *Curr Environ Health Rep* **2020**, *7* (3), 272–281. https://doi.org/10.1007/s40572-020-00285-2.

(3)   Khan, S.; Nabi, G.; Yao, L.; Siddique, R.; Sajjad, W.; Kumar, S.; Duan, P.; Hou, H. Health Risks Associated with Genetic Alterations in Internal Clock System by External Factors. *Int J Biol Sci* **2018**, *14* (7), 791–798. https://doi.org/10.7150/ijbs.23744.

(4)   Li, J.; Somers, V. K.; Xu, H.; Lopez-Jimenez, F.; Covassin, N. Trends in Use of Melatonin Supplements Among US Adults, 1999-2018. *JAMA* **2022**, *327* (5), 483. https://doi.org/10.1001/jama.2021.23652.

(5)   Szmuszkovicz, J.; Anthony, W.; Heinzelman, R. Notes- Synthesis of N-Acetyl-5-Methoxytryptamine. *J Org Chem* **1960**, *25* (5), 857–859. https://doi.org/10.1021/jo01075a623.

(6)   Cannazza, P.; Donzella, S.; Pellis, A.; Letizia Contente, M. Mycobacterium Smegmatis Acyltransferase: The Big New Player in Biocatalysis. *Biotechnol Adv* **2022**, *59*. https://doi.org/10.1016/j.biotechadv.2022.107985.

(7)   Contente, M. L.; Pinto, A.; Molinari, F.; Paradisi, F. Biocatalytic *N*-Acylation of Amines in Water Using an Acyltransferase from *Mycobacterium Smegmatis*. *Adv Synth Catal* **2018**, *360* (24), 4814–4819. https://doi.org/10.1002/adsc.201801061.

(8)   Contente, M. L.; Paradisi, F. Self-Sustaining Closed-Loop Multienzyme-Mediated Conversion of Amines into Alcohols in Continuous Reactions. *Nat Catal* **2018**, *1* (6), 452–459. https://doi.org/10.1038/s41929-018-0082-9.

(9)   Snell, E. E. Tryptophanase: Structure, Catalytic Activities, and Mechanism of Action. *Adv Enzymol Relat Areas Mol Biol* **1975**, *42*, 287–333. https://doi.org/10.1002/9780470122877.ch6.

(10) Ku, S.-Y.; Yip, P.; Howell, P. L. Structure of *Escherichia Coli* Tryptophanase. *Acta Crystallogr D Biol Crystallogr* **2006**, *62* (7), 814–823. https://doi.org/10.1107/S0907444906019895.

(11) Di Martino, P.; Fursy, R.; Bret, L.; Sundararaju, B.; Phillips, R. S. Indole Can Act as an Extracellular Signal to Regulate Biofilm Formation of *Escherichia Coli* and Other Indole-Producing Bacteria. *Can J Microbiol* **2003**, *49* (7), 443–449. https://doi.org/10.1139/w03-056.

(12) Wang, D.; Ding, X.; Rather, P. N. Indole Can Act as an Extracellular Signal in Escherichia Coli. *J Bacteriol* **2001**, *183* (14), 4210–4216. https://doi.org/10.1128/JB.183.14.4210-4216.2001/FORMAT/EPUB.

(13) Chant, E. L.; Summers, D. K. Indole Signalling Contributes to the Stable Maintenance of Escherichia Coli Multicopy Plasmids. *Mol Microbiol* **2007**, *63* (1), 35–43. https://doi.org/10.1111/J.1365-2958.2006.05481.X.

(14) Nakazawa, H.; Enei, H.; Okumura, S. Enzymatic Preparation of L-Tryptophan and 5-Hydroxy-L-Tryptophan. *FEBS Lett* **1972**, *25* (1), 43–45. https://doi.org/10.1016/0014-5793(72)80449-6.

(15) Watanabe, T.; Snell, E. E. The Interaction of Escherichia Coli Tryptophanase with Various Amino Acids and Their Analogs. *The Journal of Biochemistry* **1977**, *82* (3), 733–745. https://doi.org/10.1093/oxfordjournals.jbchem.a131750.

(16) Reusser, J. Tryptophanase and Tryptophan Decarboxylase - a Biocatalytic Path to Tryptamines. Master Thesis, Universit of Bern, Bern, 2022.

(17) Phillips, R. S.; Buisman, A. A.; Choi, S.; Hussaini, A.; Wood, Z. A. The Crystal Structure of *Proteus Vulgaris* Tryptophan Indole-Lyase Complexed with Oxindolyl- <scp>L</Scp> -Alanine: Implications for the Reaction Mechanism. *Acta Crystallogr D Struct Biol* **2018**, *74* (8), 748–759. https://doi.org/10.1107/S2059798318003352.

(18) Bellmaine, S.; Schnellbaecher, A.; Zimmer, A. Reactivity and Degradation Products of Tryptophan in Solution and Proteins. *Free Radic Biol Med* **2020**, *160*, 696–718. https://doi.org/10.1016/j.freeradbiomed.2020.09.002.

(19) Gęgotek, A.; Skrzydlewska, E. Ascorbic Acid as Antioxidant. *Vitam Horm* **2023**, *121*, 247–270. https://doi.org/10.1016/BS.VH.2022.10.008.

(20) Chatterjee, A.; Xiao, H.; Yang, P. Y.; Soundararajan, G.; Schultz, P. G. A Tryptophanyl-TRNA Synthetase/TRNA Pair for Unnatural Amino Acid Mutagenesis in E. Coli. *Angewandte Chemie International Edition* **2013**, *52* (19), 5106–5109. https://doi.org/10.1002/ANIE.201301094.

(21) Cady, S. G.; Sono, M. 1-Methyl-Dl-Tryptophan, β-(3-Benzofuranyl)-Dl-Alanine (the Oxygen Analog of Tryptophan), and β-[3-Benzo(b)Thienyl]-Dl-Alanine (the Sulfur Analog of Tryptophan) Are Competitive Inhibitors for Indoleamine 2,3-Dioxygenase. *Arch Biochem Biophys* **1991**, *291* (2), 326–333. https://doi.org/10.1016/0003-9861(91)90142-6.

(22) Williams, B. B.; Van Benschoten, A. H.; Cimermancic, P.; Donia, M. S.; Zimmermann, M.; Taketani, M.; Ishihara, A.; Kashyap, P. C.; Fraser, J. S.; Fischbach, M. A. Discovery and Characterization of Gut Microbiota Decarboxylases That Can Produce the Neurotransmitter Tryptamine. *Cell Host Microbe* **2014**, *16* (4), 495–503. https://doi.org/10.1016/j.chom.2014.09.001.

(23) McDonald, A. D.; Perkins, L. J.; Buller, A. R. Facile in Vitro Biocatalytic Production of Diverse Tryptamines. *ChemBioChem* **2019**, *20* (15), 1939–1944. https://doi.org/10.1002/cbic.201900069.

(24) De Marco, A.; De Marco, V. Bacteria Co-Transformed with Recombinant Proteins and Chaperones Cloned in Independent Plasmids Are Suitable for Expression Tuning. *J Biotechnol* **2004**, *109* (1–2), 45–52. https://doi.org/10.1016/j.jbiotec.2003.10.025.

(25) Hanahan, D. Studies on Transformation of Escherichia Coli with Plasmids. *J. Mol. Biol.* **1983**, *166* (4), 557–580. https://doi.org/10.1016/s0022-2836(83)80284-8.

(26) Tomoiaga, D.; Bubnell, J.; Herndon, L.; Feinstein, P. High Rates of Plasmid Cotransformation in E. Coli Overturn the Clonality Myth and Reveal Colony Development. *Scientific Reports 2022 12:1* **2022**, *12* (1), 1–15. https://doi.org/10.1038/s41598-022-14598-9.

(27) *Multienzymatic Assemblies*; Stamatis, H., Ed.; Methods in Molecular Biology; Springer US: New York, NY, 2022; Vol. 2487. https://doi.org/10.1007/978-1-0716-2269-8.

(28) Mathews, I.; Soltis, M.; Saldajeno, M.; Ganshaw, G.; Sala, R.; Weyler, W.; Cervin, M. A.; Whited, G.; Bott, R. Structure of a Novel Enzyme That Catalyzes Acyl Transfer to Alcohols in Aqueous Conditions. *Biochemistry* **2007**, *46* (31), 8969–8979. https://doi.org/10.1021/bi7002444.

(29) Contente, M. L.; Roura Padrosa, D.; Molinari, F.; Paradisi, F. A Strategic Ser/Cys Exchange in the Catalytic Triad Unlocks an Acyltransferase-Mediated Synthesis of Thioesters and Tertiary Amides. *Nat Catal* **2020**, *3* (12), 1020–1026. https://doi.org/10.1038/s41929-020-00539-0.

(30) Kazemi, M.; Sheng, X.; Kroutil, W.; Himo, F. Computational Study of Mycobacterium Smegmatis Acyl Transferase Reaction Mechanism and Specificity. **2018**. https://doi.org/10.1021/acscatal.8b03360.

(31) Christodoulou, M. S.; Contente, M. L.; Dallavalle, S.; Pinto, A. Enzymatic Amide Bond Formation: Synthesis of Aminooxo-Acids through a Mycobacterium Smegmatis Acyltransferase. *Green Chemistry* **2022**, *24* (11), 4432–4436. https://doi.org/10.1039/D2GC00655C.

(32) Perdomo, I. C.; Gianolio, S.; Pinto, A.; Romano, D.; Contente, M. L.; Paradisi, F.; Molinari, F. Efficient Enzymatic Preparation of Flavor Esters in Water. **2019**. https://doi.org/10.1021/acs.jafc.9b01790.

(33) Contente, M. L.; Farris, S.; Tamborini, L.; Molinari, F.; Paradisi, F. Flow-Based Enzymatic Synthesis of Melatonin and Other High Value Tryptamine Derivatives: A Five-Minute Intensified Process. **2019**, *21*, 3263. https://doi.org/10.1039/c9gc01374a.

(34) Godehard, S. P.; Badenhorst, C. P. S.; Müller, H.; Bornscheuer, U. T. Protein Engineering for Enhanced Acyltransferase Activity, Substrate Scope, and Selectivity of the *Mycobacterium Smegmatis* Acyltransferase MsAcT. *ACS Catal* **2020**, *10* (14), 7552–7562. https://doi.org/10.1021/acscatal.0c01767.

(35) Simon, P.; Filser, J. G.; Bolt, H. M. Metabolism and Pharmacokinetics of Vinyl Acetate. *Arch Toxicol* **1985**, *57* (3), 191–195. https://doi.org/10.1007/BF00290886.

(36) Sanz Sharley, D. D.; J Williams, J. M.; ChemComm COMMUNICATION, chemcomm. Acetic Acid as a Catalyst for the N-Acylation of Amines Using Esters as the Acyl Source †. *Chem. Commun* **2020**, *53*, 35. https://doi.org/10.1039/c6cc09023k.

An Alternative Chemo-Enzymatic Approach for the

Synthesis of Dimethylated Tryptamines

7.1 Aim of the Project

As outlined in Chapter 5.6, challenges in the extraction and acylation of the second intermediate were encountered during the attempted MsAct-mediated production of melatonin and other tryptamine derivatives. Consequently, we moved our research focus to coupling our enzymatic biosynthesis of tryptamines with a chemical reaction – that leads to the production of dimethylated tryptamines (DMT, 5H-DMT, and 5-MeO-DMT) using formaldehyde as the methyl donor. This reaction – so-called the Eschweiler-Clarke reaction [1]- involves the reduction of an imine intermediate (formed from the condensation of an amine with an aldehyde or ketone) using formic acid as the hydride donor to give a tertiary amine as the product. To begin our investigations into this reaction, an extensive screening of reducing agents was conducted, exploring various conditions such as temperature, pH, reagent equivalents, and reaction time. The reaction scheme is illustrated in Figure 7.1

R = H, Indole (**7**)
R= HO, 5-Hydroxyindole (**10**)
R= MeO, 5-Methoxyindole (**11**)

L-Serine (**8**)

R = H, L-Tryptophan (**9**)
R= HO, 5-Hydroxy-L-Tryptophan (**17**)
R= MeO, 5-Methoxy-L-Tryptophan (**18**)

RgTDC-W349F

R= H;*N,N*-Dimthyl tryptamine; **30**
R= OH;5-Hydroxy-*N,N*-dimthyl tryptamine; **31**
R= MeO,;5-Methoxy-*N,N*-dimthyl tryptamine; **32**

R= H;Tryptamine; **19**
R= OH;Serotonin; **20**
R= MeO;5-Methoxy tryptamine; **21**
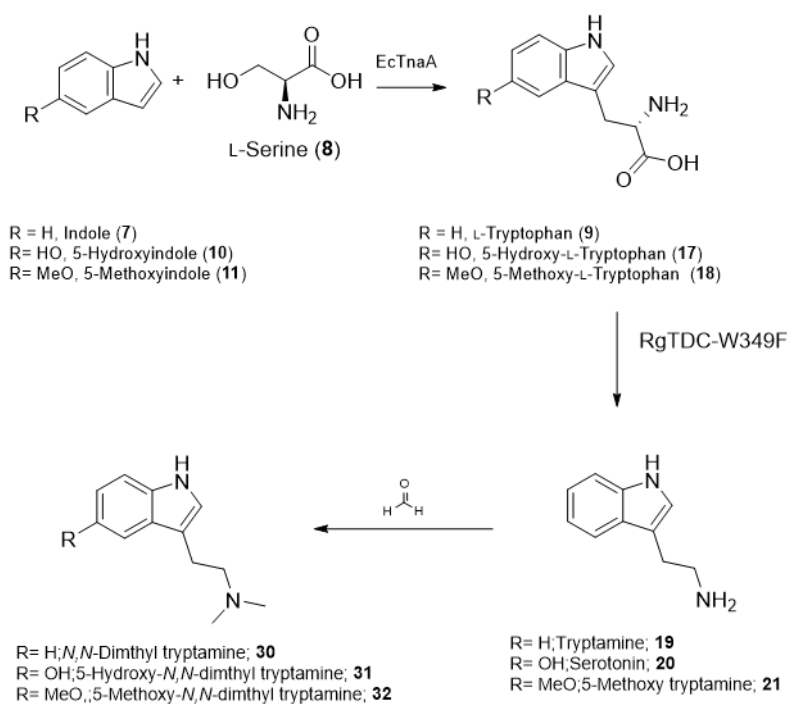
Figure 7.1 Chemo-enzymatic synthesis of three dimethylated tryptamines (**9, 17,** and **18**), starting with the coupling of analogues of indole (**7**, **10**, and **11**) with L-serine, catalysed by EcTnaA-wt or L51A-V394A. Conversion of tryptophan and analogues to tryptamine (**19**) and analogues (**20**-**21**) is catalysed by RgTDC-W349F. The chemical synthesis of DMT (**30**), 5H-DMT (**31**) 5M-DMT (**32**) involves the use of formaldehyde as the methyl donor in a reductive amination reaction using formic acid.

7.2 Introduction

Dimethylated tryptamines are a class of organic compounds that share a common structure: a tryptamine core with two methyl groups attached to the nitrogen atom. These compounds exhibit a diverse range of pharmacological properties and are often associated with psychedelic effects.[2,3] Their use is well known for religious purposes, for instance, Indigenous Amazonian tribes have long used ayahuasca, a brew containing *N,N*-dimethyl-L-tryptamine (DMT, **30**), for spiritual ceremonies.[4] In early 70's, Alexander Shulgin began pioneering work on a group of psychoactive and hallucinogenic compounds, shedding light on their synthesis and isolation, and their effects on the human body, among of which tryptamine derivatives covered a significant part of that research.[5] In recent years, the medical community have investigated the potential therapeutic applications of these compounds with a microdosing approach for various mental health conditions, including post-traumatic stress disorder (PTSD) and depression.[6–9] The full mechanism of action by which psychedelics impact perception and cognition in humans is not fully understood, but studies on 5-methoxy-*N,N*-dimethyl tryptamine (5MeO-DMT, **32**) and bufotenine (5-hydroxy-*N,N*-dimethyl tryptamine 5H-DMT, **31**) show strong interaction at the serotonin 2A receptor (5-HT2A), indicating a possible interaction with the centres responsible for mood control.[10,11] Dimethylated tryptamine derivatives can be chemically accessed from simpler precursors, such as tryptamine, using reductive amination. This often involves the use of formaldehyde as a C-1 donor coupled with a reducing agent. Sodium cyanoborohydride ($NaBH_3CN$) is commonly employed as a mild reducing agent for this reaction since it is water-soluble and prevents the competitive reduction of the ketone over the imine. However, undesired side reactions, such as the release toxic gases (HCN) during hydrolysis or acid work-up procedures prompted us to a screen other reducing agents with a lower toxicity.[12,13]

7.3 Synthesis of Dimethylated Tryptamines *via* a Reductive Amination

Reductive amination is a versatile synthetic method used to convert carbonyl compounds (such as aldehydes or ketones) into tertiary amines. A general scheme of this reaction is represented in Figure 7.2. The process involves the formation of an imine intermediate, followed by its reduction to the desired amine using hydride donors, such as sodium

borohydride (NaBH$_4$) or sodium cyanoborohydride (NaBH$_3$CN).[14] We first evaluated a range of possible conditions to perform the reaction. In our group, a similar reaction was successfully performed for the biosynthesis of hordenine from tyramine as starting material, reaching excellent conversions (96%) at a 5 mM scale using 30 equivalents of formaldehyde, in NaCO$_3$ buffer at pH 9 and 24 equivalents of picoline borane as reducing agent.[15] We therefore attempted this reaction for the production of our dimethylated tryptamine and its analogues. In our specific case, the primary amine is exemplified by tryptamine (or an analogous compound), while formaldehyde serves as the carbonyl component.
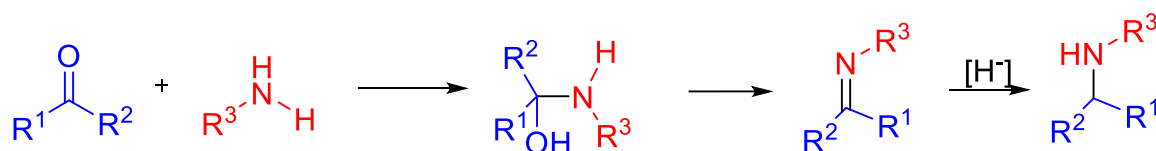
Figure 7.2 Reductive amination scheme for primary amine.

7.3.1 NaBH$_3$CN

The general mechanism of this reaction is reported in Figure 7.3: The reaction initiates with the nucleophilic attack of the amine on the activated (protonated) carbonyl (**I**), followed by the condensation to form the imine (**II**) which, under acidic conditions is protonated to give the more electrophilic iminium ion (**III**). At this stage, a hydride delivered from NaBH$_3$CN attacks the iminium ion to give mono-methylated amine (**IV**). A second reductive amination step occurs, with the same mechanism, leading to the corresponding secondary amine (**V**).

R = H = tryptamine (**19**)
R = OH = serotonin (**20**)
R = MeO = 5-methoxytryptamine (**21**)

R = H = dimethyltryptamine, DMT (**30**)
R = OH = dimethylserotonine, 5H-DMT (**31**)
R = MeO = 5-methoxydimethyltryptamine, 5MeO-DMT (**32**)
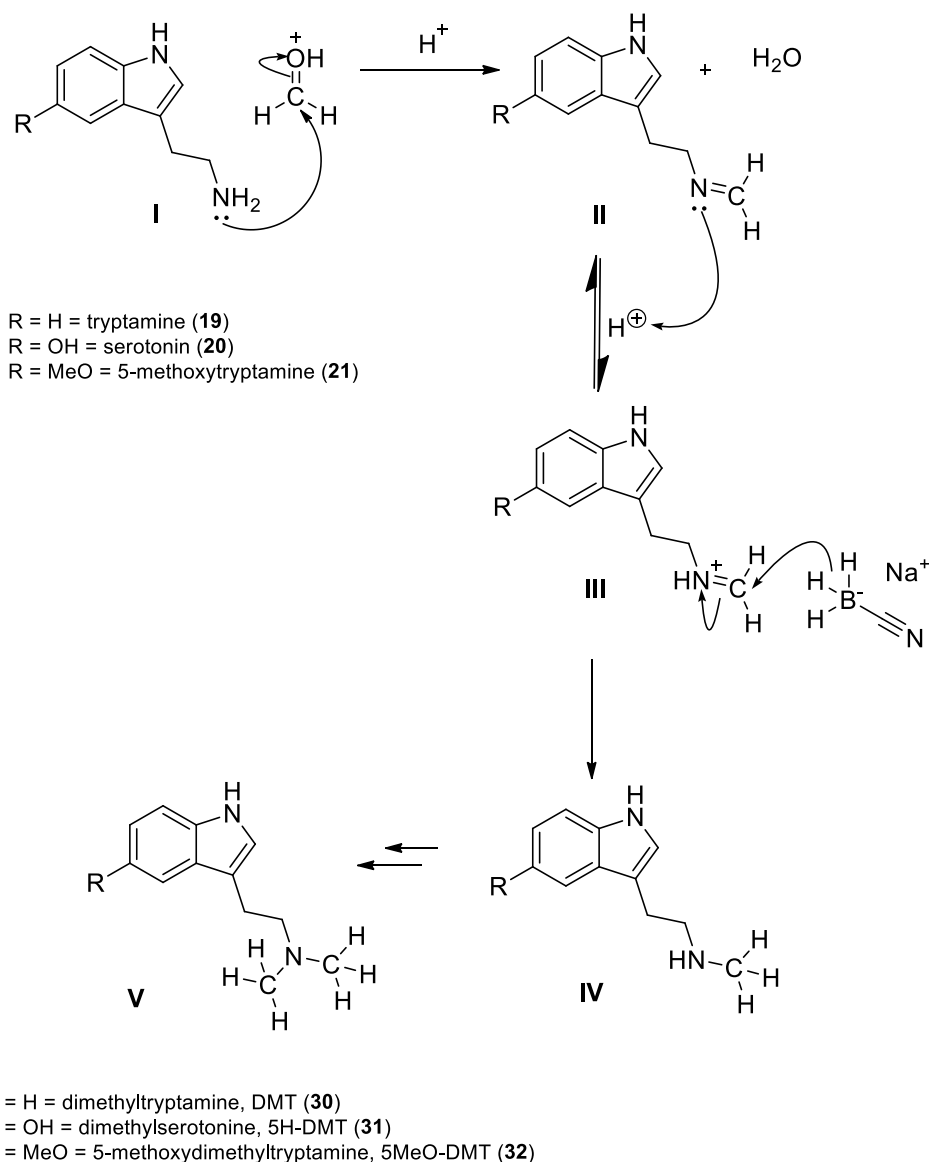
Figure 7.3 NaBH$_3$CN-mediated reductive amination of tryptamines using formaldehyde as the C-1 source.

The first substrate subjected to dimethylation was tryptamine (**19**). A solution of 150 mM of **19** was mixed with 5 equivalents of formaldehyde and 15% (*v/v*) DMSO in 50 mM KPi buffer to mimic the conditions of the enzymatic cascade, on which the dimethylation step will be performed. The pH was adjusted to 4 using acetic acid, and the reaction was incubated for one hour (Figure 7.3, **III**) before the addition of 3 equivalents of NaBH$_3$CN. After three hours, HPLC analysis revealed the presence of unknown peaks, potentially related to the dimethylated product (DMT, **30**) and other side-products, such as unreacted **19**, or mono-methylated tryptamine.[16] The product was extracted and purified on preparative TLC and its

purity was confirmed by ^{1}H-NMR and mass spectrometry and further employed as a standard reference for HPLC analyses, revealing a retention time (R_T) of 7.908 minutes.

An analogous approach was used to prepare 5-methoxydimethyltryptamine (5-M-DMT, **32**) which, upon isolation, the was injected into the HPLC, identifying the peak corresponding to **32** at 7.97 minutes.

The final substrate remaining for dimethylation was 5-hydroxytryptamine (5-HT, **20**). Following the successful approach used for the first two tryptamines, we repeated the same procedure for **20** using 150 mM of 5-hydroxydimethyltryptamine (5H-DMT, **31**) and 5 equivalents of formaldehyde. Unfortunately, under these conditions, the dimethylated product could not be detected in the reaction mixture. Despite several attempts with a number of conditions, we could never isolate **31**.

Acknowledging that further investigation are required, we decided to focus only on **30** and its 5-methoxy-derivatized analogue **32**. While NaBH₃CN effectively allowed the formation of these two substrates, it is not an optimal reducing agent due to the toxic by-products generated during the reaction work-up, such as HCN. As part of our commitment to sustainable and eco-friendly processes, we have initiated an investigation into alternative and milder reducing agents. Nevertheless, NaBH₃CN remained a valid option for synthesizing of **30** and **32** which we could then use for characterization purposes and subsequent reference standards.

7.3.2 Screening of Different Reducing Agents for Dimethylation on Commercial substrates

i. Picoline Borane

Over the past decades, numerous researchers have explored various reducing agents with varying degrees of sustainability. Unfortunately, some of these agents exhibit unfavourable properties, including issues related to stability, selectivity, secondary reactions, reaction conditions, safety hazards, and toxicity.[17] One promising alternative is 2-picoline-borane (also known as 2-methylpyridine borane or pic-BH₃, Figure 7.7). This stable solid reagent serves as a non-toxic substitute for NaBH₃CN in reductive aminations and can be effectively employed in reactions conducted in various solvents, including methanol, water, and even under solvent-free conditions.[18,19]

Figure 7.7 Structure of picoline borane complex

In our research group, pic-BH$_3$ was efficiently used to catalyse the reductive amination of tyramine at a concentration of 5 mM in batch reactions.[13] Encouraged by this result, we wanted to adopt a similar strategy to synthesize our dimethylated amines. As an initial screen, 50 mM of **19** was dissolved in 15% ethanol, 70 equivalents of formaldehyde, with 7 equivalents of pic-BH$_3$ in dH$_2$O and acidified to pH 5 using glacial acetic acid. The reaction mixture was then incubated at 25 °C and monitored after 6 and 20 hours by RP-HPLC.

The chromatographic profile revealed complete consumption of the starting material **19**, with the formation of four new peaks. Comparing this chromatographic trace with the analysis performed on compound **30** (as previously discussed), we detected the presence of the desired product. However, the conversion of this product was <0.5% of the total.

We hypothesized that at least one of the additional peaks observed may result from a side reaction between compound **19** and formaldehyde as it has been reported that the Pictet-Spengler (P-S) reaction can occur under these conditions. The P-S reaction is a transformation in which a β-arylethylamine reacts with an aldehyde (or ketone), leading to the formation of the corresponding tetrahydro-ß-carboline.[20]

1-methyl-1,2,3,4-tetrahydro-β-carboline
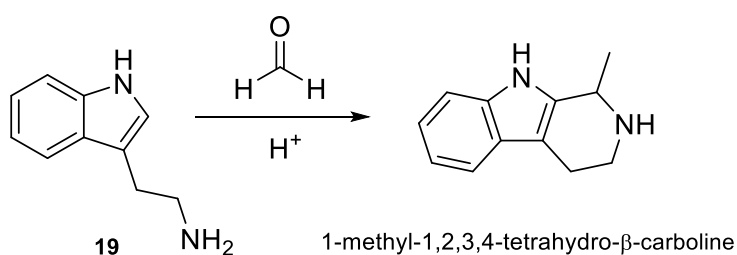
Figure 7.8 Product derived from the Pictet-Spengler reaction between **19** and formaldehyde under acidic conditions.

To verify our hypothesis, we conducted an identical experiment with the previous mentioned conditions, but omitting the addition of pic-BH$_3$. The RP-HPLC analysis of this mixture confirmed the presence of the unidentifiable peaks observed earlier, but the peak of

compound **30** is clearly missing, suggesting that they are not derived from the reduction of an intermediate imine of **30**.

In a final attempt, we increased the equivalent amount of pic-BH$_3$ to promote the reduction of the iminium bond over the condensation side-reaction. Despite this modification, the chromatographic analyses revealed a similar profile, where the majority of the peaks corresponded to the side reactions, while the production of compound **30** was limited to only 2%.

It is important to highlight that P-S products have practical applications as scaffolds for synthesizing alkaloids and biologically active compounds. However, given that these applications fall beyond the scope of our current work, we proceeded to explore other reducing agents.[21]

ii. NaBH$_4$

Another reagent which is extensively employed in reductions and is relatively green, is sodium borohydride (NaBH$_4$).[22,23] In organic synthesis, NaBH$_4$ is generally used to convert carbonyl groups (ketones and aldehydes) to alcohols, but its application in reductive amination is not unusual. Reductive amination using NaBH$_4$ couples carbonyl compounds (aldehydes or ketones) with primary amines to form secondary and tertiary amines. However, the side reaction of the reduction of the carbonyl reagent is a major drawback – a step which can be minimised by promoting the sequential formation of the imine, followed by subsequent reduction.

To screen for optimal reduction conditions, NaBH$_4$-mediated amine formation was tested on commercial samples of **19** (50 mM) at pH 5 and 9. The formation of **30** was monitored directly by HPLC but, after two hours, neither conditions showed any product. As NaBH$_4$ reacts with water, we postulated that the amount of hydride ions from borohydride available for the reduction were too low, therefore we doubled the amount of NaBH$_4$ (total of 6 equivalents). The reaction mixture was left for 20 additional hours. However, after this time, the HPLC analysis of the reaction mixture still showed a peak corresponding to the starting material, but the peak corresponding to the product was either negligible (~ 0.1% at pH 5) or completely absent (at pH 9). It is unlikely that the formation of the imine/iminium under these conditions

is a limiting factor,[24] so these results suggest that either competitive reduction of the large excess of formaldehyde or hydrolysis of NaBH$_4$ are faster than imine reduction under these conditions. Since the use of NaBH$_4$ in the reductive amination of **30** did not yield any appreciable results, we discarded the option of the use of this reducing agent in further investigations.

ii. Formic Acid

Formic acid is an alternative option for reductive amination reactions, delivering one hydride and one molecule of CO_2 per molecule of formate. This transformation - so-called the Eschweiler-Clarke reaction – requires initial iminium formation, as seen in the previous sections, followed by decarboxylative hydride transfer from formate for the reduction (Figure 7.8).[1,25]
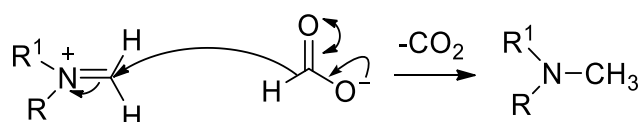

Figure 7.8 Mechanism for the reductive amination of an imine mediated by formic acid.

In a first screening for optimal conditions of the reduction, we assessed the impact of temperature, given that this reaction necessitates a certain activation energy. We set up three reactions, each containing 50 mM of **19** and 28 equivalents of formaldehyde in 100% formic acid. Three different temperatures were tested (50 °C, 100 °C, and 150 °C). Samples were collected for HPLC and ^{1}H NMR analysis at 0, 5, 15, and 60 minutes. The HPLC spectrum of the 50 °C sample did not exhibit any peak corresponding to the product, a finding corroborated by ^{1}H NMR analyses, which did not show the expected singlet peak at 2.8 ppm, while the signals corresponding to the starting materials were still present. The 100 °C reaction was the same: no formation of the dimethylated product could be detected by HPLC analysis or ^{1}H NMR. In our last effort to trigger the activation of formic acid, the temperature was increased to 150 °C. Under these conditions, we noticed a visible deterioration of the starting material during this process, with the solution transitioning from clear to brown in just 5 minutes. This degradation became more visibly pronounced over time (Figure 7.9)
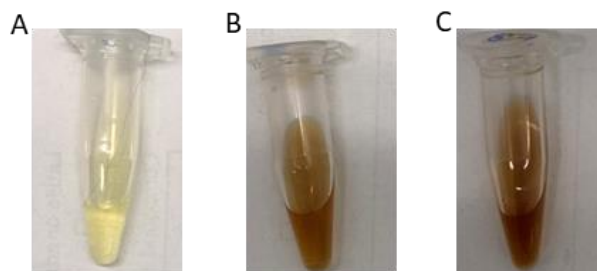
Figure 7.9 Colour change of 50 mM tryptamine solution with 28 equivalents of formaldehyde in 100 % formic acid. Upon incubation at 150 °C samples were photographed after 0 (A), 5 (B), and 15 minutes (C).

Furthermore, an analysis of the reaction mixture after 15 mins by HPLC and ^{1}H NMR showed no trace of the dimethylated product, and the peak corresponding to the starting material had completely disappeared, suggesting a degradation of **19**.

Further uses of formic acid as the reducing agent were therefore abandoned.

At the time of writing, the synthesis was successful with the commonly used NaCNBH$_3$ for compounds **30** and **32**. However, due to its inherent reactivity, the synthesis of compound **31** remains an unresolved challenge. An optimisation of the ideal conditions for the alkylation of **20** remains a work in progress.

The next section will focus on the purification of tryptamine (**19**) obtained from the cascade, as this is a trivial step for the completion of the chemoenzymatic cascade.

7.4 Tryptamine Purification for Chemoenzymatic Coupling

An excess amount of L-serine was required for the first step of the enzymatic cascade to push the reaction to completion. However, this excess poses a significant problem when we couple the multi-enzyme cascade with the final reductive amination step – the excess L-serine will also react with the C-1 donor and reducing agent, necessitating the use of large amounts of reagents. Therefore, an additional purification step was introduced in order to improve quality of the substrate needed for the final reaction, and a series of extraction conditions were investigated to determine the most effective system to extract the aromatic amine.

i. Liquid Extraction in Organic Solvent

The most straightforward method to isolate our desired amine would involve a liquid/liquid extraction with an organic solvent, in particular, ethyl acetate. This was tested on a reaction starting from indole which afforded tryptamine (**19**) with conversion of 95% over the two enzymatic steps (Section 5.5). The biocatalysts were discarded by centrifugation, and the pH adjusted to 14. Despite saturation of the aqueous phase with NaCl, upon vigorous shaking with ethyl acetate an emulsion was observed which could not be fully solved. We attributed this observation to residual denatured protein in solution that may act as a surfactant at the interface of the buffer/organic solvent. Analysed of the aqueous and organic layer by TLC indicated a poor extraction of tryptamine into the organic phase, with both **8** and **19** still present in the aqueous solution. This observation is likely due to the 15% DMSO which acts as a co-solvent and retains the compounds in the aqueous phase.

ii. Extraction with Ionic Resin

Our second strategy involved the use of ionic exchange resins. This technique is extensively used to isolate charged molecules from a mixture, often exploiting an ammonium or carboxylate functional group using an anion or cation exchange resin, respectively.[26] To assess the ability of each following resin to retain our compound of interest, a mock solution containing 50 mM of **19**, 125 mM of **8**, 0.1 mM of PLP and 15% DMSO in 50 mM KPi buffer at pH 8 was prepared. The pH of the solution was adjusted as needed for each purification protocol before the purification step.

Mixed Bed: Amberlite™ MB-3

A first attempt of purification was done with Amberlite MB-3, a mixed bed resin developed for water demineralisation purposes at industrial scale. The surface of the resin is functionalised with a mixture of strong acid cation and strong base anion groups in a proportion of 1:1. For this experiment, the mock solution was adjusted to pH 14 and loaded on a column packed with of resin suitably activated as per supplier indications so that the sulfonic acid groups are deprotonated, allowing their interaction with the ammonium groups. This allowed the separation of non-charged molecules, such as PLP and DMSO, while retaining

charged molecules on the resin. Elution with HCl should have been selective as **19** and **8** have a significant a different pKa, however we observed no separation and the use of the mixed bed resin was abandoned.

Anion Exchange: Amberlite™ HPR4811 Cl

Another approach pursued involved the use of the anion exchange resin, Amberlite™ HPR4811. This resin is widely used in industrial application for removal of strong and weak acids. Moreover, the use of a PBR packed with this resin has been employed in flow to retain, *i.e.* acids present in solution. [27] However in our case, no separation of **19** and **8** in the early fractions could be noted (Figure 7.10).
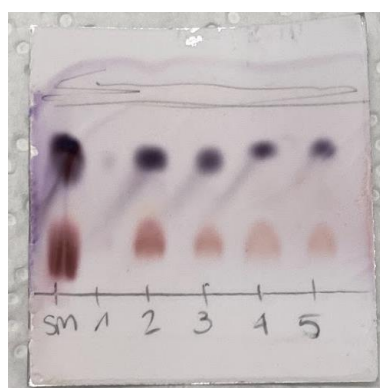

Figure 7.10 TLC analysis of the purification of tryptamine (**19**) from L-serine (**8**) with Amberlite™ HPR4811 Cl; SM: starting mixture before loading (50 mM **19**, 125 mM **8**, 0.1 mM PLP; 10 % DMSO in a 50 mM KPi buffer at pH 10). Fractions 1-3: flowthrough; Fractions 4-5: dH$_2$O wash;. Running phase 7:2:1 *n*-butanol:acetic acid:dH$_2$O

Polymeric Adsorbent Amberlite™ XAD-4

Lastly, we investigated the use of a polymeric adsorbent resin, Amberlite™ XAD-4, which is commonly employed to purify aqueous systems containing phenolic and chlorinated compounds. This resin, composed of styrene-divinylbenzene, relies on hydrophobic interactions, making it an ideal candidate for interacting with the indole ring of the structure (which is absent in **8**). Following loading of the column, several fractions were eluted with MeOH and analysed by TLC (Figure 7.11). Successful separation of compound **8** (which flushed through the resin) from compound **19** was achieved. We continued collecting fractions containing compound **19** until no blue spot was visible (Fractions 10-11, not shown).
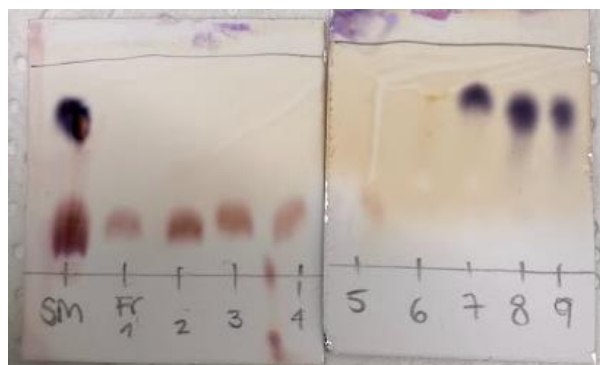
Figure 7.11 TLC analysis of the purification of tryptamine (**19**) from L-serine (**8**) with Polymeric Adsorbent Amberlite™ XAD™4; SM: starting mixture before loading (50 mM **19**, 125 mM **8**, 0.1 mM PLP; 10 % DMSO in a 50 mM KPi buffer at pH 8). Fractions 1-3: flowthrough; Fractions 4-6: dH$_2$O wash; Fractions 7-9: MeOH elution. Running phase 7:2:1 *n*-butanol:acetic acid:dH$_2$O.

The fractions containing the desired product (**19**) were pooled and the yield was estimated to be approx. 43% by HPLC. We assumed that the remaining of **19** was likely still retained on the resin. To confirm this hypothesis, we performed an additional wash with ethyl acetate, which, upon analysis by TLC, confirmed the presence of **19**.

The successful elimination of **8** from the reaction mixture prompted us to try the same approach to separate **8** from **20**. A mock solution containing **20** instead of **19** was prepared and loaded onto the resin. Fractions were collected using the same procedure as before. Figure 7.12 reports the results obtained upon TLC analysis of the fractions.
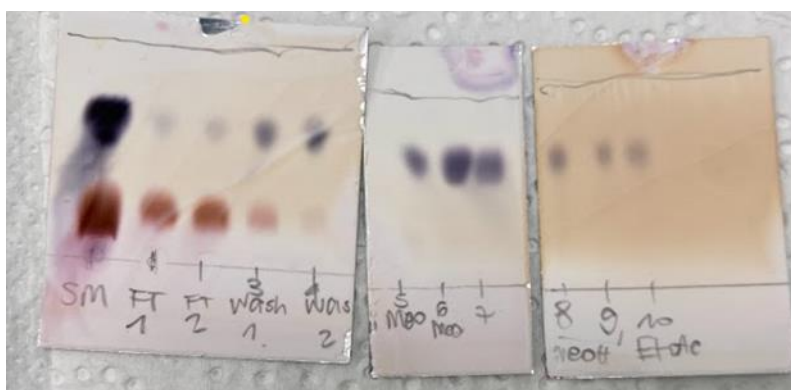
Figure 7.12 TLC analysis of the purification of 5-hydroxy tryptamine (**20**) from L-serine (**8**) using Polymeric Adsorbent Amberlite™ XAD™4; SM: initial mixture before loading (50 mM of **20**, 125 mM of **8**, 0.1 mM of PLP and 10 % DMSO in a 50 mM KPi buffer at pH 8); Fractions 1-2: flowthrough; Fractions 3-4: dH$_2$O wash; Fractions 5-9: MeOH elution; 10: final wash with EtOAc (stripping). Running phase 7:2:1 *n*-butanol:acetic acid:dH$_2$O.

The separation efficiency in this instance was lower than with **19**. This observed reduction in efficiency is likely attributed to the presence of a hydroxy group on the ring with a pK$_a$ of 9. At the current pH of 8, the hydroxy group is only partially protonated, rendering the molecule more hydrophilic than **19**. Current ongoing efforts are now dedicated to optimizing the purification procedure, involving, among other adjustments, the basification of the pH of the final solution to a target value of 10.

iii. Preparative HPLC

We also explored of the purification of **19** using preparative RP-HPLC. A particular concern was whether **19** would co-elute with L-serine **(8).** To determine the retention time of the product, the mock reaction mixture was injected directly and eluted through a C-18 column and peaks corresponding to an aromatic compound (at 260 nm) were collected. Two of the fractions recovered were found to be tryptamine but, as L-serine **(8)** does not absorb in the UV-VIS spectrum, each fraction was also analysed by TLC (Figure 7.13), staining with ninhydrin. No traces of L-serine **(8)** where **19** was present so the compound was determined to be pure and ready to be concentrated *in vacuo.*
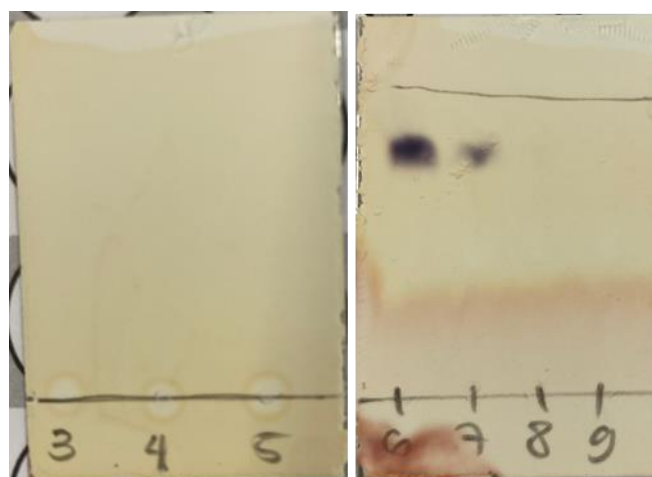
Figure 7.13 Purification of reference solution *via* semi-prep HPLC. Fraction 3-5 represents the compound absorbing at 210 nm. Fractions 6 and 7 are refer to the isolated tryptamine.

The results from the use of preparative RP-HPLC suggests that this last purification method is the most suitable for the isolation of **19** with high degree of purity compared to the other approaches. However, this chromatographic system requires a significant volume of solvents and is therefore not particularly environmentally friendly.

7.4 Conclusions

In our attempt to synthesize *N,N*-dimethyltryptamine (**30**) and its 5-substituted analogues (**31**, **32**), we examined several strategies for an environmentally-friendly reductive amination of the amine precursors. Sodium cyanoborohydride (NaBH$_3$CN) was used on tryptamine (**30**) and 5-methoxy-tryptamine (**32**), which were extracted and characterized by ^{1}H NMR and mass spectroscopy. However, the synthesis of **31,** under similar conditions, was unsuccessful. It is possible that the hydroxyl group in **20** leads to oxidative degradation. At the time of writing, experiments to synthesise **31** were still ongoing**.**

An investigation into alternative reducing agents was also performed (pic-BH$_3$, NaBH$_4$, and formic acid) that would align better with the sustainable construct of the cascade. However, only partial conversions were achieved and NaCNBH$_3$, which remains the best reducing agent for the formation of these products.

Finally, in order to minimize the number of equivalents of reagents needed for the final demethylation step, the tryptamines obtained from the enzymatic cascade were subjected to an additional a purification step. The options tested included liquid/liquid extraction with organic solvent, different resins, and preparative RP-HPLC. The best results were provided by purification with Polymeric Adsorbent Resin Amberlite XAD-4 and RP-HPLC, although in the first case the recovery yield was 43%. Both these techniques lead to the isolation of the product with a high degree of purity. The use of preparative RP-HPLC allowed also the complete removal of L-serine and DMSO from the reaction mixture. Despite its success, we are still in search for a superior alternative that can significantly reduce solvent volume and energy consumption.

7.5 Product Characterisation

In the following session, an overview of the UV-vis chromatograms- (reconstructed by raw data) and ^{1}H-NMR spectrum and chromatographic profile of the dimethylated compounds (Session 7.3.1) is given.

1. Compound **30** (Dimethyltryptamine)

   a. ^{1}H NMR (300 MHz, D$_2$O) 7.32 (dd, J = 10.5, 8.8 Hz, 1H), 7.22 (d, J = 6.4 Hz, 1H), 7.12 – 7.05 (m, 1H), 6.84 (dd, J = 8.8, 2.6 Hz, 1H), 3.80 – 3.74 (m, 1H), 3.37 (t, J = 7.4 Hz, 1H), 3.10 (t, J = 7.4 Hz, 1H), 2.80 (s, 1H);

   b. HRMS (ESI) for C$_{12}$H$_{17}$N$_2$ (M + H$^+$): Calculated 189.1386; Found: 189.1393.

2. Compound **32** (*N,N*-)-5-Methoxy dimethyltryptamine)

   a. ^{1}H NMR (300 MHz, CD$_3$OD) 7.63 – 7.58 (m, 1H), 7.37 (dt, *J* = 8.1, 1.0 Hz, 1H), 7.20 (s, 1H), 7.13 (ddd, *J* = 8.2, 7.0, 1.3 Hz, 1H), 7.05 (ddd, *J* = 8.1, 7.1, 1.2 Hz, 1H), 3.41 – 3.35 (m, 1H), 3.24 – 3.17 (m, 1H), 2.89 (s, 1H);

   b. HRMS (ESI) for C$_{12}$H$_{17}$N$_2$ (M + H$^+$): Calculated 218.1453; Found: 218.1476
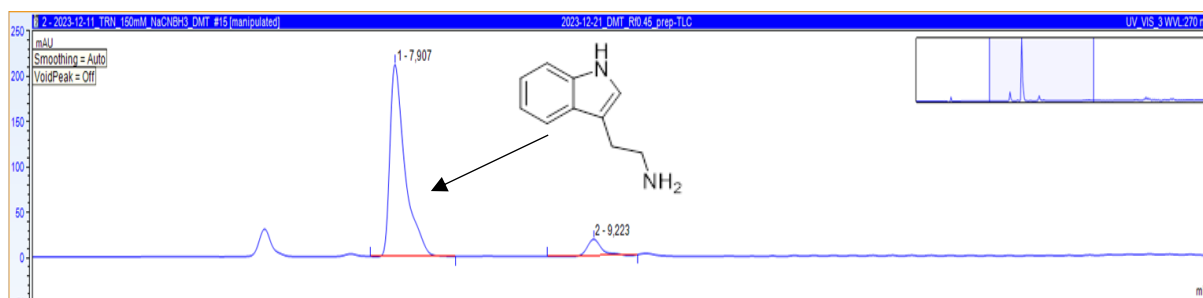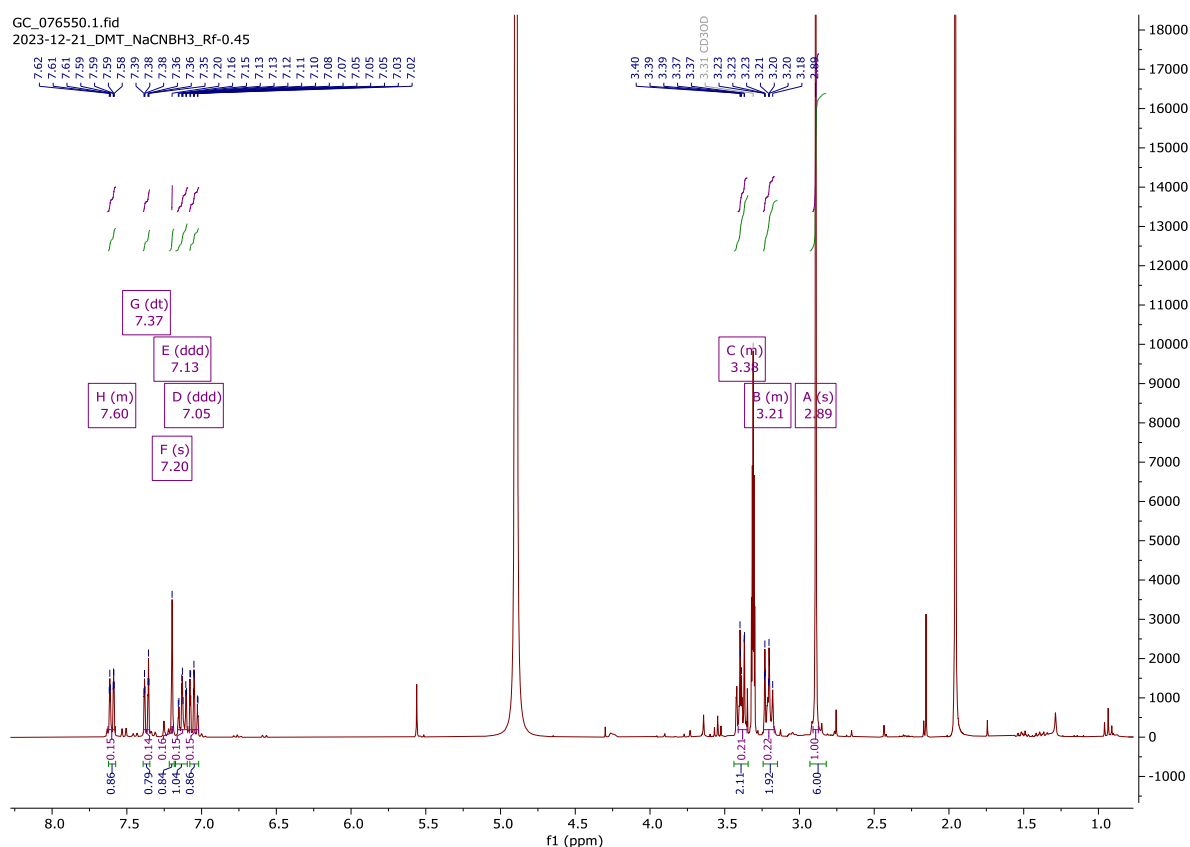
(1)   Eschweiler, W. Ersatz von an Stickstoff Gebundenen Wasserstoffatomen Durch Die Methylgruppe Mit Hülfe von Formaldehyd. *Berichte der deutschen chemischen Gesellschaft* **1905**, *38* (1), 880–882. https://doi.org/10.1002/CBER.190503801154.

(2)   Araújo, A. M.; Carvalho, F.; Bastos, M. de L.; Guedes de Pinho, P.; Carvalho, M. The Hallucinogenic World of Tryptamines an Updated Review - Araújo2015_Article_TheHallucinogenicWorldOfTrypta. *Arch Toxicol* **2015**, *89* (8), 1151–1173. https://doi.org/10.1007/s00204-015-1513-x.

(3)   Palamar, J. J.; Acosta, P. A Qualitative Descriptive Analysis of Effects of Psychedelic Phenethylamines and Tryptamines. *Human Psychopharmacology: Clinical and Experimental* **2020**, *35* (1). https://doi.org/10.1002/hup.2719.

(4)   Estrella-Parra, E. A.; Almanza-Pérez, J. C.; Alarcón-Aguilar, F. J. Ayahuasca: Uses, Phytochemical and Biological Activities. *Nat Prod Bioprospect* **2019**, *9* (4), 251–265. https://doi.org/10.1007/S13659-019-0210-5/TABLES/1.

(5)   Shulgin, A.; Shulgin, A. *TIHKAL, The Continuation*; Transform Press: United States, 1997.

(6)   Jacob, M. S.; Presti, D. E. Endogenous Psychoactive Tryptamines Reconsidered: An Anxiolytic Role for Dimethyltryptamine. *Med Hypotheses* **2005**, *64* (5), 930–937. https://doi.org/10.1016/j.mehy.2004.11.005.

(7)   Andersen, K. A. A.; Carhart-Harris, R.; Nutt, D. J.; Erritzoe, D. Therapeutic Effects of Classic Serotonergic Psychedelics: A Systematic Review of Modern-Era Clinical Studies. *Acta Psychiatr Scand* **2021**, *143* (2), 101–118. https://doi.org/10.1111/acps.13249.

(8)   Barker, S. A. Administration of N,N-Dimethyltryptamine (DMT) in Psychedelic Therapeutics and Research and the Study of Endogenous DMT. *Psychopharmacology 2022 239:6* **2022**, *239* (6), 1749–1763. https://doi.org/10.1007/S00213-022-06065-0.

(9)   Cameron, L. P.; Benson, C. J.; DeFelice, B. C.; Fiehn, O.; Olson, D. E. Chronic, Intermittent Microdoses of the Psychedelic *N* , *N* -Dimethyltryptamine (DMT) Produce Positive Effects on

Mood and Anxiety in Rodents. *ACS Chem Neurosci* **2019**, *10* (7), 3261–3270. https://doi.org/10.1021/acschemneuro.8b00692.

(10) Fantegrossi, W. E.; Harrington, A. W.; Kiessel, C. L.; Eckler, J. R.; Rabin, R. A.; Winter, J. C.; Coop, A.; Rice, K. C.; Woods, J. H. Hallucinogen-like Actions of 5-Methoxy-N,N-Diisopropyltryptamine in Mice and Rats. *Pharmacol Biochem Behav* **2006**, *83* (1), 122–129. https://doi.org/10.1016/j.pbb.2005.12.015.

(11) Sherwood, A. M.; Burkhartzmeyer, E. K.; Williamson, S. E.; Baumann, M. H.; Glatfelter, G. C. Psychedelic-like Activity of Norpsilocin Analogues. *ACS Chem Neurosci* **2024**, *15* (2), 315–327. https://doi.org/10.1021/acschemneuro.3c00610.

(12) Brandt, S. D.; Tearavarich, R.; Dempster, N.; Cozzi, N. V; Daley, P. F. Synthesis and Characterization of 5-Methoxy-2-Methyl-N,N-Dialkylated Tryptamines. **2012**. https://doi.org/10.1002/dta.398.

(13) Brandt, S. D.; Freeman, S.; Mcgagh, P.; Abdul-Halim, N.; Alder, J. F. An Analytical Perspective on Favoured Synthetic Routes to the Psychoactive Tryptamines. *J Pharm Biomed Anal* **2004**, *36*, 675–691. https://doi.org/10.1016/j.jpba.2004.08.022.

(14) Afanasyev, O. I.; Kuchuk, E.; Usanov, D. L.; Chusov, D. Reductive Amination in the Synthesis of Pharmaceuticals. *Chem Rev* **2019**, *119* (23), 11857–11911. https://doi.org/10.1021/acs.chemrev.9b00383.

(15) Gianolio, S.; Roura Padrosa, D.; Paradisi, F. Combined Chemoenzymatic Strategy for Sustainable Continuous Synthesis of the Natural Product Hordenine. *Green Chemistry* **2022**, *24* (21), 8434–8440. https://doi.org/10.1039/D2GC02767D.

(16) Brandt, S. D.; Moore, S. A.; Freeman, S.; Kanu, A. B. Characterization of the Synthesis of *N , N* -dimethyltryptamine by Reductive Amination Using Gas Chromatography Ion Trap Mass Spectrometry. *Drug Test Anal* **2010**, *2* (7), 330–338. https://doi.org/10.1002/dta.142.

(17) Shrwardi, M. H. S.; Das, S. C.; Mamun, M. A. Al. A Green Approach of Vat Dyeing of Cotton Fabric with Natural Reducing Agents. *Heliyon* **2023**, *9* (9), e19663. https://doi.org/10.1016/J.HELIYON.2023.E19663.

(18) Ruhaak, L. R.; Steenvoorden, E.; Koeleman, C. A. M.; Deelder, A. M.; Wuhrer, M. 2-Picoline-Borane: A Non-Toxic Reducing Agent for Oligosaccharide Labeling by Reductive Amination. *Proteomics* **2010**, *10* (12), 2330–2336. https://doi.org/10.1002/PMIC.200900804.

(19) Sato, S.; Sakamoto, T.; Miyazawa, E.; Kikugawa, Y. One-Pot Reductive Amination of Aldehydes and Ketones with α-Picoline-Borane in Methanol, in Water, and in Neat Conditions. *Tetrahedron* **2004**, *60* (36), 7899–7906. https://doi.org/10.1016/J.TET.2004.06.045.

(20) Stöckigt, J.; Antonchick, A. P.; Wu, F.; Waldmann, H. The Pictet–Spengler Reaction in Nature and in Organic Chemistry. *Angewandte Chemie International Edition* **2011**, *50* (37), 8538–8564. https://doi.org/10.1002/ANIE.201008071.

(21) Heravi, M. M.; Zadsirjan, V.; Malmir, M.; Guo, J.; Niu, W. Application of the Asymmetric Pictet-Spengler Reaction in the Total Synthesis of Natural Products and Relevant Biologically Active Compounds. https://doi.org/10.3390/molecules23040943.

(22) Naseem, K.; Farooqi, Z. H.; Begum, R.; Irfan, A. Removal of Congo Red Dye from Aqueous Medium by Its Catalytic Reduction Using Sodium Borohydride in the Presence of Various Inorganic Nano-Catalysts: A Review. *J Clean Prod* **2018**, *187*, 296–307. https://doi.org/10.1016/J.JCLEPRO.2018.03.209.

(23) Ghoreishi, S. M.; Haghighi, M. R. Chromophores Removal in Pulp and Paper Mill Effluent via Hydrogenation-Biological Batch Reactors. *Chemical Engineering Journal* **2007**, *127* (1–3), 59–70. https://doi.org/10.1016/J.CEJ.2006.09.022.

(24) Alam, M. A.; Nethaji, M.; Ray, M. Synthesis of a Self-Assembled Molecular Capsule That Traps Pyridine Molecules by a Combination of Hydrogen Bonding and Copper(II) Coordination. *Angewandte Chemie International Edition* **2003**, *42* (17), 1940–1942. https://doi.org/10.1002/ANIE.200250591.

(25) Zhang, M.; Li, Y.; Yuan, W.; Guo, X.; Bai, C.; Zou, Y.; Long, H.; Qi, Y.; Li, S.; Tao, G.; Xia, C.; Ma, L. Construction of Flexible Amine-Linked Covalent Organic Frameworks by Catalysis and Reduction of Formic Acid via the Eschweiler–Clarke Reaction. *Angewandte Chemie International Edition* **2021**, *60* (22), 12396–12405. https://doi.org/10.1002/ANIE.202102373.

(26) Patel, D. C.; Luo, R. G. Protein Adsorption Dissociation Constants in Various Types of Biochromatography; 1999; pp 829–845. https://doi.org/10.1016/S0167-2991(99)80573-4.

(27) Contente, M. L.; Paradisi, F. Self-Sustaining Closed-Loop Multienzyme-Mediated Conversion of Amines into Alcohols in Continuous Reactions. *Nat Catal* **2018**, *1* (6), 452–459. https://doi.org/10.1038/s41929-018-0082-9.

Chapter 8

Conclusion and Final Remarks

This thesis explored various aspects of biocatalysis, ranging from mechanistic exploration to practical applications. The central focus spanned three areas: (I) the investigation of the enantiopreference of a ω-transaminase from *Halomonas elongata*; (II) the use of encapsulin from *Mycolicibacterium hassiacum* for biocatalyst encapsulation, creating a nanoreactor that enhanced the resistance of the encapsulated enzyme to harsh conditions and protein immobilization; and (III) the development of a 3-step chemoenzymatic cascade for producing industrially valuable compounds such as melatonin and dimethyltryptamine.

In Chapter 4, we explored the ability of HeWT, traditionally *(S)*-specific, to shift towards the synthesis of the *(R)*-enantiomer in THF-amine. The transformation was monitored during variations in substrate concentrations and ionic strength. It was reported that at increased co-solvent polarity and high pH values (> 9) favoured *(S)*-selectivity, while increased ionic strength and an excess of the amino acceptor induced enantiopreference inversion. The effect was attributed to structural changes in the enzyme, possibly linked to hydrophobic interactions within the protein structure and steric discrimination within the binding pocket. Additional experiments involving mutagenesis and structure characterization under each condition are necessary for a more comprehensive understanding.

In Chapter 5, we focused on investigating a molecular nanocompartment for enzyme immobilization. Encapsulin from *M. hassiacum* was utilized to address critical issues associated with enzyme immobilization and enhance local substrate concentration. Genetic modifications of the plasmids harbouring the cargo loading peptide (CLP) allowed successful cloning and encapsulation of HeWT and HeP5CR. Unlike previous findings, in our case no benefit was observed in either system. It seems possible that substrate and cofactor migration through the encapsulin structure was not particularly efficient. The *C*-terminus anchored CLP may induce flexibility constraints, limiting enzyme conformation. While literature supports encapsulin for reaction compartmentalization, the unexpected behaviour observed suggests limitations for broader biocatalytic applications. Future directions involve screening smaller and/or monomeric enzymes and exploring larger encapsulins for broader applications.

Finally, biocatalysis was employed for practical applications in Chapters 6 and 7. The objective was to develop an enzymatic cascade, serving as an alternative to conventional synthesis to produce melatonin, acetylated melatonin, and dimethylated tryptamines. Challenges in enzyme immobilization and substrate inhibition added complexities to the cascade design and

implementation, requiring a switch to a liquid/liquid extraction design for both steps. The final step in the cascade, an enzymatic acetylation of tryptamines, was unsuccessful and ongoing studies are focussed on gaining a better understanding of the issues associated with the low concentrations of the substrates. In Chapter 8, efforts to chemoenzymatically synthesize dimethyl tryptamines (DMTs) faced challenges in synthesizing *N,N*-dimethyl-5-hydroxy tryptamine (5H-DMT) due to the inherent instability of its precursor. Ongoing experiments are addressing these issues, and alternative reducing agents are being explored for sustainability. A purification step using Amberlite XAD-4 was implemented to ensure high purity of the product and prevent unwanted by-products from being present during the subsequent dimethylation.

Acknowledgments

I wish to express my deepest gratitude to Prof. Dr. Francesca Paradisi for making this opportunity a reality. Her invaluable expertise and feedback throughout this journey were crucial for my scientific and personal growth.

I am deeply grateful to Dr. David Lim for his consistent support, both within and beyond the laboratory. His encouragement and positive mood have been essential in making all this achievable.

Dr. Stefania Gianolio, my lab buddy and friend. I am thankful for having her beside during these four years. Without her my journey would have not been the same.

To my fellows and soon-to-be doctors: Pablo, always ready to lend a hand and share a coffee, a drink, or a dive; Keir, for all the food, fun and time we shared together; and Lauriane, for her scientific advise and ensuring our work environment remained safe and organized .

I extend my deepest thanks to Laura, Glenn, Bea, Rojia, Lia, who made our team a welcoming and enjoyable work place every day. Dr. "Manos" Broumidis, Dr. Arpita Mrigwani, and Dr. Gordon Honeyman deserve recognition for their unwavering scientific and professional support. Special appreciation also goes to Dr. Roura Padrosa and Dr. Benitez-Mateos for their invaluable scientific knowledge and guidance until the very end.

I owe a great debt of gratitude to Enrico, my solid rock, who has supported me since the beginning and believed in my abilities (perhaps it is time for you to marry a doctor). There are no words to express what a beautiful soul you are. I am also grateful to Elisa, the best sister

one could ask for, and to my chosen family in this country, Paola and Veronica. Thanks to Paolo, Silvia, Dr. Martina Contente, Andrea and Franci for their caring nature and for sharing in the significant moments of the past four years, and to Fede, Mary and all my forever fiends. To Dr. Matteoli, which regular support has been invaluable.

A special thank you to Dr. Pier Paolo Giovannini, without whom I would not be where I am today.

Lastly, to my mom and dad: my greatest joy is to bring you pride. I love you both dearly.